Dynamic Polysaccharide-based Nanoparticles for Advanced Drug Delivery Applications

Dissertation

Zur Erlangung des naturwissenschaftlichen Grades
„Doktor der Naturwissenschaften“
Im Promotionsfach Chemie

am Fachbereich Chemie, Pharmazie und Geowissenschaften
der Johannes Gutenberg-Universität Mainz

vorgelegt von

M.Sc. Chemiker
Matthias Konhäuser
geboren in Mainz

Mainz, November 2019

– D77 –

Mainzer Dissertation

Dekan: [redacted]

Erstgutachter: [redacted]

Zweitgutachterin: [redacted]

Tag der Einreichung: 20.11 2019

Tag der mündlichen Prüfung: 19.12.2019

Eidesstattliche Erklärung

Die vorgelegte Dissertation wurde von 4.10.2016 bis 20.11.2019 am Institut für Pharmazie und Biochemie der Johannes Gutenberg-Universität in Mainz zur Erlangung des Grades „Doktor der Naturwissenschaften“ angefertigt.

Erstgutachter: [redacted]

Zweitgutachterin: [redacted]

Hiermit erkläre ich an Eides statt, dass ich die vorliegende Dissertation selbstständig und nur mit den angegebenen Hilfsmitteln angefertigt habe. Diese Dissertation wurde noch nicht als Prüfungsarbeit für eine andere Prüfung eingereicht. Zudem wurden bisher weder die gleiche, noch Teile der Abhandlung als Dissertation bei einer anderen Fakultät oder einem anderen Fachbereich eingereicht.

Ort, Datum Matthias Konhäuser

[redacted]

Abstract

Nanoparticles gained great importance in the medical field since their first discovery 50 years ago. Based on the ability to select from a repertoire of materials, shapes, and sizes, nanocarrier can be designed to deliver a wide range of high potent drugs. They can protect and significantly improve the bioavailability of sensitive and pharmaceutically active cargo, that otherwise would not be applicable in biological systems and thereby enabling a broad field of medical applications.

This thesis presents the further development of a biocompatible and biodegradable acid-sensitive polysaccharide-based nanocarrier system for the simultaneous delivery of hydrophilic and hydrophobic drugs. L-Asparaginase and etoposide were dual encapsulated in dextran-based nanoparticles by a double emulsion technique. Studies revealed a controlled pH-sensitive release of both drugs and a high synergistic toxicity in K562 cells *in vitro*.

For immunotherapy applications, a biocompatible and targeted transport of active agents is required to enhance the therapeutic effect and limit the undesired side effects. Therefore, the dextran-based nanoparticle system was further advanced in the second project. The introduction of a hydrophilic polyethylene glycol (PEG) layer on the surface of these particles prevents unspecific cellular uptake and prolongs circulation time. Furthermore, specific antibodies as active targeting ligands for dendritic cells were attached on PEG. *In vitro* and *in vivo* studies showed that the modified particles were preferred taken up by receptor-mediated endocytosis in dendritic cells, which enables a potential anti-tumor $CD8^+$ cytotoxic T-lymphocytes activation.

In addition, based on the pH-responsive modified dextran, an advanced biocompatible horseradish peroxidase-polysaccharide conjugate was developed through formation of a disulfide bridge. The obtained double stimuli-responsive biodegradable hybrid material self assembles in water into spherical nanoparticles. During this process the structure integrity and enzymatic activity of the enzyme conjugate was retained. Nanoparticle degradation behavior was studied in detail with a focus on triggered drug released. The highly potent, indole-3 acetic acid (IAA) prodrug was encapsulated and successfully

delivered into the cytosol of HeLa cells. Hereby the released prodrug was oxidized by the horseradish peroxidase particle material, which leads to cellular apoptosis.

Both developed dextran-based particle systems represent promising candidates for successful applications in the delivery of therapeutics.

Zusammenfassung

Seit ihrer ersten Entdeckung vor 50 Jahren haben Nanopartikel eine große Bedeutung in der Medizin erlangt. Basierend auf der Möglichkeit, aus einem Repertoire an verschiedenen Materialien, Formen und Größen auszuwählen, können Nanocarrier so konzipiert werden, dass sie eine Vielzahl an hochwirksamen Medikamenten transportieren können. Sie können die Bioverfügbarkeit von empfindlichen, pharmazeutisch aktiven Wirkstoffen erhöhen, wodurch ein breites Feld von medizinischen Anwendungen ermöglicht wird.

Diese Arbeit stellt die Weiterentwicklung eines biokompatiblen, bioabbaubaren und säureempfindlichen Zucker-basierten Nanopartikels für die gleichzeitige Abgabe von hydrophilen und hydrophoben Medikamenten dar. L-Asparaginase und Etoposid wurden in Dextran-basierten Nanopartikeln mittels einer Doppelemulsionstechnik zusammen verkapselt. Studien zeigten eine kontrollierte pH-sensitive Freisetzung beider Medikamente und eine hohe synergistische Toxizität in K562-Zellen *in vitro*.

Für die Immuntherapie ist ein biokompatibler und gezielter Wirkstofftransport notwendig, um unerwünschte Nebenwirkungen zu reduzieren und die therapeutische Effizienz zu verstärken. Das auf Dextran basierende Nanopartikelsystem wurde daher im zweiten Projekt weiterentwickelt. Die Einführung einer hydrophilen PEG-schicht auf der Oberfläche der Partikel verhindert eine unspezifische Zellaufnahme und verlängert die Zirkulationszeit Darüber hinaus wurden spezifische Antikörper als aktive Zielliganden für dendritische Zellen an PEG gebunden. *In vitro*- und *in vivo*-Studien zeigten, dass die modifizierten Partikel bevorzugt durch rezeptorvermittelte Endozytose in dendritische Zellen aufgenommen wurden. Dies ermöglicht eine potenzielle Aktivierung der gegen Tumor wirksamen, zytotoxischen $CD8^+$ T-Lymphozyten.

Darüber hinaus wurde auf Basis des pH-responsiven modifizierten Dextrans ein neuartiges, biokompatibles Meerrettich Peroxidase-Polysaccharid-Konjugat entwickelt mittels Bildung einer Disulfidbrücke. Das erhaltene doppelt Stimulus-responsive, biologisch abbaubares Hybridmaterial ordnet sich selbst in Wasser zu kugelförmigen Nanopartikeln zusammen. Hierbei konnten die Strukturintegrität und enzymatische

Aktivität des Enzym-Konjugats erhalten bleiben. Nanopartikuläres Abbauverhalten wurde detailliert untersucht, wobei der Schwerpunkt auf einer gesteuerten Medikamentenfreisetzung lag. Das hochwirksame Prodrug Indol-3-Essigsäure wurde verkapselt und erfolgreich in das Zytosol von HeLa-Zellen eingeschleust, wo das freigesetzte Prodrug durch das Meerrettich Peroxidase Partikelmaterial oxidiert wurde und schließlich zur zellulären Apoptose geführt hat.

Beide entwickelten Dextran-basierten Partikelsysteme sind vielversprechende Kandidaten für erfolgreiche Anwendungen bei der Verabreichung von Therapeutika.

Table of Content

1 Introduction and Basic Concepts

1.1 Nanoparticles as Delivery Vehicles in Medicine

1.1.1 General Concept of Nanoparticles

Traditional first line treatments for cancer include chemotherapy, surgery, and radiotherapy.[1, 2] However, all of these treatments have drawbacks and relapse can reduce the 5-year survival rate by more than 50% in aggressive cancers.[3-5] In many cases, chemotherapy is not used alone, but combined with other treatments to achieve maximum therapeutic success. Normally, chemotherapy is done by taking medications that are preferentially taken up by cancer cells due to uncontrolled and rapid growth.[6] Unfortunately, healthy cells that have rapid cell division, such as hair follicles, intestinal, oral and skin cells, can also be damaged by chemotherapy. In addition, systemically administered non-selective chemotherapeutic agents can enter tumor tissue and healthy organs in free form.[7] As a result, cancer patients suffer from the effects of the systemic toxicity of the drugs. Typical symptoms include fatigue, diarrhea, alopecia, nausea, vomiting or loss of appetite.[8]

Encapsulation of non-selective chemotherapeutic agents in a vehicle that carries the drug selectively into tumor tissue may reduce systemic toxicity. This "magic bullet" concept was first proposed by Dr. Paul Ehrlich in 1906 and nanoparticular systems could realize this concept.[7, 9]

Other benefits of a nanoparticle-based drug delivery system include sustained drug release, protection against drug degradation and crossing physiological barriers.[10] In addition, hydrophobic drugs that would contradict the Lipinski's rule of five and thus would not be bioavailable can be encapsulated in nanoparticles in order to increase the spectrum of applicable drugs.[11] Another advantage of nanoparticles is their tunable pharmacokinetics.[12] The increased bioavailability allows a lower dosage and consequently less severe side effects.[13] Since the discovery of nanoparticle formulation in 1969, a large number of nanoparticular systems have been developed which differ greatly in shape, size and properties.[14] Depending on their attributes and surface modifications, the particles can also be distinguished from each other in their medical

field of application. In **Figure 1** different nanoparticles properties are displayed and discussed in respect to their most important aspects.

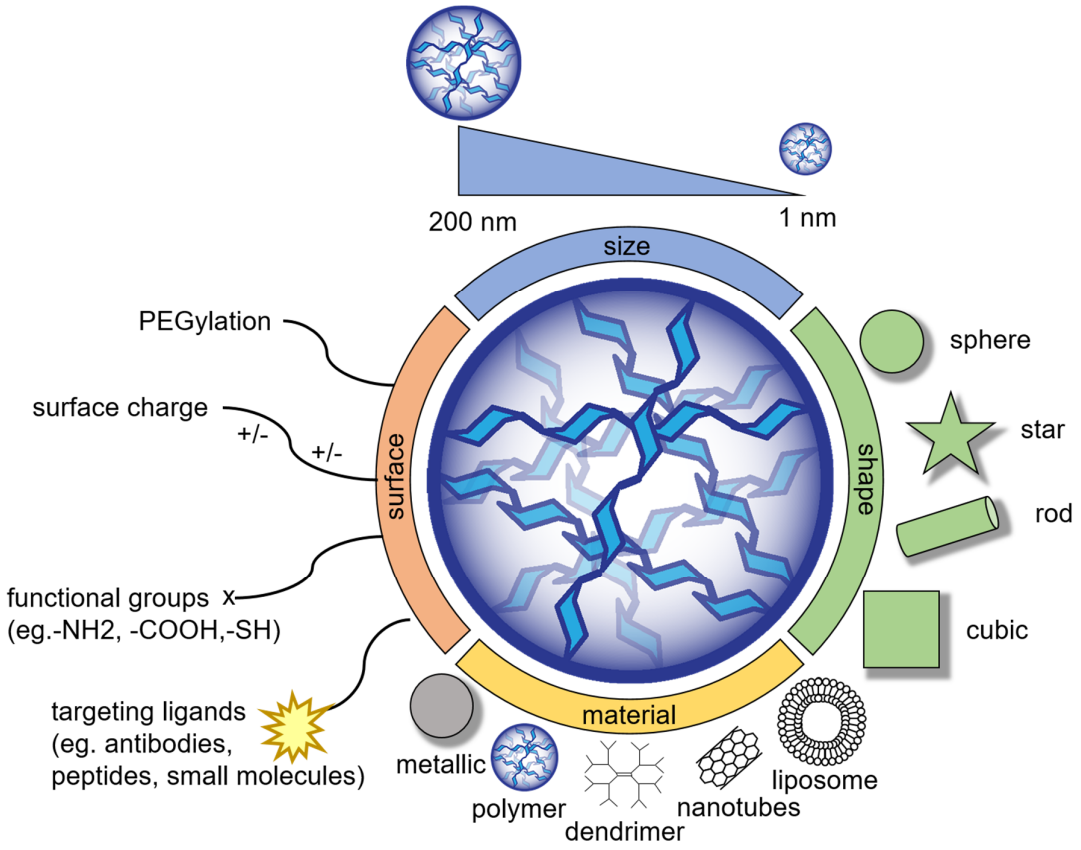

Figure 1. Overview of important nanoparticle properties. Adapted and modified from *Angewandte Chemie International Edition*.[15]

Metallic Nanoparticles

Metal nanoparticles are nano-sized particles made of pure metals (*e.g.*, iron gold, silver, platinum, titanium, zinc) or their inorganic compounds (*e.g.*, oxides, hydroxides, sulfides, phosphates, fluorides and chlorides).[16] Iron (III) oxide (Fe_2O_3) particles are characterized by their ultrafine size and magnetic properties. Superparamagnetic iron oxide nanoparticles have emerged as promising candidates for various biomedical applications, such as enhanced resolution contrast agents for magnetic resonance imaging, targeted drug delivery and imaging.[17] Gold nanoparticles provide unique optical properties which enables several applications in cellular imaging and drug delivery.[18] In contrast silver nanoparticles are typically used for threating wounds based on their antimicrobial activity.[19]

Carbon Nanotubes

Carbon nanotubes (CNTs) are a class of nanomaterials that consist of a two-dimensional hexagonal lattice of carbon atoms. Their exceptional thermal, mechanical, and electronical properties together with their tubular shape, offering a high surface area and enabling conjugation of a wide variety of therapeutic drugs, making CNTs an attractive platform for the treatment of various diseases.[20] For example it is possible to exploit their thermal conductivity in order to photothermally kill cancer cells.[21]

Dendrimers

Dendrimers are nanometer-sized, radially symmetric molecules consisting of tree-like arms or branches.[22] They are highly defined artificial macromolecules with high number of functional groups for further possible modifications.[23, 24] Applications highlighted in recent literature include drug delivery, gene transfection, catalysis and energy harvesting.[25-27]

Liposomes

Liposomes were first described 1965 and are sphere shaped vesicles consisting of one or more phospholipid bilayers.[28] They represent a promising drug delivery platform based on their biocompatibility, biodegradability, low toxicity, and ability to encapsulate both hydrophilic and hydrophobic drugs.[29, 30] On this occasion the hydrophilic drug is located in the aqueous core, while hydrophobic drugs associate with the bilayer.

Polymer Nanoparticles

Polymeric nanoparticles are researched widely as nanocarriers for controlled and sustained drug release.[31] They can be either nanocapsules or nanospheres. Nanocapsules are vesicular systems in which the drug is confined to a cavity surrounded by a polymer-membrane, while nanospheres have a matrix architecture.[32] Drugs can be either encapsulated inside the nanoparticles or adsorbed on their surface. In general, fragile molecules are better preserved from enzymatic degradation when they are encapsulated during the preparation in the nanocarrier.[33-35] Two main strategies used for preparation of polymeric nanoparticles are the “top-down” strategy and the “bottom-up” approach. The top-down strategy utilizes a preformed polymer to form polymeric nanoparticles whereas in the bottom-up approach polymerization of monomers leads to

the formation of polymeric nanoparticles.[36] Various methods are used for the preparation of polymeric nanoparticles for example self-assembly, emulsification, solvent evaporation/extraction.[37-41]

Polymers for nanoparticle formation need to fulfill several requirements.[37, 42] First, the polymer needs to be biodegradable or at least fast eliminated from the body. The polymer and the degradation products must be nontoxic and non-immunogenic.[37] Thirdly, the polymer must have suitable properties for a specialized drug delivery system. Polymeric nanoparticles consist preferably of biodegradable and biocompatible synthetic or natural polymers. As non-biodegradable materials, such as polyacrylamide, have toxic risks because of possible accumulation in the body.[43] The most widely used synthetic polymers are poly(lactic acid)(PLA), poly(glycolide) (PLG), poly(lactide-co-glycolide)(PLGA), and polycaprolactones.[44-48] Natural polymer like alginate, chitosan, dextran or proteins have been widely explored.[49-52] They show excellent biocompatibility since they are broken down by enzymatic degradation into easily metabolized peptides or saccharides in the body.[53]

Among the mentioned nanoparticle systems, polymer nanoparticles have multiple advantages, including the ability to tailor the physical, chemical, and biological properties of the nanocarrier which leads to the broadest medical applications.[54] Gold nanoparticles and iron oxide are good for imaging applications but have, in contrast to polymer nanoparticles, significant limitations for drug loading and drug release.[55] Furthermore biodegradable polymers are especially appealing since they break down in physiological or pathophysiological conditions, which generally reduces the toxicity of the carrier and facilitates systemic elimination.[56]

Size and Shape

The size and shape of nanoparticles are two important parameters for a drug delivery system. They play a crucial role in drug loading, drug release, stability and *in vivo* distribution.[57, 58] Furthermore the degradation of polymer particles can be altered based on the different size to surface area ratio.[59] Compared to microparticles, nanoparticles have a relatively higher intracellular uptake and better biodistribution based on their higher mobility.[60] For example HepG2 cell lines were found to only take up nanoparticles, while rejecting microparticles.[61] Microparticles of ~1–5 μm are further localized within

the liver where they are phagocytosed quickly by macrophages.[62, 63] Nanoparticles between 200 nm and 1 μm are easily filtered out in the spleen meanwhile smaller particles remain in blood vessels.[64] Nanoparticles should be bigger than 6 nm because otherwise they will be filtered out fast by renal clearance without reaching the therapeutic location.[65]

Generally, the optimal size of a nanoparticle system depends on the targeted location and type of therapeutically approach.[66] **Figure 2** shows the size of different nanoparticle systems.

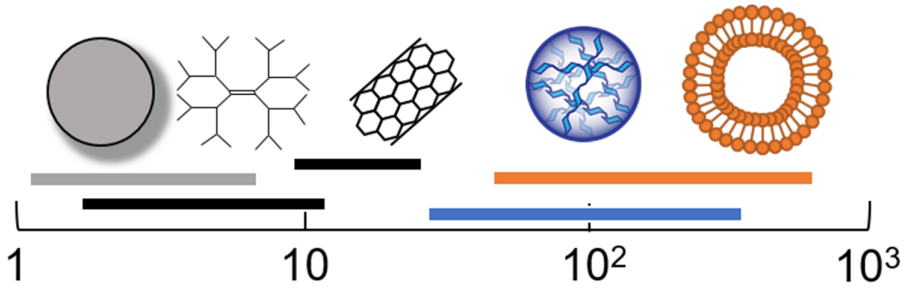

Figure 2. Size of different nanoparticle systems (metallic nanoparticles ~1–10 nm, dendrimers ~2–20 nm, carbon nanotubes~10–10 nm, polymer nanoparticles ~50–500 nm, liposomes ~60–700 nm).

The shape of nanoparticles is of equal importance as their size in drug delivery. *Chan et al*. reported that spherical gold nanoparticles have a higher chance to be internalized *in vitro* by HeLa cells compared to rod-shaped particles of similar size.[67, 68] Studies by *Vácha et al*. confirmed that spheres nanoparticles also have a higher endocytosis-rate than particles with sharp edges.[69] As summary it can be proposed spherical nanoparticles seem to be good candidates for drug delivery.[15]

Surface of Nanoparticles

In addition to both size and shape, the surface characteristics of nanoparticles represent another critical parameter in determining their drug loading efficiency, drug release biodistribution and clearance from the body.[15] Surface modifications are able to entirely alter the protein corona and thereby also the medical function.[70] The nanoparticles should have a hydrophilic surface to resist the adsorption of plasma proteins and thus escape a fast clearance by macrophages.[71, 72] The most commonly used approach to achieve this goal is to coat with hydrophilic PEG-chains.[73, 74] For further insight of surface modifications see **Chapter 1.2**.

Surface Charge of Nanoparticles

The zeta potential of a nanoparticle is commonly used to characterize its surface charge.[15, 75] It reflects the electrostatic potential of a particle and is influenced by the surface composition of the particle as well as the surrounding buffer. Nanoparticles with a zeta potential higher than ± 30 mV are stable in suspensions, as repulsion forces from the surface charges can prevent the particles from aggregation. But high surface charge also leads to more rapid opsonization by macrophages, resulting in greater clearance by the mononuclear phagocytic system (MPS).[76] Therefore, control over the surface charge can help minimize the nonspecific interactions between nanoparticles and the MPS, preventing the loss of nanoparticles in undesired locations.[77]

The complexity of finding the optimal nanoparticle size, shape and surface chemistry requires *in vivo* studies for each specific therapeutic approach.[78]

Biocompatibility and Cellular Uptake of Nanoparticles

The route of application is determined by the target organ and the properties of the nanoparticle and the encapsulated drug. For most nanoparticulate systems, intravenous administration is the first choice. On the one hand, it offers the advantage that fewer cellular barriers have to be crossed compared to a dermal application. On the other hand, an advantage is the constant neutral pH value of the blood. In contrast, the strongly acidic pH value and the digestive enzymes of the stomach pose problems for many nanoparticles during oral administration. For intravenous administration, however, the particles must be highly sterile.

After application, the size, zeta potential and solubility of the particles determine their half-life in the body.[79] **Figure 3** demonstrates different crucial parameters for the biocompatibility of nanoparticles.

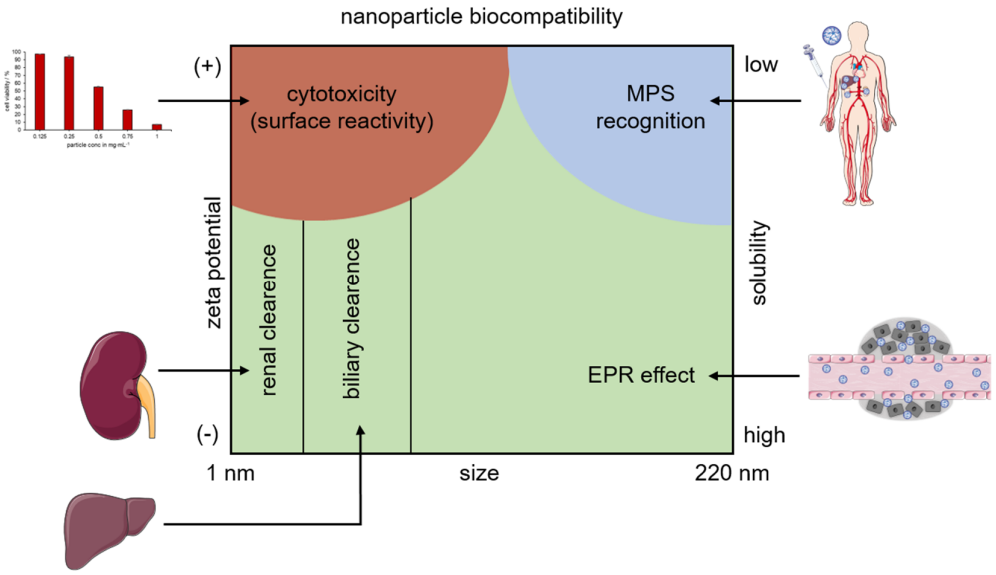

Figure 3. Nanoparticles biocompatibility dependent on size, zeta potential and solubility. Adapted and modified from *Clinical Cancer Research*.[79] Organ images modified from "Servier Medical Art" by Servier (https://smart.servier.com/) licensed under CC BY 3.0.

Endocytosis of Nanoparticles

Efficient cellular uptake of nanoparticles is important for effective intracellular drug delivery, as the target site of many drugs is located in the cytosol or cellular compartments. The endocytosis pathway of the particles significantly determines the fate and intracellular localization of the nanoparticles.[80] It can be initiated by either highly selective binding between the ligand attached to the nanoparticle and the corresponding receptor present on the cell membrane, or by nonselective binding based on hydrophobic or electrostatic interactions. There are 4 major endocytosis pathways depending on the size and surface properties of the particles.[81]

First receptor-mediated endocytosis (also known as clathrin-mediated endocystosis), is the inward budding from the plasma membrane containing receptors specific to the functionalized-particles being internalized.[82] Second, caveolae-mediated endocytosis, where extracellular molecules are internalized upon binding to specific receptors in the plasma membrane.[15] Third, macropinocytosis is a process that begins with the formation of a pocket through the invagination of the cell membrane (0.5–5 μm in size) that leads to nonspecific uptake of extracellular material together with particles. Fourth, phagocytosis, a process by which cells actively bind to- and internalize particles larger than approx. 250 nm in diameter, such as cell debris, microorganisms, or even apoptotic cells.

The phagocytosis route is mainly used by dendritic cells (DCs), neutrophils and macrophages.[83]

The internalization pathway of nanoparticles is largely determined by their size, shape and surface properties (hydrophobicity vs. hydrophilicity, charge, and the type/density of a ligand).[84, 85] Negatively charged NPs show an inferior rate of endocytosis and do not utilize the clathrin-mediated endocytosis pathway. On the other hand, positively charged and spherical NPs internalize rapidly via the clathrin-mediated pathway.[86]

While large particles are internalized through phagocytosis and macropinocytosis, small particles have to rely on clathrin- or caveolae mediated pathways.[87]

Despite different cellular entry pathways, the endosomes are mostly the first intracellular compartments encountered by the internalized nanoparticles. Early endosomes are characterized by a lower luminal pH (~6–6.5) and by a transport to lysosomes (~pH 4.5–5.2), which has been exploited to trigger the release of pH-responsive nanoparticles into the cytosol (**Figure 4**).

Intracellular Escape and Degradation of Nanoparticles

For successful delivery of therapeutic agents, the nanoparticles also need to be designed with an ability to escape from the endolysosomal network and enter the cytosol.[15] To achieve this goal nanoparticles can be coated with an amine rich polymer that is capable of buffering between pH 5.2–7.0 to enable endosomal escape through the "proton-sponge effect".[88-90] Once these cationic nanoparticles are incorporated into the acidic endolysosomal compartment, the amino groups can continuously activate the proton pumps, leading to osmotic pressure and accumulation of water molecules inside the compartment.[91] The swelling results in the rupture of the endolysosome and releasing the drug to their working site. **Figure 4** shows the different endocytosis pathways with subcellular fate and proton sponge effect.

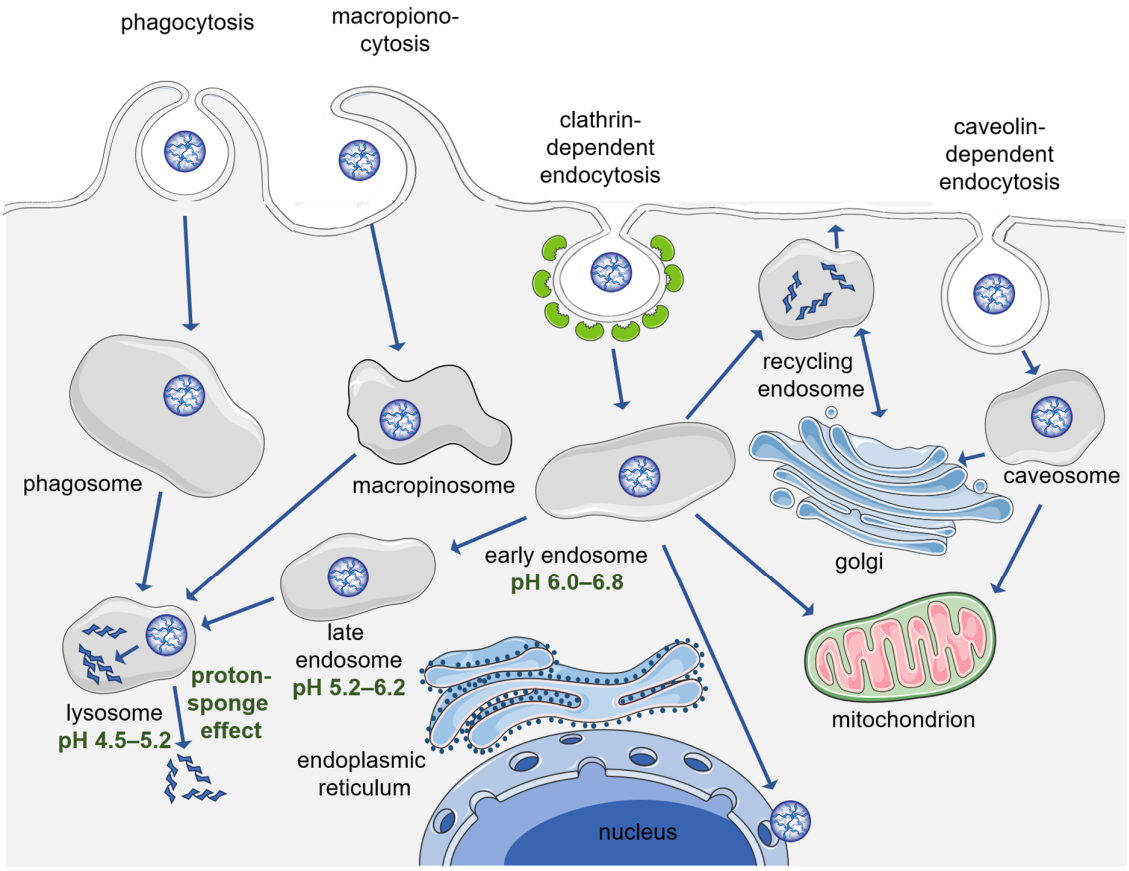

Figure 4. The endocytosis pathways with subcellular fate and proton sponge effect. Adapted and modified from *Journal of Controlled Release*.[80] Organelle images modified from "Servier Medical Art" by Servier (https://smart.servier.com/) licensed under CC BY 3.0.

Methods of Controlled Drug Release

After cellular uptake of the nanoparticle system a controlled release of the encapsulated drug is desirable. For this several stimuli-sensitive materials incorporating responsive chemical motives have been developed (see **Figure 5**). The trigger mechanism will be discussed in the next chapter.

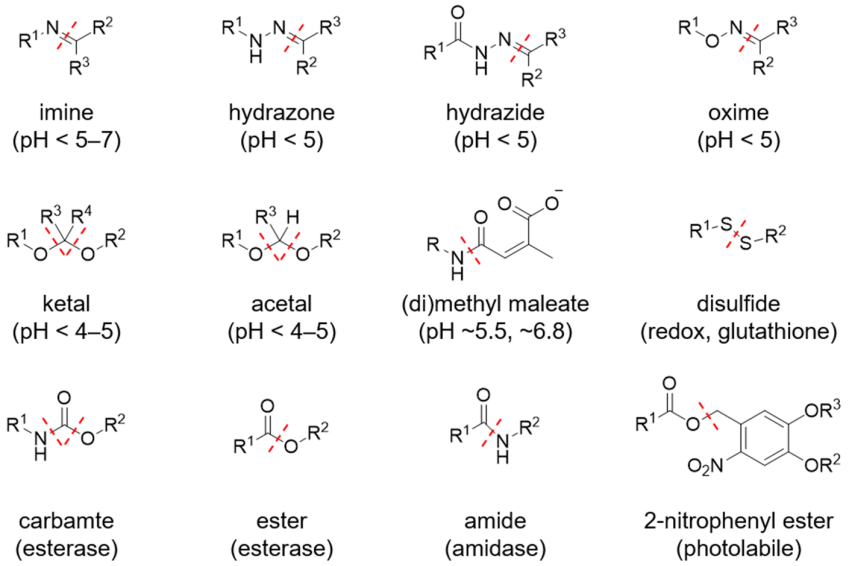

Figure 5. Cleavable linkers that have been used for stimuli-responsive drug release. The red dashed line in each molecule indicates the bond that will be broken upon activation by the corresponding stimulus. Adapted and reproduced from *Advanced Drug Delivery Reviews*.[92]

pH-sensitive Release. The variation in pH value associated with a pathological situation such as cancer or inflammation has been extensively used to trigger the release of a drug into a specific organ or intracellular compartment (*e.g*. endosome or lysosome).[93] Two main strategies exist: the use of polymers with ionizable groups that undergo conformational or solubility changes in response to environmental pH change. Commonly used polymers include poly(acrylic acid) (PAA) and poly(methyl acrylate) (PMA). With the use of these polymers, the hydrophobicity of the nanoparticle carriers change as a result of protonation or deprotonation.[94-96] Another strategy involves a system with acid-sensitive bonds whose cleavage enables the release of molecules attached to the polymer backbone.[93]

Redox-sensitive Release. The difference of redox potential (~1,000 fold) existing between the extracellular matrix and the intracellular cytosol is based on different concentrations of glutathione found in extracellular (~ 2–10 μM) and intracellular (~ 2–10 mM) compartments.[93, 97] A cytosolic drug release can be thereby obtained by reductive cleavage of disulfide bonds in the nanoparticle system.

Photo-sensitive Release. Photosensitivity is often introduced to nanoparticles through functional groups that can be cleaved or change their conformations upon irradiation with light of a specific wavelength.[98, 99] Notable examples include azobenzene, pyrene, nitrobenzene and spirobenzopyran.[15, 100, 101]

Enzyme-responsive Release. An altered expression profile of enzymes (such as proteases, phospholipases or glycosidases) observed in pathological tissue (*e.g*. cancer or inflammation) can be exploited to achieve enzyme-mediated degradation of a nanoparticle system and drug release at the desired biological target.[93, 102-104]

Thermo-responsive Release. Thermo-responsive release takes advantage of the local temperature increase caused by pathological condition like tumor, inflammation or infection.[15] Ideally, thermo-sensitive nanocarriers should retain their load at body temperature and rapidly deliver the drug within a locally heated tumor (~40–42 °C).[93] The method relies on a change of the physical properties of a temperature-sensitive material (*e.g*. liposomes or nanoparticles based on thermo-sensitive polymers) which triggers the drug release.[105, 106] Notable examples of thermo-responsive polymers are poly(*N*-isopropylacrylamide) (PNIPAAm), poly(*N*,*N*diethylacrylamide)(PDEAAm) and Pluronic (PEO-PPO-PEO).[106-108]

Dual-responsiveness. Sensitivity to more than one stimulus can even further improve nanoparticular drug delivery. pH- and redox-responsiveness can be used in combination based on the coexistence of a pH gradient and an oxidative environment in tumor- and inflammation tissues.[93] Studies by *Yoon et al*. with self-assembled nanoaggregates consisting of four-arm PEG conjugated to doxorubicin and anti-bcl-2 oligonucleotide with reducible linkers and acid-cleavable linkers showed a dual-responsive breakdown of the nanostructures. The particles degraded under reducing conditions and the oligonucleotide was released at a low pH.[109] In general, it is possible to obtain dual-responsive systems for all above mentioned different stimuli. This can be achieved by choosing the right monomers and combining them with a stimuli-responsiveness linkage group. However, the complexity of such dual-responsive systems increases dramatically.[92]

To summarize, a nanoparticle system for a wide range of therapeutic applications should consist out of a biodegradable and biocompatible polymer with a stimuli-responsive triggered drug release. The particle should have a spherical shape for high cellular uptake and to enhance the more specific clathrin-mediated endocytosis pathway. Furthermore, the particle should be able to escape the endolysosomal network through the proton sponge effect. To prevent aggregation the surface charge should be either high positive or negative. In the following chapter a polysaccharide-based particle system is described which unites the mentioned particle requirements.[110]

1.1.2 Dextran as a Material for Nanocarriers

Polysaccharides are natural polymers of monosaccharides that can be distinguished by origin and structure. Some of them are of vegetable (*e.g*. pectin), microbial (*e.g*. dextran) or animal origin (*e.g*. chitosan).[111] The polysaccharides are further divided into positively charged (*e.g*. chitosan) and negatively charged (*e.g*. heparin, pectin) polymers. Polysaccharides have a high number of reactive groups (hydroxyl, carboxyl, aldehyde, amine groups), very different molecular weights and show a large variance in chemical compositions. Furthermore, the reactive groups of the polysaccharides can easily be chemically modified and thus allowing the synthesis of various derivatives. As a natural biomaterial, polysaccharides are stable, non-toxic and biodegradable, making them an ideal nanoparticle platform. The preparation methods for polysaccharide nanoparticles are: For example covalent cross linking, ionic crosslinking, polyelectrolyte complexation and self-assembly of hydrophobically modified polysaccharides.[110]

A promising polysaccharide for nanoparticle formation is dextran. The linear dextran chain consists of D-glucose units with a length of 1.5 to 2,000 kDa, which are predominantly linked by α-1,6- glycosidic bonds.[112] Furthermore, the chains have a variable content of α-1,2 α-1,3 α-1,4-glycosidic branches.[113] The structure of α-1,6-glycosidically linked dextrans is shown in **Figure 6**.

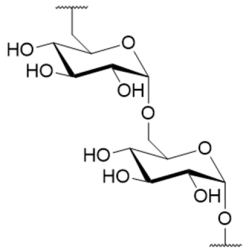

Figure 6. The structure of the linear dextran chain consists of α-1,6-glycosidically linked D-glucose units.

The synthesis of the dextrans takes place by enzymes predominantly from sucrose in bacteria of the genus *Leuconostoc mesenteroides*.[114] The macromolecules possess essential biocompatibility: Biodegradation occurs through enzymatic splitting by dextran-1,6-glucosidase found in many cell-types.[115] Furthermore, dextran lacks nonspecific cell binding and resists protein adsorption.[116] Dextran chains can be simply chemical modified, *e.g*. by reductive amination or acetalization. Dextran has proven itself as a biocompatible, biodegradable polysaccharide in medical applications. It can be used as a blood plasma substitute in emergency medicine based on the colloidal osmotic pressure of a 6 percent aqueous dextran solution with a molecular weight of 70 kDa.[117] Furthermore the use of low-molecular dextran as a thrombocyte aggregation inhibitor is possible.[118] In spite of the mentioned biocompatibility and various medical applications, *Shiratori et al*. also reports a rare hypersensitivity reaction against dextran.[119] Further use of the dextran is possible by cross-linking it with epichlorohydrin to form a copolymer which has relatively uniform pores and can be used in gel permeation chromatography.[120]

Hydrophobically-modified Dextran (AcDex)

Based on the FDA-approved polysaccharide dextran the group of *Jean Fréchet* developed a biocompatible, biodegradable, and non-toxic particle system. The particle material can be obtained by acetalation of dextran (AcDex), which changes the solubility of the polymer so that the AcDex is no longer water-soluble but soluble in organic solvents such as dichloromethane, ethyl acetate and acetone.[96]

In addition, the acetals can be cleaved under slightly acidic conditions (pH 4–5), enabling controlled drug release in sites of inflammations,[121] tumor tissue[122, 123] and lysosomes.[124] The synthesis and hydrolysis of AcDex is shown in **Figure 7**.

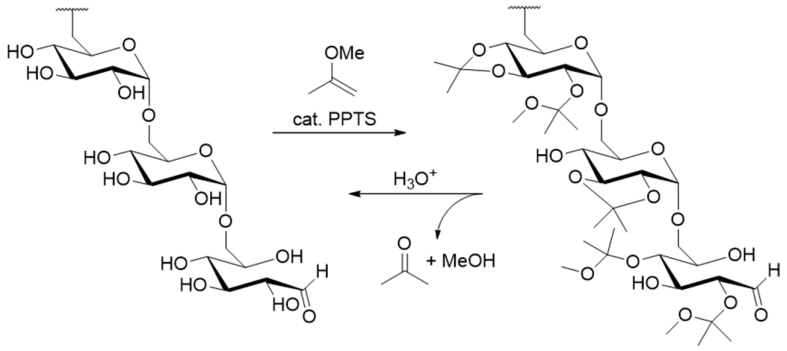

Figure 7. Synthesis and hydrolysis of AcDex.

This solubility switch enables the formation of stable particles with a top-down approach in aqueous buffers using a single or double emulsion technique.[125] For this purpose, the hydrophobic AcDex is dissolved in dichloromethane (DCM) and a phosphate-buffered saline (PBS) solution with polyvinyl alcohol (PVA) as surfactant is added. After sonification and organic solvent evaporation the particles with a size of (~100–200 nm) and a low PDI can be obtained. The particle size in this method is dependent on the type and concentration of the surfactant, sonification intensity and polymer concentration used in the process.[36, 126]

Depending on the nature of the respective cargo, small hydrophobic drugs can be encapsulated with a single emulsion procedure (w/o) and hydrophilic biomolecules with high molecular weights via a double emulsion method (w/o/w) (**Figure 8**).

With increased acetalation reaction time acyclic acetals are transferred to more stable cyclic acetals allowing a precise tuning of the hydrolysis-rate, particle degradation and hence drug release.[127, 128] AcDex with a reaction time of 10 min was almost totally degraded (90%) after incubation in acidic buffer for 10 h, meanwhile only 10% of a 60 min AcDex was hydrolyzed.[128] Another tunable aspect is the molecular weight of the applied dextran. *Kauffman et al*. showed that microparticles synthesized from AcDex with a molecular weight of 71 kDa had higher encapsulation efficiency of rapamycin and slower overall degradation than microparticles synthesized from 10 kDa AcDex.[129] The flexibility of the system gives it a major advantage over other acid-sensitive polymers, such as poly-beta amino esters (PBAEs), polyorthoester (POEs,) and polyketals, of which degradation profiles are less variable.[130]

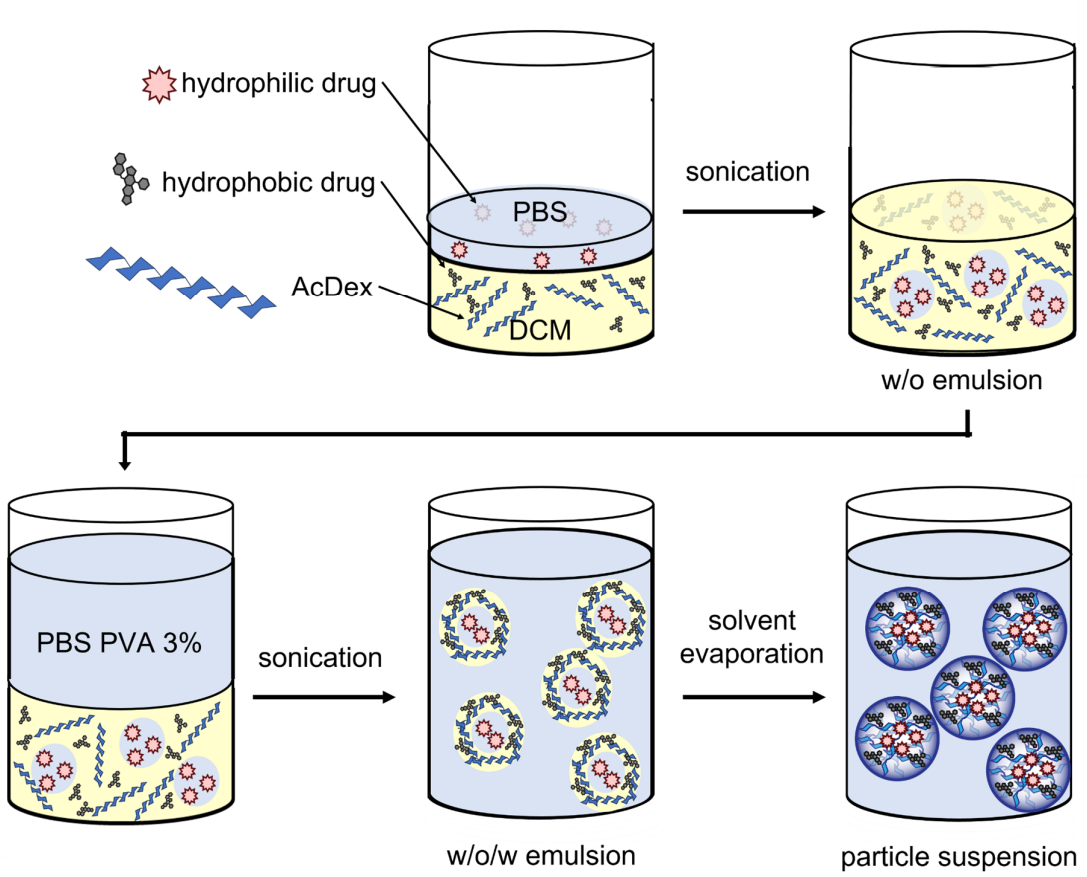

Figure 8. Double emulsion evaporation method for encapsulation of hydrophilic and hydrophobic drugs inside nanoparticles consisting of hydrophobically modified dextran.

Hydrophobic silver carbene complexes were further successfully encapsulated in AcDex nanoparticles by single emulsion. The studies by *Ornelas-Megiatto et al.* revealed a high encapsulation efficiency and a promising antibacterial property against gram-negative and gram-positive bacteria.[131]

Cohen et al. functionalized AcDex with spermine (SpAcDex) to increase the loading of siRNA by ionic interactions of the positively charged amines with the negatively charged phosphate backbone of RNA. Additionally, the cationic particle character increases the cellular-uptake and as well as the endosomal escape through the proton sponge effect, wherein the positive charge of the particles causes an influx of negatively-charged Cl^- ions into the endosome, subsequently causing osmotic rupture of the endosome.[132, 133] SpAcDex showed a high binding capacity (>75%) of encapsulated anti-luciferase siRNA. After the incubation of siLuc-loaded SpAcDex nanoparticles with HeLa-luc cells for 48 h, a successful knockdown of luciferase (up to 60%) was shown.[88]

The group of *Santos et al*. showed that a Nutlin-3a, and the cytokine granulocyte–macrophage colony-stimulating factor (GMCSF) can further be co-encapsulated in SpAcDex particles with a double emulsion technique. This enables a combination of chemo- with immunotherapy and the system is capable of inducing tumor cell death by stimulating the immune response. Due to Nut3a, the loaded NPs exert specific toxicity toward p53 cancer cells. Furthermore, the NPs show intrinsic immune adjuvancy on monocyte derived-DCs, upregulating the expression of cell surface CD83 and CD86 costimulatory markers which leads to proliferation of $CD3^+$ and cytotoxic $CD8^+$ T cells.[134] For further immunotherapy application of AcDex nanoparticles see **Chapter 1.3.2**.

A further advantage of the spermine-modified system are the easily chemically accessible amines on the particle surface. *Bamberger et al.* attached PEG and dextran chains on the particle surface through NHS-ester reaction with the primary amines of the spermine on the particle surface. The introduction of a hydrophilic PEG layer on the surface of the SpAcDex-nanoparticles prevents unwanted aggregation and decreases unspecific cell uptake. On the other hand, the introduction of a layer of low molecular weight dextran (3.5 and 5 kDa) on the particle surface encourages the nanoparticle uptake by antigen-presenting cells like macrophages and DCs. Binding of dextran modified particles to these immune cells results in a cell activation.[135, 136] *Butzbach et al.* encapsulated the photosensitizer 5, 10, 15, 20-tetraphenyl-21*H*, 23*H*-porphyrine (TPP) in SpAcDex nanoparticles and conjugated NHS-activated folic acid on the particle surface. The authors could show that the particles were successfully taken up by human HeLa-KB cells through folate-receptor-mediated endocytosis, and a light-induced cytotoxicity was observable (**Figure 9**).[137]

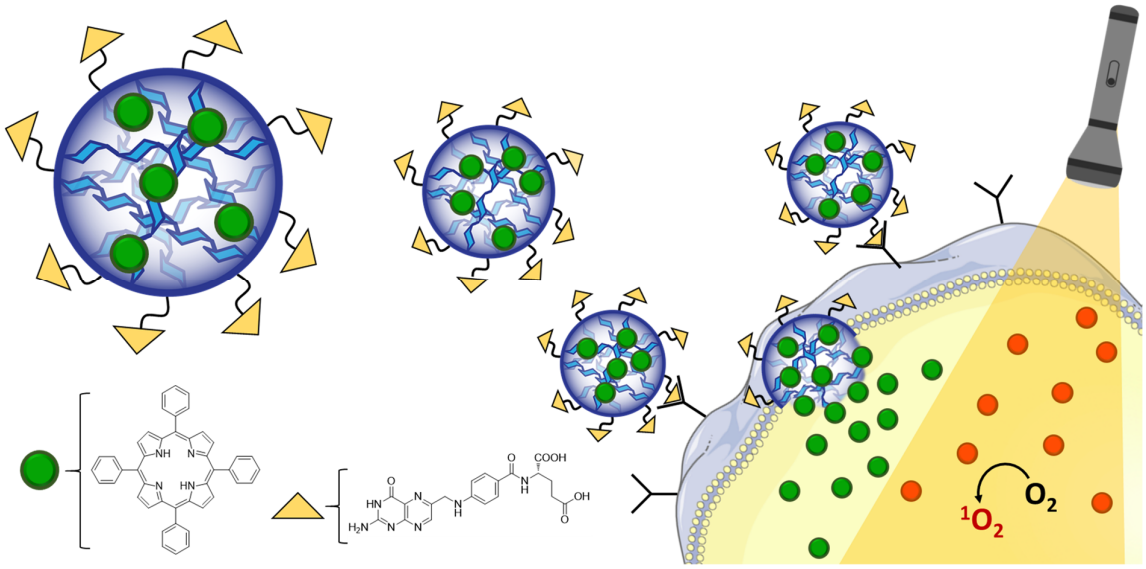

Figure 9. Folic acid functionalized SpAcDex nanoparticles with encapsulated TPP. Reproduced from *Polymers*.[137]

In summary, the AcDex system is a nontoxic, biocompatible particle material for the delivery of active small hydrophobic or huge hydrophilic drugs. The facile tunability of AcDex chemistry allows for both burst and sustained long-term release of encapsulated therapeutics using the same polymeric platform. These benefits make AcDex an ideal material for particle formulation due to their *in vivo* degradation into harmless and biological by-products.

1.2 Targeting Approaches for of Nanoparticles

1.2.1 Passive Targeting

EPR Effect

Passive targeting relies on the physicochemical properties of the nanoparticles and on the enhanced permeability and retention (EPR) effect.[138] Accumulation of nanoparticles can be observed in tumor tissue and inflammatory tissue. This is referred to as passive targeting, which is a consequence of the EPR effect and was first described in 1986 by *Maeda et al.*[139] The increased penetration of nanoparticles into tumor tissue compared to healthy tissue is due to an altered anatomy and pathophysiology based on the increased nutrient and oxygen demand of the tumor tissue.[140] As a result, tumor tissue is characterized by increased angiogenesis and a more permeable endothelial layer with disordered endothelial cell linkages.[141] In addition, the increased release of VEGF (Vascular Epithelial Growth Factor) into the tumor tissue causes an increased penetration of macromolecules.[142] The retention of NP in the tumor tissue is also favored by a deficient lymphatic drainage into the tumor tissue.[143] In contrast, nanoparticles can be relatively poorly taken up in healthy tissue due to the ordered, dense epithelial layer.[144] The accumulation of macromolecules as an effect of the EPR effect in tumor tissue compared to healthy tissue is shown schematically in **Figure 10**.

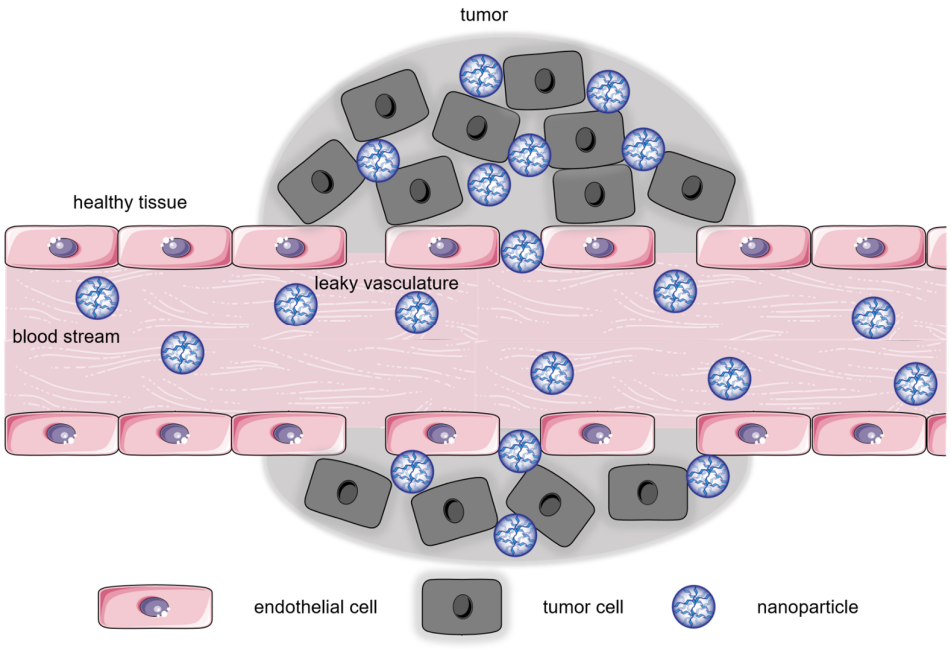

Figure 10. Accumulation of nanoparticles by the EPR effect through the permeable endothelial layer of the tumor tissue. Cell images modified from "Servier Medical Art" by Servier licensed under CC BY 3.0.

The extent of the EPR effect depends on the size and charge of the nanoparticles as well as on the type of tumor tissue and tumor microenvironment.[145, 146] A maximum EPR effect was found for particles between 10 and 100 nm, depending on the tumor tissue examined.[147] However, accumulation has also been noted for particles as large as 400 nm in an animal model.[148] Passive targeting using the EPR effect increased the nanoparticle concentration by up to 50-fold compared to healthy tissue in tumor tissue.[149] This enables the possibility of specific increase of the drug concentration in the target tissue to reduce potential side effects of the encapsulated drug. In contrast, small molecules (<10 nm) without nanoparticle packaging bear the problem that they are taken up in a comparable amount of healthy and tumor tissue and thus leading to nonspecific systemic toxicity.[7]

Stealth Effect of Surface-modified Nanoparticles

For optimal utilization of the EPR effect, a circulation time of the nanoparticles of over 6 h has been found to be ideal.[150] However, non-surface-modified nanoparticles are rapidly eliminated via the MPS system.[151] One way to increase the circulation time while reducing non-specific cell uptake of the nanoparticles is the PEGylation of the particles. A PEG shell on the nanoparticle surface causes them to be removed more slowly.[152] Bypassing the immune system by PEGylation is called the stealth effect, which is facilitated by reduced adsorption of proteins to the hydrophilic PEG chains compared to the hydrophobic nanoparticle material.[153] In particular, a lower content of opsonin on the surface of the nanoparticles causes a reduced phagocytosis rate by macrophages.[153] Another important aspect for the stealth effect is the PEG chain density. PEG coatings with a brush-like configuration reduce phagocytosis and complement activation, however a mushroom-like configuration leads to potent complement activators to induce phagocytosis.[154] In **Figure 11** the difference of mushroom-like and brush-like PEGylation is displayed.

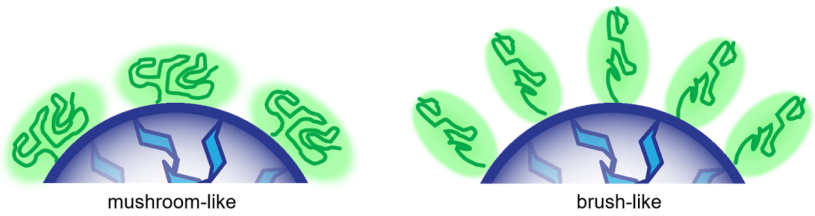

Figure 11. Mushroom-like PEGylation and brush-like PEGylation.

Figure 12 shows as an example the different biodistributions of non-PEGylated and PEGylated nanoparticles due to their difference in circulation times.

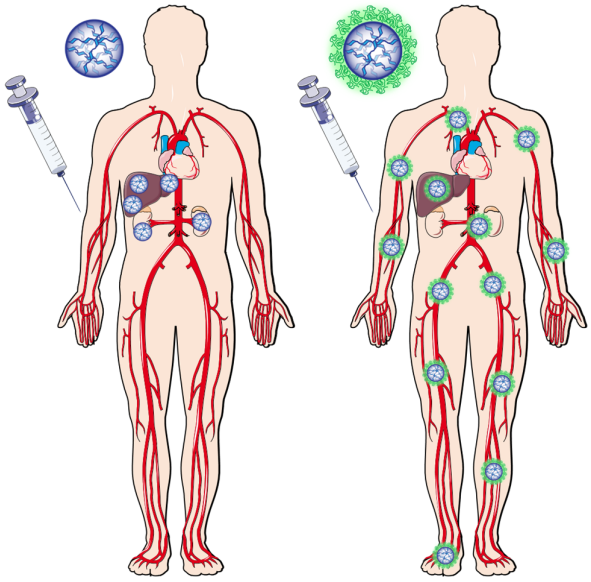

Figure 12. Biodistributions of non-PEGylated and PEGylated nanoparticles. Body images modified from "Servier Medical Art" by Servier (https://smart.servier.com/) licensed under CC BY 3.0.

According to the research results of *Wurm et al*., the stealth effect is not caused by decreased protein adsorption but rather by an altered protein corona (total adsorbed proteins on the particle surface).[155] Analysis of the protein corona of the PEGylated particles revealed more than 70% of the protein corona is clusterin. After incubation with clusterin, a reduced uptake of the nanoparticles in macrophages was also observed. This suggests that the 80 kDa chaperone clusterin plays an important role in the stealth effect. In comparison to non-PEGylated particles, the lower concentration of immunostimulatory proteins on the surface of the PEGylated nanoparticles also leads to a reduced inflammatory reaction.[156] However, there were also a few hypersensitivity reactions observed against PEG and it is not biodegradable.[142, 157] Based on this occasion, it would be useful to use PEG with a small chain length to ensure at least a fast clearance. However, polyethylene glycol with a length of less than 400 Da was found to be toxic due to oxidation to dicarboxylic acids and hydroxy carboxylic acids.[158] PEG chains above 20 kDa should be avoided because they accumulate mainly in the liver due to the reduced renal elimination based on the high molecular weight.[159] Furthermore, repeated administration of PEGylated nanoparticles leads to faster renal elimination.[160] This can be explained by the ABC effect (accelerated blood clearance). After the first exposition of

particles, a portion of the activated B cells differentiate into B memory cells, which secrete specific antibodies against particles upon re-injection of particles, resulting in accelerated opsonization by the MPS.[161] Despite these negative aspects of PEGylation, the benefits outweigh the drawbacks. To compensate for the disadvantages of PEG, many synthetic polymers are currently being investigated. A potential alternative are polyamino acids such as polyglutamic acid (PGA).[162] These amino acids have the advantage that they can be degraded *in vivo* to the corresponding amino acids and result in a reduction of the ABC effect.[163, 164] However, polyamino acids show an increased complement activation.[165] Another possible alternative for PEG are polysaccharides. They provide a hydrophilic shell on the particle surface and have several advantages such as biodegradability, low immunogenicity and toxicity.[166] These polysaccharide coated NPs have extended circulation times and carry further functional groups for the conjugation of drugs and targeting ligands.[167] Good polysaccharides candidates are derivatives of chitosan,[168] dextran[136] and hyaluronic acid.[169]

Polyglycerols are biocompatible polyether polyols, prepared in branched or linear forms.[170] The stealth effect of hyperbranched polyglycerols is comparable to PEG, while they are less susceptible to oxidation than PEG.[167] In addition, polyglycerols contain a high amount of hydroxyl groups, which can be further functionalized.[171] A major drawback for Polyglycerols is the possible accumulation in tissues based on the non-biodegradability.[172]

A successful combination of the EPR and stealth effect is the approved nanoparticle preparation Doxil®. It consists of a PEGylated liposome loaded with the anthracycline doxorubicin. In comparison to free doxorubicin, PEGylated Doxil is characterized by a significant increase of the circulation time from 10 min to 74 h. In addition, Doxil has a reduced cardiac risk, as the drug accumulates up to 10 times more frequently in tumor tissue due to the EPR effect.[173]

However, the extent of the EPR effect may be inconsistent due to the heterogeneity of the tumor tissue. For a higher specific tumor accumulation and cellular uptake, a next generation of nanoparticles has been developed that allow active targeting by ligands on the surface.[174, 175]

1.2.2 Active Targeting

Passive targeting relies on the physicochemical properties of the nanoparticles and on the EPR effect, with non-receptor-mediated cell uptake being limiting.[138] Active targeting, on the other hand, is based on attached target structures on the surface of the nanoparticles against certain organs, tissues or cells. These ligands ensure specific accumulation of the nanoparticles at the target site and can thus lead to increased cell uptake by means of specific receptor-mediated endocytosis.[176] This effect can lead to improved specific drug transport through PEGylation and thus extended circulation time. The increased number of passages of the nanoparticles through the target tissue allows a longer interaction time with the target receptor.[177] Due to receptor-mediated endocytosis, nanoparticles with specific ligands should reduce systemic toxicity.[178] *Sugahara et al*. show that active targeting can also lead to deeper tumor penetration and thus to better tumor destruction.[179] This is achieved by targeting of an overexpressed tumoral receptor. The key to active targeting is the selection of the right ligand-receptor pair. A large number of ligand species have already been investigated. Among them there are vitamins,[137, 180, 181] sugars,[182] aptamers,[183] peptides,[184] and proteins.[185] Due to the high diversity, the majority of research focuses on antibody-functionalized nanoparticles for active targeting.[141]

Antibodies are attached to the surface of the nanoparticles, which facilitates binding and internalization of the nanoparticle via the Clathrin-mediated endocytosis pathway (**Chapter 1.1.1**).(92) The conjugation of antibodies to the nanoparticle surface may be by non-covalent physical or covalent interactions.[186, 187] For both routes it is necessary that the functionality of the antibody for active targeting is maintained. Typical non-covalent conjugations comprise adsorption of the antibody onto the nanoparticle surface by electrostatic attraction, Van der Waals interactions, hydrogen bonds, hydrophobic interactions or a combination of these forces. Physical adsorption has the advantage that rapid binding occurs and chemical modification steps are omitted.[188] However, the adsorption site may be located near the antigen site and thus reduce the functionality of the antibody.[189, 190] Furthermore, physical binding *in vivo* may be susceptible to competitive exchange with serum proteins.[191] This problem can be avoided by chemical conjugation of the antibody. This can be done either directly or via linker molecules.[141] In contrast to direct coupling, the linker strategy requires a further synthesis step by derivatizing the antibody, but the orientation of the antibody on the nanoparticle surface

can be better controlled.[192] Nanoparticles with active targeting have advantages over non-targeted nanoparticles such as higher accumulation in the desired tissue, increased cell uptake, higher therapeutic efficiency and lower systemic toxicity.[193] It has also been shown that targeted nanoparticles can overcome multiple drug resistance because glycoprotein membrane transporters are incapable of removing the nanoparticles when infiltrated via receptor-mediated endocytosis.[143] In addition to these advantages of active targeting, the modification of the surface of the nanoparticles can also lead to problems: the attached antibodies alter the properties of the corona of the nanoparticles. On the one hand, this can result in a change in hydrophobicity and charge and thus influence the uptake by cells.[189] On the other hand, excessive introduction of antibodies on the surface can lead to increased excretion by the MES, since the Fc part of the antibodies favors opsonization by activating the complement system.[194] A possible strategy to circumvent this problem is to conjugate only the FAB fragment instead of the entire antibody. Another solution is the use of human antibodies instead of chimeric or murine antibodies. A change in the size of the nanoparticle due to attached antibodies can also influence the properties of the nanoparticular system.[195] A successful example of active targeting is trastuzumab-functionalized nanoparticles against the HER2/neu receptor. This receptor tyrosine kinase of the EGF receptor family is overexpressed in 25–30% of invasive breast carcinomas.[196, 197] In an *in vitro* cytotoxic MTT assay a 12.74 higher IC_{50} value could be measured for paclitaxel loaded PLGA nanoparticles functionalized with trastuzumab than for paclitaxel PLGA nanoparticles without antibody functionalization. Even compared to paclitaxel without particle formation, SK-BR-3 cells showed a 13.11 times higher IC_{50} value after 24 h.[198] The research results show that active targeting is a promising approach in tumor therapy. However, most of the ligands used are directed against receptors expressed not only by the target cells but also to some extent by healthy cells. This allows for unintentional uptake by other cells. For example, the folate receptor is not only present in tumors but also in the lungs, thyroid gland and kidneys.[199] Similarly, the EGF receptor is expressed in a large number of epithelial cells.[200] Only in some types of cancer cells are both receptors simultaneously overexpressed.[201] This occasion was abused by liposomes with attached folic acid and antibodies against the EGF receptor. The liposomes showed increased selectivity for KB cancer cells compared to liposomes with only one ligand.[201] In **Figure 13** the different biodistribution of unmodified nanoparticles, PEGylated particles and PEGylated

nanoparticles with active targeting ligands is shown. The unmodified particles are fast cleared from the body. The PEGylated particles have a longer circulation time and therefore show a broader biodistribution. The combination particles with active and passive targeting have a broad biodistribution too but they accumulate preferable at the targeted site based on the interaction between overexpressed receptor and attached ligand.

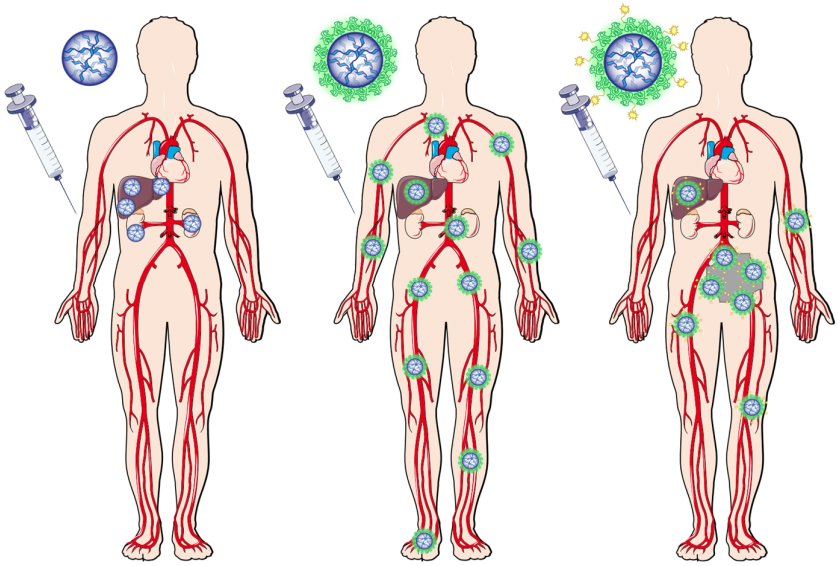

Figure 13. Difference in biodistribution between nanoparticles, PEGylated nanoparticles and PEGylated and active targeted nanoparticles. Body images modified from "Servier Medical Art" by Servier (https://smart.servier.com/) licensed under CC BY 3.0.

In summary, active and passive targeting can be combined very well. The EPR effect passively accumulates the particles in the tumor tissue and then specifically taken up into cancer cells by active targeting through receptor-mediated endocytosis. The long circulation time of the PEGylated particles also allows sufficient time for interaction between ligand and receptor. Furthermore, the PEG shell can also be used for further surface modification with the help of newly introduced functional groups. It has to be considered that on the one hand, the stealth effect allows a long circulation time for active targeting. On the other hand, the stealth effect can be reduced by the attachment of antibodies. In addition, steric hindrance from the PEG layer can also interfere with active targeting. Therefore, it is important to find the right balance between active targeting and passive targeting.[202]

Figure 14 shows an ideal combined nanoparticle with dual encapsulation, PEGylation and targeting ligands.

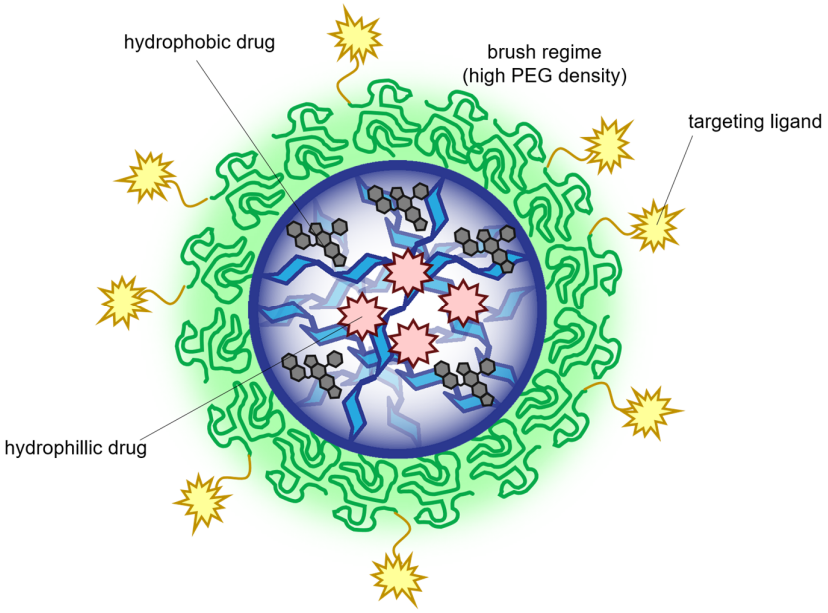

Figure 14. Combined nanoparticle with dual drug encapsulation, a stealth PEG-shell and targeting ligands.

To summarize the first two chapters, effects of size, shape, surface and targeting ligands on uptake by cells of nanoparticles are strongly correlated and all parameters must be modified equally to ensure the desired retention time and maximum drug delivery.[160]

1.3 Nanoparticles in Cancer- and Immunotherapy

1.3.1 Chronic Myeloid Leukemia Therapy

Chronic myeloid leukemia (CML) affects about one individual per 100,000 population per year and accounts for 15% of all new cases of leukemia.[203] The standard treatment of CML is imatinib characterizing in a 5 year follow up study a progression-free survival in 84% of patients.[204] In case of imatinib resistant or intolerant CML alternative therapeutic options are needed.[205] L-Asparaginase is widely used for decades in the treatment of acute lymphoblastic leukemia (ALL) and it was observed that asparaginase induces apoptosis also in chronic myeloid leukemia cells and therefore can be used for imatinib resistant cancer types.[206] The enzyme can destroy asparagine-dependent tumors by degrading circularly L-asparagine into L-aspartic acid and ammonia and therefore leads ultimately to famishing malignant cells because of their reduced L-asparagine synthetase (ASNS) level in leukemia cells.[207, 208] Etoposide is a topoisomerase II inhibitor and the resulting permanent DNA strand breaks leading to mutagenesis, chromosomal translocation, and cell death.[209] Studies by *Panosyan et al*. showed that L-asparaginase and etoposide have a synergistic effect.[210] This effect could be exploited by dual drug delivery with NPs. A codelivery of L-asparaginase and etoposide in one particle system has several advantages: First the ability to exploit the synergistic interaction by simultaneous delivering and controlled release of the drugs in a single nanoparticle carrier,[211] second improved drug solubility of the hydrophobic etoposide,[212] and third adjusted pharmacokinetics of L-asparaginase and less hypersensitive reaction against E. coli L-asparaginase are possible.[213] Further active and passive targeting of the particle system is possible (**Chapter 1.2**). As mentioned in **Chapter 1.1.2**Fehler! Verweisquelle konnte nicht gefunden werden. the SpAcDex nanoparticles represent a highly promising carrier system for the dual encapsulation of asparaginase and etoposide.

1.3.2 Immunotherapy

Cancer cells can avoid immune surveillance and exploit the immune system to grow and metastasize. This incident has encouraged the discovery of small molecules, peptides, and monoclonal antibodies to stimulate the body's own immune defense system to eradicate cancer.[214] Despite the development of these new immunotherapies, efficacy is limited due to challenges in targeted delivery and controlled release. Nanoparticle systems bear

the potential to overcome this barrier to elicit innate and adaptive immune responses to eradicate cancer cells without off-target toxicities and nonspecific immune-activation.[215, 216] This can be accomplished by either training resident immune cells to recognize and eliminate cells with tumor-associated antigens or by providing external stimuli to enhance tumor cell apoptosis in the immunosuppressive tumor microenvironment.[214] In the following, some applications for nanoparticles (in particular AcDex particles) in immunotherapy are discussed.

Delivery of Adjuvant through Nanoparticles

Oftentimes, adjuvants are required to cue a robust immune response against tumor-associated or -specific antigens.[217-220] One possible adjuvant to prime cytotoxic T-lymphocytes (CTLs) is the stimulator of interferon receptor (STING) which is a cytoplasmic adapter protein that functions as a DNA sensor.[221] The group of *Ainslie* used acetalated dextran microparticles with encapsulated STING agonist 3'3'-cyclic GMP-AMP (cGAMP) combined with soluble PAMPS. The studies revealed that a codelivery of cGAMP MPs and soluble Toll-like receptor 7/8 agonist resiquimod elicited the broadest cytokine response on primary mouse bone marrow derived dendritic cells (BMDCs).[222] In another study *Ainslie et al*. showed that incubation of RAW macrophages with vaccine adjuvants poly I:C and CpG loaded AcDex particles, led enhanced immune activity in RAW macrophages.[223]

Modulation of the Immune-suppressive TME using Nanoparticles

Tumor associated macrophages (TAM) have been known to exhibit either pro- or anti-inflammatory activities and they are implicated in tumor survival, growth, and metastasis.[224, 225] Macrophages are divided in M1 and M2 macrophages.[226, 227] Typically M1 induce immune response thereby causing the phagocytosis of tumor cells. In contrast, M2 TAMs have anti-inflammatory properties thereby stimulating immunosuppression and formation of abnormal tumor vasculature, indirectly contributing to tumor progression.[228, 229] Studies by *Zheng et al*. showed that in an invasive cancer, polarization of M1 to M2 macrophages takes place.[230] Based on this discovery, anti-tumor macrophage therapy is primarily focused either on depletion or re-programming M2 macrophages.[231, 232] Recent advances in nanotechnology show that it is possible to shift

tumor macrophages with toll-like receptor (TLR) agonists encapsulated in NPs from M2 to M1 and cure cancer in mice.[233, 234]

AcDex microparticles encapsulated with the TLR agonist imiquimod successful activated macrophages and BMDCs. After treatment with AcDex, M1 activation markers like inducible nitric oxide synthase (iNOS) and inflammatory cytokines were enhanced.[235] Overall, nanoparticles are a promising treatment approach to modulate macrophage polarization in the tumor microenvironment.[236]

Dendritic Cell Targeting

Nanoparticles can elicit cross-presentation of antigens, whereby particle associated antigens enter the cytosol of antigen presenting cells (APCs) and are processed for presentation onto major histocompatibility complexes class I (MHC-I) to stimulate antigen-specific CTL responses, and subsequent killing of antigen expressing tumor cells.[237-239] DCs as the main APC play a prominent role in the initiation of immune responses by CTL activation.[240-242] Therefore, the majority of recent nano-immunotherapy research has been dedicated towards the targeting of DCs.[2] Nanoparticle properties for delivery of antigens and adjuvants has shown promising results in DC-based immunotherapy by elevating CTL responses without eliciting undesirable immune responses when using targeting ligands.[241, 243-245] A specific targeting of DCs is desired to minimize side effects (exogenous soluble antigens are usually weakly antigenic) and enhance therapeutic efficiency.[214] A PEG-layer can support this targeting by preventing undesirable uptake by scavenger cells and therefore increasing the *in vivo* circulation time (**Chapter 1.2.1**).[241, 246] The targeting can be further advanced through precise receptor-mediated endocytosis by specialized functionalized nanoparticles (**Chapter 1.2.2**).[141] On this occasion antibodies have an outstanding selectivity and a high structural variety which leads to receptor-mediated endocytosis whereby the antigen is optimally delivered to the APCs (**Chapter 1.2.2**).[247] One potential antibody target is DEC205, a lectin-like endocytic receptor that is expressed at high levels by different DC subsets.[248, 249] A major function of this endocytic receptor is binding dying cells for uptake and cross-presentation of antigens by DCs.[250] Several studies have demonstrated that *ex vivo* targeting of mouse DCs with ovalbumin (OVA)-conjugated anti-DEC205 antibodies induces potent MHC-I cross-presentation to OVA-specific $CD8^+$ T-cells (see **Figure 15** for mechanism of $CD8^+$ T-cells activation).[247, 251-253]

A possible application for nanocarriers is the vaccination of patients suffering from malignant melanoma, an aggressive type of skin cancer.[254] This can be arranged through *in vivo* DC-targeting with encapsulated therapeutic payloads such as the tumor-specific antigen (Ag) itself or tumor antigen-encoding plasmid DNA.[255] DCs have the capacity to process internalized antigens for cross-presentation through MHC-I. By stimulating anti-tumor $CD8^+$ T-cell they are able to initiate host T-cell responses against foreign antigens and tumors.[256]

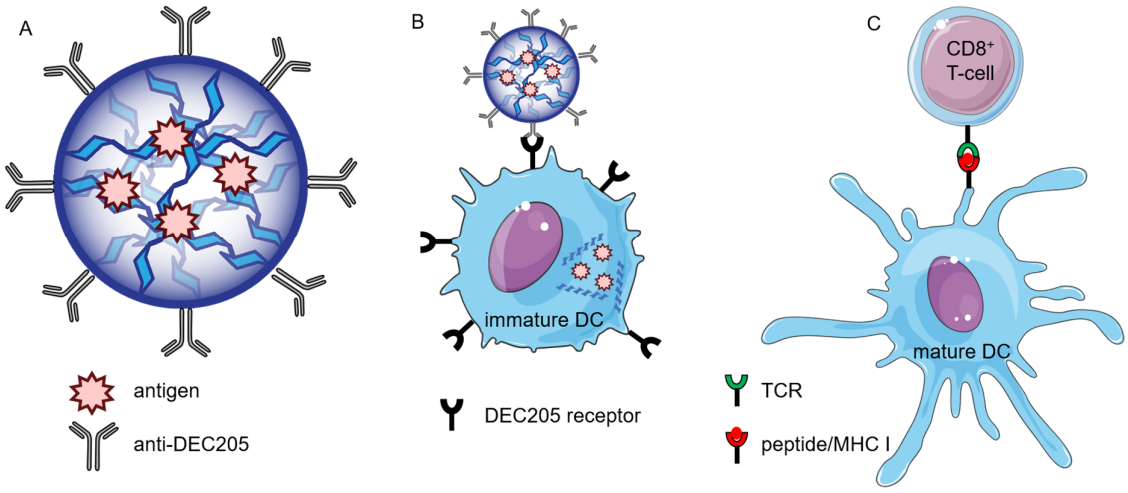

Figure 15. Schematic representation of the CTL activation by DC-targeting acid-labile NP. (a) Antigen was encapsulated in an acid labile anti-DEC205 labeled particle. (b) The particles were incorporated into DEC-205 expressing immature DC. After hydrolysis in the acid lysosomes of the DCs, the encapsulated Ag is released into the cytoplasm. (c) Intracellularly the antigen is processed, and the resulting peptides are presented on mature DC MHC-I. The recognition of the corresponding T cell receptor of $CD8^+$ T-cells in a secondary lymphatic organ leads to differentiation into CTLs. Cell and receptor images modified from "Servier Medical Art" by Servier (https://smart.servier.com/) licensed under CC BY 3.0.

Instead of DEC205, other DC target receptors can be used as well, for example DC-SIGN and CD40. They may also possess DC-activating capacity[257, 258] and polymeric nanoparticles with anti-CD40 have shown increased uptake by DCs and subsequent priming of CTLs *in vivo*.[241, 259]

AcDex particles could be used for DC-targeting as studies by *Bachelder et al.* described the encapsulation of ovalbumin (OVA) in AcDex particles. Incubation of RAW macrophages with the loaded particles led to an increased MHC-I presentation of the OVA by a factor of 16 relative to free OVA. This result indicates a possible cancer vaccination against tumors where MHC-I presentation is crucial for the activation and proliferation of $CD8^+$ T-cells.[96] Studies by *Broaders et al.* further showed that not only MHC-I but also MHC-II

presentation is enhanced by OVA-AcDex particles in BMDCs.[128] The immunostimulatory effect on DC could be increased *in vitro* and *in vivo* by co-encapsulation of a CpG DNA adjuvant[260] or through modification of the particles surface with mannose using biorthogonal click-reactions. The active targeting of the mannose-receptors on DCs with OVA-loaded mannosylated particles led to enhanced endocytosis of the AcDex particles and enhanced MHC-I antigen presentation on the cell surface compared to non-modified particles.[261]

The mentioned studies reveal that nanotechnology approaches are a potent platform for efficient *in vivo* delivery of antigens and adjuvants, and successful activation of CTL responses by targeting DCs.

1.4 Amphiphilic Polymer Conjugates

1.4.1 Amphiphilic Structures

Amphiphiles are compounds containing both hydrophilic and hydrophobic segments. Due to their amphiphilicity, they are able to self-assemble into a wide variety of structures including micelles, vesicles and bilayers. Above the critical micelle concentration (CMC) a spontaneous micelle formation occurs whereby the thermodynamically stable micelles and monomers exist in a dynamic equilibrium.[262] Important natural amphiphiles are the phospholipids whereas their polar headgroup interacts with the surrounding water molecules meanwhile the hydrophobic lipid chains tend to aggregate to minimize the contact with water and thereby increasing the free energy (**Figure 16**).

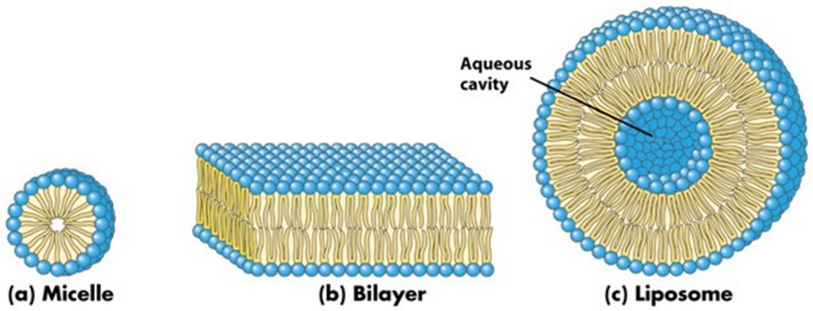

Figure 16. Various structures formed by phospholipids in aqueous solution. A micelle consists of an inner hydrophobic core, shielded from surrounding water by the hydrophilic headgroups. Two layers of phospholipids can assemble to a linear bilayer sheet. A liposome is a spherical vesicle formed of a lipid bilayer with an aqueous core (**Chapter 1.1.1**). Modified from.[263]

The structural concept of natural amphiphiles can be mimicked by block copolymers.[264, 265] Block copolymers consist of covalently linked polymers with different solubility behavior. The synthetic strategies mainly include the sequential addition of monomers via controlled polymerization techniques (*e.g.* atom transfer radical polymerization (ATRP) or ring opening polymerizations (ROP)) and coupling between active chain ends.[266-269] Based on their ambivalent architecture they are capable of self-assembly and form various nanostructures in solution.[270-272] Self assembled block-copolymer aggregates can be used for various applications such as surfactants, surface coatings and drug delivery.[273-275] Like the before mentioned polymer nanoparticles (**Chapter 1.1.1**) micelles can be vehicles for water insoluble hydrophobic drugs based on their core-shell structures.[276, 277]

For instance, a full polysaccharide amphiphilic block copolymer was prepared by *Breitenbach et al.*[278, 279] Here, the combination of an end-functionalized hydrophilic dextran block with a hydrophobic AcDex (**Chapter 1.1.2**) block results in a reduction- and pH-responsive amphiphilic structure that turns water-soluble upon acid treatment. The material has a low critical micelle concentration and self-assembles in water to spherical micellar nanoparticles. The amphiphilic polysaccharide can further stabilize the hydrophobic photosensitizer phthalocyanine zinc by hydrophobic interactions in aqueous solutions over extended time periods. A cellular uptake and photo switchable intracellular activity of the cargo upon irradiation at wavelengths in the near infrared region were shown (**Figure 17**).[278, 279]

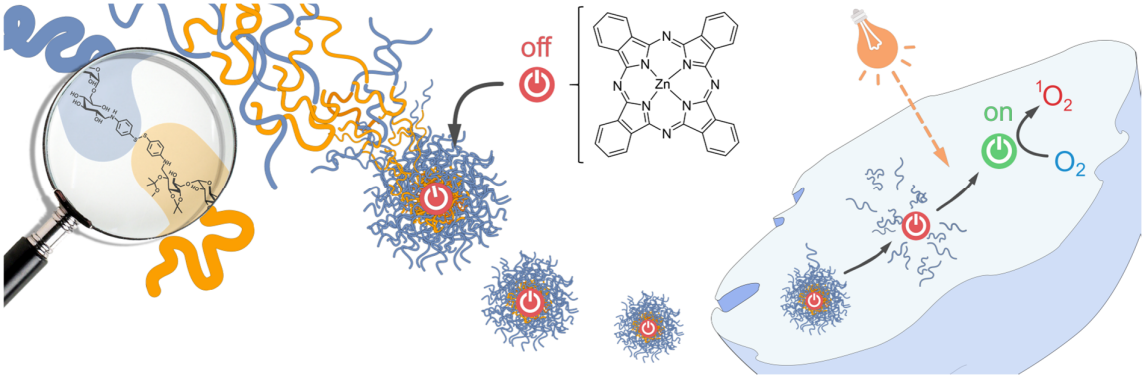

Figure 17. Reproduced with permission from *The Royal Society of Chemistry*. [279]

The drug delivery with micelles should lower a systemic leakage of the drug, reduce side-effects and should lead to an accumulation of the drug in tumors through the EPR effect (**Chapter 1.2.1**).[280, 281]

Popular methods used to encapsulate drugs in micelles include direct dissolution,[282] solvent evaporation,[283, 284] co-solvent evaporation,[285, 286] and dialysis.[287, 288] Direct dissolution is the simplest method but is only possible for highly soluble surfactants that form micelles spontaneously upon addition to water.[282] The other methods allow for dissolution of drug and polymer in an organic solvent with removal of the organic phase being accomplished by either evaporation and subsequent reconstitution with water or by slow replacement with water through a semi-permeable membrane with a molecular weight cutoff below that of the surfactant unimers.[287, 288] Co-solvent evaporation involves the addition of drug and surfactant to a mixture of organic solvent and water,

where the organic solvent is then removed to leave behind surfactant micelles in water. This method is particularly effective for high molecular weight core-forming blocks that do not re-constitute with water easily.[281]

Other commonly used hydrophobic polymers used are poly(amides), poly(lactide), poly(ε-caprolactone) poly(glycolide) and poly(styrene).[289-291] For the hydrophilic counterpart, poly(ethylene glycol) or polyglycerol is typically used.[265, 292] Dextran (and AcDex, respectively) as a natural polymer has several advantages over the most mentioned polymers because of their low toxicity, low immunogenicity, high biodegradability and can be easily chemical modified.

1.4.2 Protein-Polymer Conjugates

Proteins are one of the most impressive (bio)polymers. They can efficiently catalyze (bio)chemical reactions in a selectivity manner; they are strong and tough materials and have an incredible diversity of structure and function.[293, 294] Combining proteins with the stability and chemical diversity of synthetic or natural polymers can lead to hybrid materials with new advantageous functions of both components.[295] The new material has the potential to overcome the application limitations of enzymes due to temperature, pH, organic solvents, and biodegradation sensitivity. The polymer segment can further increase the stability, enzymatic activity and can add the ability to self-assembly like block copolymer (**Chapter 1.4.1**).[295-298] The most famous protein modification is the PEGylation which leads to favorable protein pharmacokinetics and stability.[299, 300] The modification even makes nanoparticle formation by an emulsion-based method possible.[52]

Conjugation Strategies

The goal of obtaining a well-defined linkage can be achieved by choosing a bioconjugation reaction that achieves site-specific modification in a high yield. The choice of the right bioconjugation reactions is limited by reactions in aqueous solution, near neutral pH, and in the presence of a wide array of other of side chain functional groups.[295]

A number of different bioconjugation reactions have emerged that target different amino acids on the protein surface (**Figure 18**). Alternately the protein structure can be

alternated to achieve specific functional groups on the surface, however these modifications can change the protein structure and function.

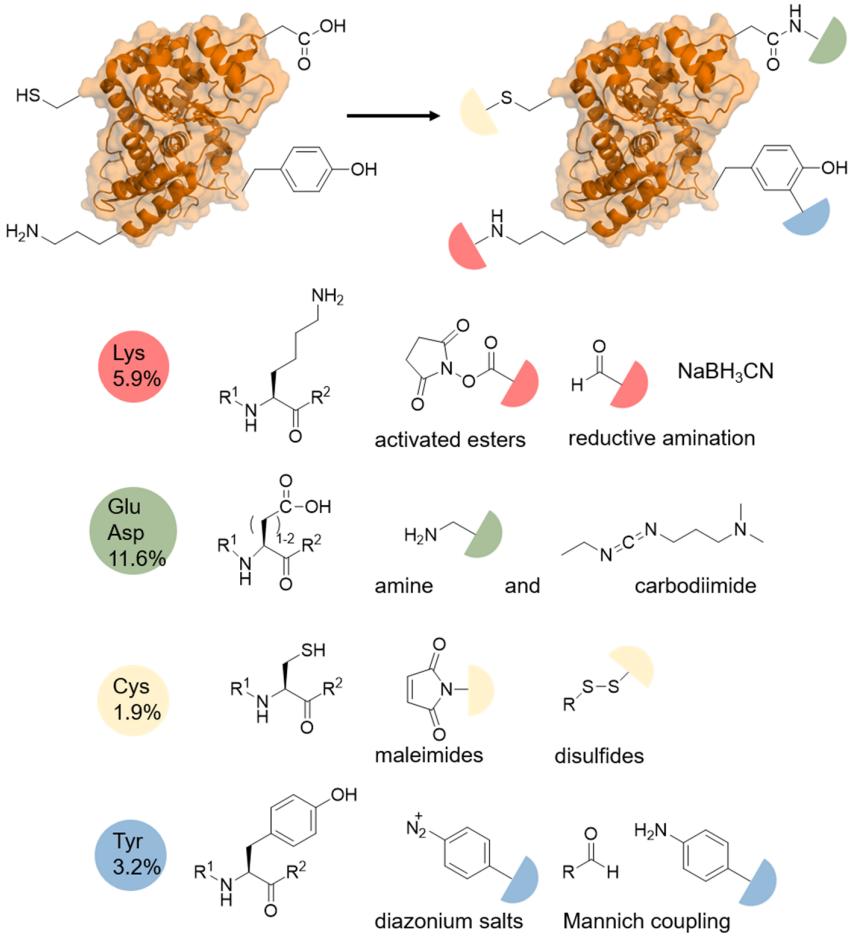

Figure 18. Bioconjugation methods for the modification of native amino acids with polymers. Adapted and modified from *ACS Macro Letters*.[294]

The modification of lysine by NHS-ester or reductive amination is quite well-known and often used. Aspartate and glutamate are typical modified by amines via carbodiimide reaction. Lysine, aspartate and glutamate are quite present (5.9%; 11.6%) on the protein surface therefore these amino acids are typically modified for a high amount of conjugated polymer instead of site-selectivity.

Based on the low presence the nucleophilic side chain of cysteine can be targeted for a more site-specific bioconjugation by thiol-Michael addition reactions or by disulfide exchange reaction.[301] Probably the most employed thiol-based conjugation method is the

thiol-Michael addition.[302] Typical Michael acceptors in thiol-Michael addition reactions are electron-deficient enes such as acrylates, methacrylates, vinyl sulfones, and maleimide. The structure of the activated ene plays an important role in the kinetic profile of the reaction. Typically, the more electron-deficient the C=C bond ,the more susceptible it is to a Michael addition reaction.[303] The reactivity of commonly used vinyl groups is shown in **Figure 19**.

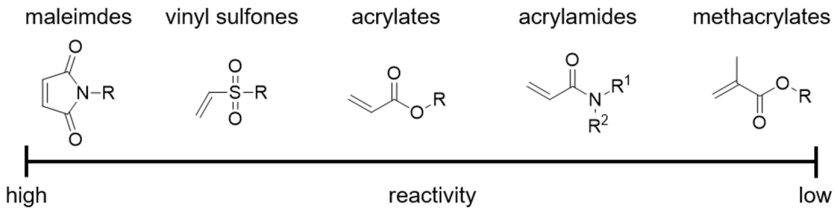

Figure 19. Reactivity of commonly utilized vinyl groups in thiol-Michael addition reactions. Adapted and modified from *Chemistry of Materials*.(301)

Based on the high reactivity of maleimides the nucleophilic addition with the cysteine residue can be done selectively with mild reaction conditions (pH range 6.5–7.5, room temperature) which is favorable for the protein structure and function preservation.[304] Studies by *Li et al*. showed maleimide-terminated poly(N-isopropylacrylamide) (PNIPAM) temperature-responsive polymers were covalently conjugated to albumin by two Michael addition thiol–ene reactions. The thermo-responsive nature of PNIPAM was conferred to the protein-polymer conjugate, as demonstrated by formation of intermolecular aggregates at elevated temperatures.[305] Studies by *Johnson et al*. revealed that maleimide thiol reaction can be used to connect N-(2-hydroxypropyl)-methacrylamide (HPMA) copolymers with FAB´ fragments of CD20 antibodies. The multivalent product had the strongest apoptotic activity against cancer B-cells with CD20 overexpression whereas cells without overexpression were not harmed.[306]

Alternatively, activated polymers with pyridyl, alkoxycarbonyl and o-nitrophenyl disulfide end-groups form protein–polymer conjugates via disulfide formation. Pyridyl disulfide is hereby the most prominent way for disulfide formation. The driving force for the reaction is the stable yellow leaving group pyridine-2-thione which allows easy monitoring of the rate of the reaction.[307] One appeal of this approach is that the bond is reversible, and the protein can be released from the polymer under reducing conditions.[304] The stimuli-responsiveness enhance a conjugate's versatility across

applications in biological and pharmacological areas and allow a targeted release of therapeutic molecules (**Chapter 1.1.1**).[308]

For proteins with no or a low number of thiols a unique cysteine can be introduced, that can be modified site-selectively to create a well-defined bioconjugate. Those artificial thiols can be added for example by modification of lysine with *N*-succinimidyl *S*-acetylthioacetate (SATA), *N*-succinimidyl-*S*-acetylthiopropionate (SATP) or site-directed mutagenesis.

The amino acid tyrosine can be modified with electrophilic reagents via azo coupling with diazonium salts or Mannich-type coupling.[309, 310]

Another strategy for site-selective modification of proteins relies on the N-terminus. There are more generally applicable procedures such as pyridoxal-5′-phosphate transamination mediated and others that require a specific amino acid at the N-terminus.[295, 311]

Shu et al. explored coiled-coil helix bundle forming peptides in which hydrophobic polystyrene (1,000 g·mol^{-1}) was conjugated onto the N-terminus. These conjugates were able to form micelles of 10 nm in diameter in the presence of surfactant.[312]

Recent work on bioconjugation reactions has developed two alternative approaches the use of artificial amino acids or the introduction of artificial functionality to proteins to enable the use of cycloaddition “click” reactions, for site-selectively modified proteins.[313, 314]

Independently of the conjugation chemistry, the formation of covalent polymer biomolecule hybrids can be accomplished by grafting a polymer “from” or “to” a protein (**Figure 20**).

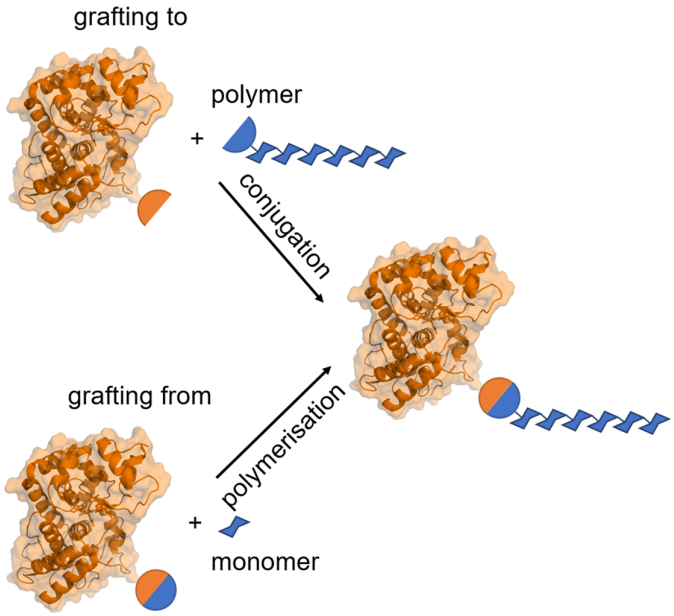

Figure 20. "Grafting To" and "Grafting from From" approaches.

"Grafting To" Method

Grafting To refers to the conjugation approach in which a preformed polymer with a reactive chain-end is directly conjugated to a suitably reactive protein.[315] In contrast to other conjugation methods, it provides a simple characterization and synthesis of the polymer and the protein remains unaffected by the harsh polymerization methods. However, high molecular weight polymers may inhibit effective conjugation, and purification after conjugation can be challenging.[316]

"Grafting From" Method

Grafting From refers to the conjugation approach in which a small molecule initiator is attached to the biomolecule and subsequently grows a polymer directly from the protein in the presence of monomers.[315] Similarly to the earlier discussed techniques, grafting from can be designed for site-specific or random attachment. When compared to the grafting to method, grafting-from provides a simple purification after conjugation and higher grafting density. However, this method may lead to protein denaturation based on the polymerization method used and often to polymers with a high polydispersity because of suboptimal polymerization conditions needed to maintain the protein structure and function.[316] Typically used polymerization techniques are atom transfer radical polymerization (ATRP) or reversible addition–fragmentation chain transfer (RAFT).[317]

Regardless of the selected method, appropriate purification steps must be performed. The purification of protein–polymer conjugates requires removal of unreacted polymer (grafting to) or monomer (grafting from) and unmodified protein. The selected purification strategy must be protein compatible such as affinity chromatography, size exclusion chromatography, precipitation or dialysis.[318]

Giant Amphiphiles

Giant amphiphiles are compounds composed of an enzyme or protein as the polar headgroup and a hydrophobic polymeric tail attached.[319] In aqueous media they are able to form self-assembled aggregate structures similar to those formed by conventional amphiphilic block copolymers (**Chapter 1.4.1**).[312] The particle formation enables a broad range of applications in bio- and nanotechnology. It can help to enhance the circulation time of the therapeutic enzyme by less proteolytic degradation and it is possible to encapsulated drugs in aqueous media.[320] Further, stimuli-responsiveness can be introduced (**Chapter 1.1.1**). Photo-sensitive polymers have been used as a molecular on/off switch, which regulates enzyme activity by controlling the accessibility of the active site of an enzyme.[321] Other stimuli-responsiveness for example pH or reductive can lead to a disassembly of the particle and therefore drug release.

Stenzel and coworkers established the preparation of albumin-based giant amphiphiles via one pot strategy. [322] Albumin (66.5 kDa) is the most abundant plasma protein and has the capacity to adsorb and transport hydrophobic molecules. The protein's surface is characterized by a single cysteine permitting site selective attachment of a polymer chain.[322] The cysteine was conjugated to a maleimide-terminated poly(methyl methacrylate) (5,400 $g \cdot mol^{-1}$) which has been prepared via a reversible addition fragmentation chain transfer (RAFT) polymerization.[323] Curcumin was added to the reaction mix of the polymer and albumin. With the formation of the conjugate, self-assembly into micelles occurred, accomplished by the entrapment of the hydrophobic model drug curcumin into the hydrophobic polymeric segments. The main challenge for the particle formation is the slow addition of the albumin solution in phosphate-buffered saline (PBS) buffer to the polymer solution in dimethyl sulfoxide (DMSO). Increasing amounts of water in the DMSO solution can lead to the precipitation of polymer while the presence of DMSO causes the protein to precipitate. After dialysis against water albumin-

coated PMMA nanoparticles where obtained which had a high selectivity towards cancerous cells (see **Figure 21**).[323]

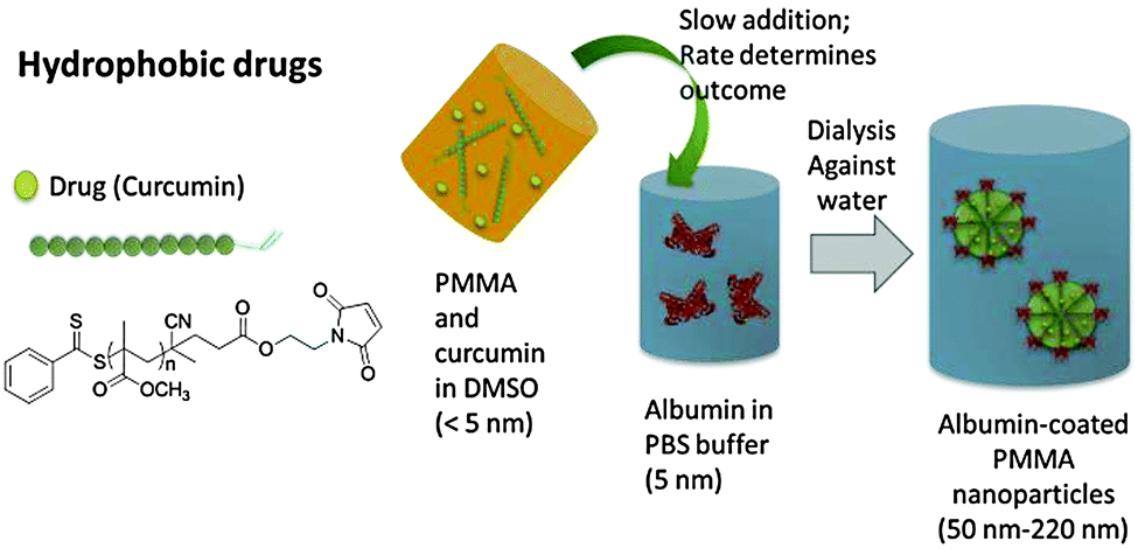

Figure 21. One pot synthesis of albumin coated PMMA nanoparticles with encapsulated curcumin. Reproduced from *Chemical Communications*.[323]

Boerakker et al. investigated the synthesis of an enzyme-polymer conjugate by coupling of a hydrophobic polystyrene (9,458 g·mol^{-1}) to horseradish peroxidase (HRP) through cofactor reconstitution.[324] They selected the redox enzyme HRP as the biological component because it contains a cofactor (ferriprotoporphyrin IX) that can be easily modified with hydrophobic chains on its carboxylic acid functional groups. The resulting giant amphiphile retained still some catalytic activity and formed vesicles (80–400 nm) in aqueous media (**Figure 22**).[324]

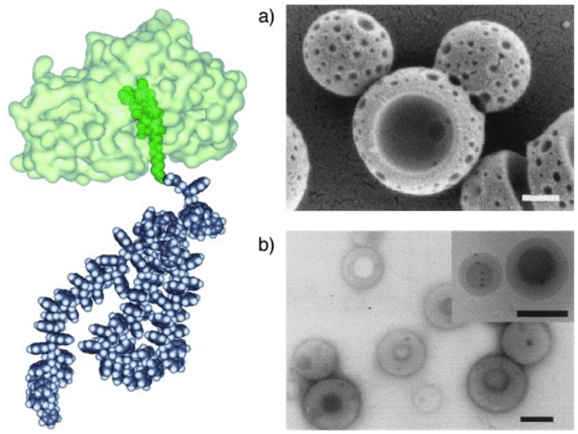

Figure 22. Computer-generated model of the HRP-polystyrene-based giant amphiphile (left). a) SEM micrograph of aggregates formed in aqueous solution; b) TEM images of aggregates of complexes formed in aqueous solution. Reproduced from *Angewandte Chemie International Edition*. [324]

2 Motivation and Aim of the Work

As described in **Chapter 1.1.1**, polymer nanoparticles represent a promising delivery vehicle for high potent drugs. Nanoparticles can protect the encapsulated drug from degradation and alter the pharmacokinetics which leads to a distinct and safe transport of the drug. Moreover, nanoparticles can prevent or reduce unwanted side effects due to specific delivery of the drug to target cells or organs. One goal of this work should comprise the further modification and application of the biocompatible and biodegradable acetalated dextran (AcDex) particle system. It was initially established by the *Fréchet* group and should be in this work further developed for 3 selected advanced delivery applications.[96]

Dual Encapsulation of Asp and Eto in SpAcDex Particles

One improvement could be a dual encapsulation of a hydrophobic and hydrophilic drug with a synergistic effect in one double emulsion technique. A possible combination could be L-asparaginase and etoposide (**Chapter 1.3.1**) for the treatment of CML. Investigations of the release profile of both drugs could give insight of the particle system. Further *in vitro* studies could demonstrate the therapeutic potential of this particles system with dual encapsulation.

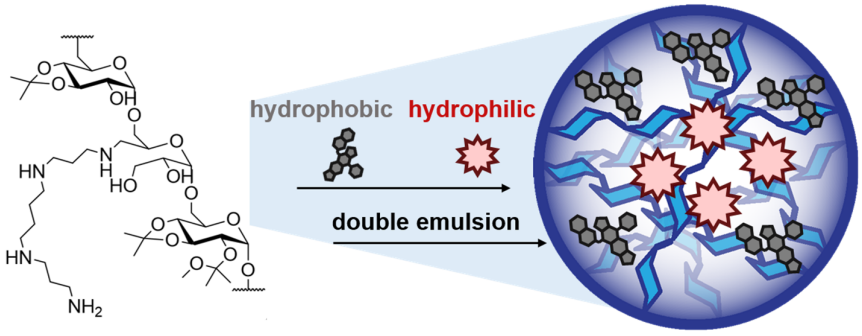

Figure 23. Dual encapsulation of a hydrophilic and hydrophobic drug in spermine-functionalized acetalated dextran nanoparticle with one double emulsion method.

Antibody-functionalized SpAcDex Particles for DC Targeting

DCs are the most effective APCs and a major key player in inducing antigen-specific T-cell immune responses.(320) Their specific targeting *in vivo* is still one of the key challenges in developing DC-based nanovaccines for cancer immunotherapy.(321) Since non-modified

dextran particles show a high unspecific uptake in several cell lines (**Chapter 1.2.2**) the particles have to be modified to exploit passive and active targeting for an immunotherapeutic DC-targeting approach. Here a targeting strategy should be developed which include a PEG-layer to maintain a long circulation time (**Chapter 1.2.1**) and attached DEC205 antibodies on the PEG-layer to receive a specific receptor mediated uptake in DCs *in vivo* (**Figure 24**). This could lead with antigen-loaded particles to a $CD8^+$ T-cell activation.

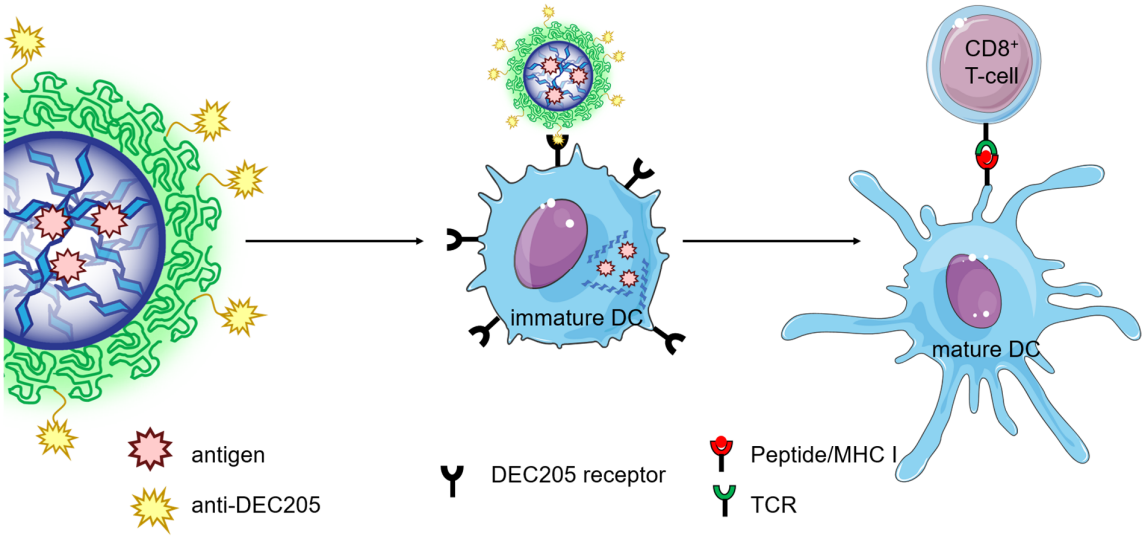

Figure 24. Schematic representation of the $CD8^+$ T-cell activation by DC-targeting with antibody functionalized and PEGylated SpAcDex NP. Cell and receptor images modified from "Servier Medical Art" by Servier (https://smart.servier.com/) licensed under CC BY 3.0.

Self-Assembled Dual-responsive HRP-AcDex Conjugates

The third project will focus on the emerging field of amphiphilic macromolecules for drug delivery applications. For this the combination of a protein with a polysaccharide by a "grafting to" strategy should result in a new hybrid material with outstanding biodegradability, biocompatibility and low immunogenicity. If the conjugate has an amphiphilic character, based on different solubility behaviors of the used biomacromolecules, it should show self-assembly properties leading to nanoparticle formation and drug encapsulation. It was the aim to conjugate hydrophobic thiol-end group activated AcDex chains with a thiol-modified horseradish peroxidase (HRP) by forming a reductive labile disulfide bond. Together with the pH-responsiveness of the AcDex chains the conjugate material should behave double stimuli-responsive. Therefore, inducing a controlled degradation of the particles and drug release by pH and redox

changes. The formed particle could be used as a nanocarrier for indole-3-acetic acid (IAA). A delivery of IAA has the advantage that a nontoxic prodrug is transported which is only toxified after release and oxidation by means of HRP.[325] The morphology of the self-assembled particles and their degradation induced by different stimuli could then be studied in detail. With the encapsulation of IAA, it should be explored whether the amphiphilic particle can successfully deliver, release and oxidize the prodrug in the cytosol of HeLa cells (**Figure 25**).

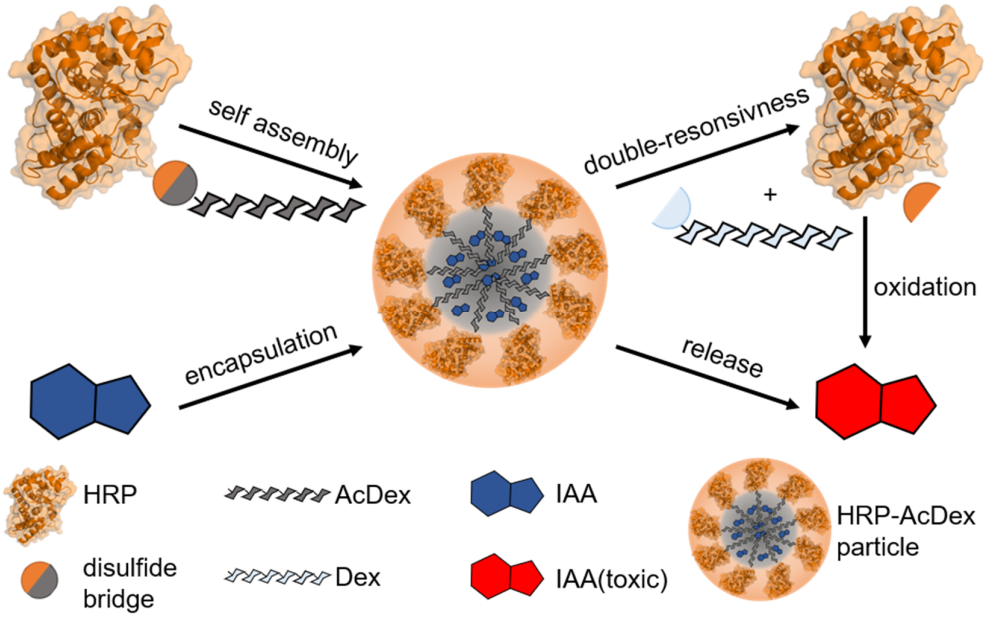

Figure 25. Self-assembly of HRP-AcDex particles with encapsulation of IAA. After stimuli-responsive particle degradation the prodrug IAA should be released and oxidizied.

3 Results and Discussion

3.1 Dual Encapsulation of Hydrophilic and Hydrophobic Drugs in Dextran Nanoparticles

As seen in **Chapter 1.1.2**, SpAcDex is a great starting material for the preparation of biopolymer nanoparticles, which can be used as drug carriers in the medical field. A dual encapsulation of L-asparaginase (Asp) and etoposide (Eto) inside SpAcDex particles could be utilized as a potential treatment in CML based on their synergistic effect (**Chapter 1.3.1**) and controlled release. For this both drugs should be encapsulated in one preparation step without losing drug encapsulation efficiency.

In this chapter, the partial oxidation, acetalation as well as reductive amination of dextran are described. The obtained SpAcDex is soluble in DCM which enables a particle preparation by double emulsion technique whereby the hydrophobic and hydrophilic drugs can be encapsulated. The quantification and the pH dependent release of both drugs are further described. Lastly, the intracellular uptake and the cytotoxicity in K562 CML cells *in vitro* are shown.

3.1.1 General Aspects of SpAcDex Nanoparticle Preparation

Synthesis of Spermine-functionalized Acetalated Dextran

Dextran was partially oxidized to introduce aldehyde functional groups besides the naturally occurring hydroxyl groups for further chemical modifications. *Cohen et al.* described the synthesis of partially oxidized dextran (Ox-Dex) with sodium (meta)periodate for 5 h.[88] Resulting in an aldehyde content of 10.3 ± 0.01 mol functions per 100 mol AGU. The specific method to maintain a solubility switch from hydrophilic to hydrophobic dextran is described by *Bachelder et al.*[96] Therefore, the dextran was dissolved in DMSO and 2-methoxypropene was added under acidic catalysis with pyridinium *p*-toluene sulfonate (PPTS) to form acetals using the hydroxyl groups of Ox-Dex. Ox-Dex was incubated with 2-methoxypropene for 10 min followed by quenching of the acetalation reaction with triethylamine (TEA). The short reaction time leads to less cyclic than acyclic acetals and therefore to a quite fast pH-sensitive degradation of the AcDex (**Chapter 1.1.2**). The isolated product contains 73.73% acetals, whereas 27.27% are cyclic and 46.6% are acyclic acetals (calculation **Chapter 5.3.1**).

The introduced aldehydes can be used to react with primary amines in the formation of imines. While these imine bonds can easily be hydrolyzed by acids, the reductive amination to an amine bond results in a stable product. Here, the polyamine spermine was used for the further functionalization of Ox-AcDex. The cationic spermine can help to increase the surface charge of the particle which enhances the cellular uptake and decreases the aggregation (**Chapter 1.1.1**). Furthermore, the remaining primary amine of the attached spermine can be used for further chemical modifications, *e.g.* using NHS (*N*-hydroxysuccinimide) chemistry to attach fluorescent dyes, PEGylation or targeting ligands. The amine functionalization helps as well to escape the endolysosomal network by the proton sponge effect (**Chapter 1.1.1**). The Ox-AcDex was dissolved in DMSO and incubated with spermine overnight to form imine bonds with the aldehydes of the modified dextran. Afterwards, sodium borohydride was added to reduce the imine bond to form more stable amine bonds. The degree of spermine functionalization results in 3.62 mol spermine per 100 mol AGU (**Chapter 5.3.1**).

3.1.2 Dual Encapsulation of L-Asparaginase and Etoposide in SpAcDex NP

After the successful functionalization of the dextran with acetals, the formation of particles is possible based on the solubility switch. In recent studies SpAcDex nanoparticles were shown to be a highly potent drug delivery platform (**Chapter 1.1.2**). Here we use this system to form co-encapsulated NPs with the synergistic drug combination of hydrophilic L-asparaginase (Asp) and hydrophobic etoposide (Eto) using a water-in-oil-in-water double emulsion method. For this the hydrophobic drug was dissolved with SpAcDex in DCM and the hydrophilic drug was added in PBS before the first sonication step (**Figure 26**). Afterwards, poly(vinyl alcohol) (3% PVA in PBS) was added as surfactant and a secondary emulsion was prepared by further sonication of the sample. The milky double emulsion was stirred overnight to evaporate all DCM. A particle solution was obtained the next day and the PVA was removed by ultracentrifugation with dd-H_2O pH 8 followed by lyophilization with PVA (0.3% in dd-H_2O pH 8) as cryoprotectant.

The control particles with only Asp encapsulated where prepared by the same double emulsion technique, whereas the empty and only Eto-encapsulated SpAcDex particles were prepared by a single emulsion technique.

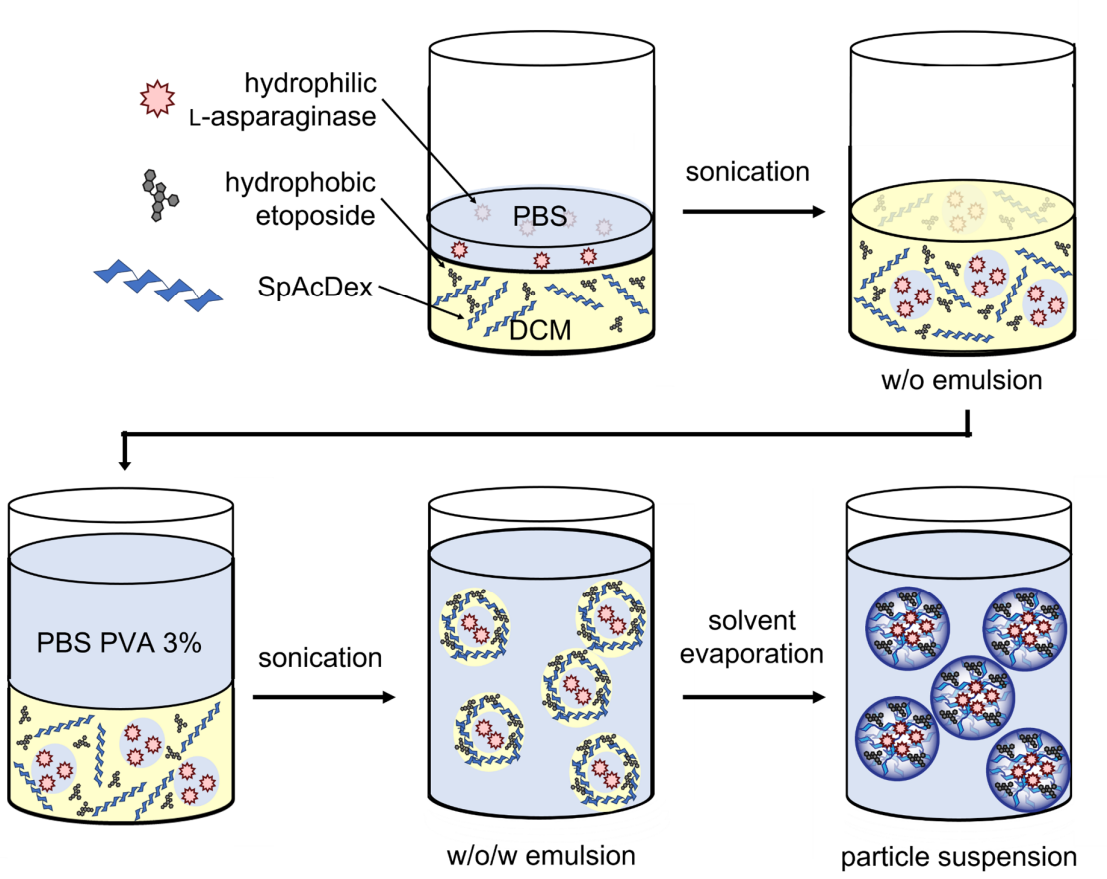

Figure 26. Dual-loaded nanoparticles preparation by double emulsion solvent evaporation method. The SpAcDex was dissolved next to etoposide in DCM and L-asparaginase in the aqueous PBS buffer phase. After the first sonication step an aqueous solution of PVA was added and a second emulsion (w/o/w) is obtained. Dual-loaded particles can be isolated by centrifugation after evaporation of the solvent.

Determination of the Nanoparticle Size and Zeta Potential

The size of the particles after purification and lyophilization was measured by Nanoparticle Tracking analysis (NTA). Therefore, particles were resuspended and diluted in H_2O pH 8 and treated thoroughly by sonication and vortexing to obtain a homogenous particle suspension without aggregates. The results of the NTA measurement are shown in **Table 1**. Mean size is calculated based on the sizes of all particles detected in the NTA measurement. Mode values describe the average size of the main particle population. The aggregation behavior can be interpreted using the standard deviation (SD) value. Particles with a mean size of approx. 194–209 nm and with a mode of 167–185 nm were obtained. With particle in the same size range it can be concluded that the dual drug encapsulation by double emulsion technique had no significant influence on the particle size compared to empty or single drug-loaded particles.

The particle surface charge has a high impact on the particle behavior *in vivo* (**Chapter 1.1.1**). Due to the negatively charged cell membrane, cationic particles probably have a higher affinity to interact with the cell membrane than negatively charged particles. This affinity can then lead to enhanced particle uptake in cells. Hence the zeta potential was measured in a HEPES buffer pH 7.4 (25 mM). The zeta potential of empty particles has a value of 11.51 mV due to exposed protonated spermine molecules on the particle surface. Based on non-covalent binding of some drugs on the particle surface the zeta potential is slightly altered for particles with encapsulated drugs (8.6–10.8 mV). The size and zeta potential of empty SpAcDex NP, SpAcDex(Asp) NP, SpAcDex(Eto) NP and SpAcDex(Asp+Eto) NP are shown in **Table 1**.

Table 1. The size and zeta potential of empty SpAcDex NP, SpAcDex(Asp) NP, SpAcDex(Eto) NP and SpAcDex(Asp+Eto) NP.

particle type	particle size measured by NTA			zeta potential in mV
	mean in d.nm	mode in d.nm	SD in d.nm	
empty SpAcDex	196.2 ± 5.7	171.2 ± 1.1	61.2 ± 6.6	11.51 ± 0.51
SpAcDex(Asp)	208.6 ± 2.8	185.3 ± 4.6	73.1 ± 8.1	9.89 ± 0.64
SpAcDex(Eto)	193.8 ± 2.6	167.3 ± 3.6	60.6 ± 1.3	10.83 ± 0.40
SpAcDex(Asp+Eto)	194.5 ± 5.8	172.3 ± 5.3	69.5 ± 1.7	8.61 ± 0.49

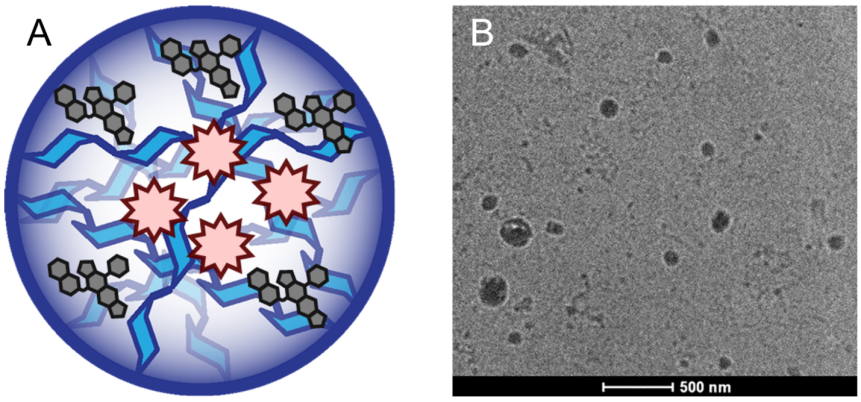

Figure 27. Characterization of the SpAcDex nanoparticles: (A) Schematic representation of dual-loaded SpAcDex(Asp+Eto) nanoparticles (Asp in red located in the hydrophilic core, blue SpAcDex particle material and Eto in grey entangled in the dextran particle backbone). Hints for this particle structure will be discussed in **Chapter 3.1.3**. (B) Representative TEM images of the structural morphology of dual-loaded SpAcDex(Asp+Eto) (1 mg·mL^{-1} in H_2O pH 8).

In **Figure 27** a schematic imagination of a dual drug-loaded SpAcDex particle and representative TEM image of recorded by [redacted] is shown and indicates solid filled spheres.

In conclusion the particle preparation of dual-loaded SpAcDex nanoparticles seems not to alter the size and zeta potential of the particles. In the next step it has to be validated if the content of dual-loaded Asp and Eto is comparable to the single-loaded drugs.

Quantification of L-Asparaginase

For the quantification of enzymatical active entrapped L-asparaginase SpAcDex(Asp) NPs, SpAcDex(Asp+Eto) NPs and empty SpAcDex NPs were incubated in NaOAc buffer at pH 5 for 48 h in a concentration of 2 mg·mL^{-1} to obtain pH-responsive released payload. The L-asparaginase assay to determine the enzymatic activity of the released Asp was based on the reaction of L-asparagine with L-asparaginase into L-aspartate and ammonium ion (**Figure 28**)and performed with the acidic particle/payload solution.

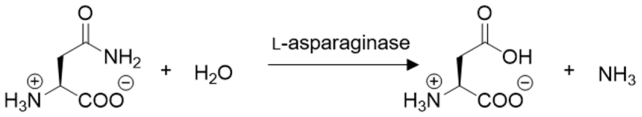

Figure 28. Reaction of L-asparagine with L-asparaginase into L-aspartate

The produced ammonium ions were then quantified with Nessler's reagent and the encapsulated Asp activity was calculated in contrast to an Asp standard with the same reaction conditions (**Figure 64**). To evaluate the encapsulation efficiency of the dual encapsulation method, the Asp content of single- and dual-loaded Asp particles were tested and compared. The results for dissolved Asp particle and Asp+Eto combination particles are with 1.14 μg per mg NP the same.

In addition to the L-asparaginase activity assay an encapsulation quantification of dissolved particles by Bradford assay is possible (**Figure 63**). The resulting absorbance shift of the dye Coomassie Brilliant Blue G-250 was calculated resulting in 3.38 μg pro mg single-loaded Asp NPs and or 3.34 μg per mg NP for dual-loaded NPs. This outcome indicates that only about a third of the encapsulated asparaginase is still active after particle formation. Maybe some Asp denatures by the DCM addition and the following first sonication step.

The encapsulation performance can be estimated by the encapsulation efficiency (EE) or loading capacity (LC) (see eq. 1 and 2).

$$EE\ (mol\%) = \frac{n_{drug,encapsulated}}{n_{drug,feed}} \cdot 100\% \qquad \text{eq. 1}$$

$$LC\ (weight\%) = \frac{m_{drug,encapsulated}}{m_{drug,encapsulated} + m_{PEGylated\ protein}} \cdot 100\% \qquad \text{eq. 2}$$

The encapsulation efficiency (EE) is with ca. 33% higher than studies by *Blackman et al*. with polymersomes (9% EE)[326], *Baran et al*. (poly(3-hydroxybutyrate-co-3-hydroxyvalerate nanocapsules with 23.7% EE)[327] and *Apolinário et al*. (5-25% EE for polymersomes).[328] The EE is further similar to PLG particles with single-loaded Asp.[329] The high EE of the SpAcDex particle system compared to other particle types compensates the only 34% of active encapsulated Asp.

The results of both Asp quantifications is summarized in **Table 2** and shows no significant difference between the content of Asp in single(Asp)- and dual(Asp+Eto)-loaded particles.

Table 2. Asparaginase encapsulation quantification

particle type	asparaginase activity in $\mu g \cdot mg^{-1}$ NP	EE in %	Bradford assay in $\mu g \cdot mg^{-1}$ NP	EE in %
SpAcDex(Asp) NP	1.14	11.4	3.38	33.8
SpAcDex(Asp+Eto) NP	1.14	11.4	3.34	33.4

Quantification of Etoposide

The etoposide quantification was performed with dissolved SpAcDex(Eto) and SpAcDex(Asp+Eto) particles in DMSO (0.5 $mg \cdot mL^{-1}$). The particle solution in DMSO was analyzed by UV-absorption and mass spectroscopy via HPLC-MS (**Figure 62**). The results are shown in **Table 3**.

Table 3. Etoposide encapsulation quantification

particle type	etoposide in $\mu g \cdot mg^{-1}$ NP	EE in %
SpAcDex(Eto) NP	7.95	8.0
SpAcDex(Asp+Eto) NP	8.06	8.1

The results for the etoposide amount inside the particle demonstrate that there is no difference between the content of single-loaded etoposide and dual-loaded etoposide. The EE and the drug loading with etoposide are lower compared to other recent etoposide-loaded particle studies.[330-332] The etoposide content was not further enhanced to visualize the synergistic effect of the particle system at a low drug dose of the high cytotoxic etoposide. With a higher etoposide content, the toxicity will be mostly dependent on etoposide without exploiting the synergistic effect within L-asparaginase and etoposide.

The dual EE for the hydrophobic and the hydrophilic drug in one particle system is higher than the studies by *Jioungou et al*. (chitosan/cyclodextrin nanoparticles; 2.48 ± 0.07% methotrexate and 2.64 ± 0.18% calcium folinate)[333] and *Niwa et al.* (PLGA nanoparticles with 5.85% indomethacin, and 2.65% 5-floururacil)[334] Meanwhile the dual EE was lower than *Español et al*. (PLGA nanoparticles; 67.7 ± 3% for dexamethasone and 54.2 ± 2% for diclofenac sodium)[335] and *Song et al*. (PLGA nanoparticles; 92.84 ± 3.4% for vincristine sulfate and 32.66 ± 2.9% for quercetin).[336] In summary, it can be said that the EE of the SpAcDex(Asp+Eto) is comparable to other studies with dual-loaded particles.
Combining the encapsulation quantifications for Asp and Eto together with the physicochemical parameter, it can be concluded that the NP preparation for both drugs in one double emulsion technique was successful and did not alter nanoparticle properties. In the following chapter the pH-dependent release of both drugs will be investigated.

3.1.3 pH-dependent Release of Asp and Eto

Release of L-Asparaginase

As described in **Chapter 1.1.2** the acetals of the SpAcDex material are hydrolyzed at low pH leading to a water-soluble particle material. As a result, the particles degrade, and the payload liberates. Hence, the release of enzymatic active L-asparaginase was carried out at pH 5 (control pH 7.4) and 37 °C to imitate the cellular lysosome environment with the same activity assay as mentioned before (**Chapter 3.1.2**). With increasing incubation time in the pH 5 buffer, the amount of released Asp increases and therefore also the measurable L-asparaginase activity based on more produced ammonium ions. The results of the L-asparaginase assay at different incubation times are shown in **Figure 29**.

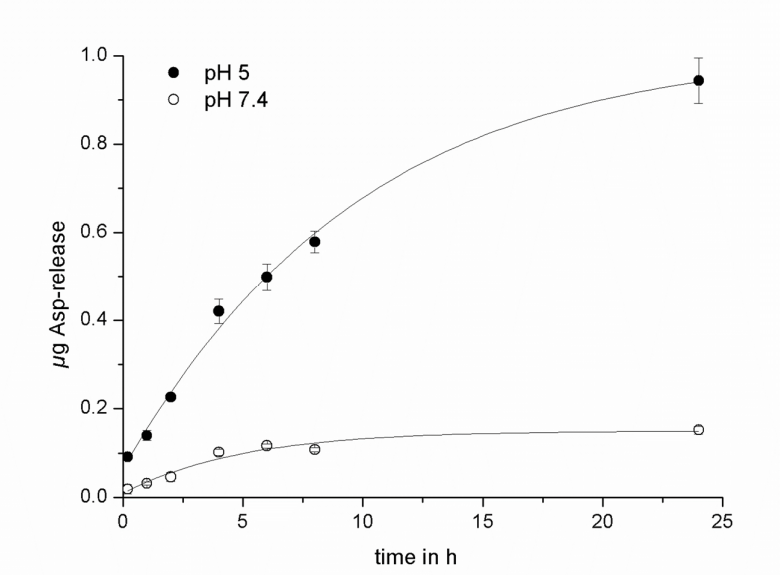

Figure 29. Release of encapsulated Asp at a pH 5 (black circles) and 7.4 (white circles) after different incubation times (0.2 h, 1 h, 2 h, 4 h, 6 h, 8 h, 24 h) at 37 °C as determined through quantification of enzymatic produced ammonium-ions through Nessler`s reagent. Data represent the mean ± standard deviation of triplicate measurements (triplet from triplets).

Until an incubation time of 8 h the release of Asp shows a linear behavior. Afterwards the slope decreases and at 24 h ca. 82% of the encapsulated Asp was released. The control particles with an incubation at pH value of 7.4 shows meanwhile a much lower enzymatic Asp-activity. Here only around 10% of the drug was released after 24 h. The results suggest that the particles could be stable in the blood stream at neutral pH but indicates a fast particle degradation und drug release of the hydrophilic drug after entering the endolyosomal network (**Chapter 1.1.1**).

Release of Etoposide

The release of etoposide was carried out similar to the Asp release at pH 5 and pH 7.4 at 37 °C. The result of the HPLC/MS quantification (like in **Chapter 3.1.2**) after 1 h, 2 h, 4 h, 6 h, and 8 h of acidic acetal hydrolysis are shown in **Figure 30**. The non-degraded particle material was separated by syringe filtration unit from etoposide.

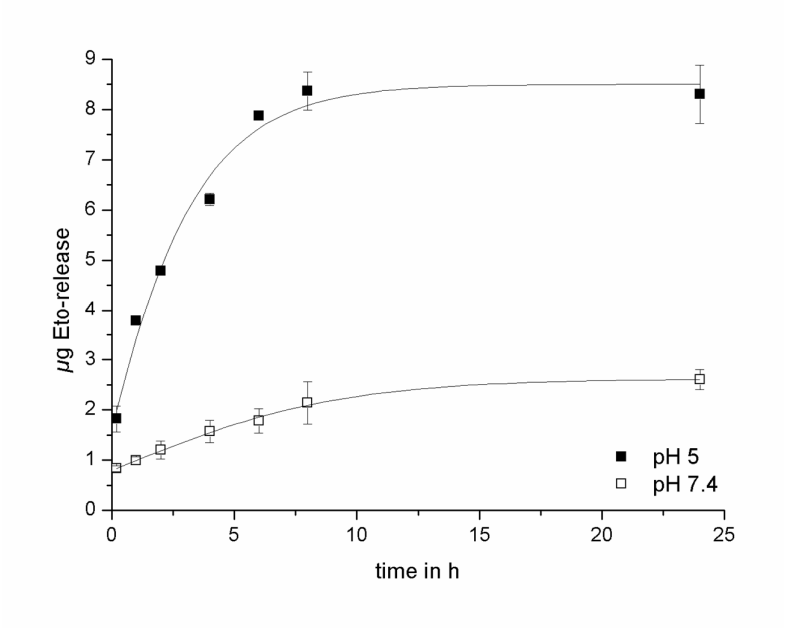

Figure 30. Release of encapsulated Eto at a pH 5 (black squares) and 7.4 (white squares) after different incubation times at 37 °C as determined by HPLC. Data represent the mean ± standard deviation of triplicate measurements.

The release of etoposide shows a fast and linear trend till 6 h incubation time. Then the release starts getting slower and after 8 h no further drug-release was detectable (100% drug release of encapsulated Eto). The control at pH 7.4 demonstrates a lower time-dependent release of etoposide. The high starting point after 20 min is maybe due to a low content of Eto (~1 μg per mg NP) non-covalently bound to the particle surface.

Comparison between the Release of Etoposide and L-Asparaginase

In general, a fast drug release is visible which correlates to a fast particle degradation in pH 5 within the first 24 h. This is since SpAcDex (10 min) with a low content of cyclic acetals was used for the particle formation. The particle degradation profile would be much slower when using a SpAcDex with a longer acetalation reaction time (**Chapter 1.1.2**).

Etoposide is faster released than L-asparaginase (no more release is detectable after 8 h for etoposide instead of the 24 h for the L-asparaginase release)(**Figure 31**). After 6 h incubation time more than 90% Eto was released, whereas in the same time only less than 45% Asp was released. This circumstance can be most likely explained by the usage of the double emulsion technique. Asp is therefore located inside the particle in a hydrophilic

core surrounded by the hydrophobic SpAcDex. Accordingly, the complete particle must be degraded before the Asp can be released. In contrast etoposide is entangled in the SpAcDex particle backbone material and because of that faster released than Asp. Another aspect of the delayed release of Asp is its higher molecular weight, hence is longer retained in the SpAcDex material. After the controlled drug release was shown within 24 h in pH 5 buffer, the next step was to verify the cellular uptake and release of the drugs *in vitro*.

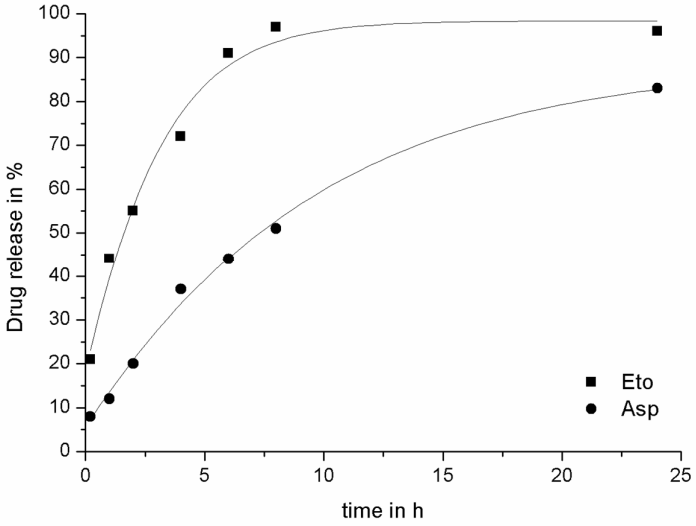

Figure 31. Comparison between Asp-release (black circles) and Eto-release (black squares) at 37 °C and pH 5 after the same incubation timepoints. The percentage release is normalized to the results of the encapsulation quantification of Asp or Eto for each particle type. Data represent the mean of triplicate measurements.

3.1.4 *In Vitro* Studies

Intracellular Uptake in K562 Cells

The confocal microscopy images (**Figure 32**) recorded by [redacted] indicate a cellular uptake and lysosomal escape based on the proton sponge effect (**Chapter 1.1.1**) after 24 h in K562 cells. This CML cell line was used based on the possible synergistic interaction of Asp and Eto in CML. For the confocal microscopy the surface amines of the SpAcDex particles were labeled with NHS-Oregon Green and Asp lysines were modified with Sulfo-NHS Cy5. It is visible that the dextran particle backbone material (green) is mostly located in the cytosol. Meanwhile Asp (red) is located all over the cell including the nucleus. Related to the cellular Asp release no difference is visible between dual-loaded Asp+Eto and the single-loaded Asp particles. Overall the confocal microscopy confirms a rapid

cellular uptake and drug release of the cationic SpAcDex particles in K562 cells. The next step is to investigate the cytotoxic potential as a dual drug delivery platform against K562 cells *in vitro*.

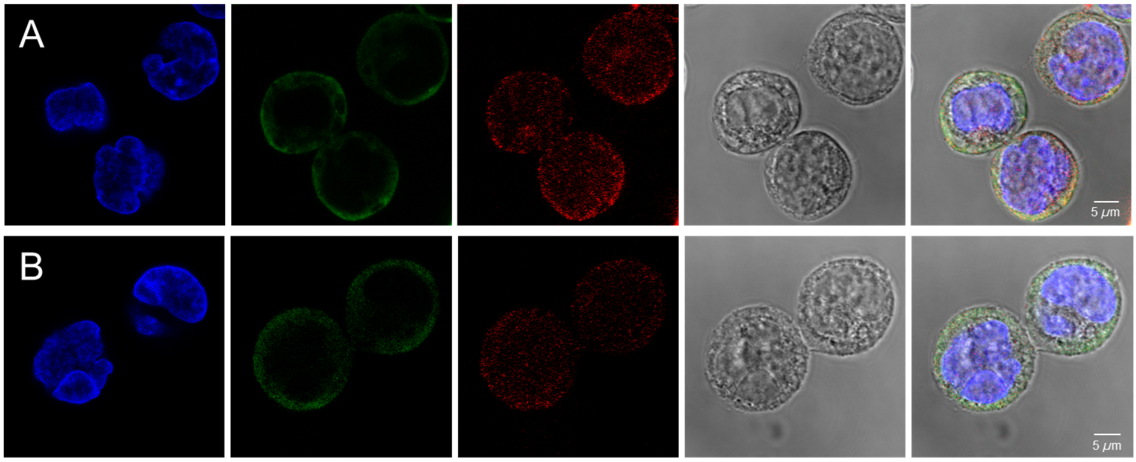

Figure 32. Confocal microscopy analysis of the intracellular uptake and Asp release of SpAcDex(Asp) particles (A) and SpAcDex(Asp+Eto) particle (B). The particles (62.5 $\mu g \cdot mL^{-1}$) were incubated with K562 cells for 24 h. The SpAcDex particle backbone had green fluorescence, Asp was labeled in red fluorescence und the cell core was dyed with DAPI.

Cytotoxicity in K562 Cells

To study the efficiency of the synergistic toxic effect of L-asparaginase and etoposide encapsulated in SpAcDex NPs in the treatment of CML the single and dual-loaded particles were tested with an MTT assay on K562 cells. MTT (3-(4,5-dimethylthiazol-2-yl)-2,5-diphenyltetrazolium bromide), is a bright yellow, water soluble salt, that can be reduced by cellular oxidoreductase enzymes. The reduction of MTT leads to a water insoluble purple formazan compound that can be quantified by absorbance measurements (**Figure 33**). The amount of reduced MTT depends on the activity of the metabolism of the K562 cells and correlates with the number of living cells. With toxic particles the cell viability of the K562 cells will decline due to a decreased number of cells per well or a decreased metabolism of the cells under toxic conditions.

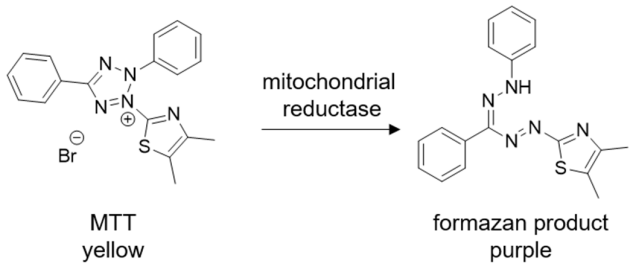

Figure 33. Reduction of a water soluble MTT salt to a purple, water insoluble formazan by mitochondrial reductases of HeLa cells.

For this NPs in a particle concentration (Asp and Eto drug loading content was the same for single-loaded and dual-loaded particles **Chapter 3.1.2**) range from 31.25 μg·mL^{-1} to 250 μg·mL^{-1} were incubated with CML K562 cells for 48 h (**Figure 34**). The MTT assay (described in detail in section **5.3.9**) shows a particle concentration dependent toxicity in the tested cells. This results in a low concentration dependence with SpAcDex(Asp) NP and a high dependence for the combination particle SpAcDex(Asp+Eto). The low active Asp content leads to a low cytotoxicity but in combination with Eto it shows a high synergistic cytotoxic effect.

The highest synergistic effect is visible at a concentration of 125 μg·mL^{-1} the cell viability is for the dual-loaded particle at 31% meanwhile for the SpAcDex(Asp) particle only at 92% and Eto-particle 82%. At a concentration of 250 μg·mL^{-1} SpAcDex(Eto) particle and SpAcDex(Asp+Eto) particle are closer. The examined synergistic cytotoxicity of the dual-loaded SpAcDex(Asp+Eto) particles is higher at a lower drug dose in contrast to studies by *Panosyan et al*. with the same drug combination in free form on GBM-ES cells.[210] Meanwhile empty NPs showed no toxicity towards K562 cells (data not shown).

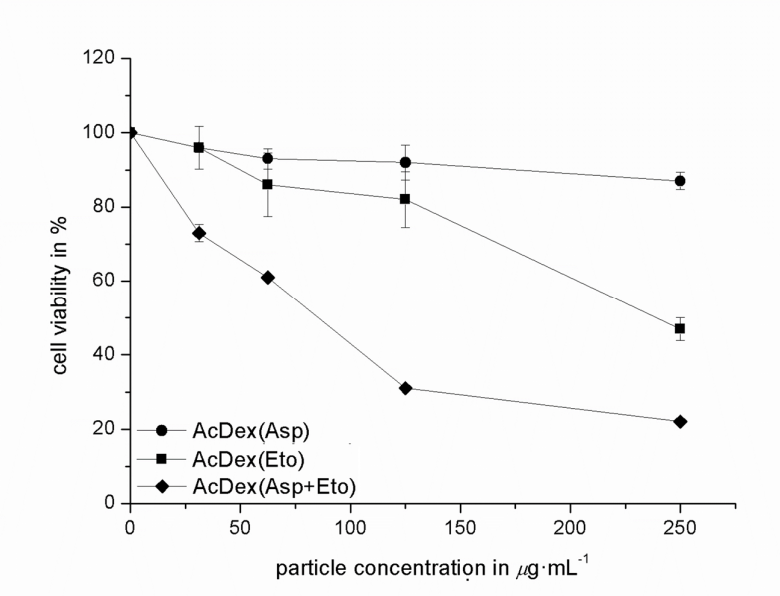

Figure 34. MTT assay to measure the cytotoxicity of SpAcDex NP carrying both Asp and Eto (black rhombus); Asp alone (black circles) or Eto alone (black squares) to K562 cells. All particles were incubated with cells for 48 h before assessing cell viability in each group and concentration (Asp and Eto drug loading content was the same for single-loaded and dual-loaded particles) (n = 3).

In conclusion several aspects highlight the therapeutic approach of SpAcDex NPs in the therapy of CML: (1) biodegradability and biocompatibility particle material; (2) hydrophilic and hydrophobic molecules can be co-transported simultaneous; (3) the combination of L-asparaginase and etoposide show a synergistic effect in K562 cells; (4) a controlled release of both drugs is with this particle system possible; (5) K562-CML cells can be reliable killed at a low drug dose. On this occasion the dual drug-loaded Asp+Eto-particles showed a high synergistic effect in contrast to the single-loaded particles. Based on the great *in vitro* cancer cell death results this co-encapsulated nanosystem has the potential to improve the treatment of CML.

3.2 Antibody-functionalized PEGylated SpAcDex NPs for the *In Vivo* Targeting of Dendritic Cells

As seen in **Chapter 3.1.4** spermine-functionalized acetalated dextran particles are fast taken up by K562 cells due to their cationic surface.[337] But as described in **Chapter 1.2.2**, for an immunotherapeutic approach a specific targeted delivery is desirable to minimize side effects and therapeutic efficacy. Therefore, further modification of the particle surface is needed to change their cationic character towards a more neutral surface to enhance the circulation time (**Chapter 1.2.1**). Further a hydrophilic layer from PEG can be attached to decrease unspecific uptake based on the mentioned stealth effect (**Chapter 1.2.1**). Afterwards, the addition of antibodies is possible to guide the particles to definite cell types and enhance a specific receptor-mediated cellular uptake. In this chapter the preparation of SpAcDex particles with a combination of passive and active targeting are analyzed regarding their specific *in vitro* and *in vivo* uptake in DEC205$^+$ DCs. The results should verify a potential use in an immunotherapeutic DC-targeting approach (**Chapter 1.3.2**).

3.2.1 Nanoparticle Preparation and PEGylation

For particle preparation the same SpAcDex material was used as described in **Chapter 3.1**. The SpAcDex particles were prepared by double emulsion with simultaneous co-encapsulation of Oregon Green dextran and CF750 dextran inside the particle. The Oregon green dye facilitates FACS and confocal microscopy measurements whereas CF750 dextran was encapsulated based on the fluorescence in near-infrared range, which makes *in vivo* biodistribution experiments possible. The quantification of the fluorescent dyes has been performed with dissolved particles in DMSO using an external standard calibration resulting in 532.25 ± 18.00 ng Oregon Green dextran (**Figure 65**) and 7.68 ± 0.11 μg CF750 dextran (**Figure 66**) per mg NP.

In the case of immunotherapeutic nanoparticles a long circulation time without recognition of the mononuclear phagocyte system is beneficial to enable the desired uptake by APCs.[338] PEGylation of the particles should enhance the hydrophilic character of the particles and reduce the positive surface charge. The unspecific cellular uptake of the SpAcDex particles was improved by the usage of bifunctional PEGylation with NHS-PEG-Mal (**Chapter 1.2.1**).[338] NHS-PEG-Mal (5 kDa) consists of an activated carbonic acid

at one end of the chain that can easily react with the primary amines of the spermine on the particle surface leading to the formation of stable amide bonds. Secondary amines are less sensitive but can also react with NHS in minimal amounts leading to the formation of stable imide bonds. The reactivity of NHS esters increases with higher pH which is favorable for the SpAcDex particle system since it undergoes no hydrolysis in basic environment. Unfortunately, the half-life of NHS esters decreases with higher pHs in aqueous buffers due to hydrolysis.[339] Furthermore the maleimide function hydrolyzes at a pH higher than 8.

Combining all factors, the particles and PEG were suspended in a PBS buffer with pH 7.4 and for the purification H_2O at pH 7 was used to minimize maleimide hydrolysis. The PEGylated particles were lyophilized and obtained as a colorless foam. In **Figure 35** the PEGylation resulting in Mal-PEG-SpAcDex particles is displayed.

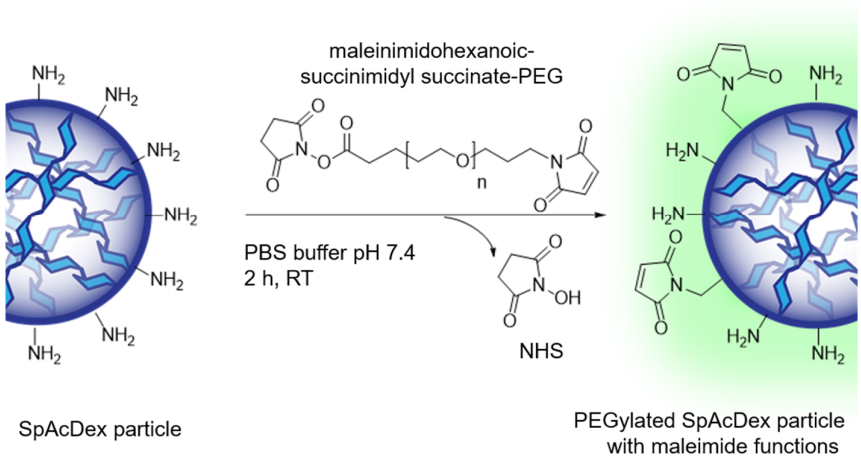

Figure 35. Primary amines on the SpAcDex nanoparticle surface were modified with the NHS-activated PEG-Mal chains in PBS buffer pH 7.4 for 2 h.

For the quantification of the extend of PEGylation on the particle surface two methods were applied. The first method is the Ellman´s excess assay. For this, a known excess of 2-aminoethanethiol was incubated for 5 h with the maleimide-functionalized particles. The unreacted 2-aminoethanthiol was afterwards quantified via Ellman`s assay with 5,5′-dithiobis(2-nitrobenzoic acid) to determine indirectly the amount of maleimide on the particle surface. Alternatively, the degree of PEGylation was determined by using a fluorescence method for the detection of the maleimides on the particle surface of the PEGylated NPs. For this, Mal-PEG-SpAcDex were incubated with Fmoc-L-cysteine for 5 h.

After purification and lyophilization the amount of conjugated Fmoc-L-Cys was quantified by fluorescence. The results of both quantification methods are shown in **Table 4**.

Table 4. Comparison of the different quantification methods of surface-PEGylation of SpAcDex nanoparticles.

quantification method	PEG on particle surface in nmol per mg
Ellman´s excess assay	25.6 ± 0.7
Fmoc-Cys determination	27.1 ± 0.8

Since the results are in a same range it can be concluded that both methods seem to be compatible for the quantification of the maleimide functions on the particle surface. With a content of 25.6–27.1 nmol PEG chains per mg NP the PEGylation is higher than previous studies by *Bamberger et al*. (19.9 nmol PEG per mg NP).[136] and the distance between 2 PEG-chains is 2.1 nm (calculation of the PEG conformation see **Chapter 5.3.6**). From this result, the conformation of the polymer on the surface of the particle surface can be calculated. The minimal distance required between grafted PEG-chains on a surface to form a mushroom conformation is defined as the Flory radius (R_F). Polymers with less space than R_F (6 nm in this case) have lower conformational freedom and hence a brush-like PEG conformation.[340] With 2.1 nm between two PEG chains for the PEGylated particles the distance is lower than Flory radius therefore a brush-like conformation can be assumed.

PEG coatings with a brush-like configuration reduce phagocytosis and complement activation, meanwhile a mushroom-like configuration is a potent complement activator to induce phagocytosis.[154] Based on the conformation calculation it can be concluded that an advantageous amount of PEG was conjugated on the particle surface to achieve the desirable stealth effect. Furthermore, the applied quantity of conjugated PEG provides a maleimide functions for the further attachment of antibodies.

3.2.2 Antibody Attachment on the Maleimide-activated Particle Surface

To enhance cellular uptake in DEC205$^+$ DCs (**Chapter 1.3.2**), that express DEC205$^+$ on the surface, anti-DEC205-PEG-SpAcDex antibody-modified NPs were synthesized by thiol-maleimide reaction with a SATA-modified antibody and the PEGylated particles (**Figure 36**). The targeting moieties are preferably conjugated at the end of the PEG-chain

for an efficient conjugation and targeting in combination with stealth effect.[341] Antibody conjugation through thiol chemistry is more selective and more precise compared to conjugation on primary amines with NHS-ester at a special pH-value. Another benefit of this reaction type is the easy addition of thiols on the antibody surface. This can be arranged by reagents like SATA or Traut´s reagent. For the anti-DEC205 antibody thiol addition SATA was used because of the acetyl protection group which enables a longtime storage of the modified antibody.

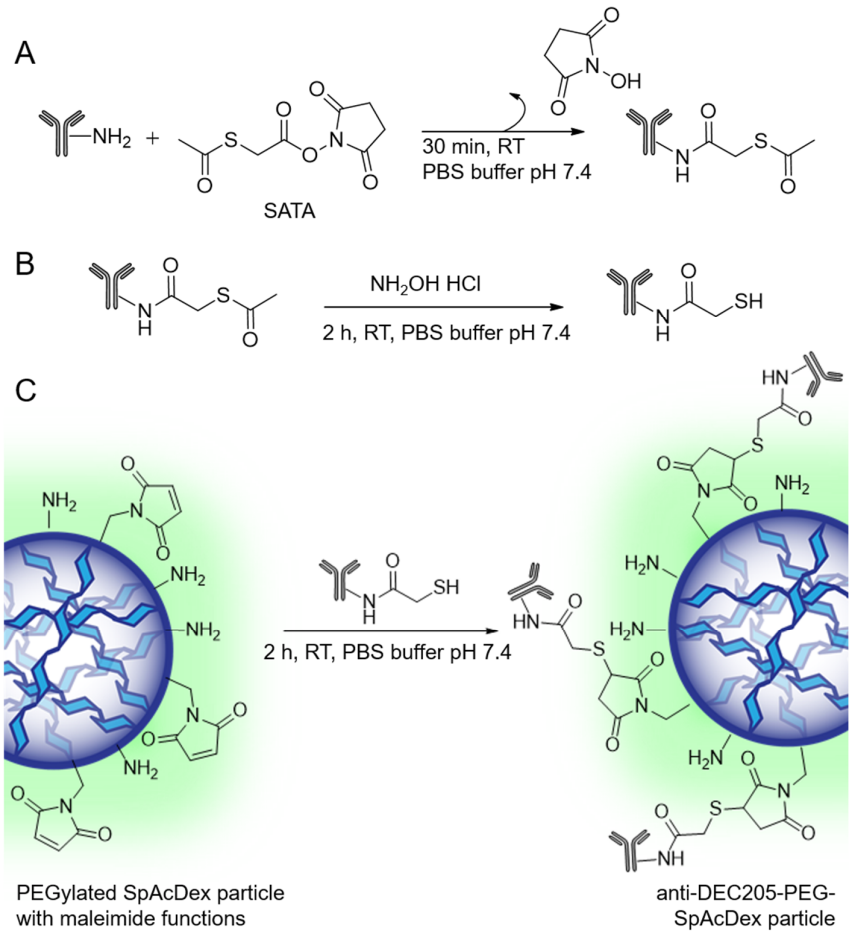

Figure 36. Antibody functionalization of PEGylated SpAcDex NPs; (A) Reaction of anti-DEC205 antibody with SATA; (B) Deacetylation of the SATA-modified anti-DEC205 antibody; (C) Conjugation of the modified anti-DEC205 antibody to the particle surface by thiol-maleimide reaction.

The increased amount of thiol groups on the anti-DEC205 antibody after SATA-modification was determined by Ellman`s assay. The results show that the native antibody has no free available cysteine meanwhile the SATA-modified antibody has an average of 0.73 ± 0.03 thiols per antibody which is quite low compared to the possible addition of up

to 6 thiols per antibody (**Figure 69**).[342] The amount of thiols per antibody was not increased as this would have led to possible undesired cross-linking between antibodies. At the same time the SATA-modification did not alter the cell binding of the monoclonal antibody (mAb) (**Figure 37**). It can therefore be assumed that SATA has not been conjugated in the proximity to the antibody epitope.

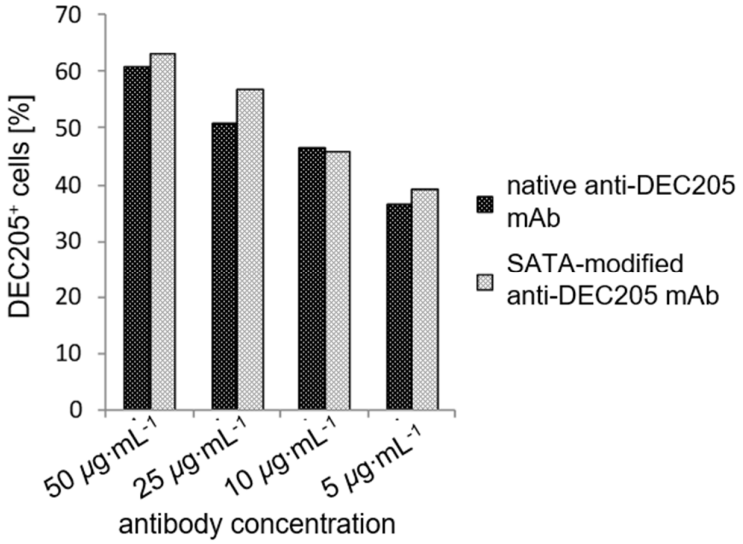

Figure 37. Cell binding of native anti-DEC205 and SATA-modified anti-DEC205 mAb. Cell tests with both antibodies were performed by [redacted].

The introduced thiol groups of the SATA-modified antibody facilitated now the following thiol-maleimide reaction with the particle (**Figure 36**). The high reactivity of maleimides (**Chapter 1.4.2**) enables a selective conjugation at neutral pH which is necessary to avoid hydrolysis of the acetalated dextran. Control particles were generated by attachment of L-cysteine (Cys) instead of the antibody.

The amount of antibodies on particle surface was quantified after conjugation, purification and lyophilization using two different methods: Bradford assay and enzyme-linked immunosorbent assay (ELISA). Bradford assay was performed with dissolved particles and ELISA with undissolved particles by [redacted] (Table 5). ELISA can detect the presence of a ligand in a liquid sample using antibodies directed against the protein to be measured. Afterwards a second detection antibody is added, forming a complex with the former antibody. The detection antibody is covalently linked to an enzyme, which enables a quantification based on a photometrically enzyme-substrate reaction.

Table 5. Antibody concentration on the particle surface quantified by Bradford assay and ELISA.

	Bradford assay		ELISA	
particle	Abs on the NP surface in μg per mg NP	number of Abs per NP	Abs on the NP surface μg per mg NP	number of Abs per NP
anti-DEC205-PEG-SpAcDex particle	2.7 ± 0.64	67.9	0.23 ± 0.027	5.8

ELISA shows, compared to the result of the Bradford assay, a ten-time lower content because of the need of an accessible antibody-epitope for the reaction with the secondary antibody. The antibody accessibility is limited on the one hand by the orientation of the conjugated antibody and shielding of the binding site by of the PEG layer. Meanwhile, the Bradford assay quantifies every antibody even if the antibody is not in an active, accessible state. For this the Bradford assay indicates the efficacy of the thiol-maleimide reaction and ELISA designates the amount of possible reactive antibody on the particle surface for receptor-mediated endocytosis.

The general amount of attached antibodies is in the lower end compared to other literatures results.[343-345] But, as seen by *Byzova et al.* and *Colombo et al*. the amount of antibody is better with a lower content.[346] In addition more attached antibodies leads to a reduced half-life of the particles based on the lower stealth effect (**Chapter 1.2.2**). Based on these findings, no further attempts to increase the antibody amount was performed.

3.2.3 Nanoparticle Size and Zeta Potential

Particle size was measured before and after both steps of surface modification using Nanoparticle Tracking Analysis (NTA) (**Table 6**). After purification and lyophilization non-modified SpAcDex particles had a mean size of approx. 180 nm in diameter with a SD-value of 56.6 nm. After PEGylation and antibody or cysteine conjugation the particles are slightly larger (approx. 210 nm).

Changes in particle properties can also be observed when looking at surface charge. The zeta potential of non-modified particles has a value of 18.5 mV due to exposed protonated spermine molecules on the particle surface. After conjugation with NHS-PEG-Mal the number of primary amines decreases. This can be seen in a lower zeta potential of the

PEGylated Cys-PEG-SpAcDex NP (+9.7 mV). The addition of the antibody leads to a negligible increase of the surface charge from 9.7 mV to 10.3 mV.

Table 6. Overview of particle size and surface potential of the modified particles in dd-H_2O pH 8.

particle modification	particle size measured by NTA			zeta potential in mV
	mean in d.nm	mode in d.nm	SD in d.nm	
SpAcDex NP	180.7 ± 5.7	162.8 ± 1.1	56.6 ± 6.6	18.5
Cys-PEG-SpAcDex NP	210.0 ± 9.1	189.7 ± 3.8	73.1 ± 8.1	9.7
anti-DEC205-PEG-SpAcDex NP	206.2 ± 2.6	195.2 ± 2.0	60.6 ± 1.3	10.3

After the full characterization of the antibody-functionalized SpAcDex particles the next step was to analyze the DC targeting potential *in vitro* and *in vivo*.

3.2.4 Analysis of Dendritic Cells Targeting *In vitro*

The following *in vitro* and *in vivo* studies of the modified particles were performed and illustrated by [redacted] (flow cytometry *in vitro* and *in vivo*), [redacted] (confocal microscopy *in vitro*) or [redacted] (biodistribution *in vivo*).

Analysis of NP uptake in BMDC by Flow Cytometry

DCs are the most effective APCs and a major key player in inducing primary antigen-specific T-cell immune responses.[347] Their specific targeting *in vivo* is still one of the key challenges in developing DC-based nanovaccines for cancer immunotherapy.[348] In order to investigate the targeting efficiency of the modified SpAcDex particles (1 μg·mL^{-1} up to 50 μg·mL^{-1}) were incubated with bone marrow-derived dendritic cells (BMDC) for 30 min at 4 °C. DEC205 is expressed at high levels on BMDC (**Figure 38A**). Cys-PEG-SpAcDex NPs served as control particles to interpret the binding efficiency of the anti-DEC205-PEG-SpAcDex NPs. For both particle types, flow cytometric analysis revealed a concentration-dependent binding to BMDC (**Figure 38B**). Cys-PEG-SpAcDex particles already show unspecific binding to BMDC in high concentrations. This might be due to their positive zeta potential.

However, specific binding can be significantly enhanced by conjugating anti-DEC205 antibody to the surface of PEG-SpAcDex NPs. Anti-DEC205-PEG-SpAcDex NPs showed an increased binding of more than 50% to DEC205$^+$ BMDC, compared to Cys-PEG-SpAcDex at lower particle concentrations (1–10 $\mu g \cdot mL^{-1}$). Unmodified SpAcDex NP showed an unspecific binding to DEC205$^+$ BMDC which was significantly reduced by more than 50% after PEGylation with NHS-PEG-Mal. These results are consistent with previously performed experiments: Due to their positive zeta potential, SpAcDex NPs bind unspecific to immune cells. Furthermore, BMDCs express high amounts of C-type lectin receptors, such as the mannose receptor CD206, which are known to bind dextran.[349] PEGylation leads to a decreased zeta potential and therefore reduces unspecific binding to cell membranes.[337, 350]

To further investigate if the improved targeting efficiency of anti-DEC205-PEG-SpAcDex NPs is based on the specific interaction between anti-DEC205 antibody and the surface receptor, a performed blocking experiments by pre-incubating BMDC with soluble anti-DEC-205 mAb was performed followed by incubation with 5 $\mu g \cdot mL^{-1}$ of anti-DEC205-PEG-SpAcDex particles. Pre-incubation with soluble anti-DEC205 antibody leads to a saturation of DEC205 receptors on the BMDC surface. Consequently, the binding efficiency of anti-DEC205-PEG-SpAcDex particles should be significantly reduced.

Flow cytometric analysis revealed a decrease (around 50%) of particle binding after pre-incubation with soluble anti-DEC205 antibody, indicating that binding of anti-DEC205-PEG-SpAcDex particles mainly occurs through the DEC205 receptor (**Figure 38C**).

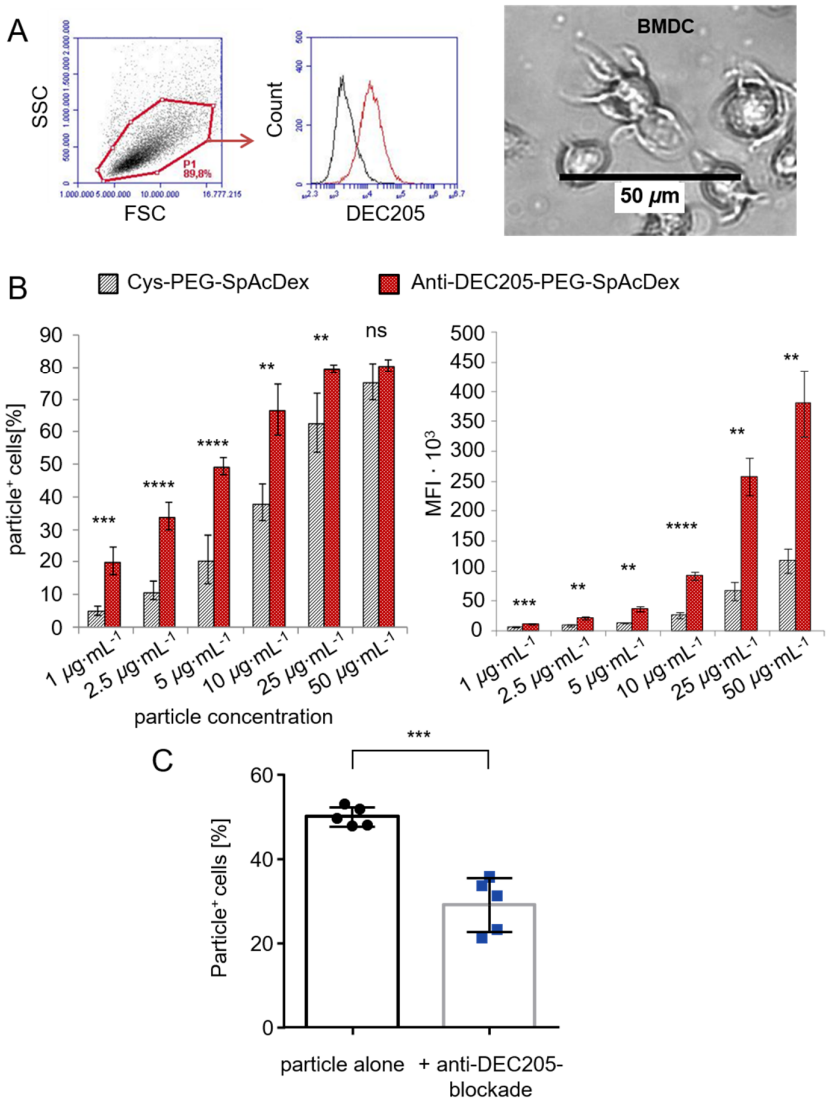

Figure 38. Anti-DEC205-PEG-SpAcDex NPs specifically target DEC205⁺ DCs through DEC205 surface molecules: (A) DEC205 expression of BMDC (left) and typical morphology of BMDC shown (right). (B) BMDC were incubated with different amounts of Oregon Green dextran-loaded particles (1–50 $\mu g \cdot mL^{-1}$) in culture medium for 30 min at 4 °C. Binding efficiency was analyzed via flow cytometry (left: percentage of Oregon Green⁺ BMDC; right: mean fluorescence intensity, MFI). Data shows mean ± SD of 5 individual experiments. Grey: Cys-PEG-SpAcDex; red: anti-DEC205-PEG-SpAcDex. (C) *In vitro* generated BMDC were pre-incubated with 50 $\mu g \cdot mL^{-1}$ of soluble anti-DEC205 antibody for 20 min followed by incubation with 5 $\mu g \cdot mL^{-1}$ of anti-DEC205-PEG-SpAcDex particles for 30 min at 4 °C (blue squares). BMDC incubated with 5 $\mu g \cdot mL^{-1}$ of anti-DEC205-PEG-SpAcDex particles alone (black dots) served as control. Binding efficiency was analyzed via flow cytometry (Oregon Green⁺ BMDC). Data shows mean ± SD of 5 individual experiments. Each dot represents one individual experiment.

Analysis of NP uptake in BMDC by Confocal Microscopy

Previously, we were able to show binding of anti-DEC205-PEG-SpAcDex particles through targeting of BMDC via the DEC205 receptor. Since DEC205 is a specific endocytosis

receptor, which is rapidly taken up by means of coated pits and vesicles,[351] we further investigated particle uptake by confocal microscopy. Therefore, BMDC were incubated with 10 μg·mL^{-1} of Oregon Green dextran encapsulated anti-DEC205-PEG-SpAcDex NPs for 1 h at 37 °C and analyzed the uptake afterwards via confocal laser scanning microscopy (CLSM). BMDC were incubated with or without 10 μg·mL^{-1} of anti-DEC205-PEG-SpAcDex or Cys-PEG-SpAcDex particles. CLSM could show that in general both particle types are taken up by BMDC after 1 h of incubation (**Figure 39**). These results are in line with our expectations. BMDC show high levels of endocytotic activity and are specialized in the uptake and processing of antigens.[352] However, by comparing the confocal images of the different groups, CLSM revealed a strong tendency for an increased uptake of anti-DEC205-PEG-SpAcDex NP in BMDC compared to the control particle Cys-PEG-SpAcDex particles.

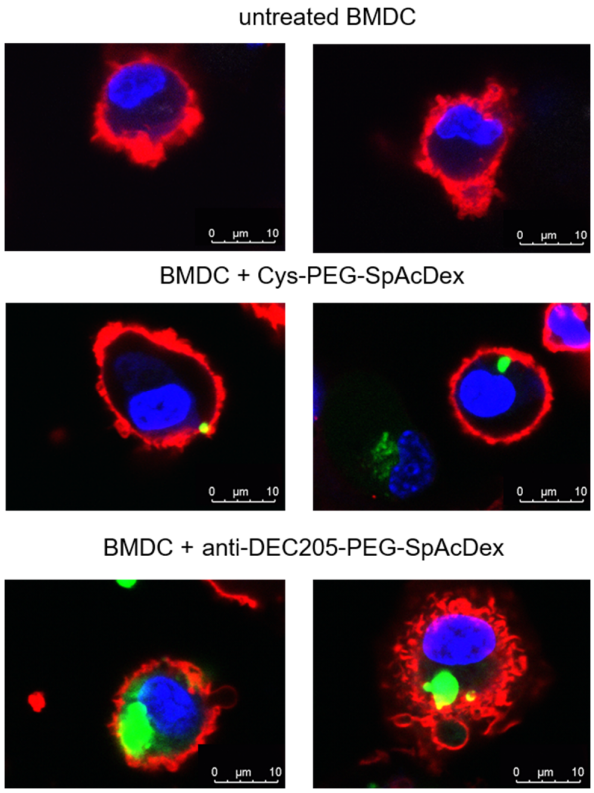

Figure 39. Enhanced uptake of anti-DEC205-PEG-SpAcDex NPs by BMDC: BMDC were incubated with 10 μg·mL^{-1} of Oregon Green-loaded anti-DEC205-PEG-Sp-Ac-Dex NPs or Cys-PEG-Sp-Ac-Dex NPs (same Oregon Green content) for 1 h at 37 °C. Untreated BMDC served as controls. Afterwards, cells were fixed with 2% PFA and stained with Hoechst dye (nuclei) and red-fluorescent dye DiD (membrane). Confocal laser scanning microscopy was carried out on a Leica TCS SP8. Blue: nuclei, red: cell membrane, green: Oregon Green dextran-loaded particles.

3.2.5 Analysis of Dendritic Cell Targeting *In vivo*

Biodistribution of anti-DEC205-PEG-SpAcDex in BALB/c Mice.

Nanoparticles have to overcome many barriers to finally deliver their cargo to specific immune cells *in vivo*. Although many NPs show an efficient targeting in *in vitro* studies, efficient addressing of immune cells *in vivo* is still a challenging problem.[353] Many particle systems get stuck in the lungs without even reaching the spleen or lymph nodes, both important lymphatic organs for the DC activation. In addition, many particles are covered by opsonin proteins when entering the blood stream (**Chapter 1.2.1**).[354] Opsonized particles are then recognized by phagocytes which rapidly digest and remove these particles from the blood stream before they can actually perform their therapeutic destination.[354] Therefore, it is mandatory to analyze the biodistribution of the different particle types.

Investigation of the biodistribution of CF750-labeled Cys-PEG-SpAcDex and anti-DEC205-PEG-SpAcDex NPs in Balb/c mice were carried out through intravenously injection of 600 μg NPs into the tail vein of each mouse and measuring fluorescence intensity 24 h after application by using an *in vivo* imaging system (IVIS). IVIS analysis showed distinct fluorescence signals in spleen, liver and lungs of mice for both particles tested (**Figure 40A**). Both particle types preferentially accumulated in the liver (60–80%) and to a lesser extent in the lungs (15–35%). These findings are consistent with previously performed experiments by *Bamberger et al.*.[355] The profound accumulation in lungs and liver can be attributed to the positive zeta potential (9.7 or 10.3 mV) of the particles and their relatively small size.[356] Importantly, also a small amount of nanoparticles (2–5%) accumulated in the spleen, one important lymphatic organ. With regard to the percent organ distribution of each mouse (**Figure 40A** pie chart + **Figure 40B**), an almost 2-fold increase of particle accumulation in spleen of mice treated with anti-DEC205-PEG-SpAcDex is observable compared to mice treated with control particles. Similar results could be found when analyzing the liver. Fluorescence intensity was increased in mice treated with anti-DEC205-PEG-SpAcDex NPs compared to Cys-PEG-SpAcDex.

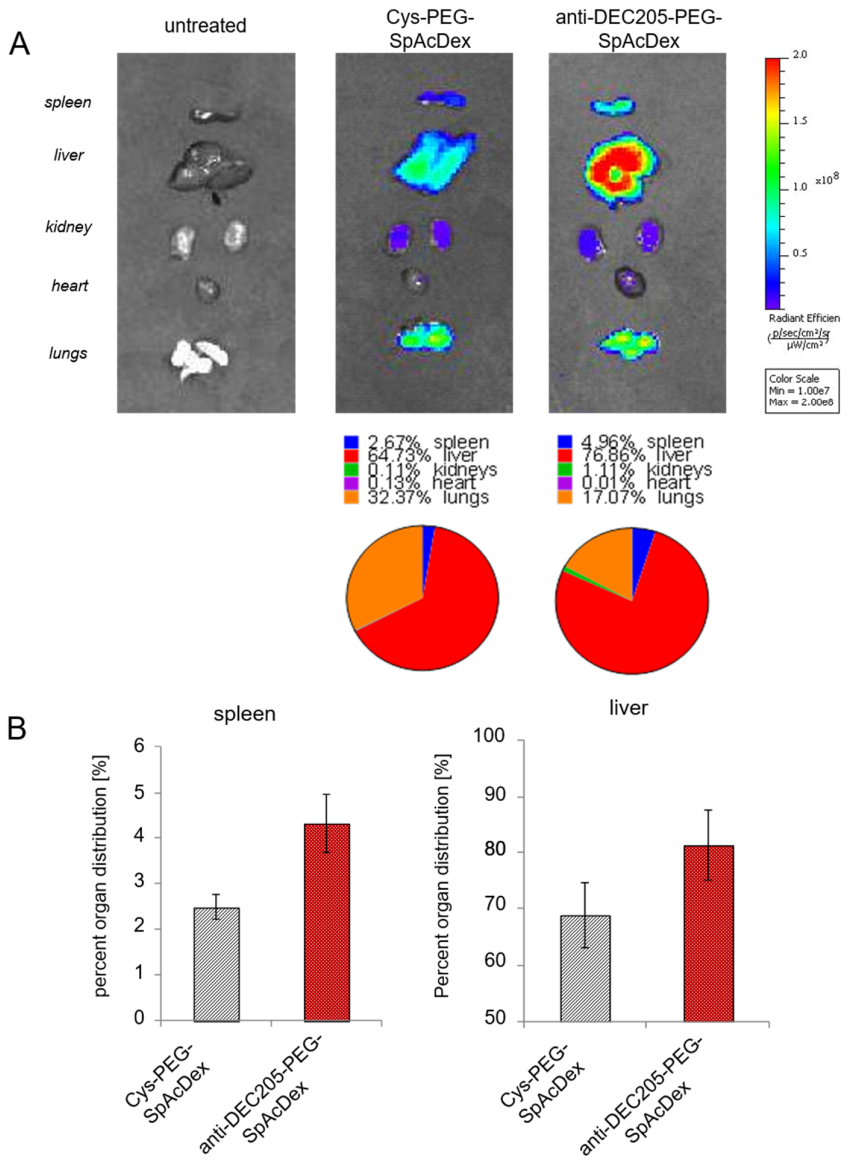

Figure 40. Biodistribution of Cys-PEG-SpAcDex and anti-DEC205-PEG-SpAcDex NPs in Balb/c mice (A) IVIS spectrum images of organs 24 h after intravenous injection of 600 μg Cys-PEG-SpAcDex or anti-DEC205-PEG-SpAcDex particles. In both particles CF750 dextran was encapsulated. Pie charts represent organ distribution of signal intensities of one individual mouse per group; (B) Data summarizes percent organ distribution of signal intensities in spleen (left) and liver (right) of both groups.

Anti-DEC205-PEG-SpAcDex NPs Uptake in Dendritic Cells and T Cells *In Vivo*.

To further analyze which cell types are targeted by SpAcDex particles *in vivo*, spleen and liver cells were isolated and binding efficiencies to important immune cells such as $CD3^+$ T cell, $F4/80^+$ macrophages and $CD11c^+$ DCs was determined (**Figure 41**). $CD11c^+CD11b^{low/-}CD8a^+$ cells are a very important DC subtype, which highly expresses DEC205 receptor and are essential for cross-presentation and priming of $CD8^+$ T

lymphocytes.[357] As desired for both organs, spleen and liver, only very low amounts of particles bound to $CD3^+$ T cells. No difference was detected between antibody-modified and control particles. With regard to the spleen, a small fraction of $F4/80^+$ macrophages bound anti-DEC205-PEG-SpAcDex particles and to a lesser extend also Cys-PEG-SpAcDex particles. Since macrophages are highly active phagocytes, it is unlikely to prevent particles from being picked up nonspecifically. The highest amount of SpAcDex particles was taken up by $CD11c^+$ DCs. Around 12% of $CD11c^+$ DC were able to bind or take up Cys-PEG-SpAcDex particles whereas approx. 22% bound the antibody-modified DEC205-PEG-SpAcDex particles. Altogether, this data shows that splenic $CD11c^+$ DCs can be efficiently targeted by anti-DEC205-PEG-SpAcDex particles *in vivo*. Regarding the liver, we observed nearly the same tendency. $CD11c^+$ DCs showed the highest frequencies of bound particles. Again, a significantly enhanced targeting of $CD11c^+$ DC could be achieved with anti-DEC205-PEG-SpAcDex particles. The binding efficiency was more than 50% higher compared to the control particles Cys-PEG-SpAcDex. Since the ratio of macrophages in the liver is higher than in the spleen, a moderate frequency of around 25% macrophages also bound anti-DEC205-Cys-PEG-SpAcDex particles. This binding can be again explained with the high phagocytotic activity of macrophages. However, the targeting efficiency of anti-DEC205-PEG-SpAcDex to $CD11c^+$ DCs was again significantly higher compared to $F4/80^+$ macrophages and much higher than $CD3^+$ T-cells.

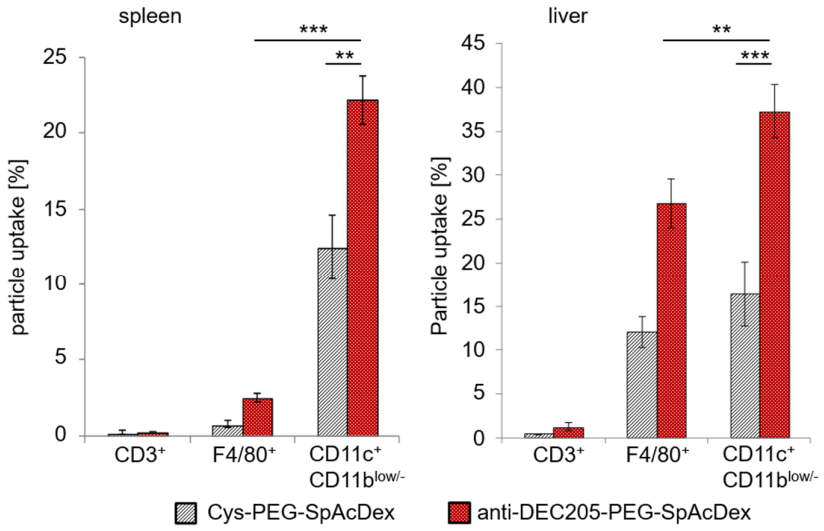

Figure 41. Specific uptake of anti-DEC205-PEG-SpAcDex NP by DC in spleen and liver: Immune cells of spleen and liver from mice treated with intravenous injection of different dextran particles were isolated and analyzed via flow cytometry regarding their particle uptake (Oregon Green+ cells). Data shows mean particle uptake ± SD of 3 independent experiments (left: spleen, right: liver). Grey: Cys-PEG-SpAcDex particles, red: anti-DEC205-PEG-SpAcDex particles.

In summary, the antibody-modified particles efficiently target DEC205+ splenic DCs. Compared to the control particles, an increase in targeting efficiency to DEC205+ cells of more than 50% was achieved.

In conclussion, several aspects highlight the immunotherapeutic potential of anti-DEC205-PEG-SpAcDex NPs: (1) biodegradability and biocompatibility particle material, (2) hydrophilic and hydrophobic molecules can be transported and therefore antigens and adjuvants can be delivered to DCs, (3) the particles have a long circulation time because of the stealth PEG-layer enabling a transport to the desired tissues and organs, (4) active targeting by antibody-receptor-mediated endocytosis leads to a high therapeutic efficiency and less side effects. The antibody functionalized SpAcDex particles have an enhanced uptake in DCs *in vitro* and *in vivo* and accumulate more in the spleen which are both favorable factors for an application as vaccination agent. As seen with the blocking experiment (**Figure 41**) the cellular uptake is in the case of anti-DEC205-PEG-SpAcDex particles DEC205-receptor mediated and therefore much more specific then the uptake of PEGylated-particles and unmodified SpAcDex particles. Another benefit of the particle system is the low binding on T-cells.

3.3 Self-Assembled Dual-responsive HRP-AcDex Conjugates

To obtain an amphiphilic protein-polysaccharide hybrid material both blocks, the protein and the polysaccharide block, have to be modified. On the one hand, the pH-responsive hydrophobic segment was achieved by thiol end functionalization at the reducing end and acetalization of dextran (AcDex-S-S-Py) (**Figure 42**). On the other hand, the hydrophilic block was HRP modified with *N*-succinimidyl-*S*-acetylthiopropionate (SATP). The conjugation can then be executed by forming a disulfide bridge between the polysaccharide and the protein which should lead to a double responsive material capable of self-assembly. Furthermore, the formed micellar nanoparticles should be competent nanocarriers for advances enzyme/drug delivery applications.

3.3.1 HRP-AcDex Synthesis

Synthesis of Thiol-modified Acetalated Dextran (AcDex-S-S-Py)

Dex-SH was synthesized with *p*-substituted aniline through end functionalized reductive amination with a microwave assisted approach.[279] *p*-substituted aniline has the advantage that it enables an easy quantification by ^1H-NMR and the low pK_a (~6.8 in contrast to a aliphatic thiol ~8) of the aromatic thiol leads to a reactive thiolate anion state at neutral pH.[358] The subsequentially reduction with tris(2-carboxyethyl)phosphine (TCEP) was observed by a quick color change from yellow to colorless. To avoid reoxidation of the introduced sulfhydryl group, the thiol-modified dextran was isolated as quickly as possible by precipitation and freeze-drying. Successful synthesis of quantitatively thiol terminated Dex-SH was confirmed by ^1H-NMR (**Figure 58**).

The activation of the thiol group at the reducing end on the dextran polymer chain was performed to reduce possible crosslinking of thiol-modified HRP in the conjugation step. The activation was carried out in DMSO under argon atmosphere with 2,2`-dipyridyl-disulfide. A yellow color emerged which is a result of the cleavage of the disulfide bridge in dipyridyl disulfide, producing the yellow pyridine-1-thione dye (**Chapter 1.4.2**). Additionally, the signal of both aromatic protons in the ^1H-NMR spectrum of the dextran derivative shifted from 7.28 to 7.45 ppm and from 6.82 to 6.74 ppm while the signal of the pyridyl group appears at 8.42, 7.90 and 7.35 ppm (**Figure 59**). Integration of the aromatic proton signals in contrast to the reducing end the results in an end group density of 97% for Dex-S-S-Py. Acetalated Dex-S-S-Py was prepared and characterized, like described for

Ox-AcDex in **Chapter 3.1.1** but with a 60 min reaction time to enhance the content of cyclic acetals in the polymer backbone. The new molecular weight and content of introduced acetals was determined by integration of the proton signal of generated acetone and MeOH during acidic cleavage of the acetals in the ^{1}H-NMR (D_2O/DCl) (**Figure 61**). The isolated product had a molecular weight of approx. 6,314 g·mol^{-1} and contained 83% acetals, whereas 31% were cyclic and 52% were acyclic acetals.

Thiol Modification of HRP

For the hydrophilic protein block we selected horseradish peroxidase. HRP is an oxidoreductase which oxidizes its substrate by catalyzing the electron transfer from substrate to hydrogen peroxide. It is an all helical enzyme with a molecular weight of 44.2 kDa. The protein bears six lysine residues and no cysteines, making SATP modification for the conjugation with AcDex-S-S-Py necessary.

Fluorescamine assay was carried out to determine indirectly the number of introduced thiol groups by SATP modification (**Figure 71**). Native HRP bearing 6 amines was used as standard and the number of amines per SATP-modified protein was calculated as 1.8 ± 0.2. Therefore 4.2 ± 0.2 thiol groups were introduced. Despite using an excess of SATP, lysine residues were not covered with thiols quantitatively. The assay revealed, that a maximum of four dextran chains is theoretically attachable under the investigated reaction conditions. The amount of possible attachable dextran chains was not further enhanced because it could lead to a decreased enzymatic activity.

HRP-AcDex Conjugation

Whereas the acetalated and thiol activated end group modified dextran served as the hydrophobic building block, thiol modified HRP was used as the hydrophilic block. Polymer and protein were linked with a disulfide bridge which is formed by the reaction of a thiol on the protein and an activated disulfide bond provided by the dextran chain. Hereby, a second stimulus-responsiveness of the conjugate besides the acid lability of the acetals was introduced. For a conjugation of compounds with different solubility behavior several issues have to be investigated *i.e.* reaction time, solvents and concentrations. The hydrophobic block was dissolved in DMSO meanwhile the hydrophilic block was dissolved in PBS buffer pH 7.4 containing 10 mM EDTA. Increasing amounts of DMSO in H_2O can lead to denaturation of the protein while a high presence of H_2O causes the

polymer to precipitate. Based on studies by Winterwerber a syringe pump was used to secure a slow (0.025 mL per h) addition of the protein (5 mg HRP-SATP in 2 mL) to the DMSO phase (4.2 mg AcDex-S-S-Py in 0.75 mL).[359] The following removal of DMSO by dialysis against H_2O pH 8 should induce a self-assembly of the amphiphilic conjugate. A micellar nanoparticular morphology should be formed with AcDex chains in the hydrophobic core and hydrophilic proteins on the surface in contact with the surrounding water. After lyophilization and addition to PBS buffer the particle formation was studied by DLS measurements.

For particles with encapsulated IAA, the drug was added to the DMSO phase and in the conjugation step encapsulated. IAA was used as payload because it functions as a prodrug that is oxidized once it is intracellular released and then induces apoptosis.

An overview of the synthesis of HRP-AcDex with particle formation and drug encapsulation is shown in **Figure 42**.

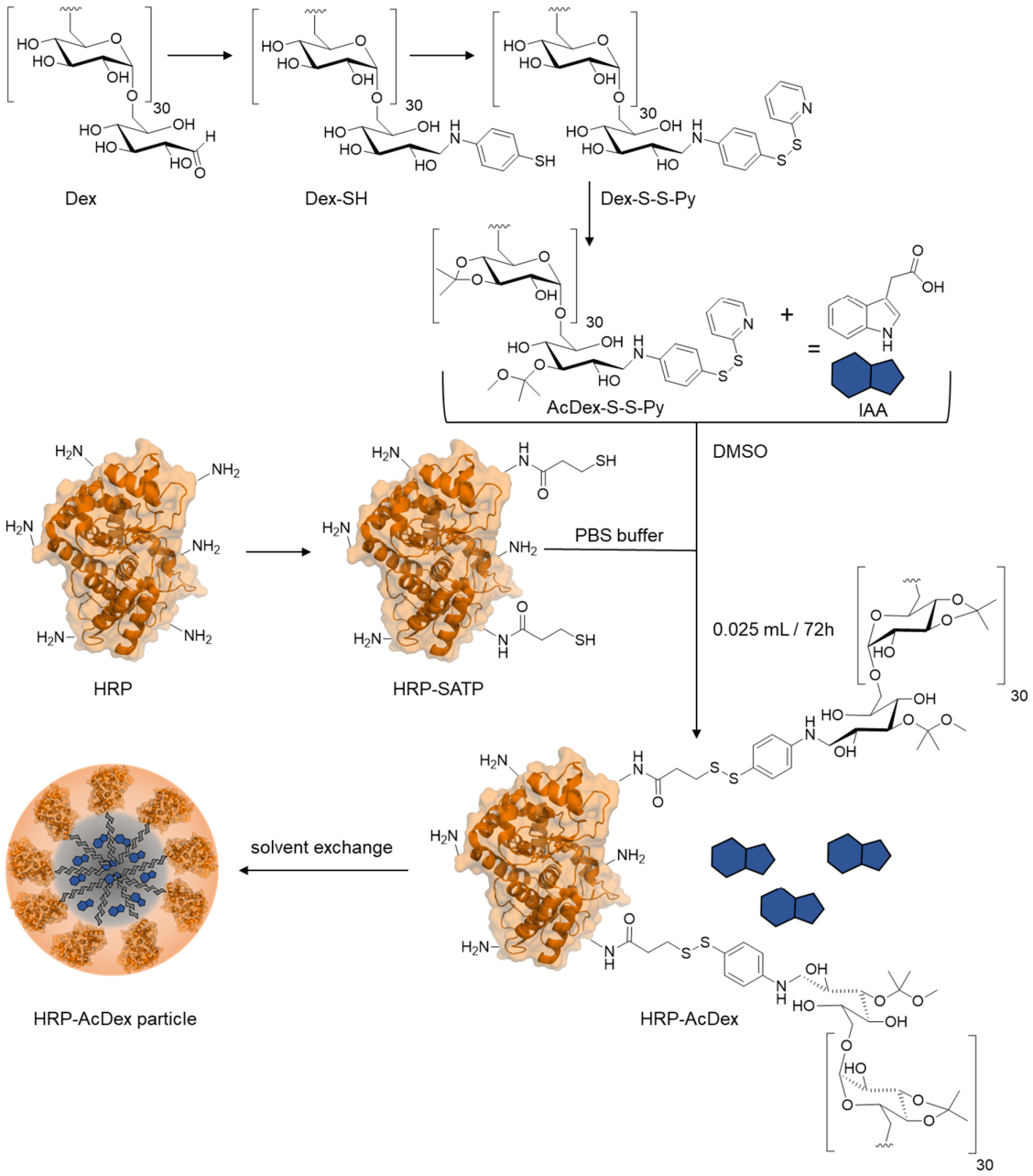

Figure 42. Overview of the synthetic route to the amphiphilic, dual-responsive HRP-AcDex conjugate with subsequent nanoparticle formulation and IAA encapsulation. For detailed reactions see **Chapter 5.4.1** and **5.4.2**.

Quantification of Attached Dextrans per HRP-AcDex

To quantify the protein content of the HRP-AcDex conjugate a BCA assay was performed resulting in a 73% protein content. Based on this result the AcDex content of the HRP-AcDex can be assumed to be remaining 27% which AcDex content resulting in 2.7 AcDex chains per HRP based on the following equation:

$$73\% = \frac{M(HRP)}{M(HRP) + x \cdot M(AcDex)} \qquad \text{eq. 3}$$

with M(HRP) is 44,174 g·mol^{-1} and M(AcDex) = 6,314 g·mol^{-1}. Resulting in an HRP-AcDex conjugate weight of 61,326 g·mol^{-1}. MALDI-TOF was not suitable for HRP-AcDex because the dextran chains degraded at the investigated MALDI-TOF ionization conditions.

Enzymatic Activity and Structure Integrity

The structural integrity and remaining enzymatic activity of HRP were further tested after conjugation with AcDex (**Figure 43**). Based on the ABTS assay the protein activity seems to be not altered and the CD spectra indicates no significant change in the secondary structure after conjugation with AcDex. Some structure elements are slightly altered but the change is only minimal and seemingly does not affect the active site of the enzyme, as can be seen in the activity assays.

After the full characterization of the HRP-AcDex material in the following the reductive-responsiveness of the material is investigated.

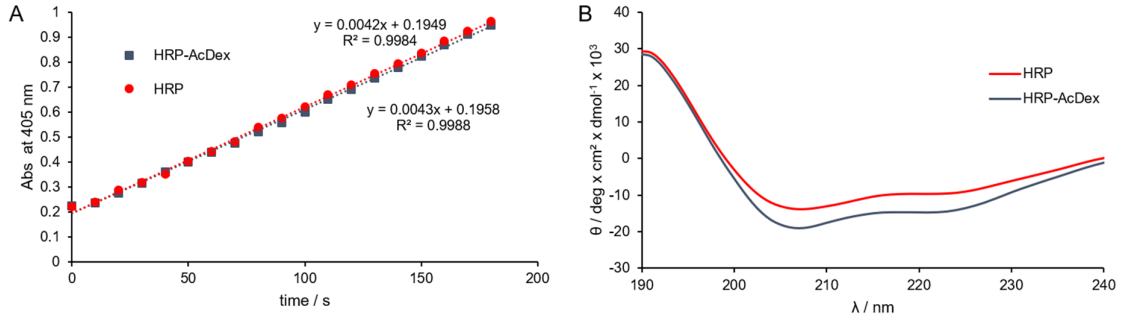

Figure 43. (A) ABTS enzyme activity assay for native HRP and HRP-AcDex sows no alteration after conjugation. (B) CD spectra indicate no significant loss of secondary structure elements after conjugation with AcDex.

Reductive-responsiveness Studies of HRP-AcDex with SDS-PAGE

SDS-PAGE (**Figure 44**) of HRP-AcDex material under non-reductive conditions shows a distribution of increasing molecular weight which correlates to the enhanced molecular weight of HRP-AcDex with 61,326 g·mol^{-1} in contrast to the molecular weight of HRP with 44,174 g·mol^{-1}. Based on different amounts of attached dextran chains the weight distribution in the SDS PAGE is broad and heterogenous. The broad distribution

disappears to some extent after reduction of the samples with Roti Load® suggesting the cleavage of disulfide bonds between protein and polymer.

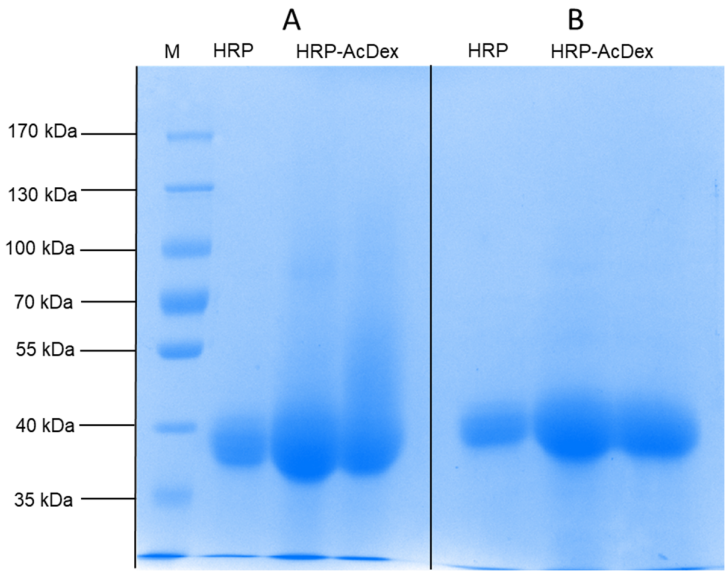

Figure 44. Molecular weight determination of HRP and HRP-AcDex with SDS-PAGE (8%) under non-reductive (A) and reductive (B) conditions. Non-reductive conditions were achieved in the absence of mercaptoethanol, whereas RotiLoad® gives reductive conditions. PageRuler Prestained Protein Ladder was used as Marker (M). The gel was stained with coomassie blue.

3.3.2 HRP-AcDex Particle Characterization

Size and Zeta Potential

The formation of particles after dialysis was confirmed by DLS measurements. Particle sizes in diameter are described by the Z-average, number, intensity and PDI. The Z-average describes the hydrodynamic cumulants mean size of all particles in the sample, whereas the number value describes the mean size of the particles forming the biggest population in the sample. The intensity describes the particle size distribution within the sample, depending on their scattering intensities. The PDI describes the polydispersity of the sample. PDIs smaller than 0.05 are rarely seen other than with highly monodisperse standards. Values greater than 0.7 indicate that the sample has a very broad size distribution and is probably not suitable for DLS. In **Table 7** and **Figure 45** the Z-average, PDI, zeta potential and intensity is shown for HRP-AcDex and HRP-AcDex with encapsulated IAA (HRP-AcDex(IAA). The particle sizes in numbers will be later used for characterization of particle degradation.

Table 7. Z. avg, PDI and zeta potential of empty and IAA-loaded HRP-AcDex particles

particle type	z. avg in nm	PDI	zeta potential in mV
HRP-AcDex(empty)	208.4	0.198	-18.3
HRP-AcDex(IAA)	203.6	0.115	-21.0

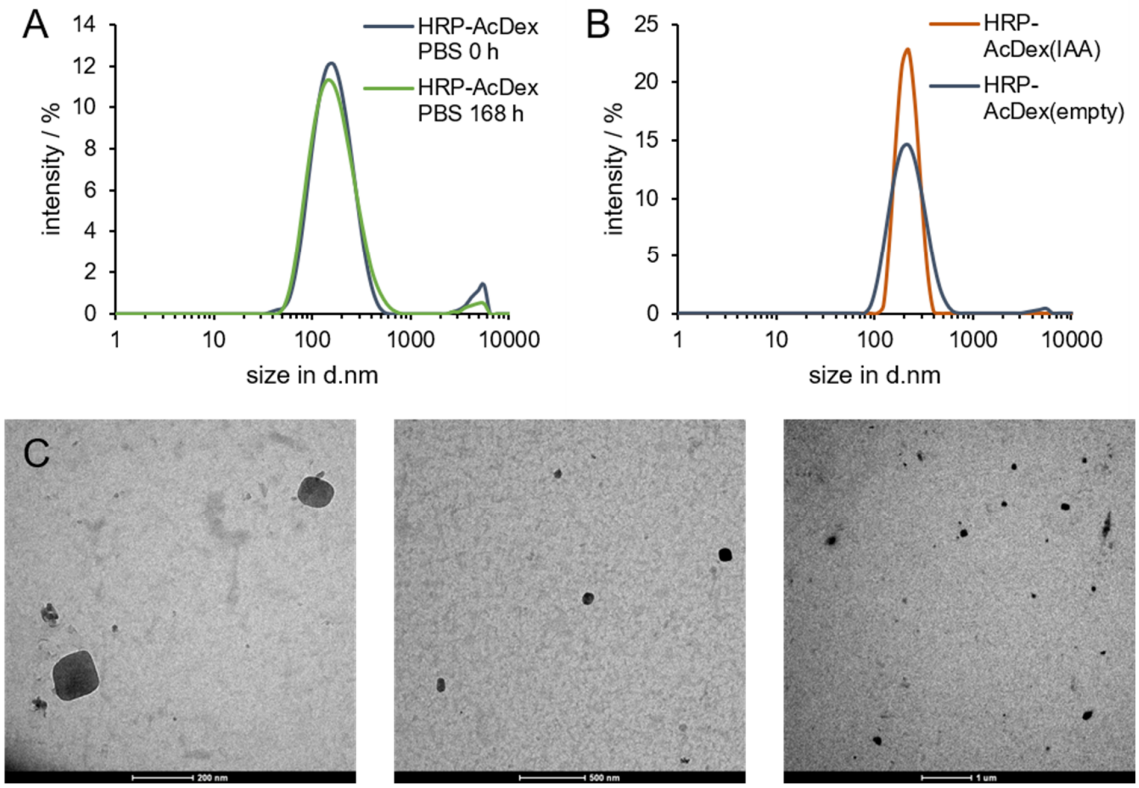

Figure 45. (A) DLS of HRP-AcDex particles in PBS buffer directly (blue) and after 1 week (green) incubation time. Sizes are shown in intensities. (B) DLS of HRP-AcDex(IAA) (orange) and empty HRP-AcDex (dark blue) in PBS buffer. Sizes are shown in intensities. (C) TEM images with different scales showing filled and solid spheres (1 mg·mL^{-1}).

The self-assembled empty HRP-AcDex particles have an average diameter of 208.4 nm and a good PDI of 0.198. Encapsulation of IAA leads to more compact particles with a great monodispersity (PDI 0.115) and smaller particle size. This circumstance can be explained by hydrophobic interactions in the micellar nanoparticle hydrophobic core between AcDex and IAA.

The AcDex-modified proteins have a more negative potential than native HRP due to the functionalization of the positively charged amino acids on the surface of the proteins and

a resulting dominance of carboxylates. The encapsulation of IAA leads to a further increase of the negative zeta potential most likely based on some content of adsorbed IAA on the particle surface. The negative zeta potential of the final nanoparticles is beneficial for a stable particle suspension since it prevents unwanted nonspecific interactions for example with blood proteins and aggregation based on the coulomb force.[360, 361] After the full characterization of the HRP-AcDex nanoparticles in the following the pH stimuli-responsive particle degradation and IAA release will be examined.

3.3.3 HRP-AcDex Particle Degradation

As seen in **Chapter 3.3.2** the particles are stable at neutral pH in PBS buffer and DMEM for over a week. The acetals of the conjugated AcDex chains can hydrolyze under acidic conditions enabling the desired stimuli-responsive particle degradation (**Chapter 1.1.1**). To study the particle breakdown, the HRP-AcDex nanoparticles were incubated in sodium acetate buffer pH 5 and the change in the size and particle concentration was analyzed by measurement of numbers and derived count-rate. Numbers was used to monitor the change in size of highest population of particles (**Figure 46A**). Observing the signal of intensities would lead to wrong conclusions based on higher light scattering of emerging aggregates. The derived count rate is a theoretical count rate measured by DLS that can be useful to quantify the signal strength from different samples. Here it can be used to monitor the particle concentrations over a period of time (**Figure 46B**).

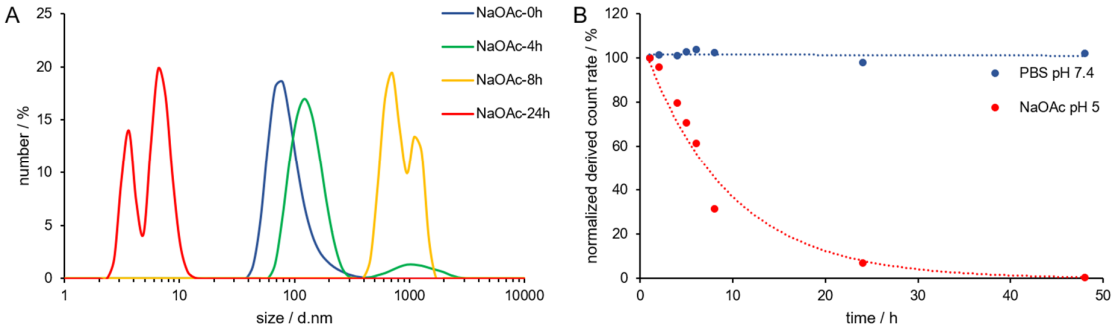

Figure 46. (A) HRP-AcDex nanoparticles incubated in NaOAc buffer (50 mM) at pH 5. After 24 h, all acetals are hydrolyzed, and a hydrophilic material (HRP with dextran chains) is regained which shows small sizes. All sizes are shown in numbers. (B) Amount of HRP-AcDex particles incubated within 48 h in NaOAc buffer pH 5 and PBS buffer pH 7.4. The number of particles was analyzed with the normalized derived count rate. A high time dependent degradation of HRP-AcDex particles is visible at pH 5. Meanwhile the number of particles at pH 7.4 is consistent in the examined period.

Within the first 8 h after particle incubation at pH 5, a shift towards higher particle sizes is visible, as the acetals in the polysaccharide backbone are slowly cleaved, and most likely aggregation of the half-degraded particles occurs (**Figure 46A**). After 24 h, all acetals are hydrolyzed, resulting in a hydrophilic material with small sizes below 10 nm, which correlates to the size of the HRP-Dex conjugate. A similar trend can be seen when looking at the change of particle numbers over time. The number of HRP-AcDex particles incubated within 48 h in NaOAc buffer pH 5 was analyzed with the normalized derived count rate (normalized to the amount of particles at the incubation starting point) (**Figure 46B**). A steady logarithmic particle degradation of the particles is visible at pH 5, which leads to almost no particles after 48 h. Meanwhile the number of particles at pH 7.4 is constant in the examined period. In conclusion a strong pH-dependent particle degradation can be confirmed. At the same time a concentration of 10 mM DTT leads to no particle degradation (data not shown). Either the disulfide bond could not be cleaved at the examined DTT concentrations or AcDex forms a highly stable hydrophobic core even after HRP separation. This circumstance needs to be investigated in detail with further studies.

The next step was to study the acid-triggered IAA release due to the disassembly of the particle system.

3.3.4 Indole 3-Acetic Acid Encapsulation Quantification and Release

For the quantification of encapsulated IAA, the HRP-AcDex(IAA) particles were dissolved in DMSO at a concentration of 1 mg·mL^{-1}. The following HPLC/MS measurements lead to 38.20 ± 0.68 μg·mL^{-1} IAA per mg particle. Based on the quantification a high loading capacity of 3.82% (mg per mg particle material) and an encapsulation efficiency of 3.6% was calculated. The encapsulation efficiency is quite low based on the high drug feed used in the particle conjugation step. Therefore, it can be concluded that most of the added IAA was not encapsulated and removed within the dialysis step.

To visualize the release of IAA under acidic conditions the particles (5 mg·mL^{-1}) were dialyzed against NaOAc buffer (pH 5) or phosphate buffer (pH 7.4). The dialysis buffer was exchanged after different incubation times and each dialyzed sample was lyophilized. The resulting pellet were resuspended, and the UV absorbance measured. The resulting release of encapsulated IAA at 37 °C demonstrates an excellent pH-dependent release of

IAA. At a neutral pH only a small proportion of IAA is released within 48 h. Meanwhile a huge release with a high burst release is visible at pH 5. After 8 h the release starts to slow down and after 48 h no further release of IAA is visible at pH 5. At this point 83% of the IAA encapsulated content was released.

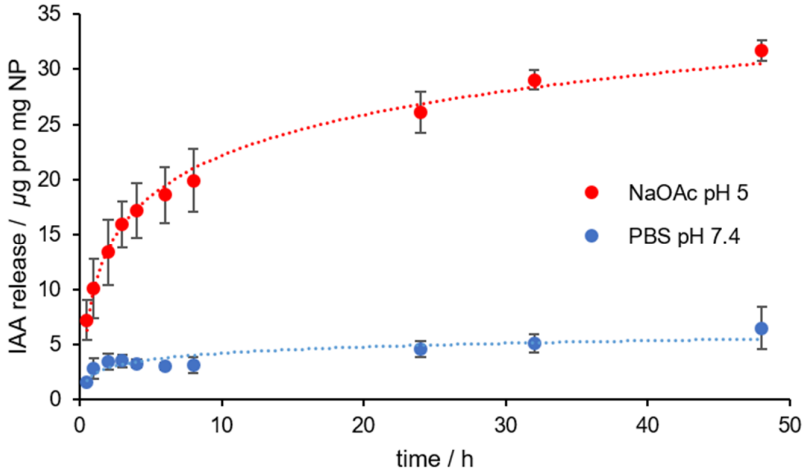

Figure 47. Release profile of IAA in NaOAc pH 5 and PBS buffer pH 7.4 dialysis experiment with HRP-AcDex(IAA) 1 mg·mL^{-1} MWCO 6–8 kDa at 37°C and 1,000 rpm. The release at pH 7.4 shows a low release of IAA in the analyzed time. In the meantime, a high time dependent release at pH 5 is displayed (experiments were carried out in triplets).

In conclusion the HRP-AcDex particles behave pH stimuli-responsive enabling a potential controlled particle degradation and drug release in lysosomes, cancer or inflammation tissue. To investigate the effect of HRP-AcDex particles on HeLa cells, the results of the confocal measurements and MTT assays are shown in the next chapter.

3.3.5 *In Vitro* Studies

Intracellular Payload Release

For an efficient particle supported therapy it is desirable to obtain control over delivery and release of a pharmaceutically active cargo within a specific tissue. In addition, the nanoparticle system has to ensure protection of the cargo from loss of function. The desired cellular uptake and intracellular payload release of the HRP-AcDex NP was investigated by confocal microscopy measurements with HeLa cells.

To visualize the potential release of IAA the model fluorescence dye 5/6 carboxyflourescein (5/6 FAM) was encapsulated instead of IAA during the conjugation

step. 5/6 FAM was used because it has structure similarities to IAA, and it is membrane-impermeant.[362] Hence 5/6 FAM can only be transported inside the cell through delivery by HRP-AcDex particles. The lysines of the HRP were labeled with Sulfo-Cy5-NHS ester to see if the particle material and the released payload have different localization inside the cell after the particle degradation in the lysosome. HeLa Cells were incubated with Cy5-HRP-AcDex(5/6 FAM) particles at a concentration of 0.75 mg·mL^{-1} for 24 h and the particle uptake was studied by confocal microscopy (**Figure 48**).

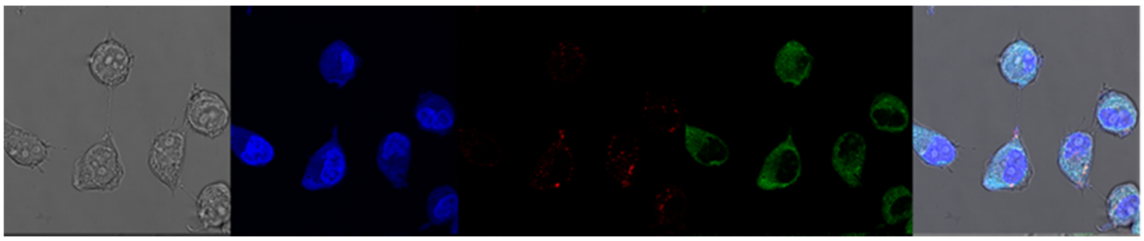

Figure 48. HeLa cells incubated with Cy5-HRP-AcDex particles loaded with 5/6 FAM (0.75 mg·mL^{-1}) over 24 h. From left to right the panels show the transmitted light image, DAPI stained cell nuclei (blue), Cy5 fluorescence of the Cy5 labeled HRP-AcDex particle material in cells (red), 5/6 FAM fluorescence of the released 5/6 FAM in cells (green) and the overlay of all three images.

The released green-fluorescent 5/6 FAM signal is spread all over the cytosol meanwhile the red-labeled HRP seems to be located still in the lysosome. It can be concluded, that the particle payload was successful delivered into the cells after 24 h incubation time. The different locations of the particle material and 5/6 FAM indicates a complete payload release. After the confirmation of the particle uptake in HeLa cells the next step was to verify if HRP-AcDex(IAA) NP can induce an *in vitro* toxicity based on the intracellular release of IAA and oxidation by HRP-AcDex.

In Vitro Cytotoxicity of IAA-loaded Particles

The enzyme/prodrug pair produces free radicals and toxic 3-methylene-2-oxindole, which can cause membrane lipid peroxidation and DNA damage, resulting in cell death.[363, 364] The possible oxidation mechanism is shown in **Figure 49**.

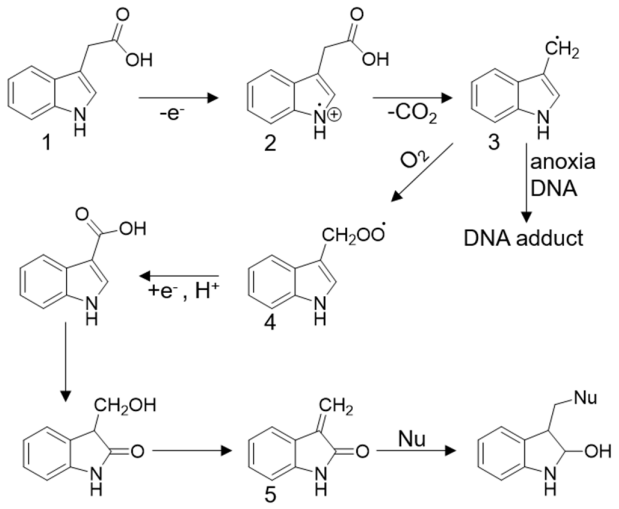

Figure 49. Mechanisms involved in toxicity of IAA. IAA (**1**) is oxidized by HRP to the radical cation (**2**), which fragments rapidly to the skatolyl radical (**3**). In anoxia (total depletion of oxygen), this forms adducts, *e.g*., with DNA.[365] Otherwise, the skatolyl radical reacts with oxygen to form the peroxyl radical (**4**), which forms 3-methylene-2-oxindole by reduction and rearrangement (**5**). The latter can react with cellular nucleophiles (Nu), *e.g*., protein thiols and DNA to form adducts.[366] Modified and adapted from [367].

The cytotoxicity of HRP-AcDex particles with encapsulated IAA was analyzed by using an MTT cell viability assay with HeLa cells after incubation for 72 h (**Figure 50**). The MTT assay reflects the cellular uptake results and shows a high particle concentration dependent toxicity in the tested HeLa cells which results in 7% remaining living cells for 1 mg·mL^{-1} particles. With regard to the same IAA concentration (180 μM) this toxicity is higher (7% remaining living cells) than studies by *Hung et al*. with HRP-immobilized mesoporous silica nanocontainers (~40% remaining living cells).[368] This observation might be explained by the high preserved enzymatic activity of HRP-AcDex. In the meantime, empty HRP-AcDex particles and simply IAA without HRP addition showed no toxicity towards HeLa cells in the same examined concentrations. Therefore, it can be concluded that only the combination of HRP-AcDex with encapsulated IAA can induce apoptosis in cells.

Together with the confocal microscopy it can be summarized that the prodrug IAA is at a low pH intracellular released and then oxidized by the HRP particle material and induces high cytotoxicity *in vitro*.

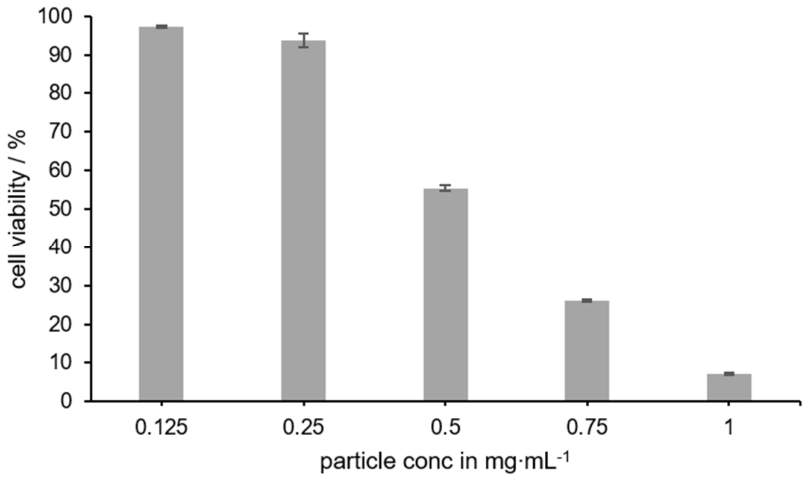

Figure 50. MTT assay with Hela cells incubated with HRP-AcDex(IAA) for 72 h. Particles concentrations from 0.125 mg·mL^{-1} up to 1 mg·mL^{-1} (equal to 4.78 ± 0.09 μg·mL^{-1} up to 38.20 ± 0.68 μg·mL^{-1} encapsulated IAA) were investigated (experiments were carried out in triplets and standard deviation shown).

In summary, an HRP-AcDex conjugate was successfully synthesized by forming a disulfide bridge between the hydrophobic AcDex chain and the hydrophilic HRP. The conjugate is still enzymatic active and was capable of self-assembly into micellar nanoparticles with a low PDI and sizes of 200 nm. The pH-responsiveness of the polymer component has been shown by a fast particle degradation and drug release. A highly potent drug delivery nanocarrier with a high loading capacity and the ability to oxidize the encapsulated prodrug and induce apoptosis was discovered which was validated in first promising *in vitro* results.

4 Conclusion and Outlook

Dual Encapsulation of Asp and Eto in SpAcDex Particles

In the first project of the thesis, it was shown that the SpAcDex particle preparation by double emulsion technique can be used to encapsulate simultaneously hydrophilic and hydrophobic drugs. Based on the known synergistic effect a combination of L-asparaginase and etoposide were entrapped inside the pH-sensitive, biodegradable and biocompatible SpAcDex particle material. A successful dual encapsulation was confirmed by the same drug content for both drugs in dual-loaded in contrast to single-loaded particles. The subsequent release studies at pH 5 revealed that the hydrophobic Eto is released much faster than the hydrophilic Asp (after 6 h incubation time more than 90% Eto and only 45% Asp were released). This indicates that Eto is entrapped in the hydrophobic SpAcDex particle material throughout the whole particle and the bigger Asp is most likely congregated in the area of the particle core (**Figure 51**). Confocal microscopy experiments with K562-CML cells validated an intracellular controlled drug release. Further *in vitro* studies showed a high synergistic toxicity for the dual-loaded SpAcDex(Asp+Eto) particles in contrast to the single-loaded particles. At a concentration of 125 $\mu g \cdot mL^{-1}$ the cell viability is for the dual-loaded particle at 31%, meanwhile for the SpAcDex(Asp) particle only at 92% and for the SpAcDex(Eto) particle at 82%. Based on the successful *in vitro* results this co-encapsulated nanosystem has the potential to improve the treatment of imatinib-resistant CML at a low drug dose.

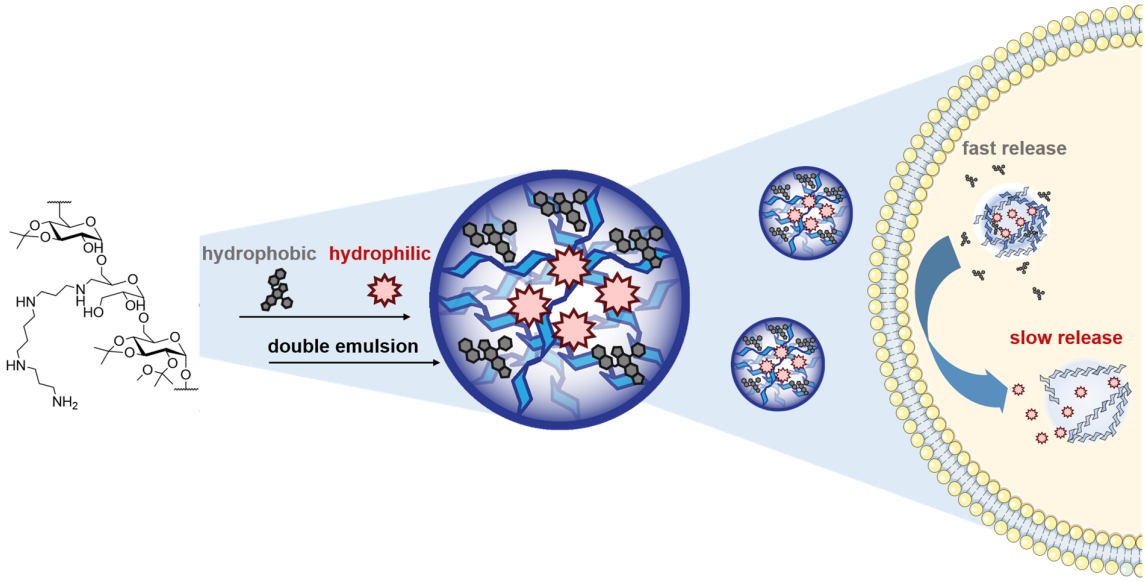

Figure 51. Dual encapsulation of a hydrophilic and hydrophobic drug in spermine-functionalized acetalated dextran nanoparticle with one double emulsion method. The subsequently cellular uptake and controlled release is shown.

Further studies should include the testing of the cytotoxicity on other leukemia cell lines for example on AML or ALL cells to see if the cytotoxicity is on the same level. On top of that, the transferability of the system to *in vivo* studies should be investigated. For this, the particles have to be PEGylated to maintain a long circulation time to reach the desired location.[350] In this context, an active targeting should be considered which has the potential to reduce side effects and enhance the therapeutic efficacy of the particle system with dual-loaded drugs. A potential target structure is transferrin whose transferrin like receptor (TfR) expression is increased in CML cells.[369]

Antibody-functionalized SpAcDex Particles for DC Targeting

The main focus of the second project was the further development of the SpAcDex nanoparticle system by using targeting mechanisms to enable a specific cell uptake (**Chapter 1.2**). Accordingly, the shielding properties of a PEG-layer with an attachment of anti-DEC205 mAb for active DC-targeting were combined on the particle surface. These modifications should prevent unspecific cellular uptake, prolong blood circulation time and enhance the efficiency in immunotherapeutic approaches. PEGylation was successful introduced onto surface amines of the nanoparticles with NHS-PEG-Mal. The maleimide function quantification on the attached PEG chains by Ellman´s excess assay and Fmoc-

Cys determination resulted in 25.6–27.1 nmol per mg which correlates to the desired brush-like PEG conformation (**Chapter 1.2.1**). The DEC205 antibody was modified with SATA and then attached at the PEG-layer by thiol-maleimide reaction. The resulting nanoparticles with 5.8 antibodies per nanoparticle (quantified by ELISA) showed a favorable DC targeting *in vitro* in contrast to unmodified particles and PEGylated particles. Furthermore, an antibody specific through receptor-mediated endocytosis of the particles was confirmed by experiments with pre-treatment of high amounts of soluble anti-DEC205 mAb resulting in a significantly reduced binding of anti-DEC205-PEG-SpAcDex nanoparticles on BMDCs. *In vivo* the anti-DEC205-PEG-SpAcDex NPs showed a favorable biodistribution and a 50% greater specific cellular uptake in DEC205$^+$ DCs than the control particles (**Figure 52**). Overall the results indicate that this particle system has the potential to activate specific DCs.

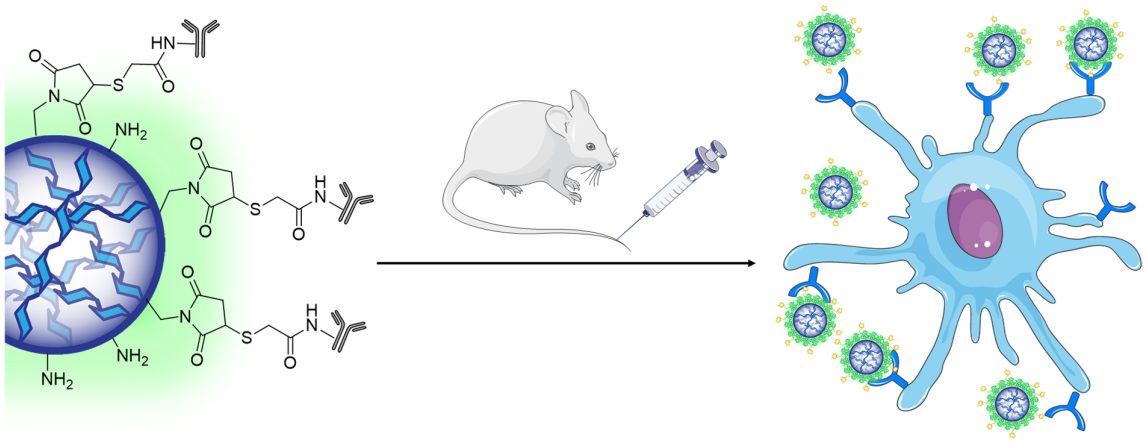

Figure 52. Antibody-functionalized and PEGylated SpAcDex nanoparticles for the *in vivo* targeting of dendritic cells.

Additional investigations should test if antigen-loaded anti-DEC205-PEG-SpAcDex particles taken up by DCs result in an efficient great anti-tumor CD8$^+$ cytotoxic T-lymphocytes activation *in vivo*.[370, 371] As a proof of concept, the induction of experimental autoimmune encephalomyelitis (EAE) could be considered to determine the immunotherapy potential of the antibody-functionalized particle system. Further studies could include a switch of the particle system from PEG to an alternative stealth polymer with advantageous properties, for example dextran or PGA (**Chapter 1.2.1**).

Self-Assembled Dual-responsive HRP-AcDex Conjugates

Conjugation of thiol-modified HRP was performed by dipyridyldithiol-mediated thiol exchange reaction with pH-responsive thiol-modified AcDex. This reaction lead to a polysaccharide-protein conjugate with 2.7 AcDex chains per HRP. During the conjugation step the prodrug IAA was efficiency encapsulated and after solvent exchange, self-assembled HRP-AcDex(IAA) nanoparticles were obtained. The biocompatible particles had a great PDI (0.115) with a good drug loading capacity (3.8%). The new hybrid protein-polysaccharide material had the same enzymatic activity as the native HRP, and no significant change in the secondary structure of the protein was observed. DLS measurements showed a fast particle degradation within 24 h at pH 5. Further, the encapsulated IAA was pH-sensitive controlled released (83% at 48 h) meanwhile only a low amount of IAA was released at pH 7.4. The reductive-responsiveness of the disulfide bridge between the protein and the AcDex was only confirmed with an SDS-PAGE but not with DLS experiments. This could be explained by a hydrophobic stable AcDex core even after disulfide cleavage. *In vitro* studies revealed an intracellular uptake accompanied by a cargo release in HeLa cells. Lastly, the MTT assay in HeLa cells revealed high cytotoxicity of HRP-AcDex(IAA) through oxidation of the stimuli-responsive released IAA by the HRP particle material. The results are especially attractive in the field of enzyme/prodrug delivery, where protein-polysaccharide particles could overcome the limitation of traditional enzyme therapies. The maintained enzymatic activity and stimuli-responsive prodrug release should lead to a more controlled therapy with better pharmacokinetics.

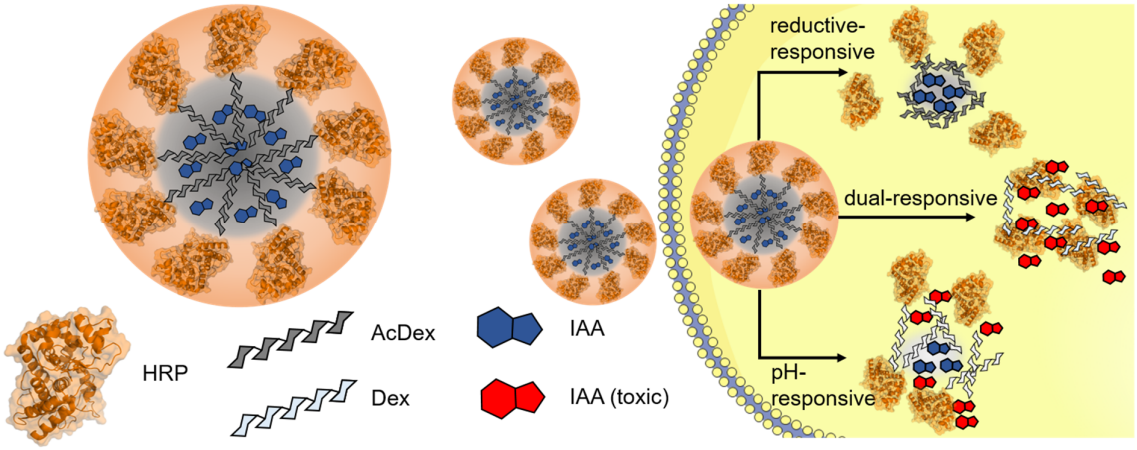

Figure 53. The HRP-AcDex particles applied as a delivery system for the prodrug indole-3-acetic acid into the cytosol of HeLa cells. Hereby inducing a cytotoxic effect after stimuli-responsive release and oxidation by HRP-AcDex.

Additional studies could confirm the applicability of the HRP-AcDex(IAA) carrier system *in vivo*. Further experiments should investigate if the established HRP-AcDex system is transferable to other enzymes which would open up a field of possible enzyme/drug combinations. Techniques like transmission electron cryomicroscopy (cryoTEM) and static light scattering (SLS) could give a valuable insight in particle morphology. A detailed understanding of the underlying mechanism could help to obtain full control over nanoparticle design and size distribution.

5 Experimental Part

5.1 Materials

5.1.1 Reagents

Chemical	Supplier	CAS
2,2'-azino-bis(3-ethylbenzothiazoline-6-sulphonic acid) (ABTS)	Alfa Aesar	30931-67-0
Acetic acid	Sigma-Aldrich	64-19-7
Acetonitrile	Sigma Aldrich	75-05-8
N-Acetyl-L-cysteine	Sigma-Aldrich	616-91-1
4-Aminothiophenol	TCI	1193-02-8
Anti-mouse CD205 (DEC205)	Bio X Cell	
L-Asparaginase	Abcam	9015-68-3
L-Asparagine	VWR chemicals	70-47-3
5(6)-Carboxyfluorescein	Sigma- Aldrich	72088-94-9
Coomasie Blue G 250	Sigma Aldrich	6104-58-1
L-Cysteine	Sigma Aldrich	52-90-4
Deuterium chloride 38% in deuterium oxide	Carl Roth	7698-05-7
Deuterium oxide	Deutero	7789-20-0
Dextran T5 from *Leuconostoc mesenteroides*	Pharmacosmos	
Dextran T10 from *Leuconostoc mesenteroides*	Pharmacosmos	
Dextran, Oregon Green® 488; 10,000 MW	Life Technologies	
Dextran, CF750 10,000 MW	Linaris	
4′,6-diamidino-2-phenylindole (DAPI)	Thermo Scientific	28718-90-3
Dichloromethane anhydrous, ≥99.8%	Sigma-Aldrich	75-09-2
Dimethyl sulfoxide anhydrous, ≥99.9%	Sigma-Aldrich	67-68-5
2,2'-Dipyridyl disulfide	TCI	127-03-9
5,5'-Dithiobis(2-nitrobenzoic acid) (DTNB, Ellman's reagent)	Sigma-Aldrich	69-78-3
1,4-Dithiothreitol	Alfa Aesar	3483-12-3
DMEM GlutaMAX™ (Dulbecco's Modified Eagle's Medium high glucose)	Thermo Scientific	
Ethanol	Fisher Scientific	64-17-5

Chemical	Supplier	CAS
Ethylenediaminetetraacetic acid (EDTA)	Sigma-Aldrich	60-00-4
Etoposide	Abcam	33419-42-0
Fetal Calf Serum (FCS)	Life Technologies	
Fluorescamine	TCI	38183-12-9
Fmoc-L-Cysteine	Iris Biotech	135248-89
Glycerol	Sigma-Aldrich	56-81-5
Glycine	Sigma-Aldrich	56-40-6
n-Hexylamine	Sigma-Aldrich	111-26-2
Horseradish peroxidase	Alfa Aesar	9003-99-0
Hydrochloric acid 37%	Carl Roth	7647-01-0
N-Hydroxysuccinimide (NHS)	Sigma-Aldrich	6066-82-6
Indole-3-acetic acid	Sigma Aldrich	87-51-4
Methanol	Sigma-Aldrich	67-56-1
2-Methoxypropene	Sigma-Aldrich	116-11-0
Nessler`s Reagent	VWR chemicals	7783-33-7
Oregon Green® 488-X, Succinimidyl Ester, 6-isomer	Life Technologies	
PageRuler Prestained Protein Ladder	Thermo Scientific	
Phosphate buffered saline (10x concentrate)	Sigma-Aldrich	
PEG (CH_3O-PEG-NHCO-C_2H_4-CONHS 5 kDa)	Rapp Polymere	
PEG (PEG-(NHCO-C_2H_4-CONHS)$_2$ 2 kDa)	Rapp Polymere	
PEG-Malhex	Rapp Polymere	
Penicillin-streptomycin Gibco™	Thermo Scientific	
Poly-L-lysin (300,000 kDa)	Biochrom	25988-63-0
Poly(vinyl alcohol)	Sigma-Aldrich	9002-89-5
Pyridinium *p*-toluenesulfonate	Sigma-Aldrich	24057-28-1
RPMI-1640 GlutaMAX™	Thermo Scientific	
Roti®-Histofix 4% acid free (pH 7)	Carl Roth	
Rotiload	Carl Roth	
N-succinimidyl *S*-acetylthioacetate (SATA)	Thermo Scientific	76931-93-6
N-succinimidyl *S*-acetylthiopropionate (SATP)	Thermo Scientific	84271-78-3
Sodium acetate	Sigma-Aldrich	127-09-3

Chemical	Supplier	CAS
Sodium borohydride	Sigma-Aldrich	16940-66-2
Sodium chloride	Carl Roth	7647-14-5
Sodium dodecyl sulfate (SDS)	Sigma Aldrich	151-21-3
Sodium hydroxide	Carl Roth	1310-73-2
Sodium (*meta*)periodate	Sigma-Aldrich	7790-28-5
Sodium pyruvate (100 mM) Gibco™	Thermo Scientific	
Spermine	Iris Biotech	71-44-3
Sulfo-Cyanine 5 NHS-Ester	Lumiprobe	
Triethylamine	Carl Roth	121-44-8
Tris(2-carboxyethyl)phosphine (TCEP)	Carl Roth	51805-45-9
Water, sterile-filtered, BioReagent, suitable for cell culture	Sigma-Aldrich	7732-18-5

5.1.2 Buffers and Media

All buffers were filtered through a sterile syringe filter with a pore size of 0.22 μm (CME membrane, Rotilabo®). Aqueous buffers were stored at 4 °C to prevent bacterial contamination unless otherwise noticed.

Acetate Buffer (0.1 M, pH 5)

13.6 g sodium acetate trihydrate (Sigma-Aldrich, M_W 136.08 g·mol^{-1}) were dissolved in 1 L dd-H_2O and adjusted to pH 5 with acetic acid.

Borate Buffer (0.1 M, pH 8.5)

6.2 g boric acid (Sigma-Aldrich, M_W 61.83 g·mol^{-1}) were dissolved in 1 L dd-H_2O and adjusted to pH 8.5 with NaOH.

Coomassie Staining Solution

250 mg Coomassie Brillant Blue R-250 were dissolved in a mixture of water (45 mL), acetic acid (10 mL) and ethanol (45 mL).

dd-H_2O (pH 8)

dd-H_2O was adjusted to pH 8 with TEA (30 μL TEA per 1 L dd-H_2O).

Destaining Solution for Coomassie Stained Gels

A mixture of water (450 mL), ethanol (450 mL) and acetic acid (100 mL) was used.

DMEM for HeLa cells

DMEM GlutaMAX™ (high glucose) with phenol red was mixed with 10% FCS, 1% sodium-pyruvate and 1% penicillin-streptomycin.

DTT (10 mM, pH 7.4)

10 mM DTT in PBS buffer pH 7.4

Glycine Buffer (0.1 M, pH 10.5)

7.5 g glycine (Sigma-Aldrich, M_W 75.07 g·mol^{-1}) and 5.8 g sodium chloride (Carl Roth, M_W 58.44 g·mol^{-1}) were dissolved in 1 L dd-H_2O and adjusted to pH 10.5 with NaOH.

HEPES Buffer (25 mM, pH 7.4)

6.0 g 4-(2-hydroxyethyl)-1-piperazineethanesulfonic acid (Amresco, M_W 238.30 g·mol^{-1}) were dissolved in 1 L dd-H_2O and the pH was adjusted to pH 7.4 with NaOH.

PBS Buffer (pH 7.4)

PBS 10x concentrate (Sigma-Aldrich, 100 mL) was diluted with dd-H_2O (900 mL); containing 154 mM NaCl, 8 mM $NaHPO_4$ and 2 mM KH_2PO_4 with a final pH of 7.4.

PBS Buffer (pH 8)

PBS buffer (1x) was adjusted to pH 8 with NaOH.

PBS Buffer (10 mM EDTA, pH 7.4)

PBS buffer (1x) was mixed with 3.72 g ethylenediaminetetraacetic acid disodium salt (Alfa, M_W 372.24 g·mol^{-1}) and adjusted to pH 7.4 with NaOH.

3% PVA in PBS pH 7.4

30 g poly(vinyl alcohol) (Sigma-Aldrich, M_W 13,000–23,000 g·mol^{-1}) were dissolved in 970 mL 1x PBS under heating (90 °C).

0.3% PVA as Cryoprotectant

3 g poly(vinyl alcohol) (Sigma-Aldrich, M_W 13,000–23,000 g·mol^{-1}) were dissolved in 997 mL dd-H_2O under heating (90 °C).

RPMI for K562 cells

RPMI-1640 with phenol red was mixed with 10% FCS, 1% sodium-pyruvate and 1% penicillin-streptomycin.

Running Buffer for Gel Electrophoresis (5x concentrated)

15.1 g Tris and 94 g glycine and a solution of SDS in water (20%, 25 mL) were dissolved with water to final volume of 1 L.

SDS 20% in Water

20 g sodium dodecyl sulfate were dissolved in water to a final volume of 100 mL.

5.1.3 Disposables

Consumables	Manufacturer
BRAND® UV cuvettes micro (c = 8.5 mm)	VWR
CELLSTAR® cell culture flasks 25 cm^2, 75 cm^2, 225 cm^2	Greiner Bio-One
Coverslips, precision (diameter 1.8 cm, thickness of 0.17 ±0.005 mm, borosilicate glass)	Carl Roth GmbH
Disposable pipettes 5 mL, 10 mL, 25 mL	Sarstedt
Disposable syringes 1 mL, 2 mL, 5 mL, 10 mL, 20 mL	B.Braun
Eppendorf Tubes 1.5 mL, 2 mL	Eppendorf
Filtropur S 0.2 (sterile, non-pyrogenic)	Sarstedt
Glass pipettes	Carl Roth GmbH
Locking clips for dialysis	Carl Roth GmbH
Micro-centrifuge tubes for high G-force 1.5 mL	VWR
Microplate 12-well, flat bottom, clear, sterile	Greiner Bio-One
Microplate 96-well, flat bottom, clear	Sarstedt
Microplate 96-well, flat bottom, clear, sterile	Greiner Bio-One
Microplate 96-well, flat bottom, black	Greiner Bio-One
Microplate 96-well, flat bottom, UV-Star	Greiner Bio-One
NMR tubes	Sigma-Aldrich
Parafilm	Pechiney Plastic Packing
Pipette tips 2 μL, 200 μL, 1000 μL	Sarstedt
Pipette tips sterile 100 μL, 300 μL, 1250 μL	Greiner Bio-One
SuperSpin™ Microcentrifuge Tubes, polypropylene (1.5 mL, max. rcf 35 k)	VWR
Tubes 13 mL, 100x16 mm, PP	Sarstedt
Tubes 15 mL, 120x17 mm, PP	Sarstedt
Tubes 50 mL, 114x28 mm, PP	Sarstedt
ZelluTrans/Roth Mini Dialyzer MD100 MwCO 6,000–8,000 $g \cdot mol^{-1}$	Carl-Roth GmbH

5.1.4 Cell Lines

HeLa Cells

An adherent epitheloid cervix carcinoma cell line. Cells were a kind gift from the group of Prof. Dr. Bernd Epe (Institute of Pharmacy and Biochemistry, Johannes Gutenberg-University, Mainz).

K562 cells

A non-adherent human immortalized myelogenous leukemia cell line. Cells were a kind gift from the group of PD Dr. rer. physiol. Udo F. Hartwig (Department of Internal Medicine III, Hematology, Oncology and Pneumology, University Medical Center of the Johannes Gutenberg-University, Mainz).

5.2 Equipment

Absorption and Fluorescence Measurements

Equipment: Infinite® M200 Pro Plate Reader, Tecan Group Ltd., Switzerland. Analysis was carried out using i-control 1.7 software and Microsoft Excel or Origen 7.5 V5.

Absorption measurements were performed with clear 96-well microplates (flat bottom). Fluorescence measurements were performed with black 96-well microplates (flat bottom).

Bath-Sonicator

Equipment: Sonorex Super RK 102 H, Bandelin electronic.

Samples were sonicated until complete dissolving could be observed. Nanoparticles were suspended until no aggregates were detectable.

Biological Safety Cabinet

All cell culture experiments were performed in a sterile environment using a biological safety cabinet from Herasafe™, Kendro Laboratory Products, Langenselbold, Germany.

Centrifuges

Equipment: Heraeus™ Multifuge™ X3R, Thermo Scientific.
Heraeus™ Megafuge™ 8 R, Thermo Scientific
BECKMAN Type Avanti™ J-25

Dialysis

Equipment: Spectra/Por® 6, regenerated cellulose, MWCO 1,000 $g \cdot mol^{-1}$, Carl Roth GmbH.
ZelluTrans Roth, regenerated cellulose, MWCO 3,500 $g \cdot mol^{-1}$, Carl Roth GmbH.

Dialysis membranes were inserted in d-H_2O for 15 min and rinsed with water before loading with the samples. Dialysis was performed against d-H_2O pH 8 in a beaker glass under constant stirring. Water was changed 6-times in 24 hours.

Incubator

Equipment: Heraeus® BB15 FUNCTION Line, Thermo Scientific.

Cell incubations were performed in a humidified incubator at 37 °C with 5% CO_2 atmosphere.

Inert Gas

Equipment: Argon gas bomb in 99.998% purity N46, Air Liquide Deutschland GmbH.

Argon was used as inert gas to flood flasks and reaction containers. Balloons were attached to the reaction flasks to prevent the contact of reagents with air.

Lyophilizer

Equipment: ALPHA 1-4 LSC, Martin Christ Gefriertrocknungsanlagen GmbH.

Samples were dissolved or suspended in water, frozen in liquid nitrogen and then stored in the lyophilizer for freeze-drying. Before lyophilization of nanoparticles, 30 μL 0.3% PVA in dd-H_2O were added as a standard cryoprotectant.

HPLC/MS

Equipment: HP Agilent 1100 with Proshell 120 EC-C18-column

Fluorescence Microscopy

Equipment: Leica TCS SP5 Microscope

Nuclear Magnetic Resonance (NMR)

Equipment: Bruker Topspin Fourier 300 MHz.

For standard analytical purpose ^1H-NMR spectra were recorded at 300 MHz. The experiments were performed at room temperature using $CDCl_3$ and D_2O as solvents. The chemical shifts were reported in ppm against the solvent signal of TMS. For the description of the signals the following abbreviations were used: s = singlet, d = doublet, t = triplet, q = quartet, m = multiplet, br = broad signal. Integrals were calculated by using MestReNova Software. Assignments were carried out according to literature. Peaks resulting from solvent residues were determined by literature.[372]

The degree of acetalation of the modified polysaccharide and the amphiphilic block copolymers was determined by ^1H-NMR. Therefore, approx. 10 mg of modified

polysaccharide was dissolved under vortexing in 550 μL D_2O by adding three drops of DCl. Integration of the signals of nascent Acetone and Methanol compared to the signal of all AGU protons allowed the determination of the ratio of cyclic to acyclic acetals

Theoretical molecular weight calculation of acetalized dextrans. The average g·mol^{-1} of AcDex ($M_{n,NMR}$) was calculated by ^1H-NMR using equation:

$$\begin{aligned} \text{n AGU} \cdot \Big(& 202.22\ \text{g} \cdot \text{mol}^{-1}\, \frac{\%}{100}\, \text{cyclic} + 234.26\ \text{g} \cdot \text{mol}^{-1}\, \frac{\%}{100}\, \text{acyclic} \\ & + 162.12\ \text{g} \cdot \text{mol}^{-1}\, \frac{\%}{100}\, \text{no acetals} \Big)\ \text{g} \cdot \text{mol}^{-1} \\ & = M_{n,NMR}\ \text{g} \cdot \text{mol}^{-1} \end{aligned} \qquad \text{eq. 4}$$

Particle Sonicator

Equipment: Bandelin Ultrasonic Homogenisator Sonoplus UW 70 (v220-240w), microtip MS 73 SH70G Stufenhorn 20 kHz, BANDELIN electronic GmbH & CO. KG, Berlin, Germany.

Sonication of all nanoparticle samples was carried out while cooling the samples on an ice bath (Settings: power 75%, cycle 70% MS 72/D).

pH Measurement

Equipment: SevenCompact™ pH/Ion S220 with a InLab® Micro special electrode, Mettler Toledo, Mettler-Toledo Ltd., Beaumont Leys, Leicester, United Kingdom.

The pH-meter was calibrated with commercially available buffer standards (pH 4.00, pH 7.00, and pH 11.00).

Scales

Equipment: Mettler Toledo Excellence Plus.
Sartorius™ M-Prove™ Scales AY303, Sartorius, Göttingen, Germany.

Samples below 200 mg were weighed on the fine balance from Mettler. For samples above 200 mg, the standard laboratory balance from Sartorius was used.

SDS Gel Electrophoresis

Equipment: Mini Vertical Electrophoresis Unit Hoefer SE260, Hoefer Inc., Holliston, Massachusetts, USA.

Syringe Pump

Equipment: World Precision Instruments, Sarasota, Florida, Model No. AL-4000

Protein-polymer conjugations were carried out using a syringe pump to ensure the slow and defined addition of one solution to another. The rate was set on 0.025 mL per h with a syringe diameter of 9 mm.

Particle Size Measurements

Equipment: Malvern Zetasizer Nano ZS, Malvern Instruments GmbH, Herrenberg, Germany.

NanoSight LM 10 microscope, Malvern Instruments GmbH, Herrenberg, Germany.

Sample Incubation

Equipment: Thermomixer pro, CellMedia, Elsteraue, Germany

Solvents

All solvents were either bought dry or dried before use. Methanol (Sigma-Aldrich) was purified before use by distillation with a rotary evaporator.

Water

Equipment: Direct-Q® 5 UV Remote Water Purification System, Merck Millipore, Germany.

Water (dd-H_2O) for buffers and particle washing steps was purified by a Direct-Q® 5 UV Remote Water Purification System. Water (dd-H_2O) used for the particle treatment was adjusted to pH 8 with triethylamine (TEA, Carl Roth, Germany, approx. 0.0015% (V/V)).

Zeta Potential

Equipment: Malvern Zetasizer Nano ZS, Malvern Instruments GmbH, Herrenberg, Germany.

5.3 SpAcDex Nanoparticles

5.3.1 Synthesis of Spermine-Functionalized Acetalated Dextran

The Synthesis of spermine-functionalized acetalated dextran was described before by *Cohen et al*..[88] The first step is the partial oxidation of dextran followed by an acetalation and functionalization with spermine.

Partial Oxidation of Dextran (OxDex)

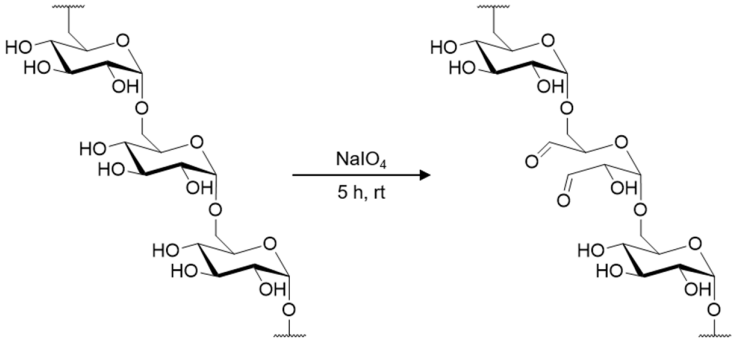

Sodium periodate (M = 213.89 g·mol^{-1}, 0.48 g, 2.25·10^{-3} mol, 0.2 eq) was added to a solution of dextran (M = 9–11 kDa, 2 g, 12.34·10^{-3} mol) in dd-H_2O (8 mL) and stirred for 5 h at room temperature. The resulting yellowish solution was dialyzed against dd-H_2O for 96 h using a regenerated cellulose membrane with MWCO of 3,500 g·mol^{-1}. After lyophilization overnight a colorless powder was obtained.

Yield: 1.6 g (80%)

Aldehyde content: 10.3 ± 0.01 mol aldehyde pro 100 mol AGU

Acetalation of Partially Oxidized Dextran (OxAcDex)

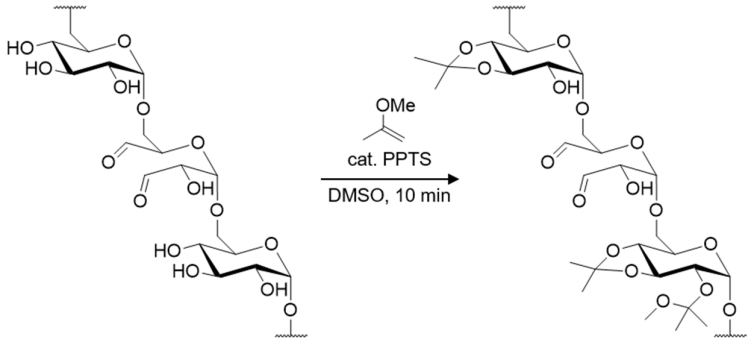

Partially oxidized dextran (1 g, $6.17 \cdot 10^{-3}$ mol) was dissolved in DMSO (12.5 mL) at room temperature. 2-methoxypropene (M = 72.11 g·mol^{-1}, 2.6 g, $3.6 \cdot 10^{-2}$ mol) was added slowly after addition of pyridinium *p*-toluenesulfonate (M = 251.30 g·mol^{-1}, 22 mg, $8.8 \cdot 10^{-5}$ mol). After 10 min the acetalation was quenched with the help of triethylamine (1 mL) The resulting reaction mixture was precipated in dd-H_2O pH 8 (100 mL) and isolated by centrifugation (12,000 g, 20 min, 4 °C). The product was further 5 times washed with dd-H_2O pH 8 and lyophilized overnight. The OxAcDex was obtained as a colorless powder. The degree of substitution (DS) of the Ox-AcDex was determined by ^1H-NMR spectroscopy in D_2O/DCl.[128] The acidic environment led to the deacetalation of Ox-AcDex back to Ox-Dex as well as methanol and acetone as by-products. Cyclic acetals disintegrate in acetone, whereas acyclic acetals break down in acetone and methanol. The resulting ^1H-NMR peaks were integrated and the following formulas were used to calculate the DS (**Figure 55**).

$$\mathrm{DS_{cyclic}} = \int \text{1 H MeOH} \div \int \text{1 H Polysaccharide Backbone} \qquad \text{eq. 5}$$

$$\mathrm{DS_{acyclic}} = \left[\left(\int \text{1 H Acetone} - \int \text{1 H MeOH}\right) \times 2\right] \div \int \text{1 H Polysaccharide Backbone} \qquad \text{eq. 6}$$

$$\text{Total DS} = \left(\mathrm{DS_{cyclic}} + \mathrm{DS_{acyclic}}\right) \div \text{Number Hydroxyl Groups per AGU} \qquad \text{eq. 7}$$

Yield: 0.77 g (64%)

Acetal content: acyclic content: 27.27% cyclic content: 46.46% total content: 73.73%

Modification of OxAcDex with Spermine (SpAcDex)

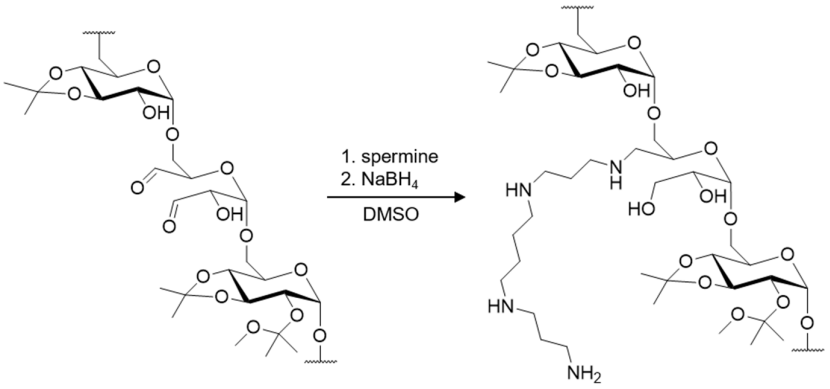

OxAcDex (770 mg) was dissolved in DMSO (3.8 mL) and spermine (M = 202.34 g·mol^{-1}, 770 mg, 3.8·10^{-3} mol) was added under Ar-atmosphere. The reaction mixture was stirred for 20 h at 40 °C. Sodium borohydride (37.83 g·mol^{-1}, 384 mg, 1·10^{-2} mol) was added and the reaction was stirred for additional 22 h at 50 °C. The resulting product was precipated in dd-H_2O pH 8 and the pellet isolated by centrifugation (12,000 g, 20 min, 4 °C) and washed 5 times with dd-H_2O pH 8 (20 mL) (12,000 g, 20 min, 4 °C). The colorless SpAcDex powder was obtained after lyophilization.

Yield: 810 mg (95%)

The degree of functionalization was determined by elementary analysis (C = 52,2%, H = 8,07%, N = 1,25%). Resulting in 3.62 mol spermine per 100 mol AGU

5.3.2 Preparation of SpAcDex Nanoparticles

Preparation of Empty SpAcDex Nanoparticles by Single Emulsion

SpAcDex nanoparticles were prepared by a single emulsion method using a probe sonicator. 10 mg SpAcDex were dissolved in 400 μL dichloromethane (DCM) and 2 mL polyvinyl alcohol (PVA) solution (3% w/w in PBS, 13–27 kDa, 87–89% party hydrolyzed) was added and an oil-in-water emulsion was performed by sonication for 30 s. The resulting emulsion was stirred overnight to remove all DCM by evaporation. SpAcDex NP were purified by ultracentrifugation (45,000 g, 20 min, 20 °C) and washed twice with dd-H_2O (pH 8). Before lyophilization 100 μL PVA solution (0.3% w/w in dd-H_2O pH 8) was added as cryoprotectant. The particle yield was about 65%, based on the initial SpAcDex material.

Encapsulation of Etoposide

1 mg etoposide was added next to 10 mg SpAcDex to the 400 μL DCM before the first sonification step of the single emulsion of the particle preparation.

Preparation of Empty SpAcDex Nanoparticles by Double Emulsion

As previously described SpAcDex nanoparticles were prepared by a double emulsion method using a probe sonicator. 10 mg SpAcDex were dissolved in 800 μL dichloromethane (DCM) and 100 μL PBS buffer was added for the first sonication step of 10 s. Then 4 mL PVA solution (3% w/w in PBS) was added and the secondary water-in-oil-in-water emulsion was performed by sonication for 30 s. The resulting emulsion was stirred overnight to remove all DCM by evaporation. SpAcDex NP were purified by ultracentrifugation (45,000 g, 20 min, 20 °C) and washed twice with dd-H_2O (pH 8). Before lyophilization 100 μL PVA solution (0.3% w/w in dd-H_2O pH 8) was added as cryoprotectant. The particle yield was about 65%, based on the initial SpAcDex material.

Encapsulation of Oregon Green 488 Dextran and CF750 Dextran

50 μg Oregon Green 488 dextran or a mixture of 50 μg Oregon Green 488 dextran and 150 μg CF750 dextran were added to the 100 μL PBS buffer before the first sonification step of the double emulsion particle preparation.

Encapsulation of L-Asparaginase

100 μg L-asparaginase was added to the 100 μL PBS buffer before the first sonification step of the double emulsion of the particle preparation. Particles with fluorescent-labeled L-asparaginase were prepared the same way.

L-Asparaginase labeling with Sulfo-Cyanin 5-NHS-Ester

The fluorescent-labeling was performed with a mixture of 1 mg L-asparaginase and $3.15 \cdot 10^{-8}$ mol Sulfo-Cyanin 5-NHS Ester in PBS buffer pH 7.4 for 2 h at RT. The non-reacted fluorescent dye was removed by NAP25-column purification.

Dual Encapsulation of L-Asparaginase and Etoposide by Double Emulsion

Dual-loaded SpAcDex nanoparticles were prepared by a double emulsion method using a probe sonicator. 10 mg SpAcDex were dissolved in 800 μL dichloromethane (DCM) with

1 mg etoposide and 100 μL PBS containing 100 μg L-asparaginase was added for the first sonication step of 10 s. Then 4 mL PVA solution (3% w/w in PBS) was added and the secondary water-in-oil-in-water emulsion was performed by sonication for 30 s. The resulting double emulsion was stirred overnight to remove all DCM by evaporation. SpAcDex NP were purified by ultracentrifugation (45,000 g, 20 min, 20 °C) and washed twice with dd-H_2O (pH 8). Before lyophilization 50 μL PVA solution (0.3% w/w in dd-H_2O pH 8) was added as cryoprotectant. The particle yield was about 65%, based on the initial SpAcDex material. Particles with fluorescent-labeled L-asparaginase were prepared the same way.

Preparation of SpAcDex Nanoparticles labeled with Oregon Green 488 NHS

Particles were suspended in PBS buffer pH 8 (2 mg·mL^{-1}) and 0.4 μL per mg particle Oregon Green® 488 NHS-ester in DMSO (10 mM) was added and stirred for 2 h at RT in the dark. Afterwards the unreacted dye was removed by Amicon® centrifugal filter (MWCO 30 kDa) (7,500 g, 10 min) and rinsing the pellet with dd-H_2O at pH 8 (five times, 2 mL each). Before lyophilization, 0.3% PVA was added as cryoprotectant and a yellow fluffy powder was obtained (approximately 90% of the initial weight).

Quantification of Conjugated Oregon Green 488 on SpAcDex Particle Surface

Oregon Green® 488-SpAcDex particles were dissolved in DMSO (1 mg·mL^{-1}) 100 μL particle solution were transferred in triplets to a black 96-well microtiter plate. A standard curve was prepared with the Oregon Green dye diluted in DMSO in a concentration from 31.25 to 1000 pmol·mL^{-1}. Each standard was transferred in triplets (100 μL) to the microplate and the fluorescence of Oregon Green 488 was detected with a Tecan microplate reader ($\lambda_{ex.}$ 488 nm, $\lambda_{em.}$ 514 nm).

5.3.3 Particle Characterization

Nanoparticle Tracking Analysis

The size of SpAcDex particles was determined by nanoparticle tracking analysis (NTA) with a NanoSight LM 10 microscope equipped with a green laser (532 nm) and a sCMOS camera. All NP samples were measured after sonication with videos of 30 s at 25 °C in triplets. The size calculation was performed with NTA software version 3.1 build 3.1.54

(software settings: Capture: screen gain: 1.0, camera level: 9; Process: screen gain 1.0, detection threshold 5).

Dynamic Light Scattering

Dynamic Light Scattering (DLS) was performed with nanoparticle samples suspended in PBS (filtered 0.22 μm) with a concentration of about 20 μg·mL^{-1} and sonicated for 20 seconds before measurements. Samples were prepared in polystyrene micro cuvettes (Brand) using 110 μL of freshly prepared particle solution. Generally, after equilibration to 20 °C, three measurements each consisting of 12 runs were performed. The refractive index (RI) of the dispersant (preset: water) was set to 1.330 and the viscosity to 1.0031 cP, respectively. The RI of the particle was set to 1.590. Both attenuator and measurement position were controlled by the instrument and Mark-Houwink parameters and all measurements were performed at a scattering angle of 173° (backscatter, NIBS default).

Zeta Potential

Zeta potential (particle charge) was measured with a Malvern Zetasizer Nano ZS instrument using a clear disposable zeta cell. Three measurements with 20 individual runs were performed at 25 °C. Particle samples were prepared at concentrations of 0.1 mg·mL^{-1} in HEPES buffer (25 mM, pH 7.4). The refractive index (RI) of the dispersant (preset: water) was adjusted to 1.330 and the viscosity to 0.8872 cP with a dielectric constant of 78.5. The RI of the particle material dextran was set to 1.590. The resulting data was analyzed using the model of Smoluchowski and the Malvern Zetasizer software 6.20.

5.3.4 Determination of Encapsulation

Quantification of Encapsulated Oregon Green 488 Dextran and CF750 Dextran.

The Oregon Green-labeled SpAcDex particles (5 mg·mL^{-1}) were dissolved in 0.1 M acetate buffer (pH 5) for 24 h under stirring. To analyze the content of encapsulated Oregon Green® 488 dextran, 10 μL of NP suspension was added to 90 μL PBS buffer pH 8 and measured by fluorescence spectroscopy in triplets using a Tecan Infinite M200 Pro microplate reader ($\lambda_{ex.}$ 496 nm, $\lambda_{em.}$ 524 nm). The concentration was calculated using a

calibration curve in the range of 0.031 μg·mL^{-1} to 2 μg·mL^{-1} (**Figure 65**). Analogical the quantification with CF750 Dextran was performed with a calibration curve in the range of 0.093 μg·mL^{-1} to 6 μg·mL^{-1} ($\lambda_{ex.}$ 750 nm, $\lambda_{em.}$ 780 nm) (**Figure 66**).

Quantification of Active Encapsulated L-Asparaginase

For the quantification of enzymatical active entrapped L-asparaginase SpAcDex(Asp) NPs, SpAcDex(Asp+Eto) NPs and empty SpAcDex NPs were incubated in NaOAc buffer at pH 5 for 48 h in a concentration of 2 mg·mL^{-1}. 100 μL dissolved particle suspension or 100 μL asparaginase standard solution were added to 500 μL 0.1 M TRIS pH 8.6 and 250 μL 0.01 M L-asparagine in 0.1 M TRIS pH 8.6. The asparaginase reaction was carried out for 30 min at 37 °C and then quenched with 250 μL 15% TCA. After addition of 250 μL Nessler's reagent and incubation for 10 min the number of produced ammonium-ions was quantified by absorption at a wavelength of λ = 425 nm. The calculation of the L-asparaginase activity was performed with an asparaginase standard in a concentration range from 0.03125–3 μg·mL^{-1} combined with Asp-loaded particles in contrast to empty particles (**Figure 64**).

For quantification of the released encapsulated L-asparaginase the test was performed analogous after different incubation times (0 h, 1 h, 2 h, 4 h, 6 h, 8 h, 24 h) in NaOAc buffer at pH 5 (2 mg·mL^{-1}) or PBS buffer pH 7.4 (2 mg·mL^{-1}) and 37 °C.

BCA Assay for Quantification of the Encapsulated L-Asparaginase

BCA assay for the L-asparaginase quantification was carried out analogous to Roti® Quant instructions for microtiter-plates by Carl Roth®. For this a standard curve with asparaginase from 1.25 μg·mL^{-1} to 40 μg·mL^{-1} in 0.1 M NaOAc buffer at pH 5 was performed (**Figure 63**). SpAcDex(Asp) and SpAcDex(Asp+Eto) particles were dissolved in the same buffer for 48 h in a concentration of 2 mg·mL^{-1}. 50 μL of standard/sample was added as a triplet to 100 μL BCA-solution in a 96-Well transparent plate. After 10 min incubation time the protein content quantified at a wavelength of λ = 595 nm. The calculation was performed with SpAcDex(Asp) and SpAcDex(Asp+Eto) in contrast to empty SpAcDex particles.

Quantification of Encapsulated Etoposide

For the quantification of encapsulated etoposide, the particles were dissolved in DMSO at a concentration of 0.5 mg·mL^{-1}. Afterwards the analyses were made with an HPLC-Agilent 1100 instrument at λ = 254 nm equipped with a C18 column. The solvent system consisted of acetonitrile:water 65:35 v/v, an injection volume of 5 μL and a flow rate of 0.6 mL·min^{-1}. Etoposide was detected at a retention time of 3.6 min.

For the quantification a standard was used in a range from 1.56–100 μg·mL^{-1} and the encapsulation was calculated with Microsoft Excel (**Figure 62**).

The release of encapsulated etoposide was performed with particles in 0.1 M NaOAc buffer at pH 5 or PBS buffer pH 7.4 at a concentration of 0.5 mg·mL^{-1}. The content of etoposide was quantified like the payload by the same HPLC-method but after different incubation times (0 h, 1 h, 2 h, 4 h, 6 h, 8 h) at 37 °C.

5.3.5 PEGylation of SpAcDex NPs

PEGylation of SpAcDex Nanoparticles with NHS-PEG-Mal

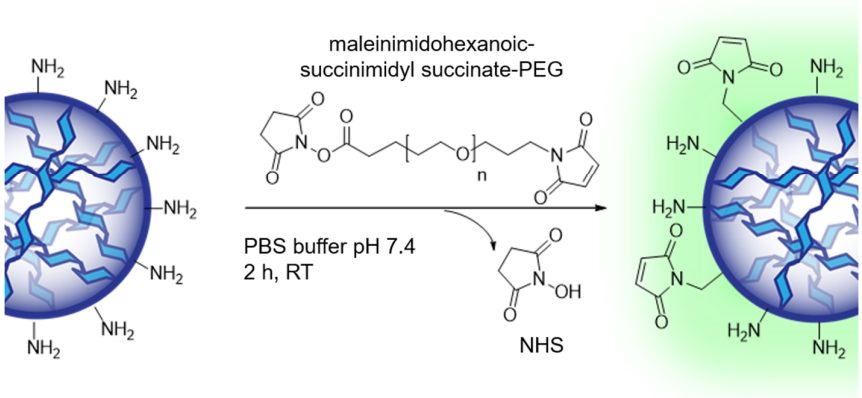

NP were resuspended in PBS (pH 7.4) at a concentration of 2 mg·mL^{-1} and α-maleinimidohexanoic-ω-NHS PEG (NHS-PEG-Mal, 5 kDa, dissolved in PBS (50 mg·mL^{-1})) was added. The required amount of conjugation reagent was, as previously described, estimated based on average results shown by fluorescamine assays.[355] The reaction mixture was incubated under stirring for 2 h at RT. Particles were purified by ultracentrifugation (45,000 g, 20 min, 20 °C) and rinsing the pellet with dd-H_2O at pH 7 (twice, 2 mL each). Before lyophilization, 0.3% PVA in dd-H_2O at pH 7 was added as cryoprotectant and a colorless fluffy powder was obtained (approx. 75% of the initial weight).

5.3.6 Determination of PEGylation

Quantification of Maleimide-PEG on Surface of SpAcDex particles by Ellman's Assay

The particles were suspended in PBS (10 mM EDTA, pH 7.4, 1 mg·mL^{-1}) with an excess of 2-aminoethanethiol (750 nmol·mg^{-1} NP). After 5 h reaction time the unreacted 2-aminoethanthiol was quantified via Ellman`s assay to determine indirectly the amount of maleimide on the particle surface. For this, 30 μL DNTB (4 mg·mL^{-1} in reaction buffer) was added to a standard row of 2-aminoethanethiol (0.3–1.65 mM in reaction buffer), blank and the NP suspension (100 μL). The solutions were incubated for 15 min under gentle agitation and the absorbance was read with a Tecan microplate reader at λ = 412 nm after addition of 100 μL DMSO to all samples to dissolve the nanoparticles. All samples were prepared and measured in triplets (**Figure 68**).

Fluorescence Assay for Maleimide-PEG Quantification with Fmoc-*L*-Cysteine

Alternatively, the degree of PEGylation was determined by using a fluorescence method (using Fmoc-L-cysteine) for the detection of the maleimides on the particle surface of the PEGylated NPs. For this, Mal-PEG-Sp-Ac-Dex NPs were suspended in PBS (1 mM EDTA pH 7.4, 1 mg·mL^{-1}) and Fmoc-L-Cys-OH*H_2O (5x molar excess, 750 nmol·mg^{-1}) was added. After 5 h reaction time the particles were purified by ultracentrifugation (45,000 g, 20 min, 20 °C) and rinsing the pellet with dd-H_2O pH 8 (4-times, 2 mL). Before lyophilization, 0.3% PVA was added as cryoprotectant and after freeze-drying a white fluffy powder was obtained (yield: approx. 85% from initial weight).

For the determination of Fmoc-L-Cys molecules, nanoparticles were dissolved in DMSO at concentrations of 1 mg·mL^{-1}. Pure Fmoc-L -Cys-OH dissolved in DMSO was used in a standard curve with concentrations ranging from of 6.25–100 nmol·mL^{-1} (**Figure 67**). Each standard and sample (100 μL) was added in triplets to a black, flat bottom 96-well microplate and the fluorescence was read with a Tecan microplate reader ($\lambda_{ex.}$ 265 nm, $\lambda_{em.}$ 315 nm). The amount of Fmoc-L-Cys on the particle surface was calculated in Microsoft Excel.

Surface Density of Maleimide-PEG on Surface

SpAcDex particles with an average diameter of 180 nm have a surface area of 101,787 nm^2. In the case of 29,286 PEG chains (5 kDa) on the particle surface (determined by Ellman´s excess assay, Fmoc-Cys determination); one PEG chain is grafted per 3.5 nm^2 for 5 kDa PEG. Hence the distance between two PEG chains is approx. 2.1 nm. From this

distance, the conformation of the polymer on the surface of the particle surface can be estimated. The minimal distance required between grafted polymers on a surface to form a mushroom conformation is defined as the Flory radius (R). Polymers with less space than R have lower conformational freedom and a brush conformation is obtained. The following equation 8 is used to calculate R with the polymer chain length (n), monomer length (α) and solvent type (ν):

$$R = \alpha n^{\nu} \qquad \text{eq. 8}$$

For a 5 kDa PEG chain in water this results in R = 6 nm (α = 0.35 nm, n = 114, ν = 3/5). The distance between the chains is therefore smaller than the Flory radius. Accordingly, it can be concluded that a brush like structure of the PEG chains is present.

5.3.7 Antibody Conjugation on PEGylated SpAcDex NPs

Modification of DEC205 Antibody with SATA

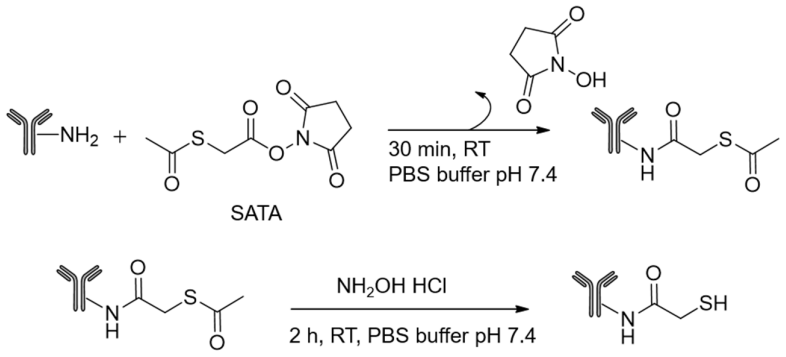

The modification with *N*-Succinimidyl-*S*-acethylthioacetate (SATA) was carried out according to manufacturer's protocol. Briefly, 5 μL SATA (dissolved in DMSO, 55 mM) was added to a 35 μM antibody solution (in PBS, pH 7.4) and incubated at room temperature for 30 min. Afterwards, SATA-modified antibodies were washed and purified with PBS (pH 7.4) via Vivaspin® 15R filter (6,000 g, 12.5 mL, 25 min). Deacetylation of the SATA-modified antibody was accomplished with a deacetylation solution containing 0.5 M hydroxylamine and 25 mM EDTA within a reaction time of 2 h at room temperature. The purification afterwards was carried out via Vivaspin® 15R filter (MWCO 30 kDa) with 10 mM EDTA in PBS (pH 7.4, 6,000 g, 12.5 mL, 25 min).

Conjugation of SATA-modified Antibody to Mal-PEG-SpAcDex Nanoparticles

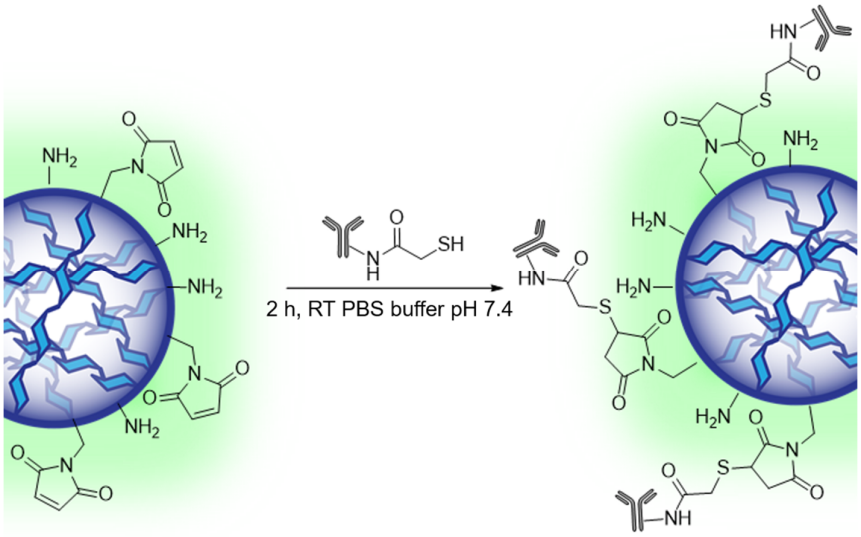

The conjugation between thiol-modified anti-DEC205 mAb and Mal-PEG-SpAcDex NP was performed by mixing 4 mg particles with 3.675 mg antibody in a total volume of 1 mL PBS (pH 7.4) for 2 h at RT. Then 50 mM L-cysteine was added to get rid of non-reacted maleimide. As a control, Mal-PEG-SpAcDex NPs were incubated only with L-cysteine for 16 h without any further addition of antibodies. Particles were purified by centrifugation (30,000 g, 20 min, 20 °C) and washed twice with dd-H_2O pH 8. Before lyophilization 40 μL PVA solution (0.3% w/w in dd-H_2O pH 8) was added as cryoprotectant.

5.3.8 Determination of Antibody-functionalization of SpAcDex NPs

Ellman's Assay for Quantification of SATA-Modification on Antibody

Ellman's reagent (5,5'-dithio-bis-(2-nitrobenzoic acid), DTNB) was used to determine the amount of introduced and deprotected sulfhydryl groups of the SATA-modified antibody. The reaction of DTNB with the sulfhydryl groups of the sample leads to the yellow by-product TNB^{2-} (2-nitro-5-thiobenzoic acid) with an absorbance maximum at 412 nm. SATA-modified and unmodified antibody, as negative control, were dissolved in PBS buffer (7.35 mg·mL^{-1}) for further analysis. DTNB was dissolved in sodium phosphate buffer (0.1 M, pH 8 containing 1 mM EDTA) and 4 μL of Ellman`s reagent solution has been added to a mixture of 200 μL reaction buffer and 25 μL sample/standard in a 96-well microplate. *N*-acetyl-*L*-cysteine was prepared in a concentration of 31.25 μM to 1 mM and used as standard (**Figure 69**). After incubation for 15 min the absorbance of all samples

and standards were measured with a Tecan pro 200M microplate reader at a wavelength of λ = 412 nm to determine the amount of thiol groups.

Bradford Assay for Quantification of the Attached Antibody

Bradford assay for the antibody quantification was carried out analogous to Roti®-Quant instructions for microtiter-plates by Carl Roth®. For this a standard curve with anti-DEC205 from 10 μg·mL^{-1} to 100 μg·mL^{-1} in NaOAc buffer at pH 5 was performed (**Figure 70**). Mal-PEG-SpAcDex and anti-DEC205-PEG-SpAcDex particles were dissolved in the same buffer overnight in a concentration of 2 mg·mL^{-1}. 50 μL of standard or sample was added as a triplet to 200 μL Bradford solution (5.5 parts buffer to 2 parts conc. dye) in a 96-Well transparent plate. After 10 min incubation time the protein content was quantified at a wavelength of λ = 495 nm with a Tecan plate reader. The calculation was performed with Microsoft Excel with anti-DEC205-PEG-SpAcDex in contrast to Mal-PEG-SpAcDex particles.

Estimation of the Average Number of Antibodies per Nanoparticle

Assuming that the SpAcDex NPs have a density like PLGA NPs (1.34 g·cm^{-3})

$$m_{NP} = \rho \cdot V = 1.34 \frac{g}{cm^3} \cdot 4.99 \cdot 10^{-15} cm^3 = 6.68 \cdot 10^{-15} g \quad \text{eq. 9}$$

$$\text{Amount of NPs in 1 mg sample: } = \frac{0.001\ g}{6.68 \cdot 10^{-15} g} = 1.496 \cdot 10^{11} \text{NPs per mg} \quad \text{eq. 10}$$

$$\text{Antibody (Bradford) } 2.7 \frac{\mu g}{mg}\ ;\ n = \frac{2.7\ \mu g}{160{,}000 \frac{g}{mol}} \quad \text{eq. 11}$$

$$\text{Antibody are } 1.69 \cdot 10^{-11} \text{mol} \cdot \text{Avogadro constant} = 1.01 \cdot 10^{13} \quad \text{eq. 12}$$

$$\text{Amount of antibody per particle are: } \frac{1.01 \cdot 10^{13}}{1.496 \cdot 10^{11}} = 67.9 \quad \text{eq. 13}$$

Analogous for ELISA

Antibody (ELISA): 0.23 $\frac{\mu g}{mg}$

Amount of antibody per particle are: 5.78

5.3.9 Cell Culture

K562 cells were grown in preheated Roswell Park Memorial Institute medium (RPMI L-Glutamine) supplemented with 10% (V/V) fetal calf serum (FCS), 1% pyruvate, and 1% penicillin-streptomycin. Cell incubations were performed in a humidified incubator at 37 °C with 5% CO_2 atmosphere.

Determination of Cell Viability by MTT Assay with K562 Cells

The cytotoxic effects of the SpAcDex(Asp) NP SpAcDex(Eto) NP and the SpAcDex(Asp+Eto) NPs were evaluated by MTT assay using non adherent human myelogenous leukemia K562 cells. Cells were precultured in RPMI and seeded at a concentration of 15,000 cells per well in a 96 well-plate and a volume of 50 μL. The nanoparticle samples were prepared with RPMI in a concentration range from 62.5 $\mu g \cdot mL^{-1}$ to 2 $mg \cdot mL^{-1}$. 50 μL of the sample solutions as well as RPMI as blank solutions were added to each well. All measurements were carried out in triplets. After 48 h incubation at 37 °C 50 μL MTT solution (5 $mg \cdot mL^{-1}$ in RPMI) was added to each well and incubated at 37 °C for 2 h.

A mixture of 89 μL DMSO and 11 μL glycine buffer (0.1 M glycine, 0.1 M NaCl, pH 10.5) was added to each well and shaken for 30 min. The absorbance of the formazan was determined at a wavelength of λ = 595 nm and a reference wavelength of λ = 670 nm using a Tecan Infinite 200 PRO microplate reader. Cell viability (%) was calculated relative to the control wells that contained the cell culture medium without samples.

Confocal Microscopy

K562 cells were incubated with 62.5 $\mu g \cdot mL^{-1}$ Oregon Green 488-SpAcDex(Asp-Cy5) NP and Oregon Green 488-SpAcDex(Asp-Cy5+Eto) particles in a 12-well plate (350,000 cells per well). After 4 h, the cells were plated on Poly-L-lysin (0.1 $mg \cdot mL^{-1}$ MW > 300,000) coated cover slips in 12-well plates for 20 h. Afterwards the cells were washed 3 times with PBS and fixed with Roti®-Histofix. After 30 min incubation time at 4 °C fixed cells were incubated with DAPI solution (1 $\mu g \cdot mL^{-1}$) in PBS for 30 min and washed 3 times with fresh PBS. The cover slips were put on mounting medium on object slides and analyzed with a Leica TCS SP5 Microscope. The image analysis was performed with Fiji software.

5.4 HRP-AcDex Nanoparticles

5.4.1 Synthesis of Thiol-functionalized Acetalated Dextran

The Synthesis of thiol-functionalized acetalated dextran was described before by *Breitenbach et al*..[279] The first step is the thiol modification of dextran followed by a thiol activation with 2,2'-Dipyridyl disulfide and acetalation of the dextran.

Thiol End-Functionalized Dextran (Dex-SH)

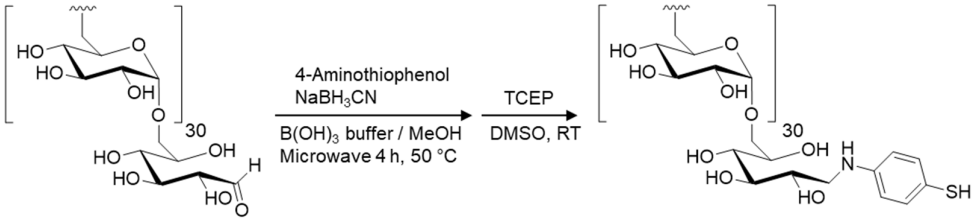

Dextran 5 kDa (200 mg, 0.04 mmol, 1 eq) was dissolved in 1.6 mL of $B(OH)_3$ buffer (0.1 M, pH 8.5) in a sealed microwave vial. 4-Aminothiophenol (50.2 mg, 0.4 mmol, 10 eq) in 1.6 mL MeOH and $NaCNBH_3$ (30.2 mg, 0,48 mmol, 12 eq) were added under stirring. The reductive amination in the microwave was performed for 4 h at 50 °C with maximum microwave power set to 100 W. The product was precipitated in a 10-fold excess of MeOH, centrifuged down (12,000 g, 20 min, 4 °C) and washed 2 times with MeOH. The resulting pellet was dissolved in 2 mL dd-H_2O and adding of TCEP (22.9 mg, 0.08 mmol, 2 eq) induced a change of the solution color from yellow to colorless. The solution was left to stir overnight, precipitated in MeOH and centrifuged (12,000 g, 20 min, 4 °C). After washing with MeOH for additional 2 times, the pellet was dissolved in dd-H_2O and freeze-dried. The purified product was obtained as a colorless powder.

Yield: 155 mg (78%)

^{1}*H*-NMR (300 MHz, D_2O): δ = 7.27 (d, 2 H), 6.79 (d, 2 H), 5.37–4.87 (m, 30 H), 4.07–3.35 (m, AGU).

Thiol-Activated Dextran (Dex-S-S-Py)

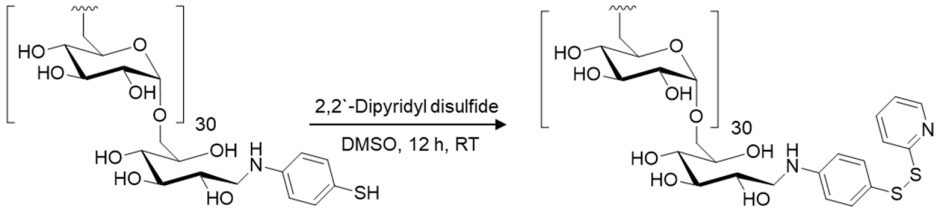

Dex-SH (137 mg, 0.03 mmol, 1 eq) was dissolved in DMSO (additional 3% dd-H_2O) and mixed with 2,2'-dipyridyl disulfide (14.0 mg, 0.05 mmol, 2 eq) in DMSO. The final volume of DMSO was 10.6 mL, whereas Dex-SH was dissolved in the greater amount of about 9 mL. The solution was allowed to stir overnight. The crude product was precipitated in a 10-fold excess of MeOH and centrifuged (15,000 g, 20 min, 4 °C). After washing with MeOH for two times, the resulting yellowish pellet was dissolved in 3 mL dd-H_2O and dialyzed against d-H_2O (MWCO 1 kDa) for 24 h. After freeze drying, the purified product was obtained as a yellowish powder.

Yield: 89 mg (65%)

^{1}*H*-NMR (300 MHz, D_2O): δ = 8.41 (1 H), 7.85 (2 H), 7.45 (2 H), 7.33 (1 H), 6.73 (2 H), 5.39–4.89 (m, 30 H), 4.09–3.33 (m, AGU).

Acetalated Thiol-Activated Dextran (AcDex-S-S-Py)

The acetalization was carried out after a protocol by the Fréchet group as follows: A sealed vial was charged with Dex-S-S-Py (86 mg, 0.02 mmol, 1 eq) in anhydrous DMSO (1.75 mL) and mixed with PPTS (2.8 mg, 0.01 mmol, 0.64 eq) under an argon atmosphere. Then, 0.75 mL of 2-methoxypropene (6.5 mmol, 380 eq) were added dropwise and the solution was stirred for 60 min. The reaction was quenched by adding 0.18 mL of TEA, and the product was precipitated in dd-H_2O (pH 8). The product was isolated by centrifugation (15,000 g, 20 min, 20 °C) after 3 washing steps. The pellet was lyophilized, and the product was obtained as a fluffy colorless powder.

Yield: 99 mg (91%)

^{1}H-NMR (300 MHz, D_2O): δ = 3.88–3.23 (m, AGU), 3.12 (s, MeOH), 2.00 (s, acetone).

Acetal content: determined by ^{1}H-NMR 300 MHz, D_2O/DCl): total acetals 83%, 31% acyclic acetals, 52% cyclic acetals.

5.4.2 HRP Modification

SATP Modification of HRP

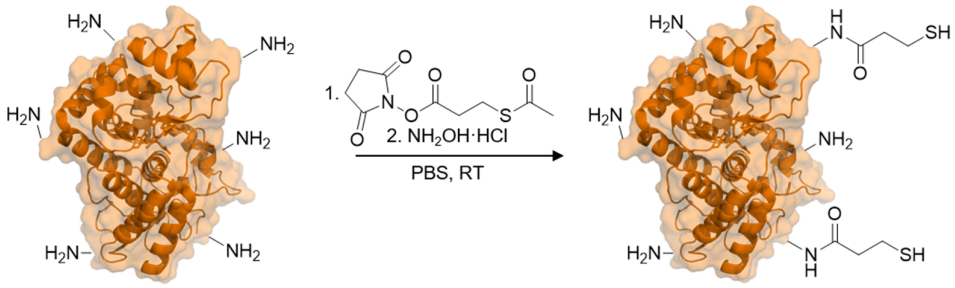

Thiol modified HRP were prepared according to the procedure described by the distributor (Thermo Scientific) as follows: HRP was dissolved in 1 mL PBS buffer and combined with 10 μL of a freshly prepared SATP solution (55 μM in DMSO). The combined components were incubated for 1 h and centrifuged 5 times with PBS at 7,500 g, for 10 min at 4 °C with a centrifugal filter unit (MWCO 10 kDa). To deprotect the thiol groups the protein was dissolved in 1 mL PBS buffer and mixed with 100 μL deacetylation solution (87 mg $NH_2OH{\cdot}HCl$, 18.3 mg Na_2EDTA, 2 mL PBS buffer, 0.5 mL dd-H_2O). After 2 hours of incubation at room temperature and 4 centrifugation runs using PBS buffer with 10 mM EDTA, the protein was used for conjugation immediately.

Cy5-Modification of HRP

10 mg·mL^{-1} HRP in phosphate buffer 0.1 M pH 7.4 was mixed with 0.19 mg Cy5-Sulfo NHS. The combined components were incubated for 1.5 h at rt in the dark and centrifuged with a centrifugal filter unit (MWCO 10 kDa) 8 times with dd-H_2O (7,500 g, 15 min, 4 °C). After resuspending in dd-H_2O the blue product was lyophilized (yield 60%).

Quantification of Cy5 (Cy5-HRP)

The Cy5-labeled HRP (1 mg·mL^{-1}) was dissolved in DMSO. To analyze the content of Cy5 the fluorescence was measured in triplets using a Tecan Infinite M200 Pro microplate

reader ($\lambda_{ex.}$ 645 nm, $\lambda_{em.}$ 675 nm). The concentration was calculated using a calibration curve in the range of 0.04 μg·mL^{-1} to 5 μg·mL^{-1} (**Figure 76**).

Fluorescamine Assay

For the quantification of the SATP-modification samples of modified protein were prepared in a concentration of 2 mg·mL^{-1}. 125 μL of PBS buffer were pipetted into each well of 96-black-well-microplate and 25 μL of standard native HRP (11–23 μM) or sample solution were added in triplets (**Figure 71**). After addition of 50 μL of an ice-cold 0.3 mg·mL^{-1} fluorescamine solution (in acetone), the emission was immediately measured ($\lambda_{ex.}$ 380 nm, $\lambda_{em..}$ 460 nm).

5.4.3 Preparation of HRP-AcDex Particles

Conjugation of SATA-modified HRP with AcDex-S-S-Py

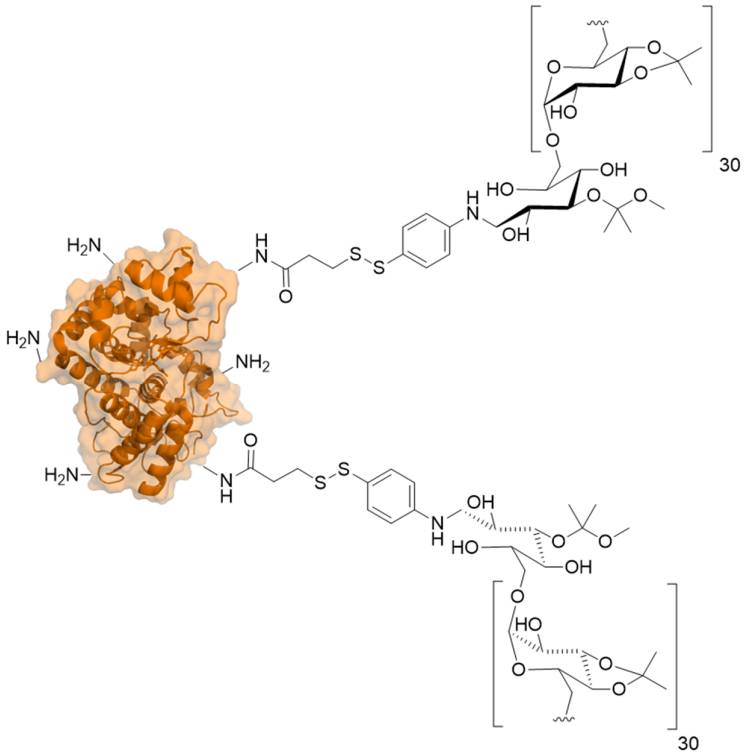

Freshly deprotected SATP-modified HRP (5 mg) was dissolved in 2 mL 10 mM EDTA PBS buffer and AcDex-S-S-Py (4.2 mg) in DMSO (750 μL), respectively. For conjugation both solutions were mixed 0.025 mL·h^{-1} slowly under stirring at room temperature using a syringe pump (protein to polymer conjugation).

For encapsulation of IAA (5 mg) or 5/6 FAM (5 mg) these substances were present in the DMSO-phase next to the AcDex-S-S-Py in the conjugation step. Afterwards the reaction mixture was dialyzed against dd-H_2O pH 8 for 24 h. Following a centrifugation step (7,500 g, 10 min, 4 °C). The supernatant was lyophilized, and a light-brown powder was obtained

Yield: 3.92 mg

5.4.4 Particle Characterization

Dynamic Light Scattering

Dynamic Light Scattering (DLS) was performed with nanoparticle samples suspended in PBS (filtered 0.22 μm) with a concentration of about 100 $\mu g \cdot mL^{-1}$. Samples were prepared in polystyrene micro cuvettes using 130 μL of freshly prepared particle solution. Generally, after equilibration to 20 °C, three measurements each consisting of 12 runs were performed. The refractive index (RI) of the dispersant (preset: water) was set to 1.330 and the viscosity to 1.0031 cP, respectively. The RI of the particle was set to 1.590. Both attenuator and measurement position were controlled by the instrument and Mark-Houwink parameters and all measurements were performed at a scattering angle of 173° (backscatter, NIBS default).

Zeta Potential

Zeta potential (particle charge) was measured with a Malvern Zetasizer Nano ZS instrument using a clear disposable zeta cell. Three measurements with 20 individual runs were performed at 25 °C. Particle samples were prepared at concentrations of 0.1 $mg \cdot mL^{-1}$ in HEPES buffer (25 mM, pH 7.4). The refractive index (RI) of the dispersant (preset: water) was adjusted to 1.330 and the viscosity to 0.8872 cP with a dielectric constant of 78.5. The RI of the particle material dextran was set to 1.590. The resulting data was analyzed using the model of Smoluchowski and the Malvern Zetasizer software 6.20.

BCA Assay for Quantification of the Protein Content in HRP-AcDex

BCA assay for the quantification of HRP within HRP-AcDex was carried out analogous to Roti®-Quant instructions for microtiter-plates by Carl Roth®. For this a standard curve

with HRP from 0.06 mg·mL^{-1} to 1 mg·mL^{-1} in dd-H_2O was performed (**Figure 72**). HRP-AcDex particles were dissolved in the same solvent in a concentration of 0.4 mg·mL^{-1}. 50 μL of standard/sample was added as a triplet to 100 μL BCA-solution in a 96-Well transparent plate. After 10 min incubation time the protein content quantified at a wavelength of λ = 492 nm. The quantification was analyzed with Microsoft Excel.

Degradation Experiment of HRP-AcDex Particles

A stock solution of freeze-dried particles was prepared with 20 mg·mL^{-1} and diluted with either NaOAc buffer, DTT, PBS or DMEM solution to reach a concentration of 10 mg·mL^{-1} in NaOAc buffer (50 mM, pH 5), DTT (10 mM), PBS buffer or DMEM. The samples were placed in a micro cuvette and measured for 24 h by DLS.

Quantification Cy5 Content of HRP-AcDex

The Cy5-labeled HRP-AcDex (1 mg·mL^{-1}) was dissolved in DMSO. To analyze the content of Cy5 the fluorescence was measured in triplets using a Tecan Infinite M200 Pro microplate reader ($\lambda_{ex.}$ 645 nm, $\lambda_{em.}$ 675 nm). The concentration was calculated using a calibration curve of Sulfo-Cy5-NHS in the range of 0.04 μg·mL^{-1} to 5 μg·mL^{-1} in DMSO (**Figure 76**).

Quantification of Encapsulated IAA in HRP-AcDex(IAA)

For the quantification of encapsulated IAA, the HRP-AcDex(IAA) particles were dissolved in DMSO at a concentration of 1 mg·mL^{-1}. Afterwards the analyses were made with an HPLC-Agilent 1100 instrument at 254 nm equipped with a C18 column. The solvent system consisted of acetonitrile:water 20:80 v/v, an injection volume of 5 μL and a flow rate of 0.6 mL·min^{-1}. IAA was detected at a retention time of 4.2 min.

For the quantification a standard was used in a range from 3.125–200 μg·mL^{-1} and the encapsulation was calculated with Microsoft Excel.

Release of Encapsulated IAA from HRP-AcDex(IAA)

IAA was encapsulated in HRP-AcDex particles, like described in the experimental section. To visualize the release of IAA under acidic conditions and from the particles, four samples of the particle solution (5 mg·mL^{-1}, 100 μL) were placed in a ZelluTrans Mini Dialyzer MD100 (MwCO 6,000–8,000, Carl-Roth, Germany) and dialyzed against 1.6 mL

NaOAc buffer (0.1 M, pH 5) or phosphate buffer (0.1 M, pH 7.4). The dialysis buffer was exchanged after 1, 2, 3, 4, 6, 8, 24, 32, 48 h. Each dialyzed sample was lyophilized, and the resulting pellet resuspended in 100 μL. The absorbance was recorded as triplet in a 96-well microplate on an Infinite® 200 PRO Tecan plate reader at λ = 280 nm. Quantification of the released IAA content was calculated with a standard curve in the range of 0.2 μg·mL^{-1} to 100 μg·mL^{-1} and calculated with Microsoft Excel (**Figure 74**).

ABTS Assay

The peroxidase activity of HRP-AcDex was measured by using 2,2'-azinobis-(2-ethylbenzthiazoline-6-sulfonate) (ABTS). The assay mixture contained 1 M phosphate pH 7.4 buffer, 0.3% hydrogen peroxide (6.7 μL), the native enzyme and HRP-AcDex (0.01 mg·mL^{-1} enzyme, 3.3 μL) and ABTS (0.05 mM) in a total volume of 200 μL. The reaction was initiated by addition of H_2O_2. The assay was performed in a 96-wellmicroplate and the increase in absorbance at 405 nm was measured with a Tecan Infinite® M200 Pro Plate Reader. All measurements were investigated for 3 min and analyzed with Microsoft Excel.

SDS-PAGE

For HRP and HRP-AcDex an 8% Gel was performed. Samples were prepared by mixing 15 μL of a 4 mg·mL^{-1} stock solution (in H_2O) with 5 μL of sample loading buffer and incubating in a heating water bath for 15 min. Therefore, Roti®-Load 1 was used when reduction of disulfide bridges was desired, otherwise a loading buffer (80 mg·L^{-1} bromophenol blue, 0.22 g·L^{-1} TRIS, 30% glycerin in H_2O) was used. 0.8 g SDS (8% w/v). Stock solution of native proteins were prepared in a concentration of 1 mg·mL^{-1}. 20 μL of each sample or 5 μL PageRuler prestained protein ladder were pipetted into the gel pockets, empty pockets were loaded with 5 μL loading buffer. A voltage of 90 mV up to 200 mV was applied until sufficient separation of the samples could be observed. The gel was stained with coomassie blue G250.

CD-Spectroscopy

CD spectra were recorded on a J-815 (JASCO) using the software Spectra Manager 2.12.00. UV CD spectra (X-190 nm) were recorded at 20 °C with a total enzyme concentration of 0.1 mg·mL^{-1} in 10 mM K_3PO_4 / 50 mM Na_2SO_4 pH 7 buffer using quartz cells with a path

length of 1 mm. All spectra were corrected by subtraction from the background (buffer). Data points were collected at a resolution of 1 nm. DICHROWEB using CONTIN-LL method (reference set 7)

TEM

HRP-AcDex particles have been diluted in dd-H_2O (1 mg·mL^{-1}). 5 μL of the nanoparticle solution were dropped on a 300-mesh copper carbon grid from Plano GmbH for TEM measurements. TEM images were recorded on a Tecnai T12 (FEI, acceleration voltage: 120 kV, lens: BIO-TWIN, electron source: LaB6 cathode) equipped with a 4K CCD camera (Tietz).

5.4.5 Cell Culture

Hela cells were grown in preheated DMEM GlutaMax supplemented with 10% (V/V) fetal calf serum (FCS), 1% pyruvate, and 1% penicillin-streptomycin. Cell incubations were performed in a humidified incubator at 37 °C with 5% CO_2 atmosphere

Determination of Cell Viability by MTT Assay with HeLa Cells

HeLa cells were cultured in 96-well microplates at a concentration of 15,000 cells per well and a volume of 100 μL of DMEM. HRP-AcDex(IAA) was dissolved at a concentration of 0.125 mg·mL^{-1} up to 1 mg·mL^{-1} in medium and added as triplets to the HeLa cells. After an incubation time of 72 h (37 °C, 5% CO_2) a solution of 3-(4,5-dimethyl-2-thiazolyl)-2,5-diphenyl-2H-tetrazolium bromide (MTT) in medium (40 μL, 3 mg·mL^{-1}) was added directly to each well and the plate was incubated for additional 20 min. The complete medium was removed and replaced by 200 μL of DMSO and 25 μL of glycine buffer (0.1 M glycine, 0.1 M NaCl, pH 10.5), followed by 20 min shaking to dissolve the purple formazan crystals. Finally, the absorbance was measured at λ = 595 nm using a Tecan Infinite® M200 Pro Plate Reader. Furthermore, the background was measured at λ = 670 nm and subtracted from the data obtained from the first read out. Cell viability was normalized to the absorbance measured from untreated cells. The resulting data was analyzed with Microsoft Excel.

Confocal Microscopy

HeLa cells were incubated with 0.75 mg·mL^{-1} Cy5-HRP-AcDex(5/6 FAM) in a 12-well plate (80,000 cells per well) for 24 h. Afterwards the cells were washed 3 times with PBS and fixed with Roti®-Histofix (1 mL). After 30 min incubation time at 4 °C fixed cells were incubated with DAPI solution (1 μg·mL^{-1}) in methanol for 30 min and washed 3 times with methanol. The cover slips were put on mounting medium on object slides and analyzed with a Leica TCS SP5 Microscope. The image analysis was performed with Fiji software.

6 Appendix

6.1 List of Abbreviations

Abbreviation	Meaning
Ø	diameter
Abs.	absorbance
ABTS	2,2'-azino-bis(3-ethylbenzothiazoline-6-sulphonic acid)
Ac	acetalated
Ag	antigen
AGU	anhydrous glucose unit
ALL	acute lymphoblastic leukemia
AML	acute myeloid leukemia
Anti	antibody
APC	antigen-presenting cell
Approx.	approximately
ASNS	asparagine synthetase
Asp	L-asparaginase
BMDC	bone-marrow derived dendritic cell
CD	cluster of differentiation
CD	circular dichroism
$CDCl_3$	deuterated chloroform
CML	chronic myelogenous leukemia
CLSM	confocal laser scanning microscopy
conc.	concentration
CTL	cytotoxic T cell
L-Cys	L-cysteine
dd-	double distilled
Da	dalton
DAPI	4',6-diamidino-2-phenylindole
DC	dendritic cell
DCl	deuterium chloride
DCM	dichloromethane
Dex	dextran
DLS	dynamic light scattering
DMEM	Dulbecco's modified Eagle's medium
DMSO	dimethyl sulfoxide
d.nm	particle size in diameter (nm scale)
DS	degree of substitution
DTNB	5,5'-dithio-bis-(2-nitrobenzoic acid)
EDC	*N*-(3-dimethylaminopropyl)-*N*′-ethylcarbodiimide

Abbreviation	Meaning
EDTA	ethylenediaminetetraacetic acid
ELISA	enzyme-linked immunosorbent assay
em.	emission
EPR	enhanced permeability and retention
eq.	equivalent
Eto	etoposide
EtOH	ethanol
ex.	excitation
FACS	flow cytometry
FCS	fetal calf serum
FDA	Food and Drug Administration
Fmoc	fluorenylmethyloxycarbonyl
FTIR	fourier transform infrared spectroscopy
HeLa	tumor cells from the patient Henrietta Lacks
HEPES	4-(2-hydroxyethyl)-1-piperazineethanesulfonic acid
HRP	horseradish peroxidase
IR	Infrared
K562	myelogenous leukemia cell line
Λ	Wavelength
LC-MS	liquid chromatography-mass spectrometry
mAb	monoclonal antibody
Mal	Maleimide
MeOH	Methanol
MHC	major histocompatibility complex
mPEG	methoxy poly(ethylene glycol)
MPS	mononuclear phagocytic system
MTT	3-(4,5-dimethylthiazol-2-yl)-2,5-diphenyl-tetrazoliumbromide
M_W	molecular weight
MWCO	molecular weight cut-off
$NaBH_4$	sodium borohydride
NHS	*N*-hydroxysuccinimide
NMR	nuclear magnetic resonance
NP	Nanoparticle
NTA	nanoparticle tracking analysis
Ox	Oxidized
PAGE	polyacrylamide gel electrophoresis
PBS	phosphate buffered saline
PDI	polydispersity index
PEG	poly(ethylene glycol)

Abbreviation	Meaning
PLGA	poly(lactic *co*-glycolic acid)
P/S	penicillin-streptomycin
PVA	poly(vinyl alcohol)
RI	refractive index
RPMI	Roswell Park Memorial Institute
RT	room temperature
SATA	*N*-succinimidyl *S*-acetylthioacetate
SATP	*N*-succinimidyl *S*-acetylthiopropionate
SD	standard deviation
SDS-PAGE	sodium dodecyl sulfate polyacrylamide gel electrophoresis
SMCC	succinimidyl 4-(*N*-maleimidomethyl)cyclohexane-1-carboxylate
Sp	Spermine
TEA	Triethylamine
TfR	transferrin receptor
TLR	toll-like receptor
UV	Ultraviolet

6.2 Collaboration Partners

[redacted]

6.3 Publications

[1] D. Bamberger, D. Hobernik, M. Konhäuser, M. Bros, P. R. Wich, Surface Modification of Polysaccharide-Based Nanoparticles with PEG and Dextran and the Effects on Immune Cell Binding and Stimulatory Characteristics, *Mol. Pharm.*, *14*, 4403–4416.

[2] B. Breitenbach, E. Steiert, M. Konhäuser, L. M. Voigt, Y. Wang, S. H. Parekh, P. R. Wich, Double stimuli-responsive polysaccharide block copolymers as green macrosurfactants for near-infrared photodynamic therapy, *Soft Matter*, *15*, 1423–1434.

[3] J. Kühlborn, M. Konhäuser, J. Groß, P. R. Wich, T. Opatz, Xylochemical Synthesis of Cytotoxic 2-Aminophenoxazinone-Type Natural Products Through Oxidative Cross Coupling, *ACS Sustainable Chem. Eng.*, *7*, *4*, 4414–4419.

[4] K. Butzbach†, M. Konhäuser†, M. Fach, D. N. Bamberger, B. Breitenbach, B. Epe and P. R. Wich, Receptor-mediated Uptake of Folic Acid-functionalized Dextran Nanoparticles for Applications in Photodynamic Therapy, *Polymers, 11*.

[5] M. Konhäuser, J. Schlöder, J. Schupp, M. Diken, A. Tuettenberg, H. Jonuleit, and P. R. Wich, Antibody-conjugated Dextran Nanoparticles for the *In Vivo* Targeting of Dendritic Cells, submitted.

[6] F. Barthels, G. Marincola, T. Marciniak, M. Konhäuser, S. Hammerschmidt, J. Bierlmeier, P. R. Wich, U. Distler, S. Tenzer, D. Schwarzer, W. Ziebuhr, T. Schirmeister, Asymmetric Disulfanylbenzamides as Irreversible and Selective Inhibitors of Staphylococcus aureus Sortase A, in preparation.

[7] M. Konhäuser, E. Steiert, K. Schwickert, T. Schirmeister, P. R. Wich Co-encapsulation of L-Asparaginase and Etoposide in Acetalated-Dextran Nanoparticles for the Treatment of CML, in preparation.

[8] F. Foerster, M. Konhäuser, P. R. Wich, LPS-encapsulated PEGylated Dextran Nanoparticles for M1 Macrophages Repolarisation *In Vivo*, in preparation.

[9] M. Konhäuser, E. Steiert, P. Winterwerber, B. Breitenbach,P. R. Wich, Self-Assembled Dual-responsive Enzyme-Polysaccharide Conjugates with Encapsulated Indole-3-acetic-acid for Tumor Cytotoxicity, in preparation.

6.4 Literature

[1] A. A. Gupta, X. Yao, S. Verma, H. Mackay, and L. Hopkins. Systematic Chemotherapy for Inoperable, Locally Advanced, Recurrent, or Metastatic Uterine Leiomyosarcoma: A Systematic Review. *Clinical Oncology* **2013**, *25*, 346-355.

[2] P. Velpurisiva, A. Gad, B. Piel, R. Jadia, and P. Rai. Nanoparticle Design Strategies for Effective Cancer Immunotherapy. *J Biomed (Syd)* **2017**, *2*, 64-77.

[3] L. Maciejko, M. Smalley, and A. Goldman. Cancer Immunotherapy and Personalized Medicine: Emerging Technologies and Biomarker-Based Approaches. *J Mol Biomark Diagn* **2017**, *8*, 350.

[4] A. Goldman, A. Kulkarni, M. Kohandel, P. Pandey, P. Rao, S. K. Natarajan, V. Sabbisetti, and S. Sengupta. Rationally Designed 2-in-1 Nanoparticles Can Overcome Adaptive Resistance in Cancer. *ACS Nano* **2016**, *10*, 5823-5834.

[5] K. Shao, S. Singha, X. Clemente-Casares, S. Tsai, Y. Yang, and P. Santamaria. Nanoparticle-based immunotherapy for cancer. *ACS Nano* **2015**, *9*, 16–30.

[6] S.-S. Feng, and S. Chien. Chemotherapeutic engineering: Application and further development of chemical engineering principles for chemotherapy of cancer and other diseases. *Chem. Eng. Sci.* **2003**, *58*, 4087-4114.

[7] H. Wang, J. Yu, X. Lu, and X. He. Nanoparticle systems reduce systemic toxicity in cancer treatment. *Nanomedicine* **2015**, *11*, 103-106.

[8] A. Coates, S. Abraham, S. B. Kaye, T. Sowerbutts, C. Frewin, R. M. Fox, and M. H. N. Tattersall. On the receiving end—patient perception of the side-effects of cancer chemotherapy. *European Journal of Cancer and Clinical Oncology* **1983**, *19*, 203-208.

[9] K. Strebhardt, and A. Ullrich. Paul Ehrlich`s magic bullet concept: 100 years of progress. *Nature Reviews Cancer* **2008**, *8*, 473.

[10] L. Mu, and S. S. Feng. A novel controlled release formulation for the anticancer drug paclitaxel (Taxol®): PLGA nanoparticles containing vitamin E TPGS. *J. Controlled Release* **2003**, *86*, 33-48.

[11] S. E. McNeil. Nanotechnology for the biologist. *J. Leukocyte Biol.* **2005**, *78*, 585-594.

[12] M. Li, K. T. Al-Jamal, K. Kostarelos, and J. Reineke. Physiologically Based Pharmacokinetic Modeling of Nanoparticles. *ACS Nano* **2010**, *4*, 6303-6317.

[13] K. R. Vega-Villa, J. K. Takemoto, J. A. Yáñez, C. M. Remsberg, M. L. Forrest, and N. M. Davies. Clinical toxicities of nanocarrier systems. *Adv. Drug Delivery Rev.* **2008**, *60*, 929-938.

[14] S. C. Khanna, M. Soliva, and P. Speiser. Epoxy Resin Beads as a Pharmaceutical Dosage Form II: Dissolution Studies of Epoxy-Amine Beads and Release of Drug. *J. Pharm. Sci.* **1969**, *58*, 1385-1388.

[15] T. Sun, Y. S. Zhang, B. Pang, D. C. Hyun, M. Yang, and Y. Xia. Engineered Nanoparticles for Drug Delivery in Cancer Therapy. *Angew. Chem. Int. Ed.* **2014**, *53*, 12320-12364.

[16] E. Piñón-Segundo, N. Mendoza-Muñoz, and D. Quintanar-Guerrero. Chapter 23 - Nanoparticles as Dental Drug-Delivery Systems, in *Nanobiomaterials in Clinical Dentistry* (Subramani, K., Ahmed, W., and Hartsfield, J. K., Eds.) **2013**, pp 475-495, William Andrew Publishing.

[17] V. V. Mody, R. Siwale, A. Singh, and H. R. Mody. Introduction to metallic nanoparticles. *J Pharm Bioallied Sci* **2010**, *2*, 282-289.

[18] D. A. Giljohann, D. S. Seferos, W. L. Daniel, M. D. Massich, P. C. Patel, and C. A. Mirkin. Gold Nanoparticles for Biology and Medicine. *Angew. Chem. Int. Ed.* **2010**, *49*, 3280-3294.

[19] F. Furno, K. S. Morley, B. Wong, B. L. Sharp, P. L. Arnold, S. M. Howdle, R. Bayston, P. D. Brown, P. D. Winship, and H. J. Reid. Silver nanoparticles and polymeric medical devices: a new approach to prevention of infection? *J. Antimicrob. Chemother.* **2004**, *54*, 1019-1024.

[20] G. Herlem, F. Picaud, C. Girardet, and O. Micheau. Chapter 16 - Carbon Nanotubes: Synthesis, Characterization, and Applications in Drug-Delivery Systems, in *Nanocarriers for Drug Delivery* (Mohapatra, S. S., Ranjan, S., Dasgupta, N., Mishra, R. K., and Thomas, S., Eds.) **2019**, pp 469-529, Elsevier.

[21] W. Ahmed, A. Elhissi, V. Dhanak, and K. Subramani. Chapter 18 - Carbon nanotubes: Applications in cancer therapy and drug delivery research, in *Emerging Nanotechnologies in Dentistry (Second Edition)* (Subramani, K., and Ahmed, W., Eds.) **2018**, pp 371-389, William Andrew Publishing.

[22] E. Abbasi, S. F. Aval, A. Akbarzadeh, M. Milani, H. T. Nasrabadi, S. W. Joo, Y. Hanifehpour, K. Nejati-Koshki, and R. Pashaei-Asl. Dendrimers: synthesis, applications, and properties. *Nanoscale Res Lett* **2014**, *9*, 247-247.

[23] D. A. Tomalia, and J. M. J. Fréchet. Discovery of dendrimers and dendritic polymers: A brief historical perspective*. *J. Polym. Sci., Part A: Polym. Chem.* **2002**, *40*, 2719-2728.

[24] S. M. Grayson, and J. M. J. Fréchet. Convergent Dendrons and Dendrimers: from Synthesis to Applications. *Chem. Rev.* **2001**, *101*, 3819-3868.

[25] B. Noriega-Luna, L. A. Godinez, F. J. Rodriguez, A. Rodriguez, G. Zaldivar-Lelo de Larrea, C. F. Sosa-Ferreyra, R. F. Mercado-Curiel, J. Manriquez, and E. Bustos.

Applications of Dendrimers in Drug Delivery Agents, Diagnosis, Therapy, and Detection. *Journal of Nanomaterials* **2014**, *2014*, 19.

[26] C. Fu, and J.-P. Li. Application of Dendrimers in Analytical Chemistry. *Chinese Journal of Analytical Chemistry* **2013**, *41*, 1762-1772.

[27] R. W. J. Scott, O. M. Wilson, and R. M. Crooks. Synthesis, Characterization, and Applications of Dendrimer-Encapsulated Nanoparticles. *The Journal of Physical Chemistry B* **2005**, *109*, 692-704.

[28] A. D. Bangham, M. M. Standish, and J. C. Watkins. Diffusion of univalent ions across the lamellae of swollen phospholipids. *J. Mol. Biol.* **1965**, *13*, 238-IN27.

[29] M. J. W. Johnston, S. C. Semple, S. K. Klimuk, S. Ansell, N. Maurer, and P. R. Cullis. Characterization of the drug retention and pharmacokinetic properties of liposomal nanoparticles containing dihydrosphingomyelin. *Biochim. Biophys. Acta* **2007**, *1768*, 1121-1127.

[30] A. Akbarzadeh, R. Rezaei-Sadabady, S. Davaran, S. W. Joo, N. Zarghami, Y. Hanifehpour, M. Samiei, M. Kouhi, and K. Nejati-Koshki. Liposome: classification, preparation, and applications. *Nanoscale Res Lett* **2013**, *8*, 102-102.

[31] A. Kumari, S. K. Yadav, and S. C. Yadav. Biodegradable polymeric nanoparticles based drug delivery systems. *Colloids Surf. B. Biointerfaces* **2010**, *75*, 1-18.

[32] K. S. Soppimath, T. M. Aminabhavi, A. R. Kulkarni, and W. E. Rudzinski. Biodegradable polymeric nanoparticles as drug delivery devices. *J. Controlled Release* **2001**, *70*, 1-20.

[33] G. Lambert, E. Fattal, H. Pinto-Alphandary, A. Gulik, and P. Couvreur. Polyisobutylcyanoacrylate Nanocapsules Containing an Aqueous Core as a Novel Colloidal Carrier for the Delivery of Oligonucleotides. *Pharm. Res.* **2000**, *17*, 707-714.

[34] C. Perez, A. Sanchez, D. Putnam, D. Ting, R. Langer, and M. J. Alonso. Poly(lactic acid)-poly(ethylene glycol) nanoparticles as new carriers for the delivery of plasmid DNA. *J. Controlled Release* **2001**, *75*, 211-224.

[35] N. Nafee, S. Taetz, M. Schneider, U. F. Schaefer, and C.-M. Lehr. Chitosan-coated PLGA nanoparticles for DNA/RNA delivery: effect of the formulation parameters on complexation and transfection of antisense oligonucleotides. *Nanomed. Nanotechnol. Biol. Med.* **2007**, *3*, 173-183.

[36] R. Rai, S. Alwani, and I. Badea. Polymeric Nanoparticles in Gene Therapy: New Avenues of Design and Optimization for Delivery Applications. *Polymers* **2019**, *11*.

[37] C. Vauthier, and K. Bouchemal. Methods for the Preparation and Manufacture of Polymeric Nanoparticles. *Pharm. Res.* **2009**, *26*, 1025-1058.

[38] N. Anton, J.-P. Benoit, and P. Saulnier. Design and production of nanoparticles formulated from nano-emulsion templates—A review. *J. Controlled Release* **2008**, *128*, 185-199.

[39] S. Freitas, H. P. Merkle, and B. Gander. Microencapsulation by solvent extraction/evaporation: reviewing the state of the art of microsphere preparation process technology. *J. Controlled Release* **2005**, *102*, 313-332.

[40] K. Bouchemal, S. Briançon, E. Perrier, and H. Fessi. Nano-emulsion formulation using spontaneous emulsification: solvent, oil and surfactant optimisation. *Int. J. Pharm.* **2004**, *280*, 241-251.

[41] R. H. Staff, K. Landfester, and D. Crespy. Recent Advances in the Emulsion Solvent Evaporation Technique for the Preparation of Nanoparticles and Nanocapsules, in *Hierarchical Macromolecular Structures: 60 Years after the Staudinger Nobel Prize II* (Percec, V., Ed.) **2013**, pp 329-344, Springer International Publishing, Cham.

[42] L. Y. Qiu, and Y. H. Bae. Polymer Architecture and Drug Delivery. *Pharm. Res.* **2006**, *23*, 1-30.

[43] M. Kuruppuarachchi, H. Savoie, A. Lowry, C. Alonso, and R. W. Boyle. Polyacrylamide Nanoparticles as a Delivery System in Photodynamic Therapy. *Mol. Pharmaceutics* **2011**, *8*, 920-931.

[44] R. Singh, and J. W. Lillard. Nanoparticle-based targeted drug delivery. *Experimental and Molecular Pathology* **2009**, *86*, 215-223.

[45] G. G. Pitt, M. M. Gratzl, G. L. Kimmel, J. Surles, and A. Sohindler. Aliphatic polyesters II. The degradation of poly (DL-lactide), poly (ε-caprolactone), and their copolymers in vivo. *Biomaterials* **1981**, *2*, 215-220.

[46] C. E. Astete, and C. M. Sabliov. Synthesis and characterization of PLGA nanoparticles. *Journal of Biomaterials Science, Polymer Edition* **2006**, *17*, 247-289.

[47] F. Rancan, D. Papakostas, S. Hadam, S. Hackbarth, T. Delair, C. Primard, B. Verrier, W. Sterry, U. Blume-Peytavi, and A. Vogt. Investigation of Polylactic Acid (PLA) Nanoparticles as Drug Delivery Systems for Local Dermatotherapy. *Pharm. Res.* **2009**, *26*, 2027-2036.

[48] J. Molpeceres, M. Guzman, M. R. Aberturas, M. Chacon, and L. Berges. Application of Central Composite Designs to the Preparation of Polycaprolactone Nanoparticles by Solvent Displacement. *J. Pharm. Sci.* **1996**, *85*, 206-213.

[49] F. R. Wurm, and C. K. Weiss. Nanoparticles from renewable polymers. *Frontiers in chemistry* **2014**, *2*, 49-49.

[50] L. Qi, Z. Xu, X. Jiang, C. Hu, and X. Zou. Preparation and antibacterial activity of chitosan nanoparticles. *Carbohydr. Res.* **2004**, *339*, 2693-2700.

[51] E. Steiert, L. Radi, M. Fach, and P. R. Wich. Protein-Based Nanoparticles for the Delivery of Enzymes with Antibacterial Activity. *Macromol. Rapid Commun.* **2018**, *39*, 1800186.

[52] M. Fach, L. Radi, and P. R. Wich. Nanoparticle Assembly of Surface-Modified Proteins. *J. Am. Chem. Soc.* **2016**, *138*, 14820-14823.

[53] L. S. Nair, and C. T. Laurencin. Biodegradable polymers as biomaterials. *Prog. Polym. Sci.* **2007**, *32*, 762-798.

[54] J. Karlsson, H. J. Vaughan, and J. J. Green. Biodegradable Polymeric Nanoparticles for Therapeutic Cancer Treatments. *Annual Review of Chemical and Biomolecular Engineering* **2018**, *9*, 105-127.

[55] J. Gilleron, W. Querbes, A. Zeigerer, A. Borodovsky, G. Marsico, U. Schubert, K. Manygoats, S. Seifert, C. Andree, M. Stöter, H. Epstein-Barash, L. Zhang, V. Koteliansky, K. Fitzgerald, E. Fava, M. Bickle, Y. Kalaidzidis, A. Akinc, M. Maier, and M. Zerial. Image-based analysis of lipid nanoparticle–mediated siRNA delivery, intracellular trafficking and endosomal escape. *Nat. Biotechnol.* **2013**, *31*, 638.

[56] R. Gref, Y. Minamitake, M. T. Peracchia, V. Trubetskoy, V. Torchilin, and R. Langer. Biodegradable long-circulating polymeric nanospheres. *Science (New York, N.Y.)* **1994**, *263*, 1600.

[57] N. Kamaly, Z. Xiao, P. M. Valencia, A. F. Radovic-Moreno, and O. C. Farokhzad. Targeted polymeric therapeutic nanoparticles: design, development and clinical translation. *Chem. Soc. Rev.* **2012**, *41*, 2971-3010.

[58] V. Mohanraj, and V. Chen. Nanoparticles – A Review. *Tropical Journal of Pharmaceutical Research* **2006**, *5*, 561-573.

[59] E. Seydoux, B. Rothen-Rutishauser, I. M. Nita, S. Balog, A. Gazdhar, P. A. Stumbles, A. Petri-Fink, F. Blank, and C. von Garnier. Size-dependent accumulation of particles in lysosomes modulates dendritic cell function through impaired antigen degradation. *International journal of nanomedicine* **2014**, *9*, 3885-3902.

[60] J. Panyam, and V. Labhasetwar. Biodegradable nanoparticles for drug and gene delivery to cells and tissue. *Adv. Drug Delivery Rev.* **2003**, *55*, 329-347.

[61] W. Zauner, N. A. Farrow, and A. M. R. Haines. In vitro uptake of polystyrene microspheres: effect of particle size, cell line and cell density. *J. Controlled Release* **2001**, *71*, 39-51.

[62] L. Ilium, S. S. Davis, C. G. Wilson, N. W. Thomas, M. Frier, and J. G. Hardy. Blood clearance and organ deposition of intravenously administered colloidal particles. The effects of particle size, nature and shape. *Int. J. Pharm.* **1982**, *12*, 135-146.

[63] Y. Tabata, and Y. Ikada. in *New Polymer Materials***1990**, pp 107-141, Springer Berlin Heidelberg, Berlin, Heidelberg.

[64] M. Caldorera-Moore, N. Guimard, L. Shi, and K. Roy. Designer nanoparticles: incorporating size, shape and triggered release into nanoscale drug carriers. *Expert Opin Drug Deliv* **2010**, *7*, 479-495.

[65] W. M. Deen, M. J. Lazzara, and B. D. Myers. Structural determinants of glomerular permeability. *American Journal of Physiology-Renal Physiology* **2001**, *281*, F579-F596.

[66] S. K. Hobbs, W. L. Monsky, F. Yuan, W. G. Roberts, L. Griffith, V. P. Torchilin, and R. K. Jain. Regulation of transport pathways in tumor vessels: role of tumor type and microenvironment. *Proceedings of the National Academy of Sciences of the United States of America* **1998**, *95*, 4607-4612.

[67] B. D. Chithrani, and W. C. W. Chan. Elucidating the Mechanism of Cellular Uptake and Removal of Protein-Coated Gold Nanoparticles of Different Sizes and Shapes. *Nano Lett.* **2007**, *7*, 1542-1550.

[68] W. Jiang, B. Y. S. Kim, J. T. Rutka, and W. C. W. Chan. Nanoparticle-mediated cellular response is size-dependent. *Nature Nanotechnology* **2008**, *3*, 145.

[69] R. Vácha, F. J. Martinez-Veracoechea, and D. Frenkel. Receptor-Mediated Endocytosis of Nanoparticles of Various Shapes. *Nano Lett.* **2011**, *11*, 5391-5395.

[70] M. Lundqvist, J. Stigler, G. Elia, I. Lynch, T. Cedervall, and K. A. Dawson. Nanoparticle size and surface properties determine the protein corona with possible implications for biological impacts. *Proceedings of the National Academy of Sciences* **2008**, *105*, 14265.

[71] Z. Amoozgar, and Y. Yeo. Recent advances in stealth coating of nanoparticle drug delivery systems. *Wiley Interdisciplinary Reviews: Nanomedicine and Nanobiotechnology* **2012**, *4*, 219-233.

[72] G. Caracciolo, S. Palchetti, V. Colapicchioni, L. Digiacomo, D. Pozzi, A. L. Capriotti, G. La Barbera, and A. Laganà. Stealth Effect of Biomolecular Corona on Nanoparticle Uptake by Immune Cells. *Langmuir : the ACS journal of surfaces and colloids* **2015**, *31*, 10764-10773.

[73] J. S. Suk, Q. Xu, N. Kim, J. Hanes, and L. M. Ensign. PEGylation as a strategy for improving nanoparticle-based drug and gene delivery. *Adv. Drug Delivery Rev.* **2016**, *99*, 28-51.

[74] J. V. Jokerst, T. Lobovkina, R. N. Zare, and S. S. Gambhir. Nanoparticle PEGylation for imaging and therapy. *Nanomedicine* **2011**, *6*, 715-728.

[75] P. Couvreur, G. Barratt, E. Fattal, and C. Vauthier. Nanocapsule Technology: A Review. **2002**, *19*, 36.

[76] M. Elsabahy, and K. L. Wooley. Design of polymeric nanoparticles for biomedical delivery applications. *Chem. Soc. Rev.* **2012**, *41*, 2545-2561.

[77] M. E. Davis, Z. Chen, and D. M. Shin. Nanoparticle therapeutics: an emerging treatment modality for cancer. *Nature Reviews Drug Discovery* **2008**, *7*, 771.

[78] N. Hoshyar, S. Gray, H. Han, and G. Bao. The effect of nanoparticle size on in vivo pharmacokinetics and cellular interaction. *Nanomedicine (London, England)* **2016**, *11*, 673-692.

[79] W. C. Zamboni, V. Torchilin, A. K. Patri, J. Hrkach, S. Stern, R. Lee, A. Nel, N. J. Panaro, and P. Grodzinski. Best Practices in Cancer Nanotechnology: Perspective from NCI Nanotechnology Alliance. *Clin. Cancer. Res.* **2012**, *18*, 3229.

[80] B. Yameen, W. I. Choi, C. Vilos, A. Swami, J. Shi, and O. C. Farokhzad. Insight into nanoparticle cellular uptake and intracellular targeting. *J. Controlled Release* **2014**, *190*, 485-499.

[81] M. Zheng, C. Yue, Y. Ma, P. Gong, P. Zhao, C. Zheng, Z. Sheng, P. Zhang, Z. Wang, and L. Cai. Single-Step Assembly of DOX/ICG Loaded Lipid–Polymer Nanoparticles for Highly Effective Chemo-photothermal Combination Therapy. *ACS Nano* **2013**, *7*, 2056-2067.

[82] E. J. Ungewickell, and L. Hinrichsen. Endocytosis: clathrin-mediated membrane budding. *Curr. Opin. Cell Biol.* **2007**, *19*, 417-425.

[83] L.-A. H. Allen, and A. Aderem. Mechanisms of phagocytosis. *Curr. Opin. Immunol.* **1996**, *8*, 36-40.

[84] H. Herd, N. Daum, A. T. Jones, H. Huwer, H. Ghandehari, and C.-M. Lehr. Nanoparticle Geometry and Surface Orientation Influence Mode of Cellular Uptake. *ACS Nano* **2013**, *7*, 1961-1973.

[85] C. Huang, Y. Zhang, H. Yuan, H. Gao, and S. Zhang. Role of Nanoparticle Geometry in Endocytosis: Laying Down to Stand Up. *Nano Lett.* **2013**, *13*, 4546-4550.

[86] O. Harush-Frenkel, N. Debotton, S. Benita, and Y. Altschuler. Targeting of nanoparticles to the clathrin-mediated endocytic pathway. *Biochem. Biophys. Res. Commun.* **2007**, *353*, 26-32.

[87] R. A. Petros, and J. M. DeSimone. Strategies in the design of nanoparticles for therapeutic applications. *Nature Reviews Drug Discovery* **2010**, *9*, 615.

[88] J. L. Cohen, S. Schubert, P. R. Wich, L. Cui, J. A. Cohen, J. L. Mynar, and J. M. J. Fréchet. Acid-degradable cationic dextran particles for the delivery of siRNA therapeutics. *Bioconjugate Chem.* **2011**, *22*, 1056-1065.

[89] J. E. Fuller, G. T. Zugates, L. S. Ferreira, H. S. Ow, N. N. Nguyen, U. B. Wiesner, and R. S. Langer. Intracellular delivery of core–shell fluorescent silica nanoparticles. *Biomaterials* **2008**, *29*, 1526-1532.

[90] M. V. Yezhelyev, L. Qi, R. M. O'Regan, S. Nie, and X. Gao. Proton-Sponge Coated Quantum Dots for siRNA Delivery and Intracellular Imaging. *J. Am. Chem. Soc.* **2008**, *130*, 9006-9012.

[91] I. Richard, M. Thibault, G. De Crescenzo, M. D. Buschmann, and M. Lavertu. Ionization Behavior of Chitosan and Chitosan–DNA Polyplexes Indicate That Chitosan Has a Similar Capability to Induce a Proton-Sponge Effect as PEI. *Biomacromolecules* **2013**, *14*, 1732-1740.

[92] E. Fleige, M. A. Quadir, and R. Haag. Stimuli-responsive polymeric nanocarriers for the controlled transport of active compounds: Concepts and applications. *Adv. Drug Delivery Rev.* **2012**, *64*, 866-884.

[93] S. Mura, J. Nicolas, and P. Couvreur. Stimuli-responsive nanocarriers for drug delivery. *Nature Materials* **2013**, *12*, 991.

[94] A. V. Ambade, E. N. Savariar, and S. Thayumanavan. Dendrimeric Micelles for Controlled Drug Release and Targeted Delivery. *Mol. Pharmaceutics* **2005**, *2*, 264-272.

[95] J. Kost, and R. Langer. Responsive polymeric delivery systems. *Adv. Drug Delivery Rev.* **2001**, *46*, 125-148.

[96] E. M. Bachelder, T. T. Beaudette, K. E. Broaders, J. Dashe, and J. M. J. Fréchet. Acetal-Derivatized Dextran: An Acid-Responsive Biodegradable Material for Therapeutic Applications. *J. Am. Chem. Soc.* **2008**, *130*, 10494-10495.

[97] F. Q. Schafer, and G. R. Buettner. Redox environment of the cell as viewed through the redox state of the glutathione disulfide/glutathione couple. *Free Radical Biol. Med.* **2001**, *30*, 1191-1212.

[98] N. Fomina, C. McFearin, M. Sermsakdi, O. Edigin, and A. Almutairi. UV and Near-IR Triggered Release from Polymeric Nanoparticles. *J. Am. Chem. Soc.* **2010**, *132*, 9540-9542.

[99] J. S. Katz, and J. A. Burdick. Light-Responsive Biomaterials: Development and Applications. *Macromol. Biosci.* **2010**, *10*, 339-348.

[100] C. Alvarez-Lorenzo, and A. Concheiro. Smart drug delivery systems: from fundamentals to the clinic. *Chem. Commun.* **2014**, *50*, 7743-7765.

[101] S. Sortino. Photoactivated nanomaterials for biomedical release applications. *J. Mater. Chem.* **2012**, *22*, 301-318.

[102] T. Akagi, M. Higashi, T. Kaneko, T. Kida, and M. Akashi. Hydrolytic and Enzymatic Degradation of Nanoparticles Based on Amphiphilic Poly(γ-glutamic acid)-graft-l-Phenylalanine Copolymers. *Biomacromolecules* **2006**, *7*, 297-303.

[103] I. I. Vlasova, A. A. Kapralov, Z. P. Michael, S. C. Burkert, M. R. Shurin, A. Star, A. A. Shvedova, and V. E. Kagan. Enzymatic oxidative biodegradation of nanoparticles: Mechanisms, significance and applications. *Toxicol. Appl. Pharmacol.* **2016**, *299*, 58-69.

[104] J. Hu, G. Zhang, and S. Liu. Enzyme-responsive polymeric assemblies, nanoparticles and hydrogels. *Chem. Soc. Rev.* **2012**, *41*, 5933-5949.

[105] T. Ta, and T. M. Porter. Thermosensitive liposomes for localized delivery and triggered release of chemotherapy. *J. Controlled Release* **2013**, *169*, 112-125.

[106] T.-Y. Liu, S.-H. Hu, D.-M. Liu, S.-Y. Chen, and I. W. Chen. Biomedical nanoparticle carriers with combined thermal and magnetic responses. *Nano Today* **2009**, *4*, 52-65.

[107] J. Zhang, H. Chen, L. Xu, and Y. Gu. The targeted behavior of thermally responsive nanohydrogel evaluated by NIR system in mouse model. *J. Controlled Release* **2008**, *131*, 34-40.

[108] S. H. Lee, S. H. Choi, S. H. Kim, and T. G. Park. Thermally sensitive cationic polymer nanocapsules for specific cytosolic delivery and efficient gene silencing of siRNA: Swelling induced physical disruption of endosome by cold shock. *J. Controlled Release* **2008**, *125*, 25-32.

[109] S. Yoon, W. J. Kim, and H. S. Yoo. Dual-Responsive Breakdown of Nanostructures with High Doxorubicin Payload for Apoptotic Anticancer Therapy. *Small (Weinheim an der Bergstrasse, Germany)* **2013**, *9*, 284-293.

[110] Z. Liu, Y. Jiao, Y. Wang, C. Zhou, and Z. Zhang. Polysaccharides-based nanoparticles as drug delivery systems. *Adv. Drug Delivery Rev.* **2008**, *60*, 1650-1662.

[111] V. R. Sinha, and R. Kumria. Polysaccharides in colon-specific drug delivery. *Int. J. Pharm.* **2001**, *224*, 19-38.

[112] R. Mehvar. Dextrans for targeted and sustained delivery of therapeutic and imaging agents. *J. Controlled Release* **2000**, *69*, 1-25.

[113] M. H. P. B. Vettori, S. M. M. Franchetti, and J. Contiero. Structural characterization of a new dextran with a low degree of branching produced by Leuconostoc mesenteroides FT045B dextransucrase. *Carbohydr. Polym.* **2012**, *88*, 1440-1444.

[114] C. E. Ioan, T. Aberle, and W. Burchard. Structure Properties of Dextran. 2. Dilute Solution. *Macromolecules* **2000**, *33*, 5730-5739.

[115] E. L. Rosenfeld, and I. S. Lukomskaya. The splitting of dextran and isomaltose by animal tissues. *Clin. Chim. Acta* **1957**, *2*, 105-114.

[116] S. P. Massia, J. Stark, and D. S. Letbetter. Surface-immobilized dextran limits cell adhesion and spreading. *Biomaterials* **2000**, *21*, 2253-2261.

[117] G. Heinemeyer. Clinical Pharmacokinetic Considerations in the Treatment of Increased Intracranial Pressure. *Clinical Pharmacokinetics* **1987**, *13*, 1-25.

[118] U. Klotz, and H. Kroemer. Clinical Pharmacokinetic Considerations in the Use of Plasma Expanders. *Clinical Pharmacokinetics* **1987**, *12*, 123-135.

[119] T. Shiratori, A. Sato, M. Fukuzawa, N. Kondo, and S. Tanno. Severe Dextran-Induced Anaphylactic Shock during Induction of Hypertension-Hypervolemia-Hemodilution Therapy following Subarachnoid Hemorrhage. *Case Reports in Critical Care* **2015**, *2015*, 5.

[120] A. Tiselius, J. Porath, and P.-A. Albertsson. Separation and Fractionation of Macromolecules and Particles. *Science (New York, N.Y.)* **1963**, *141*, 13.

[121] Y. Hu, T. Litwin, A. R. Nagaraja, B. Kwong, J. Katz, N. Watson, and D. J. Irvine. Cytosolic Delivery of Membrane-Impermeable Molecules in Dendritic Cells Using pH-Responsive Core−Shell Nanoparticles. *Nano Lett.* **2007**, *7*, 3056-3064.

[122] E. S. Lee, Z. Gao, and Y. H. Bae. Recent progress in tumor pH targeting nanotechnology. *J. Controlled Release* **2008**, *132*, 164-170.

[123] K. Engin, D. B. Leeper, J. R. Cater, A. J. Thistlethwaite, L. Tupchong, and J. D. McFarlane. Extracellular pH distribution in human tumours. *International Journal of Hyperthermia* **1995**, *11*, 211-216.

[124] W. Ulbrich, and A. Lamprecht. Targeted drug-delivery approaches by nanoparticulate carriers in the therapy of inflammatory diseases. *Journal of The Royal Society Interface* **2010**, *7*, S55-S66.

[125] T. T. Beaudette, J. A. Cohen, E. M. Bachelder, K. E. Broaders, J. L. Cohen, E. G. Engleman, and J. M. J. Fréchet. Chemoselective ligation in the functionalization of polysaccharide-based particles. *J. Am. Chem. Soc.* **2009**, *131*, 10360-10361.

[126] D. Lemoine, and V. Préat. Polymeric nanoparticles as delivery system for influenza virus glycoproteins. *J. Controlled Release* **1998**, *54*, 15-27.

[127] T. H. Fife, and L. K. Jao. Substituent Effects in Acetal Hydrolysis. *The Journal of Organic Chemistry* **1965**, *30*, 1492-1495.

[128] K. E. Broaders, J. A. Cohen, T. T. Beaudette, E. M. Bachelder, and J. M. J. Fréchet. Acetalated dextran is a chemically and biologically tunable material for particulate immunotherapy. *Proceedings of the National Academy of Sciences of the United States of America* **2009**, *106*, 5497-5502.

[129] K. J. Kauffman, N. Kanthamneni, S. A. Meenach, B. C. Pierson, E. M. Bachelder, and K. M. Ainslie. Optimization of rapamycin-loaded acetalated dextran microparticles for immunosuppression. *Int. J. Pharm.* **2012**, *422*, 356-363.

[130] N. Chen, M. A. Collier, M. D. Gallovic, G. C. Collins, C. C. Sanchez, E. Q. Fernandes, E. M. Bachelder, and K. M. Ainslie. Degradation of acetalated dextran can be broadly tuned based on cyclic acetal coverage and molecular weight. *Int. J. Pharm.* **2016**, *512*, 147-157.

[131] C. Ornelas-Megiatto, P. N. Shah, P. R. Wich, J. L. Cohen, J. A. Tagaev, J. A. Smolen, B. D. Wright, M. J. Panzner, W. J. Youngs, J. M. J. Fréchet, and C. L. Cannon. Aerosolized Antimicrobial Agents Based on Degradable Dextran Nanoparticles Loaded with Silver Carbene Complexes. *Mol. Pharmaceutics* **2012**, *9*, 3012-3022.

[132] S. Yang, and S. May. Release of cationic polymer-DNA complexes from the endosome: A theoretical investigation of the proton sponge hypothesis. *The Journal of Chemical Physics* **2008**, *129*, 185105.

[133] A. Akinc, M. Thomas, A. M. Klibanov, and R. Langer. Exploring polyethylenimine-mediated DNA transfection and the proton sponge hypothesis. *The Journal of Gene Medicine* **2005**, *7*, 657-663.

[134] T. Bauleth-Ramos, M.-A. Shahbazi, D. Liu, F. Fontana, A. Correia, P. Figueiredo, H. Zhang, J. P. Martins, J. T. Hirvonen, P. Granja, B. Sarmento, and H. A. Santos. Nutlin-3a and Cytokine Co-loaded Spermine-Modified Acetalated Dextran Nanoparticles for Cancer Chemo-Immunotherapy. *Adv. Funct. Mater.* **2017**, *27*, 1703303.

[135] F. Foerster, D. Bamberger, J. Schupp, M. Weilbächer, L. Kaps, S. Strobl, L. Radi, M. Diken, D. Strand, A. Tuettenberg, P. R. Wich, and D. Schuppan. Dextran-based therapeutic nanoparticles for hepatic drug delivery. *Nanomedicine* **2016**, *11*, 2663-2677.

[136] D. Bamberger, D. Hobernik, M. Konhäuser, M. Bros, and P. R. Wich. Surface Modification of Polysaccharide-Based Nanoparticles with PEG and Dextran and the Effects on Immune Cell Binding and Stimulatory Characteristics. *Mol. Pharmaceutics* **2017**, *14*, 4403-4416.

[137] K. Butzbach, M. Konhäuser, M. Fach, N. D. Bamberger, B. Breitenbach, B. Epe, and R. P. Wich. Receptor-mediated Uptake of Folic Acid-functionalized Dextran Nanoparticles for Applications in Photodynamic Therapy. *Polymers* **2019**, *11*.

[138] S. Goodall, M. L. Jones, and S. Mahler. Monoclonal antibody-targeted polymeric nanoparticles for cancer therapy – future prospects. *Journal of Chemical Technology & Biotechnology* **2015**, *90*, 1169-1176.

[139] Y. Matsumura, and H. Maeda. A New Concept for Macromolecular Therapeutics in Cancer Chemotherapy: Mechanism of Tumoritropic Accumulation of Proteins and the Antitumor Agent Smancs. *Cancer Res.* **1986**, *46*, 6387.

[140] C. J. Gulledge, and M. W. Dewhirst. Tumor oxygenation: a matter of supply and demand. *Anticancer Res.* **1996**, *16*, 741-749.

[141] F. Fay, and C. J. Scott. Antibody-targeted nanoparticles for cancer therapy. *Immunotherapy* **2011**, *3*, 381-394.

[142] K. Knop, R. Hoogenboom, D. Fischer, and U. S. Schubert. Poly(ethylene glycol) in Drug Delivery: Pros and Cons as Well as Potential Alternatives. *Angew. Chem. Int. Ed.* **2010**, *49*, 6288-6308.

[143] Z. Cheng, A. Al Zaki, J. Z. Hui, V. R. Muzykantov, and A. Tsourkas. Multifunctional nanoparticles: cost versus benefit of adding targeting and imaging capabilities. *Science (New York, N.Y.)* **2012**, *338*, 903-910.

[144] S. K. Golombek, J.-N. May, B. Theek, L. Appold, N. Drude, F. Kiessling, and T. Lammers. Tumor targeting via EPR: Strategies to enhance patient responses. *Adv. Drug Delivery Rev.* **2018**, *130*, 17-38.

[145] T. Stylianopoulos. EPR-effect: utilizing size-dependent nanoparticle delivery to solid tumors. *Therapeutic Delivery* **2013**, *4*, 421-423.

[146] B. Zhang, Y. Hu, and Z. Pang. Modulating the Tumor Microenvironment to Enhance Tumor Nanomedicine Delivery. *Frontiers in pharmacology* **2017**, *8*, 952-952.

[147] F. Danhier, O. Feron, and V. Préat. To exploit the tumor microenvironment: Passive and active tumor targeting of nanocarriers for anti-cancer drug delivery. *J. Controlled Release* **2010**, *148*, 135-146.

[148] J.-H. Kim, Y.-S. Kim, K. Park, S. Lee, H. Y. Nam, K. H. Min, H. G. Jo, J. H. Park, K. Choi, S. Y. Jeong, R.-W. Park, I.-S. Kim, K. Kim, and I. C. Kwon. Antitumor efficacy of cisplatin-loaded glycol chitosan nanoparticles in tumor-bearing mice. *J. Controlled Release* **2008**, *127*, 41-49.

[149] D. Peer, J. M. Karp, S. Hong, O. C. Farokhzad, R. Margalit, and R. Langer. Nanocarriers as an emerging platform for cancer therapy. *Nature Nanotechnology* **2007**, *2*, 751.

[150] K. Greish, J. Fang, T. Inutsuka, A. Nagamitsu, and H. Maeda. Macromolecular Therapeutics. *Clinical Pharmacokinetics* **2003**, *42*, 1089-1105.

[151] L. Grislain, P. Couvreur, V. Lenaerts, M. Roland, D. Deprez-Decampeneere, and P. Speiser. Pharmacokinetics and distribution of a biodegradable drug-carrier. *Int. J. Pharm.* **1983**, *15*, 335-345.

[152] M. Longmire, P. L. Choyke, and H. Kobayashi. Clearance properties of nano-sized particles and molecules as imaging agents: considerations and caveats. *Nanomedicine* **2008**, *3*, 703-717.

[153] S. Salmaso, and P. Caliceti. Stealth Properties to Improve Therapeutic Efficacy of Drug Nanocarriers. *Journal of Drug Delivery* **2013**, *2013*, 19.

[154] K. Yang, and Y.-Q. Ma. Computer simulation of the translocation of nanoparticles with different shapes across a lipid bilayer. *Nature Nanotechnology* **2010**, *5*, 579.

[155] S. Schöttler, G. Becker, S. Winzen, T. Steinbach, K. Mohr, K. Landfester, V. Mailänder, and F. R. Wurm. Protein adsorption is required for stealth effect of poly(ethylene glycol)- and poly(phosphoester)-coated nanocarriers. *Nature Nanotechnology* **2016**, *11*, 372.

[156] Z. J. Deng, M. Liang, M. Monteiro, I. Toth, and R. F. Minchin. Nanoparticle-induced unfolding of fibrinogen promotes Mac-1 receptor activation and inflammation. *Nature Nanotechnology* **2010**, *6*, 39.

[157] I. Gonzalez-Mahave, M. D. Del Pozo, A. Blasco, T. Lobera, and M. Venturini. Urticaria due to pentoxyfylline. *Allergy* **2005**, *60*, 705-705.

[158] D. A. Herold, K. Keil, and D. E. Bruns. Oxidation of polyethylene glycols by alcohol dehydrogenase. *Biochem. Pharmacol.* **1989**, *38*, 73-76.

[159] G. Pasut, and F. M. Veronese. Polymer–drug conjugation, recent achievements and general strategies. *Prog. Polym. Sci.* **2007**, *32*, 933-961.

[160] A. S. Abu Lila, H. Kiwada, and T. Ishida. The accelerated blood clearance (ABC) phenomenon: Clinical challenge and approaches to manage. *J. Controlled Release* **2013**, *172*, 38-47.

[161] T. Ishihara, M. Takeda, H. Sakamoto, A. Kimoto, C. Kobayashi, N. Takasaki, K. Yuki, K.-i. Tanaka, M. Takenaga, R. Igarashi, T. Maeda, N. Yamakawa, Y. Okamoto, M. Otsuka, T. Ishida, H. Kiwada, Y. Mizushima, and T. Mizushima. Accelerated Blood Clearance Phenomenon Upon Repeated Injection of PEG-modified PLA-nanoparticles. *Pharm. Res.* **2009**, *26*, 2270-2279.

[162] C. Li, and S. Wallace. Polymer-drug conjugates: Recent development in clinical oncology. *Adv. Drug Delivery Rev.* **2008**, *60*, 886-898.

[163] J. M. Metselaar, P. Bruin, L. W. T. de Boer, T. de Vringer, C. Snel, C. Oussoren, M. H. M. Wauben, D. J. A. Crommelin, G. Storm, and W. E. Hennink. A Novel Family of l-Amino Acid-Based Biodegradable Polymer−Lipid Conjugates for the Development of Long-Circulating Liposomes with Effective Drug-Targeting Capacity. *Bioconjugate Chem.* **2003**, *14*, 1156-1164.

[164] B. Romberg, C. Oussoren, C. J. Snel, M. G. Carstens, W. E. Hennink, and G. Storm. Pharmacokinetics of poly(hydroxyethyl-l-asparagine)-coated liposomes is superior over that of PEG-coated liposomes at low lipid dose and upon repeated administration. *Biochim. Biophys. Acta* **2007**, *1768*, 737-743.

[165] B. Romberg, J. M. Metselaar, L. Baranyi, C. J. Snel, R. Bünger, W. E. Hennink, J. Szebeni, and G. Storm. Poly(amino acid)s: Promising enzymatically degradable stealth coatings for liposomes. *Int. J. Pharm.* **2007**, *331*, 186-189.

[166] T. Kean, and M. Thanou. Biodegradation, biodistribution and toxicity of chitosan. *Adv. Drug Delivery Rev.* **2010**, *62*, 3-11.

[167] Z. Amoozgar, and Y. Yeo. Recent advances in stealth coating of nanoparticle drug delivery systems. *Wiley interdisciplinary reviews. Nanomedicine and nanobiotechnology* **2012**, *4*, 219-233.

[168] L. Fan, F. Li, H. Zhang, Y. Wang, C. Cheng, X. Li, C.-h. Gu, Q. Yang, H. Wu, and S. Zhang. Co-delivery of PDTC and doxorubicin by multifunctional micellar nanoparticles to achieve active targeted drug delivery and overcome multidrug resistance. *Biomaterials* **2010**, *31*, 5634-5642.

[169] K. Y. Choi, H. Chung, K. H. Min, H. Y. Yoon, K. Kim, J. H. Park, I. C. Kwon, and S. Y. Jeong. Self-assembled hyaluronic acid nanoparticles for active tumor targeting. *Biomaterials* **2010**, *31*, 106-114.

[170] R. K. Kainthan, J. Janzen, E. Levin, D. V. Devine, and D. E. Brooks. Biocompatibility Testing of Branched and Linear Polyglycidol. *Biomacromolecules* **2006**, *7*, 703-709.

[171] C. Siegers, M. Biesalski, and R. Haag. Self-Assembled Monolayers of Dendritic Polyglycerol Derivatives on Gold That Resist the Adsorption of Proteins. *Chemistry – A European Journal* **2004**, *10*, 2831-2838.

[172] N. Hadjesfandiari, and A. Parambath. 13 - Stealth coatings for nanoparticles: Polyethylene glycol alternatives, in *Engineering of Biomaterials for Drug Delivery Systems* (Parambath, A., Ed.) **2018**, pp 345-361, Woodhead Publishing.

[173] Z. Symon, A. Peyser, D. Tzemach, O. Lyass, E. Sucher, E. Shezen, and A. Gabizon. Selective delivery of doxorubicin to patients with breast carcinoma metastases by stealth liposomes. *Cancer* **1999**, *86*, 72-78.

[174] P. Zhang, L. Zhang, Z. Qin, S. Hua, Z. Guo, C. Chu, H. Lin, Y. Zhang, W. Li, X. Zhang, X. Chen, and G. Liu. Genetically Engineered Liposome-like Nanovesicles as Active Targeted Transport Platform. *Adv. Mater.* **2018**, *30*, 1705350.

[175] J. Jakoby, F. Beuschlein, S. Mentz, C. Hantel, and R. Süss. Liposomal doxorubicin for active targeting: surface modification of the nanocarrier evaluated in vitro and in vivo: challenges and prospects. *Oncotarget* **2015**, *6*, 43698-43711.

[176] R. van der Meel, L. J. C. Vehmeijer, R. J. Kok, G. Storm, and E. V. B. van Gaal. Ligand-targeted particulate nanomedicines undergoing clinical evaluation: Current status. *Adv. Drug Delivery Rev.* **2013**, *65*, 1284-1298.

[177] V. P. Torchilin. Targeted pharmaceutical nanocarriers for cancer therapy and imaging. *AAPS J* **2007**, *9*, E128-E147.

[178] J. D. Byrne, T. Betancourt, and L. Brannon-Peppas. Active targeting schemes for nanoparticle systems in cancer therapeutics. *Adv. Drug Delivery Rev.* **2008**, *60*, 1615-1626.

[179] K. N. Sugahara, T. Teesalu, P. P. Karmali, V. R. Kotamraju, L. Agemy, O. M. Girard, D. Hanahan, R. F. Mattrey, and E. Ruoslahti. Tissue-Penetrating Delivery of Compounds and Nanoparticles into Tumors. *Cancer Cell* **2009**, *16*, 510-520.

[180] S. H. Kim, J. H. Jeong, K. W. Chun, and T. G. Park. Target-Specific Cellular Uptake of PLGA Nanoparticles Coated with Poly(l-lysine)−Poly(ethylene glycol)−Folate Conjugate. *Langmuir : the ACS journal of surfaces and colloids* **2005**, *21*, 8852-8857.

[181] M. O. Oyewumi, S. Liu, J. A. Moscow, and R. J. Mumper. Specific Association of Thiamine-Coated Gadolinium Nanoparticles with Human Breast Cancer Cells Expressing Thiamine Transporters. *Bioconjugate Chem.* **2003**, *14*, 404-411.

[182] Y.-I. Jeong, S.-J. Seo, I.-K. Park, H.-C. Lee, I.-C. Kang, T. Akaike, and C.-S. Cho. Cellular recognition of paclitaxel-loaded polymeric nanoparticles composed of poly(γ-benzyl l-glutamate) and poly(ethylene glycol) diblock copolymer endcapped with galactose moiety. *Int. J. Pharm.* **2005**, *296*, 151-161.

[183] J. K. Herr, J. E. Smith, C. D. Medley, D. Shangguan, and W. Tan. Aptamer-Conjugated Nanoparticles for Selective Collection and Detection of Cancer Cells. *Anal. Chem.* **2006**, *78*, 2918-2924.

[184] R. M. Schiffelers, A. Ansari, J. Xu, Q. Zhou, Q. Tang, G. Storm, G. Molema, P. Y. Lu, P. V. Scaria, and M. C. Woodle. Cancer siRNA therapy by tumor selective delivery with ligand-targeted sterically stabilized nanoparticle. *Nucleic Acids Res.* **2004**, *32*, e149-e149.

[185] N. C. Bellocq, S. H. Pun, G. S. Jensen, and M. E. Davis. Transferrin-Containing, Cyclodextrin Polymer-Based Particles for Tumor-Targeted Gene Delivery. *Bioconjugate Chem.* **2003**, *14*, 1122-1132.

[186] M. K. Yu, J. Park, and S. Jon. Targeting strategies for multifunctional nanoparticles in cancer imaging and therapy. *Theranostics* **2012**, *2*, 3-44.

[187] K. E. Sapsford, W. R. Algar, L. Berti, K. B. Gemmill, B. J. Casey, E. Oh, M. H. Stewart, and I. L. Medintz. Functionalizing Nanoparticles with Biological Molecules: Developing Chemistries that Facilitate Nanotechnology. *Chem. Rev.* **2013**, *113*, 1904-2074.

[188] V. H. Shargh, H. Hondermarck, and M. Liang. Antibody-targeted biodegradable nanoparticles for cancer therapy. *Nanomedicine* **2015**, *11*, 63-79.

[189] P. Kocbek, N. Obermajer, M. Cegnar, J. Kos, and J. Kristl. Targeting cancer cells using PLGA nanoparticles surface modified with monoclonal antibody. *J. Controlled Release* **2007**, *120*, 18-26.

[190] M. E. Wiseman, and C. W. Frank. Antibody Adsorption and Orientation on Hydrophobic Surfaces. *Langmuir : the ACS journal of surfaces and colloids* **2012**, *28*, 1765-1774.

[191] L. Illum, P. D. Jones, R. W. Baldwin, and S. S. Davis. Tissue distribution of poly(hexyl 2-cyanoacrylate) nanoparticles coated with monoclonal antibodies in mice bearing human tumor xenografts. *J. Pharmacol. Exp. Ther.* **1984**, *230*, 733.

[192] W. R. Algar, D. E. Prasuhn, M. H. Stewart, T. L. Jennings, J. B. Blanco-Canosa, P. E. Dawson, and I. L. Medintz. The Controlled Display of Biomolecules on Nanoparticles: A Challenge Suited to Bioorthogonal Chemistry. *Bioconjugate Chem.* **2011**, *22*, 825-858.

[193] A. Z. Wang, F. Gu, L. Zhang, J. M. Chan, A. Radovic-Moreno, M. R. Shaikh, and O. C. Farokhzad. Biofunctionalized targeted nanoparticles for therapeutic applications. *Expert Opin Biol Ther* **2008**, *8*, 1063-1070.

[194] F. Alexis, E. Pridgen, L. K. Molnar, and O. C. Farokhzad. Factors Affecting the Clearance and Biodistribution of Polymeric Nanoparticles. *Mol. Pharmaceutics* **2008**, *5*, 505-515.

[195] H. Cabral, Y. Matsumoto, K. Mizuno, Q. Chen, M. Murakami, M. Kimura, Y. Terada, M. R. Kano, K. Miyazono, M. Uesaka, N. Nishiyama, and K. Kataoka. Accumulation of sub-100 nm polymeric micelles in poorly permeable tumours depends on size. *Nature Nanotechnology* **2011**, *6*, 815.

[196] B. Sun, and S.-S. Feng. Trastuzumab-functionalized nanoparticles of biodegradable copolymers for targeted delivery of docetaxel. *Nanomedicine* **2009**, *4*, 431-445.

[197] D. J. Slamon, W. Godolphin, L. A. Jones, J. A. Holt, S. G. Wong, D. E. Keith, W. J. Levin, S. G. Stuart, J. Udove, A. Ullrich, and a. et. Studies of the HER-2/neu proto-oncogene in human breast and ovarian cancer. *Science (New York, N.Y.)* **1989**, *244*, 707.

[198] B. Sun, B. Ranganathan, and S.-S. Feng. Multifunctional poly(d,l-lactide-co-glycolide)/montmorillonite (PLGA/MMT) nanoparticles decorated by Trastuzumab for targeted chemotherapy of breast cancer. *Biomaterials* **2008**, *29*, 475-486.

[199] S. D. Weitman, R. H. Lark, L. R. Coney, D. W. Fort, V. Frasca, V. R. Zurawski, and B. A. Kamen. Distribution of the Folate Receptor GP38 in Normal and Malignant Cell Lines and Tissues. *Cancer Res.* **1992**, *52*, 3396.

[200] D. S. Salomon, R. Brandt, F. Ciardiello, and N. Normanno. Epidermal growth factor-related peptides and their receptors in human malignancies. *Crit. Rev. Oncol./Hematol.* **1995**, *19*, 183-232.

[201] J. M. Saul, A. V. Annapragada, and R. V. Bellamkonda. A dual-ligand approach for enhancing targeting selectivity of therapeutic nanocarriers. *J. Controlled Release* **2006**, *114*, 277-287.

[202] J. Cui, M. Björnmalm, Y. Ju, and F. Caruso. Nanoengineering of Poly(ethylene glycol) Particles for Stealth and Targeting. *Langmuir : the ACS journal of surfaces and colloids* **2018**, *34*, 10817-10827.

[203] J. F. Apperley. Chronic myeloid leukaemia. *The Lancet* **2015**, *385*, 1447-1459.

[204] B. J. Druker, F. Guilhot, S. G. O'Brien, I. Gathmann, H. Kantarjian, N. Gattermann, M. W. N. Deininger, R. T. Silver, J. M. Goldman, R. M. Stone, F. Cervantes, A. Hochhaus, B. L. Powell, J. L. Gabrilove, P. Rousselot, J. Reiffers, J. J. Cornelissen, T. Hughes, H. Agis, T. Fischer, G. Verhoef, J. Shepherd, G. Saglio, A. Gratwohl, J. L. Nielsen, J. P. Radich, B. Simonsson, K. Taylor, M. Baccarani, C. So, L. Letvak, and R. A. Larson. Five-Year Follow-up of Patients Receiving Imatinib for Chronic Myeloid Leukemia. *New Engl. J. Med.* **2006**, *355*, 2408-2417.

[205] D. Bixby, and M. Talpaz. Mechanisms of resistance to tyrosine kinase inhibitors in chronic myeloid leukemia and recent therapeutic strategies to overcome resistance. *ASH Education Program Book* **2009**, *2009*, 461-476.

[206] P. Song, L. Ye, J. Fan, Y. Li, X. Zeng, Z. Wang, S. Wang, G. Zhang, P. Yang, Z. Cao, and D. Ju. Asparaginase induces apoptosis and cytoprotective autophagy in chronic myeloid leukemia cells. *Oncotarget* **2015**, *6*, 3861-3873.

[207] C. Daniele, T. Saverio, B. Ovidio, R. C. Laurent, V. P. Maria, D. Rita, V. Giovanna, and S. Claudia. Expanding Targets for a Metabolic Therapy of Cancer: L-Asparaginase. *Recent Patents on Anti-Cancer Drug Discovery* **2012**, *7*, 4-13.

[208] M. Wolf, M. Wirth, F. Pittner, and F. Gabor. Stabilisation and determination of the biological activity of l-asparaginase in poly(d,l-lactide-co-glycolide) nanospheres. *Int. J. Pharm.* **2003**, *256*, 141-152.

[209] E. L. Baldwin, and N. Osheroff. Etoposide, topoisomerase II and cancer. *Curr Med Chem Anticancer Agents* **2005**, *5*, 363-372.

[210] E. H. Panosyan, Y. Wang, P. Xia, W. N. Lee, Y. Pak, D. R. Laks, H. J. Lin, T. B. Moore, T. F. Cloughesy, H. I. Kornblum, and J. L. Lasky, 3rd. Asparagine depletion potentiates the cytotoxic effect of chemotherapy against brain tumors. *Mol. Cancer Res.* **2014**, *12*, 694-702.

[211] L. Zhang, A. F. Radovic-Moreno, F. Alexis, F. X. Gu, P. A. Basto, V. Bagalkot, S. Jon, R. S. Langer, and O. C. Farokhzad. Co-delivery of hydrophobic and hydrophilic drugs from nanoparticle-aptamer bioconjugates. *ChemMedChem* **2007**, *2*, 1268-71.

[212] H.-C. Shin, A. W. G. Alani, D. A. Rao, N. C. Rockich, and G. S. Kwon. Multi-drug loaded polymeric micelles for simultaneous delivery of poorly soluble anticancer drugs. *J. Controlled Release* **2009**, *140*, 294-300.

[213] M. H. Woo, L. J. Hak, M. C. Storm, J. T. Sandlund, R. C. Ribeiro, G. K. Rivera, J. E. Rubnitz, P. L. Harrison, B. Wang, W. E. Evans, C.-H. Pui, and M. V. Relling. Hypersensitivity or Development of Antibodies to Asparaginase Does Not Impact Treatment Outcome of Childhood Acute Lymphoblastic Leukemia. *Journal of Clinical Oncology* **2000**, *18*, 1525-1532.

[214] J. B. Cole, T. Pamela, M. B. Eric, and M. A. Kristy. Drug Delivery for Cancer Immunotherapy and Vaccines. *Pharmaceutical Nanotechnology* **2018**, *6*, 232-244.

[215] W. E. Carson, J. E. Dierksheide, S. Jabbour, M. Anghelina, P. Bouchard, G. Ku, H. Yu, H. Baumann, M. H. Shah, M. A. Cooper, J. Durbin, and M. A. Caligiuri. Coadministration of interleukin-18 and interleukin-12 induces a fatal inflammatory response in mice: critical role of natural killer cell interferon-γ production and STAT-mediated signal transduction. *Blood* **2000**, *96*, 1465.

[216] G. Q. Phan, J. C. Yang, R. M. Sherry, P. Hwu, S. L. Topalian, D. J. Schwartzentruber, N. P. Restifo, L. R. Haworth, C. A. Seipp, L. J. Freezer, K. E. Morton, S. A. Mavroukakis, P. H. Duray, S. M. Steinberg, J. P. Allison, T. A. Davis, and S. A. Rosenberg. Cancer regression and autoimmunity induced by cytotoxic T lymphocyte-associated antigen 4 blockade in patients with metastatic melanoma. *Proceedings of the National Academy of Sciences* **2003**, *100*, 8372.

[217] C. B. Chesson, and A. Zloza. Nanoparticles: augmenting tumor antigen presentation for vaccine and immunotherapy treatments of cancer. *Nanomedicine* **2017**, *12*, 2693-2706.

[218] M. L. Bookstaver, S. J. Tsai, J. S. Bromberg, and C. M. Jewell. Improving Vaccine and Immunotherapy Design Using Biomaterials. *Trends Immunol.* **2018**, *39*, 135-150.

[219] D. R. Wilson, R. Sen, J. C. Sunshine, D. M. Pardoll, J. J. Green, and Y. J. Kim. Biodegradable STING agonist nanoparticles for enhanced cancer immunotherapy. *Nanomed. Nanotechnol. Biol. Med.* **2018**, *14*, 237-246.

[220] D. Paßlick, K. Piradashvili, D. Bamberger, M. Li, S. Jiang, D. Strand, P. R. Wich, K. Landfester, M. Bros, S. Grabbe, and V. Mailänder. Delivering all in one: Antigen-nanocapsule loaded with dual adjuvant yields superadditive effects by DC-directed T cell stimulation. *J. Controlled Release* **2018**, *289*, 23-34.

[221] X. Cai, Y.-H. Chiu, and Zhijian J. Chen. The cGAS-cGAMP-STING Pathway of Cytosolic DNA Sensing and Signaling. *Mol. Cell* **2014**, *54*, 289-296.

[222] M. A. Collier, R. D. Junkins, M. D. Gallovic, B. M. Johnson, M. M. Johnson, A. N. Macintyre, G. D. Sempowski, E. M. Bachelder, J. P. Y. Ting, and K. M. Ainslie. Acetalated Dextran Microparticles for Codelivery of STING and TLR7/8 Agonists. *Mol. Pharmaceutics* **2018**, *15*, 4933-4946.

[223] K. J. Peine, E. M. Bachelder, Z. Vangundy, T. Papenfuss, D. J. Brackman, M. D. Gallovic, K. Schully, J. Pesce, A. Keane-Myers, and K. M. Ainslie. Efficient Delivery of the Toll-

like Receptor Agonists Polyinosinic:Polycytidylic Acid and CpG to Macrophages by Acetalated Dextran Microparticles. *Mol. Pharmaceutics* **2013**, *10*, 2849-2857.

[224] C. Fernandes, D. Suares, and M. C. Yergeri. Tumor Microenvironment Targeted Nanotherapy. *Frontiers in Pharmacology* **2018**, *9*, 1230.

[225] D. F. Quail, and J. A. Joyce. Molecular Pathways: Deciphering Mechanisms of Resistance to Macrophage-Targeted Therapies. *Clin. Cancer. Res.* **2017**, *23*, 876.

[226] C. D. Mills, K. Kincaid, J. M. Alt, M. J. Heilman, and A. M. Hill. M-1/M-2 Macrophages and the Th1/Th2 Paradigm. *The Journal of Immunology* **2000**, *164*, 6166.

[227] C. Mills. M1 and M2 Macrophages: Oracles of Health and Disease. **2012**, *32*, 463-488.

[228] K. Ley. M1 Means Kill; M2 Means Heal. *The Journal of Immunology* **2017**, *199*, 2191.

[229] M. Jarosz-Biej, N. Kamińska, S. Matuszczak, T. Cichoń, J. Pamuła-Piłat, J. Czapla, R. Smolarczyk, D. Skwarzyńska, K. Kulik, and S. Szala. M1-like macrophages change tumor blood vessels and microenvironment in murine melanoma. *PloS one* **2018**, *13*, e0191012.

[230] X. Zheng, K. Turkowski, J. Mora, B. Brüne, W. Seeger, A. Weigert, and R. Savai. Redirecting tumor-associated macrophages to become tumoricidal effectors as a novel strategy for cancer therapy. *Oncotarget* **2017**, *8*, 48436-48452.

[231] K. K. Goswami, T. Ghosh, S. Ghosh, M. Sarkar, A. Bose, and R. Baral. Tumor promoting role of anti-tumor macrophages in tumor microenvironment. *Cell. Immunol.* **2017**, *316*, 1-10.

[232] S. Hoves, C.-H. Ooi, C. Wolter, H. Sade, S. Bissinger, M. Schmittnaegel, O. Ast, A. M. Giusti, K. Wartha, V. Runza, W. Xu, Y. Kienast, M. A. Cannarile, H. Levitsky, S. Romagnoli, M. De Palma, D. Rüttinger, and C. H. Ries. Rapid activation of tumor-associated macrophages boosts preexisting tumor immunity. *The Journal of Experimental Medicine* **2018**, *215*, 859.

[233] C. B. Rodell, S. P. Arlauckas, M. F. Cuccarese, C. S. Garris, R. Li, M. S. Ahmed, R. H. Kohler, M. J. Pittet, and R. Weissleder. TLR7/8-agonist-loaded nanoparticles promote the polarization of tumour-associated macrophages to enhance cancer immunotherapy. *Nat Biomed Eng* **2018**, *2*, 578-588.

[234] Y. Wang, Y.-X. Lin, S.-L. Qiao, H.-W. An, Y. Ma, Z.-Y. Qiao, R. P. Y. J. Rajapaksha, and H. Wang. Polymeric nanoparticles promote macrophage reversal from M2 to M1 phenotypes in the tumor microenvironment. *Biomaterials* **2017**, *112*, 153-163.

[235] E. M. Bachelder, T. T. Beaudette, K. E. Broaders, J. M. J. Fréchet, M. T. Albrecht, A. J. Mateczun, K. M. Ainslie, J. T. Pesce, and A. M. Keane-Myers. In Vitro Analysis of Acetalated Dextran Microparticles as a Potent Delivery Platform for Vaccine Adjuvants. *Mol. Pharmaceutics* **2010**, *7*, 826-835.

[236] D. Reichel, M. Tripathi, and J. M. Perez. Biological Effects of Nanoparticles on Macrophage Polarization in the Tumor Microenvironment. *Nanotheranostics* **2019**, *3*, 66-88.

[237] L. D. Falo, M. Kovacsovics-Bankowski, K. Thompson, and K. L. Rock. Targeting antigen into the phagocytic pathway in vivo induces protective tumour immunity. *Nat. Med.* **1995**, *1*, 649-653.

[238] M. Kovacsovics-Bankowski, K. Clark, B. Benacerraf, and K. L. Rock. Efficient major histocompatibility complex class I presentation of exogenous antigen upon phagocytosis by macrophages. *Proceedings of the National Academy of Sciences of the United States of America* **1993**, *90*, 4942-4946.

[239] D. B. Graham, L. M. Stephenson, S. K. Lam, K. Brim, H. M. Lee, J. Bautista, S. Gilfillan, S. Akilesh, K. Fujikawa, and W. Swat. An ITAM-signaling pathway controls cross-presentation of particulate but not soluble antigens in dendritic cells. *The Journal of Experimental Medicine* **2007**, *204*, 2889.

[240] L. M. Kranz, M. Diken, H. Haas, S. Kreiter, C. Loquai, K. C. Reuter, M. Meng, D. Fritz, F. Vascotto, H. Hefesha, C. Grunwitz, M. Vormehr, Y. Hüsemann, A. Selmi, A. N. Kuhn, J. Buck, E. Derhovanessian, R. Rae, S. Attig, J. Diekmann, R. A. Jabulowsky, S. Heesch, J. Hassel, P. Langguth, S. Grabbe, C. Huber, Ö. Türeci, and U. Sahin. Systemic RNA delivery to dendritic cells exploits antiviral defence for cancer immunotherapy. *Nature* **2016**, *534*, 396.

[241] R. A. Rosalia, L. J. Cruz, S. van Duikeren, A. T. Tromp, A. L. Silva, W. Jiskoot, T. de Gruijl, C. Löwik, J. Oostendorp, S. H. van der Burg, and F. Ossendorp. CD40-targeted dendritic cell delivery of PLGA-nanoparticle vaccines induce potent anti-tumor responses. *Biomaterials* **2015**, *40*, 88-97.

[242] S. N. Thomas, E. Vokali, A. W. Lund, J. A. Hubbell, and M. A. Swartz. Targeting the tumor-draining lymph node with adjuvanted nanoparticles reshapes the anti-tumor immune response. *Biomaterials* **2014**, *35*, 814-824.

[243] L. Jeanbart, M. Ballester, A. de Titta, P. Corthésy, P. Romero, J. A. Hubbell, and M. A. Swartz. Enhancing Efficacy of Anticancer Vaccines by Targeted Delivery to Tumor-Draining Lymph Nodes. *Cancer Immunology Research* **2014**, *2*, 436.

[244] J. Conniot, J. M. Silva, J. G. Fernandes, L. C. Silva, R. Gaspar, S. Brocchini, H. F. Florindo, and T. S. Barata. Cancer immunotherapy: nanodelivery approaches for immune cell targeting and tracking. *Frontiers in Chemistry* **2014**, *2*.

[245] S. N. Mueller, S. Tian, and J. M. DeSimone. Rapid and Persistent Delivery of Antigen by Lymph Node Targeting PRINT Nanoparticle Vaccine Carrier To Promote Humoral Immunity. *Mol. Pharmaceutics* **2015**, *12*, 1356-1365.

[246] Z. Xu, S. Ramishetti, Y.-C. Tseng, S. Guo, Y. Wang, and L. Huang. Multifunctional nanoparticles co-delivering Trp2 peptide and CpG adjuvant induce potent

cytotoxic T-lymphocyte response against melanoma and its lung metastasis. *J. Controlled Release* **2013**, *172*, 259-265.

[247] C. Macri, C. Dumont, A. P. Johnston, and J. D. Mintern. Targeting dendritic cells: a promising strategy to improve vaccine effectiveness. *Clin Transl Immunology* **2016**, *5*, e66-e66.

[248] M. Guo, S. Gong, S. Maric, Z. Misulovin, M. Pack, K. Mahnke, M. C. Nussenzweig, and R. M. Steinman. A monoclonal antibody to the DEC-205 endocytosis receptor on human dendritic cells. *Hum. Immunol.* **2000**, *61*, 729-738.

[249] K. Mahnke, M. Guo, S. Lee, H. Sepulveda, S. L. Swain, M. Nussenzweig, and R. M. Steinman. The Dendritic Cell Receptor for Endocytosis, Dec-205, Can Recycle and Enhance Antigen Presentation via Major Histocompatibility Complex Class II–Positive Lysosomal Compartments. *The Journal of Cell Biology* **2000**, *151*, 673.

[250] R. E. Shrimpton, M. Butler, A.-S. Morel, E. Eren, S. S. Hue, and M. A. Ritter. CD205 (DEC-205): A recognition receptor for apoptotic and necrotic self. *Mol. Immunol.* **2009**, *46*, 1229-1239.

[251] L. Bonifaz, D. Bonnyay, K. Mahnke, M. Rivera, M. C. Nussenzweig, and R. M. Steinman. Efficient Targeting of Protein Antigen to the Dendritic Cell Receptor DEC-205 in the Steady State Leads to Antigen Presentation on Major Histocompatibility Complex Class I Products and Peripheral CD8+ T Cell Tolerance. *The Journal of Experimental Medicine* **2002**, *196*, 1627.

[252] L. C. Bonifaz, D. P. Bonnyay, A. Charalambous, D. I. Darguste, S.-I. Fujii, H. Soares, M. K. Brimnes, B. Moltedo, T. M. Moran, and R. M. Steinman. In vivo targeting of antigens to maturing dendritic cells via the DEC-205 receptor improves T cell vaccination. *The Journal of experimental medicine* **2004**, *199*, 815-824.

[253] D. Dudziak, A. O. Kamphorst, G. F. Heidkamp, V. R. Buchholz, C. Trumpfheller, S. Yamazaki, C. Cheong, K. Liu, H.-W. Lee, C. G. Park, R. M. Steinman, and M. C. Nussenzweig. Differential Antigen Processing by Dendritic Cell Subsets in Vivo. *Science (New York, N.Y.)* **2007**, *315*, 107.

[254] M. A. Berciano-Guerrero, A. Montesa-Pino, G. Castaneda-Penalvo, L. Munoz-Fernandez, and J. Rodriguez-Flores. Nanoparticles in melanoma. *Curr. Med. Chem.* **2014**, *21*, 3701–3716.

[255] A. Garu, G. Moku, S. K. Gulla, and A. Chaudhuri. Genetic Immunization With In Vivo Dendritic Cell-targeting Liposomal DNA Vaccine Carrier Induces Long-lasting Antitumor Immune Response. *Mol. Ther.* **2016**, *24*, 385-397.

[256] S. S. Saluja, D. J. Hanlon, F. A. Sharp, E. Hong, D. Khalil, E. Robinson, R. Tigelaar, T. M. Fahmy, and R. L. Edelson. Targeting human dendritic cells via DEC-205 using PLGA nanoparticles leads to enhanced cross-presentation of a melanoma-associated antigen. *Int J Nanomedicine* **2014**, *9*, 5231–5246.

[257] L. J. Cruz, R. A. Rosalia, J. W. Kleinovink, F. Rueda, C. W. G. M. Löwik, and F. Ossendorp. Targeting nanoparticles to CD40, DEC-205 or CD11c molecules on dendritic cells for efficient CD8+ T cell response: A comparative study. *J. Controlled Release* **2014**, *192*, 209-218.

[258] C. M. Fehres, A. J. van Beelen, S. C. M. Bruijns, M. Ambrosini, H. Kalay, L. v. Bloois, W. W. J. Unger, J. J. Garcia-Vallejo, G. Storm, T. D. de Gruijl, and Y. v. Kooyk. *In situ* Delivery of Antigen to DC-SIGN^{+}CD14^{+} Dermal Dendritic Cells Results in Enhanced CD8^{+} T-Cell Responses. *Journal of Investigative Dermatology* **2015**, *135*, 2228-2236.

[259] J. Xiang, L. Xu, H. Gong, W. Zhu, C. Wang, J. Xu, L. Feng, L. Cheng, R. Peng, and Z. Liu. Antigen-Loaded Upconversion Nanoparticles for Dendritic Cell Stimulation, Tracking, and Vaccination in Dendritic Cell-Based Immunotherapy. *ACS Nano* **2015**, *9*, 6401-6411.

[260] T. T. Beaudette, E. M. Bachelder, J. A. Cohen, A. C. Obermeyer, K. E. Broaders, J. M. J. Fréchet, E.-S. Kang, I. Mende, W. W. Tseng, M. G. Davidson, and E. G. Engleman. In Vivo Studies on the Effect of Co-Encapsulation of CpG DNA and Antigen in Acid-Degradable Microparticle Vaccines. *Mol. Pharmaceutics* **2009**, *6*, 1160-1169.

[261] L. Cui, J. A. Cohen, K. E. Broaders, T. T. Beaudette, and J. M. J. Fréchet. Mannosylated Dextran Nanoparticles: A pH-Sensitive System Engineered for Immunomodulation through Mannose Targeting. *Bioconjugate Chem.* **2011**, *22*, 949-957.

[262] A. Goswami, G. Verma, P. A. Hassan, and S. S. Bhagwat. Equilibrium and Dynamic Surface Tension Behavior of Triblock Copolymer PEO-PPO-PEO in Aqueous Medium. *J. Dispersion Sci. Technol.* **2015**, *36*, 885-891.

[263] C. Smith. Biological Membranes. *https://slideplayer.com/slide/7360690/* **2015**, *18.11.2019*.

[264] C. Wang, Z. Wang, and X. Zhang. Amphiphilic Building Blocks for Self-Assembly: From Amphiphiles to Supra-amphiphiles. *Acc. Chem. Res.* **2012**, *45*, 608-618.

[265] D. Lombardo, M. A. Kiselev, S. Magaz, and P. Calandra. Amphiphiles Self-Assembly: Basic Concepts and Future Perspectives of Supramolecular Approaches. *Advances in Condensed Matter Physics* **2015**, *2015*, 22.

[266] H. Feng, X. Lu, W. Wang, N.-G. Kang, and W. J. Mays. Block Copolymers: Synthesis, Self-Assembly, and Applications. *Polymers* **2017**, *9*.

[267] C. J. Hawker, and K. L. Wooley. The Convergence of Synthetic Organic and Polymer Chemistries. *Science (New York, N.Y.)* **2005**, *309*, 1200.

[268] C. Aydogan, C. Kutahya, A. Allushi, G. Yilmaz, and Y. Yagci. Block copolymer synthesis in one shot: concurrent metal-free ATRP and ROP processes under sunlight. *Polymer Chemistry* **2017**, *8*, 2899-2903.

[269] A. Mühlebach, S. G. Gaynor, and K. Matyjaszewski. Synthesis of Amphiphilic Block Copolymers by Atom Transfer Radical Polymerization (ATRP). *Macromolecules* **1998**, *31*, 6046-6052.

[270] A. Blanazs, S. P. Armes, and A. J. Ryan. Self-Assembled Block Copolymer Aggregates: From Micelles to Vesicles and their Biological Applications. *Macromol. Rapid Commun.* **2009**, *30*, 267-277.

[271] A. Rösler, G. W. M. Vandermeulen, and H.-A. Klok. Advanced drug delivery devices via self-assembly of amphiphilic block copolymers. *Adv. Drug Delivery Rev.* **2012**, *64*, 270-279.

[272] M. Mekhail, L. Benameur, and M. Tabrizian. Chapter 25 - Self-Assembled Nanostructures (SANs), in *Biology and Engineering of Stem Cell Niches* (Vishwakarma, A., and Karp, J. M., Eds.) **2017**, pp 391-409, Academic Press, Boston.

[273] G. Gaucher, M.-H. Dufresne, V. P. Sant, N. Kang, D. Maysinger, and J.-C. Leroux. Block copolymer micelles: preparation, characterization and application in drug delivery. *J. Controlled Release* **2005**, *109*, 169-188.

[274] P. Alexandridis. Poly(ethylene oxide)/poly(propylene oxide) block copolymer surfactants. *Current Opinion in Colloid & Interface Science* **1997**, *2*, 478-489.

[275] J. H. Lee, J. Kopecek, and J. D. Andrade. Protein-resistant surfaces prepared by PEO-containing block copolymer surfactants. *Journal of Biomedical Materials Research* **1989**, *23*, 351-368.

[276] H. M. Aliabadi, S. Elhasi, A. Mahmud, R. Gulamhusein, P. Mahdipoor, and A. Lavasanifar. Encapsulation of hydrophobic drugs in polymeric micelles through co-solvent evaporation: The effect of solvent composition on micellar properties and drug loading. *Int. J. Pharm.* **2007**, *329*, 158-165.

[277] Y. H. A. Hussein, and M. Youssry. Polymeric Micelles of Biodegradable Diblock Copolymers: Enhanced Encapsulation of Hydrophobic Drugs. *Materials (Basel)* **2018**, *11*, 688.

[278] B. B. Breitenbach, I. Schmid, and P. R. Wich. Amphiphilic Polysaccharide Block Copolymers for pH-Responsive Micellar Nanoparticles. *Biomacromolecules* **2017**, *18*, 2839-2848.

[279] B. B. Breitenbach, E. Steiert, M. Konhäuser, L.-M. Vogt, Y. Wang, S. H. Parekh, and P. R. Wich. Double stimuli-responsive polysaccharide block copolymers as green macrosurfactants for near-infrared photodynamic therapy. *Soft Matter* **2019**, *15*, 1423-1434.

[280] Y. Zhang, Y. Huang, and S. Li. Polymeric micelles: nanocarriers for cancer-targeted drug delivery. *AAPS PharmSciTech* **2014**, *15*, 862-871.

[281] S. R. Croy, and G. S. Kwon. Polymeric Micelles for Drug Delivery. *Curr. Pharm. Des.* **2006**, *12*, 4669-4684.

[282] V. Y. Alakhov, E. Y. Moskaleva, E. V. Batrakova, and A. V. Kabanov. Hypersensitization of Multidrug Resistant Human Ovarian Carcinoma Cells by Pluronic P85 Block Copolymer. *Bioconjugate Chem.* **1996**, *7*, 209-216.

[283] M. L. Adams, and G. S. Kwon. Relative aggregation state and hemolytic activity of amphotericin B encapsulated by poly(ethylene oxide)-block–poly(N-hexyl-l-aspartamide)-acyl conjugate micelles: effects of acyl chain length. *J. Controlled Release* **2003**, *87*, 23-32.

[284] A. Lavasanifar, J. Samuel, and G. S. Kwon. Micelles self-assembled from poly(ethylene oxide)-block-poly(N-hexyl stearate l-aspartamide) by a solvent evaporation method: effect on the solubilization and haemolytic activity of amphotericin B. *J. Controlled Release* **2001**, *77*, 155-160.

[285] K. K. Jette, D. Law, E. A. Schmitt, and G. S. Kwon. Preparation and Drug Loading of Poly(Ethylene Glycol)-block-Poly(ε-Caprolactone) Micelles Through the Evaporation of a Cosolvent Azeotrope. *Pharm. Res.* **2004**, *21*, 1184-1191.

[286] X. Shuai, H. Ai, N. Nasongkla, S. Kim, and J. Gao. Micellar carriers based on block copolymers of poly(ε-caprolactone) and poly(ethylene glycol) for doxorubicin delivery. *J. Controlled Release* **2004**, *98*, 415-426.

[287] M. Yokoyama, A. Satoh, Y. Sakurai, T. Okano, Y. Matsumura, T. Kakizoe, and K. Kataoka. Incorporation of water-insoluble anticancer drug into polymeric micelles and control of their particle size. *J. Controlled Release* **1998**, *55*, 219-229.

[288] C. Allen, J. Han, Y. Yu, D. Maysinger, and A. Eisenberg. Polycaprolactone–b-poly(ethylene oxide) copolymer micelles as a delivery vehicle for dihydrotestosterone. *J. Controlled Release* **2000**, *63*, 275-286.

[289] J. Wang, S. Li, Y. Han, J. Guan, S. Chung, C. Wang, and D. Li. Poly(Ethylene Glycol)-Polylactide Micelles for Cancer Therapy. *Frontiers in pharmacology* **2018**, *9*, 202-202.

[290] W. Wei, T. Wang, C. Yi, J. Liu, and X. Liu. Self-assembled micelles based on branched poly(styrene-alt-maleic anhydride) as particulate emulsifiers. *RSC Advances* **2015**, *5*, 1564-1570.

[291] A. S. Mikhail, and C. Allen. Poly(ethylene glycol)-b-poly(ε-caprolactone) Micelles Containing Chemically Conjugated and Physically Entrapped Docetaxel: Synthesis, Characterization, and the Influence of the Drug on Micelle Morphology. *Biomacromolecules* **2010**, *11*, 1273-1280.

[292] A. B. Kutikov, and J. Song. Biodegradable PEG-Based Amphiphilic Block Copolymers for Tissue Engineering Applications. *ACS Biomater Sci Eng* **2015**, *1*, 463-480.

[293] R. L. Stein. A Process Theory of Enzyme Catalytic Power – the Interplay of Science and Metaphysics. *Foundations of Chemistry* **2006**, *8*, 3-29.

[294] M. A. Meyers, P.-Y. Chen, A. Y.-M. Lin, and Y. Seki. Biological materials: Structure and mechanical properties. *Prog. Mater Sci.* **2008**, *53*, 1-206.

[295] A. C. Obermeyer, and B. D. Olsen. Synthesis and Application of Protein-Containing Block Copolymers. *ACS Macro Letters* **2015**, *4*, 101-110.

[296] P. Bailon, A. Palleroni, C. A. Schaffer, C. L. Spence, W.-J. Fung, J. E. Porter, G. K. Ehrlich, W. Pan, Z.-X. Xu, M. W. Modi, A. Farid, W. Berthold, and M. Graves. Rational Design of a Potent, Long-Lasting Form of Interferon: A 40 kDa Branched Polyethylene Glycol-Conjugated Interferon α-2a for the Treatment of Hepatitis C. *Bioconjugate Chem.* **2001**, *12*, 195-202.

[297] P. Tae Gwan, and A. S. Hoffman. Synthesis and characterization of a soluble, temperature-sensitive polymer-conjugated enzyme. *Journal of Biomaterials Science, Polymer Edition* **1993**, *4*, 493-504.

[298] D. Chang, C. N. Lam, S. Tang, and B. D. Olsen. Effect of polymer chemistry on globular protein–polymer block copolymer self-assembly. *Polymer Chemistry* **2014**, *5*, 4884-4895.

[299] S. Banerjee, N. Aher, R. Patil, and J. Khandare. Poly(ethylene glycol)-Prodrug Conjugates: Concept, Design, and Applications. *Journal of drug delivery* **2012**, *2012*, 103973.

[300] E. M. Pelegri-O'Day, E.-W. Lin, and H. D. Maynard. Therapeutic Protein–Polymer Conjugates: Advancing Beyond PEGylation. *J. Am. Chem. Soc.* **2014**, *136*, 14323-14332.

[301] N. M. Giles, G. I. Giles, and C. Jacob. Multiple roles of cysteine in biocatalysis. *Biochem. Biophys. Res. Commun.* **2003**, *300*, 1-4.

[302] D. P. Nair, M. Podgórski, S. Chatani, T. Gong, W. Xi, C. R. Fenoli, and C. N. Bowman. The Thiol-Michael Addition Click Reaction: A Powerful and Widely Used Tool in Materials Chemistry. *Chem. Mater.* **2014**, *26*, 724-744.

[303] A. B. Lowe. Thiol-ene "click" reactions and recent applications in polymer and materials synthesis. *Polymer Chemistry* **2010**, *1*, 17-36.

[304] K. L. Heredia, and H. D. Maynard. Synthesis of protein–polymer conjugates. *Organic & Biomolecular Chemistry* **2007**, *5*, 45-53.

[305] M. Li, P. De, H. Li, and B. S. Sumerlin. Conjugation of RAFT-generated polymers to proteins by two consecutive thiol–ene reactions. *Polymer Chemistry* **2010**, *1*, 854-859.

[306] R. N. Johnson, P. Kopečková, and J. Kopeček. Biological Activity of Anti-CD20 Multivalent HPMA Copolymer-Fab' Conjugates. *Biomacromolecules* **2012**, *13*, 727-735.

[307] M. H. Stenzel. Bioconjugation Using Thiols: Old Chemistry Rediscovered to Connect Polymers with Nature's Building Blocks. *ACS Macro Letters* **2013**, *2*, 14-18.

[308] B. A. Paik, S. R. Mane, X. Jia, and K. L. Kiick. Responsive Hybrid (Poly)peptide-Polymer Conjugates. *J Mater Chem B* **2017**, *5*, 8274-8288.

[309] H. Sui, Y. Wang, Z. Yu, Q. Cong, X. X. Han, and B. Zhao. A rapid and ultrasensitive SERRS assay for histidine and tyrosine based on azo coupling. *Talanta* **2016**, *159*, 208-214.

[310] D. W. Romanini, and M. B. Francis. Attachment of Peptide Building Blocks to Proteins Through Tyrosine Bioconjugation. *Bioconjugate Chem.* **2008**, *19*, 153-157.

[311] L. S. Witus, T. Moore, B. W. Thuronyi, A. P. Esser-Kahn, R. A. Scheck, A. T. Iavarone, and M. B. Francis. Identification of Highly Reactive Sequences For PLP-Mediated Bioconjugation Using a Combinatorial Peptide Library. *J. Am. Chem. Soc.* **2010**, *132*, 16812-16817.

[312] J. Y. Shu, Y.-J. Huang, C. Tan, A. D. Presley, J. Chang, and T. Xu. Amphiphilic Peptide–Polymer Conjugates Based on the Coiled-Coil Helix Bundle. *Biomacromolecules* **2010**, *11*, 1443-1452.

[313] J. E. Hudak, R. M. Barfield, G. W. de Hart, P. Grob, E. Nogales, C. R. Bertozzi, and D. Rabuka. Synthesis of Heterobifunctional Protein Fusions Using Copper-Free Click Chemistry and the Aldehyde Tag. *Angew. Chem. Int. Ed.* **2012**, *51*, 4161-4165.

[314] N. Stephanopoulos, and M. B. Francis. Choosing an effective protein bioconjugation strategy. *Nat. Chem. Biol.* **2011**, *7*, 876-884.

[315] S. Averick, R. A. Mehl, S. R. Das, and K. Matyjaszewski. Well-defined biohybrids using reversible-deactivation radical polymerization procedures. *J. Controlled Release* **2015**, *205*, 45-57.

[316] T. A. Wright, R. C. Page, and D. Konkolewicz. Polymer conjugation of proteins as a synthetic post-translational modification to impact their stability and activity. *Polymer Chemistry* **2019**, *10*, 434-454.

[317] J. Liu, V. Bulmus, D. L. Herlambang, C. Barner-Kowollik, M. H. Stenzel, and T. P. Davis. In Situ Formation of Protein–Polymer Conjugates through Reversible Addition Fragmentation Chain Transfer Polymerization. *Angew. Chem. Int. Ed.* **2007**, *46*, 3099-3103.

[318] C. Boyer, X. Huang, M. R. Whittaker, V. Bulmus, and T. P. Davis. An overview of protein–polymer particles. *Soft Matter* **2011**, *7*, 1599-1614.

[319] J. M. Hannink, J. J. L. M. Cornelissen, J. A. Farrera, P. Foubert, F. C. De Schryver, N. A. J. M. Sommerdijk, and R. J. M. Nolte. Protein–Polymer Hybrid Amphiphiles. *Angew. Chem. Int. Ed.* **2001**, *40*, 4732-4734.

[320] G. N. Grover, and H. D. Maynard. Protein–polymer conjugates: synthetic approaches by controlled radical polymerizations and interesting applications. *Curr. Opin. Chem. Biol.* **2010**, *14*, 818-827.

[321] T. Shimoboji, E. Larenas, T. Fowler, S. Kulkarni, A. S. Hoffman, and P. S. Stayton. Photoresponsive polymer–enzyme switches. *Proceedings of the National Academy of Sciences* **2002**, *99*, 16592.

[322] Y. Jiang, and M. Stenzel. Drug Delivery Vehicles Based on Albumin–Polymer Conjugates. *Macromol. Biosci.* **2016**, *16*, 791-802.

[323] Y. Jiang, M. Liang, D. Svejkar, G. Hart-Smith, H. Lu, W. Scarano, and M. H. Stenzel. Albumin-micelles via a one-pot technology platform for the delivery of drugs. *Chem. Commun.* **2014**, *50*, 6394-6397.

[324] M. J. Boerakker, J. M. Hannink, P. H. H. Bomans, P. M. Frederik, R. J. M. Nolte, E. M. Meijer, and N. A. J. M. Sommerdijk. Giant Amphiphiles by Cofactor Reconstitution. *Angew. Chem. Int. Ed.* **2002**, *41*, 4239-4241.

[325] W. Peter. Indole-3-Acetic Acids and Horseradish Peroxidase: A New Prodrug / Enzyme Combination for Targeted Cancer Therapy. *Curr. Pharm. Des.* **2002**, *8*, 1363-1374.

[326] L. D. Blackman, S. Varlas, M. C. Arno, Z. H. Houston, N. L. Fletcher, K. J. Thurecht, M. Hasan, M. I. Gibson, and R. K. O'Reilly. Confinement of Therapeutic Enzymes in Selectively Permeable Polymer Vesicles by Polymerization-Induced Self-Assembly (PISA) Reduces Antibody Binding and Proteolytic Susceptibility. *ACS Cent Sci* **2018**, *4*, 718-723.

[327] E. T. Baran, N. özer, and V. Hasirci. In vivo half life of nanoencapsulated L-asparaginase. *J. Mater. Sci. Mater. Med.* **2002**, *13*, 1113-1121.

[328] C. A. Apolinário, S. M. Magoń, A. Pessoa Jr, and D. C. Rangel-Yagui. Challenges for the Self-Assembly of Poly(Ethylene Glycol)–Poly(Lactic Acid) (PEG-PLA) into Polymersomes: Beyond the Theoretical Paradigms. *Nanomaterials* **2018**, *8*.

[329] M. Gaspar, D. Blanco, and M. Cruz. Formulation of l-asparaginase-loaded poly(lactide-co-glycolide) nanoparticles: influence of polymer properties on enzyme loading, activity and in vitro release. *J. Controlled Release* **1998**, *52*, 53–62.

[330] W.-Y. Qian, D.-M. Sun, R.-R. Zhu, X.-L. Du, H. Liu, and S.-L. Wang. pH-sensitive strontium carbonate nanoparticles as new anticancer vehicles for controlled etoposide release. *International journal of nanomedicine* **2012**, *7*, 5781-5792.

[331] A. Tsend-Ayush, X. Zhu, Y. Ding, J. Yao, L. Yin, J. Zhou, and J. Yao. Lactobionic acid-conjugated TPGS nanoparticles for enhancing therapeutic efficacy of etoposide against hepatocellular carcinoma. *Nanotechnology* **2017**, *28*, 195602.

[332] B. Wang, X.-C. Yu, S.-F. Xu, and M. Xu. Paclitaxel and etoposide co-loaded polymeric nanoparticles for the effective combination therapy against human osteosarcoma. *Journal of Nanobiotechnology* **2015**, *13*, 22.

[333] J. Jingou, H. Shilei, L. Weiqi, W. Danjun, W. Tengfei, and X. Yi. Preparation, characterization of hydrophilic and hydrophobic drug in combine loaded chitosan/cyclodextrin nanoparticles and in vitro release study. *Colloids Surf. B. Biointerfaces* **2011**, *83*, 103-107.

[334] T. Niwa, H. Takeuchi, T. Hino, N. Kunou, and Y. Kawashima. Preparations of biodegradable nanospheres of water-soluble and insoluble drugs with D,L-lactide/glycolide copolymer by a novel spontaneous emulsification solvent diffusion method, and the drug release behavior. *J. Controlled Release* **1993**, *25*, 89-98.

[335] L. Español, A. Larrea, V. Andreu, G. Mendoza, M. Arruebo, V. Sebastian, M. S. Aurora-Prado, E. R. M. Kedor-Hackmann, M. I. R. M. Santoro, and J. Santamaria. Dual encapsulation of hydrophobic and hydrophilic drugs in PLGA nanoparticles by a single-step method: drug delivery and cytotoxicity assays. *RSC Advances* **2016**, *6*, 111060-111069.

[336] X. Song, Y. Zhao, S. Hou, F. Xu, R. Zhao, J. He, Z. Cai, Y. Li, and Q. Chen. Dual agents loaded PLGA nanoparticles: Systematic study of particle size and drug entrapment efficiency. *European Journal of Pharmaceutics and Biopharmaceutics* **2008**, *69*, 445-453.

[337] J. L. Cohen, S. Schubert, P. R. Wich, L. Cui, J. A. Cohen, J. L. Mynar, and J. M. Frechet. Acid-degradable cationic dextran particles for the delivery of siRNA therapeutics. *Bioconjugate Chem.* **2011**, *22*, 1056–1065.

[338] S. M. Moghimi, A. C. Hunter, and J. C. Murray. Long-circulating and target-specific nanoparticles: theory to practice. *Pharmacological reviews* **2001**, *53*, 283-318.

[339] Y. Nojima, K. Iguchi, Y. Suzuki, and A. Sato. The pH-Dependent Formation of PEGylated Bovine Lactoferrin by Branched Polyethylene Glycol (PEG) N-Hydroxysuccinimide (NHS) Active Esters. *Biol. Pharm. Bull.* **2009**, *32*, 523-526.

[340] A. R. Nicholas, M. J. Scott, N. I. Kennedy, and M. N. Jones. Effect of grafted polyethylene glycol (PEG) on the size, encapsulation efficiency and permeability of vesicles. *Biochim. Biophys. Acta* **2000**, *1463*, 167-178.

[341] N. T. Huynh, E. Roger, N. Lautram, J.-P. Benoît, and C. Passirani. The rise and rise of stealth nanocarriers for cancer therapy: passive versus active targeting. *Nanomedicine* **2010**, *5*, 1415–1433.

[342] A. S. Manjappa, K. R. Chaudhari, M. P. Venkataraju, P. Dantuluri, B. Nanda, C. Sidda, K. K. Sawant, and R. S. Murthy. Antibody derivatization and conjugation strategies: application in preparation of stealth immunoliposome to target chemotherapeutics to tumor. *J. Control. Release* **2011**, *150*, 2–22.

[343] S. Xu, F. Cui, D. Huang, D. Zhang, A. Zhu, X. Sun, Y. Cao, S. Ding, Y. Wang, E. Gao, and F. Zhang. PD-L1 monoclonal antibody-conjugated nanoparticles enhance drug delivery level and chemotherapy efficacy in gastric cancer cells. *International journal of nanomedicine* **2018**, *14*, 17-32.

[344] H. Chen, J. Gao, Y. Lu, G. Kou, H. Zhang, L. Fan, Z. Sun, Y. Guo, and Y. Zhong. Preparation and characterization of PE38KDEL-loaded anti-HER2 nanoparticles for targeted cancer therapy. *J. Controlled Release* **2008**, *128*, 209-216.

[345] S. Muro, T. Dziubla, W. Qiu, J. Leferovich, X. Cui, E. Berk, and V. R. Muzykantov. Endothelial Targeting of High-Affinity Multivalent Polymer Nanocarriers Directed to Intercellular Adhesion Molecule 1. *J. Pharmacol. Exp. Ther.* **2006**, *317*, 1161.

[346] M. Colombo, L. Fiandra, G. Alessio, S. Mazzucchelli, M. Nebuloni, C. De Palma, K. Kantner, B. Pelaz, R. Rotem, F. Corsi, W. J. Parak, and D. Prosperi. Tumour homing and therapeutic effect of colloidal nanoparticles depend on the number of attached antibodies. *Nature communications* **2016**, *7*, 13818-13818.

[347] J. Banchereau, and R. M. Steinman. Dendritic cells and the control of immunity. *Nature* **1998**, *392*, 245.

[348] R. Klippstein, and D. Pozo. Nanotechnology-based manipulation of dendritic cells for enhanced immunotherapy strategies. *Nanomedicine* **2010**, *6*, 523–529.

[349] S. Pustylnikov, D. Sagar, P. Jain, and Z. K. Khan. Targeting the C-type lectins-mediated host-pathogen interactions with dextran. *J Pharm Pharm Sci* **2014**, *17*, 371-392.

[350] D. Bamberger, D. Hobernik, M. Konhauser, M. Bros, and P. R. Wich. Surface Modification of Polysaccharide-Based Nanoparticles with PEG and Dextran and the Effects on Immune Cell Binding and Stimulatory Characteristics. *Mol. Pharmaceutics* **2017**, *14*, 4403–4416.

[351] W. Jiang, W. J. Swiggard, C. Heufler, M. Peng, A. Mirza, R. M. Steinman, and M. C. Nussenzweig. The receptor DEC-205 expressed by dendritic cells and thymic epithelial cells is involved in antigen processing. *Nature* **1995**, *375*, 151–155.

[352] T. Yonggang, M. Yiming, Z. Heying, S. Cheng, W. Qiushi, Y. Xianghong, Z. Wei, Z. Huawei, and F. Shan. Maturation and upregulation of functions of murine dendritic cells (DCs) under the influence of purified aromatic-turmerone (AR). *Human vaccines & immunotherapeutics* **2012**, *8*, 1416-1424.

[353] P. Chen, X. Liu, Y. Sun, P. Zhou, Y. Wang, and Y. Zhang. Dendritic cell targeted vaccines: Recent progresses and challenges. *Human vaccines & immunotherapeutics* **2015**, *12*, 612-622.

[354] D. E. Owens, 3rd, and N. A. Peppas. Opsonization, biodistribution, and pharmacokinetics of polymeric nanoparticles. *International journal of pharmaceutics* **2006**, *307*, 93–102.

[355] F. Foerster, D. Bamberger, J. Schupp, M. Weilbacher, L. Kaps, S. Strobl, L. Radi, M. Diken, D. Strand, A. Tuettenberg, P. R. Wich, and D. Schuppan. Dextran-based therapeutic nanoparticles for hepatic drug delivery. *Nanomedicine (Lond)* **2016**, *11*, 2663–2677.

[356] C. He, Y. Hu, L. Yin, C. Tang, and C. Yin. Effects of particle size and surface charge on cellular uptake and biodistribution of polymeric nanoparticles. *Biomaterials* **2010**, *31*, 3657–3666.

[357] J. M. den Haan, S. M. Lehar, and M. J. Bevan. CD8(+) but not CD8(-) dendritic cells cross-prime cytotoxic T cells in vivo. *J. Exp. Med.* **2000**, *192*, 1685-96.

[358] T. V. DeCollo, and W. J. Lees. Effects of Aromatic Thiols on Thiol−Disulfide Interchange Reactions That Occur during Protein Folding. *The Journal of Organic Chemistry* **2001**, *66*, 4244-4249.

[359] P. Winterwerber. Amphiphilic Protein Polysaccharide Conjugates with Double Stimuli Responsiveness, Master of Science Johannes Gutenberg University. **2018**.

[360] S. Das, and A. Chaudhury. Recent advances in lipid nanoparticle formulations with solid matrix for oral drug delivery. *AAPS PharmSciTech* **2011**, *12*, 62-76.

[361] C. Freitas, and R. H. Müller. Effect of light and temperature on zeta potential and physical stability in solid lipid nanoparticle (SLN™) dispersions. *Int. J. Pharm.* **1998**, *168*, 221-229.

[362] C. C. Woodroofe, R. Masalha, K. R. Barnes, C. J. Frederickson, and S. J. Lippard. Membrane-Permeable and -Impermeable Sensors of the Zinpyr Family and Their Application to Imaging of Hippocampal Zinc In Vivo. *Chem. Biol.* **2004**, *11*, 1659-1666.

[363] O. Greco, G. U. Dachs, G. M. Tozer, and C. Kanthou. Mechanisms of cytotoxicity induced by horseradish peroxidase/indole-3-acetic acid gene therapy. *J. Cell. Biochem.* **2002**, *87*, 221-232.

[364] F. W. Krainer, and A. Glieder. An updated view on horseradish peroxidases: recombinant production and biotechnological applications. *Appl. Microbiol. Biotechnol.* **2015**, *99*, 1611-1625.

[365] O. Augusto. Alkylation and cleavage of DNA by carbon-centered radical metabolites. *Free Radical Biol. Med.* **1993**, *15*, 329-336.

[366] L. K. Folkes, M. F. Dennis, M. R. L. Stratford, L. P. Candeias, and P. Wardman. Peroxidase-catalyzed effects of indole-3-acetic acid and analogues on lipid membranes, DNA, and mammalian cells in vitro. *Biochem. Pharmacol.* **1999**, *57*, 375-382.

[367] O. Greco, L. K. Folkes, P. Wardman, G. M. Tozer, and G. U. Dachs. Development of a novel enzyme/prodrug combination for gene therapy of cancer: horseradish peroxidase/indole-3-acetic acid. *Cancer Gene Ther.* **2000**, *7*, 1414-1420.

[368] B.-Y. Hung, Y. Kuthati, R. K. Kankala, S. Kankala, J.-P. Deng, C.-L. Liu, and C.-H. Lee. Utilization of Enzyme-Immobilized Mesoporous Silica Nanocontainers (IBN-4) in Prodrug-Activated Cancer Theranostics. *Nanomaterials (Basel)* **2015**, *5*, 2169-2191.

[369] X. Yang, J. Pang, N. Shen, F. Yan, L.-C. Wu, A. Al-Kali, M. R. Litzow, Y. Peng, R. J. Lee, and S. Liu. Liposomal bortezomib is active against chronic myeloid leukemia by disrupting the Sp1-BCR/ABL axis. *Oncotarget* **2016**, *7*, 36382-36394.

[370] E. M. Bachelder, T. T. Beaudette, K. E. Broaders, J. Dashe, and J. M. Frechet. Acetal-derivatized dextran: an acid-responsive biodegradable material for therapeutic applications. *J. Am. Chem. Soc.* **2008**, *130*, 10494–10495.

[371] L. Cui, J. A. Cohen, K. E. Broaders, T. T. Beaudette, and J. M. Frechet. Mannosylated dextran nanoparticles: a pH-sensitive system engineered for immunomodulation through mannose targeting. *Bioconjugate Chem.* **2011**, *22*, 949–957.

[372] H. E. Gottlieb, V. Kotlyar, and A. Nudelman. NMR Chemical Shifts of Common Laboratory Solvents as Trace Impurities. *J. Org. Chem.* **1997**, *62*, 7512-7515.

6.5 Supplemental Part

6.5.1 Selected ^1H-NMR Spectra

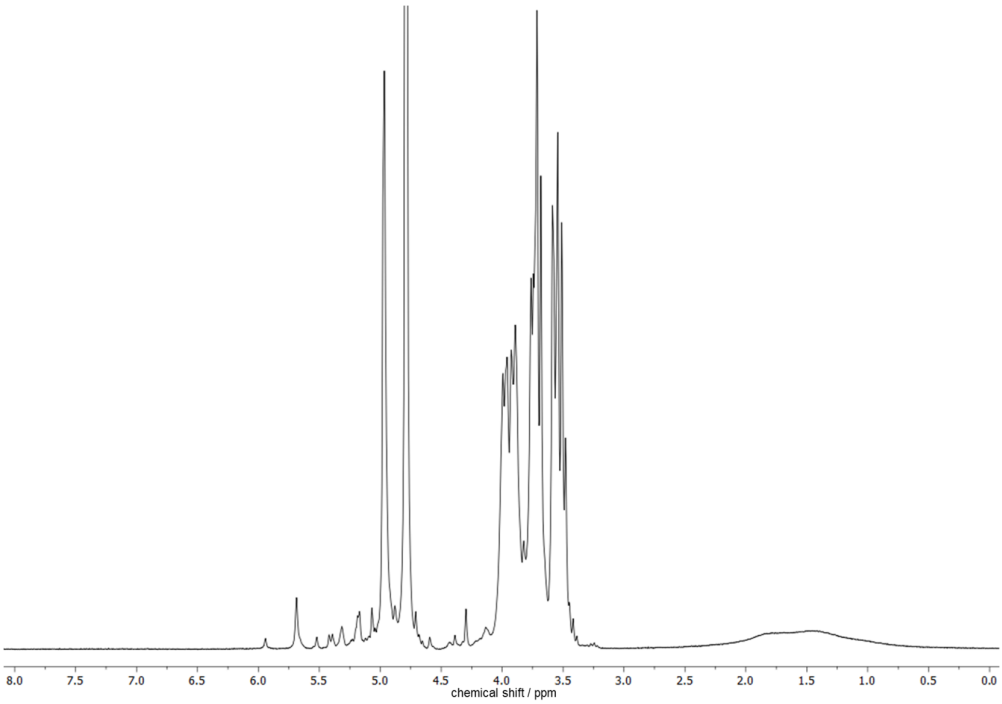

Figure 54. ^1H-NMR (D_2O, 300 MHz) of OxDex (10 kDa).

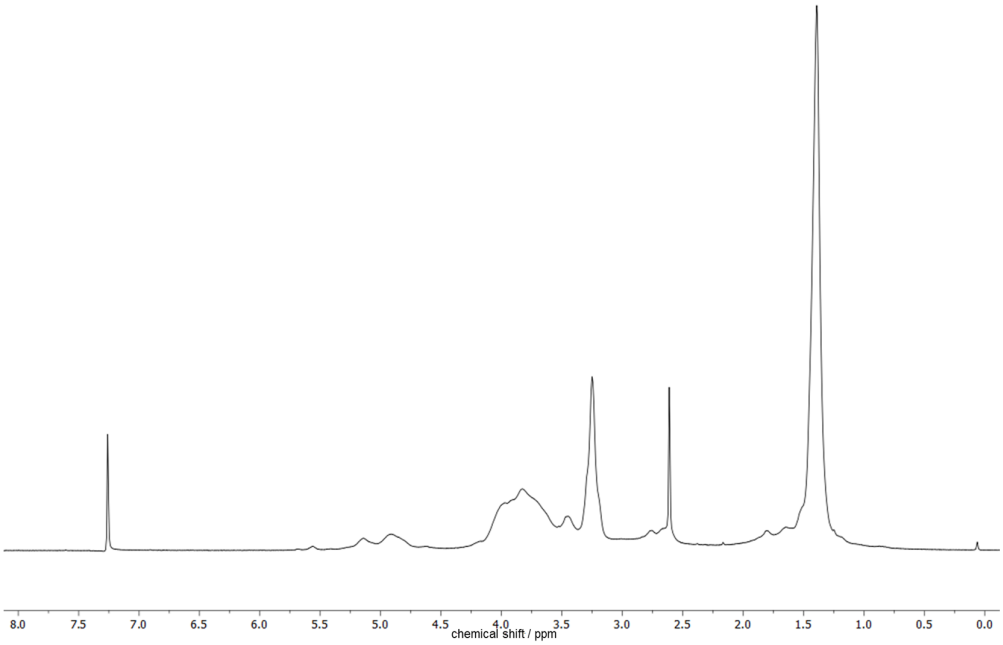

Figure 55. ^1H-NMR ($CDCl_3$, 300 MHz) of OxAcDex (10 kDa).

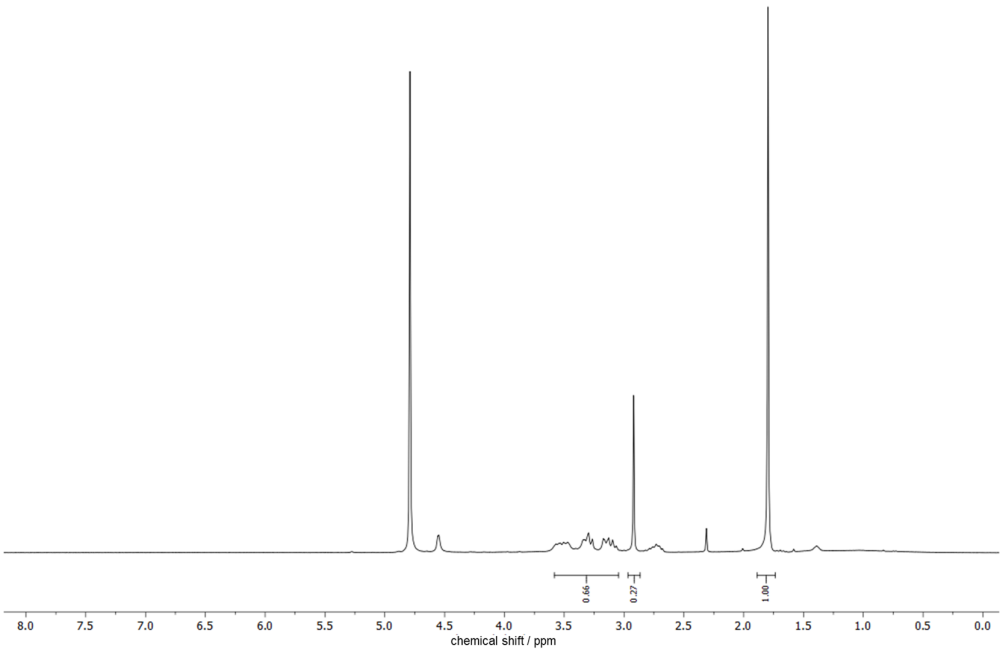

Figure 56. ^{1}H-NMR (D_2O/DCl, 300 MHz) of OxAcDex (10 kDa).

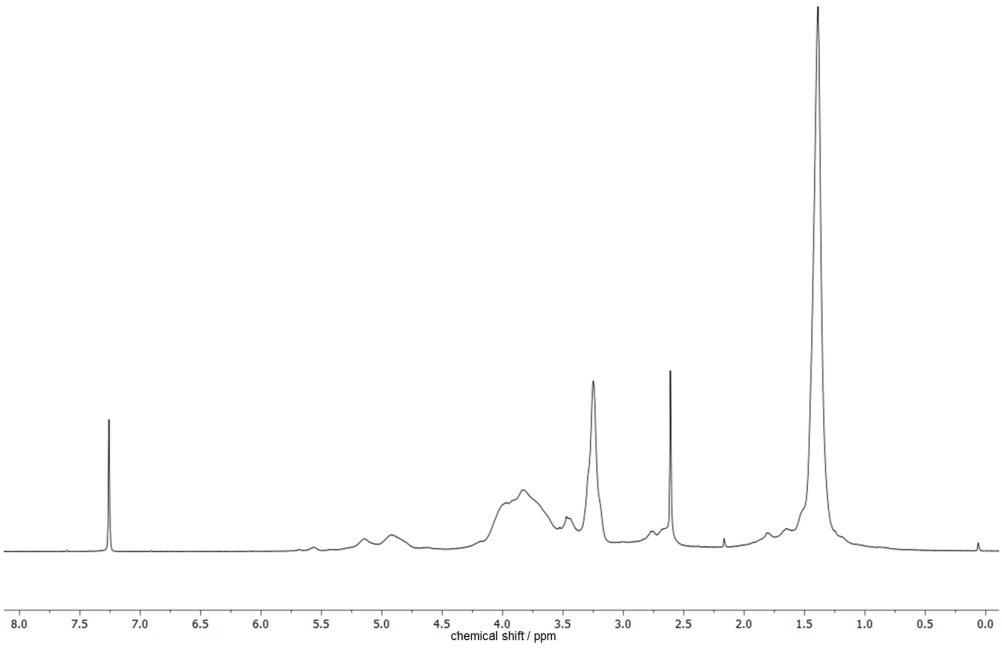

Figure 57. ^{1}H-NMR ($CDCl_3$, 300 MHz) of SpAcDex (10 kDa).

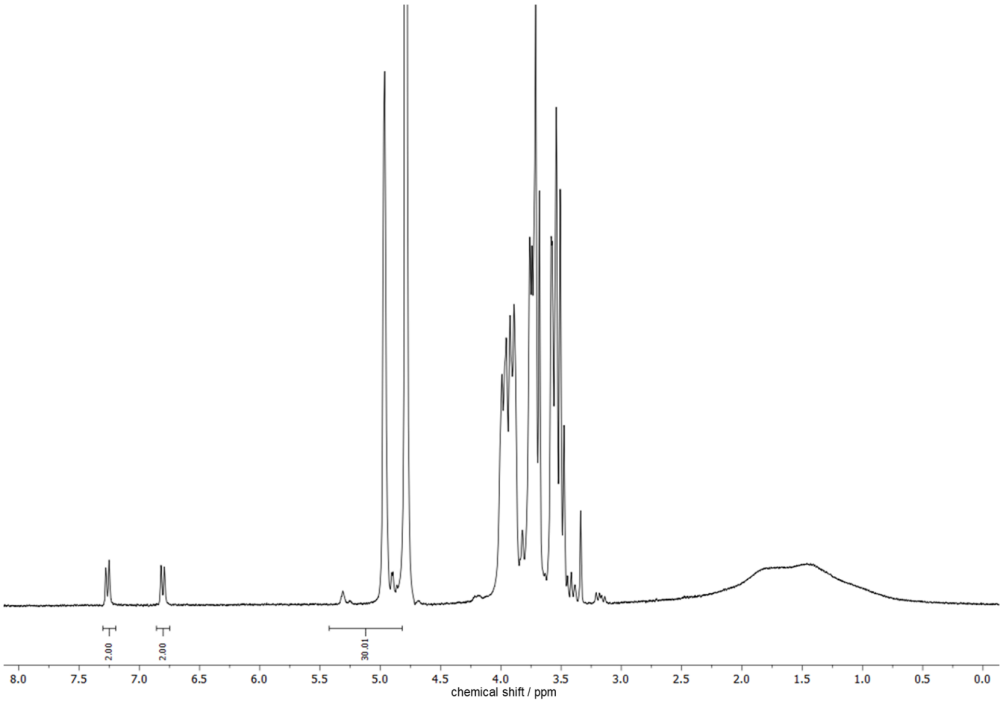

Figure 58. ^{1}H-NMR (D_2O, 300 MHz) of Dex-SH (5 kDa).

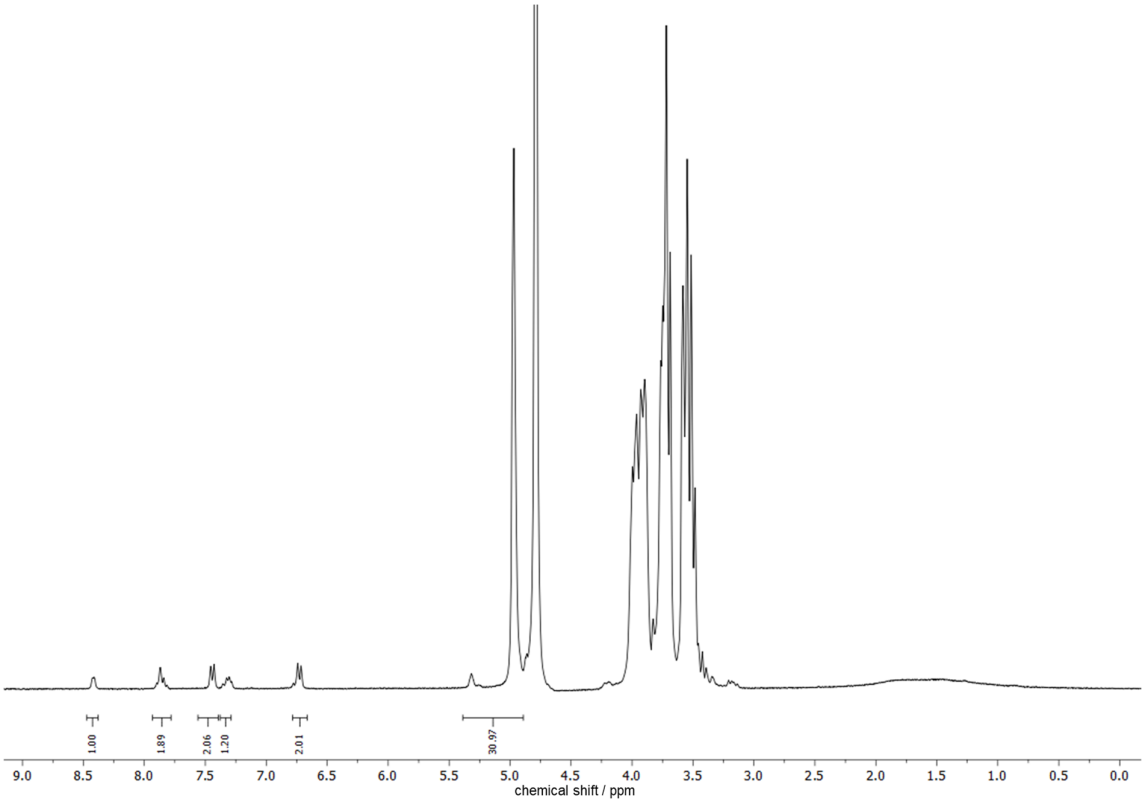

Figure 59. ^{1}H-NMR (D_2O, 300 MHz) of Dex-S-S-Py (5 kDa).

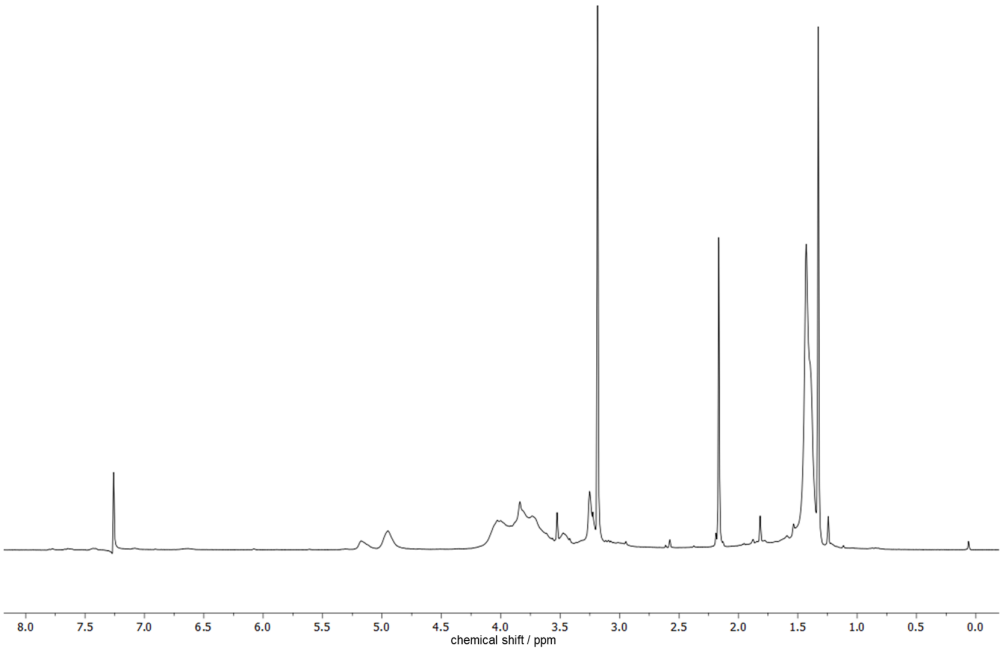

Figure 60. ^{1}H-NMR (DCl_3, 300 MHz) of AcDex-S-S-Py (5 kDa).

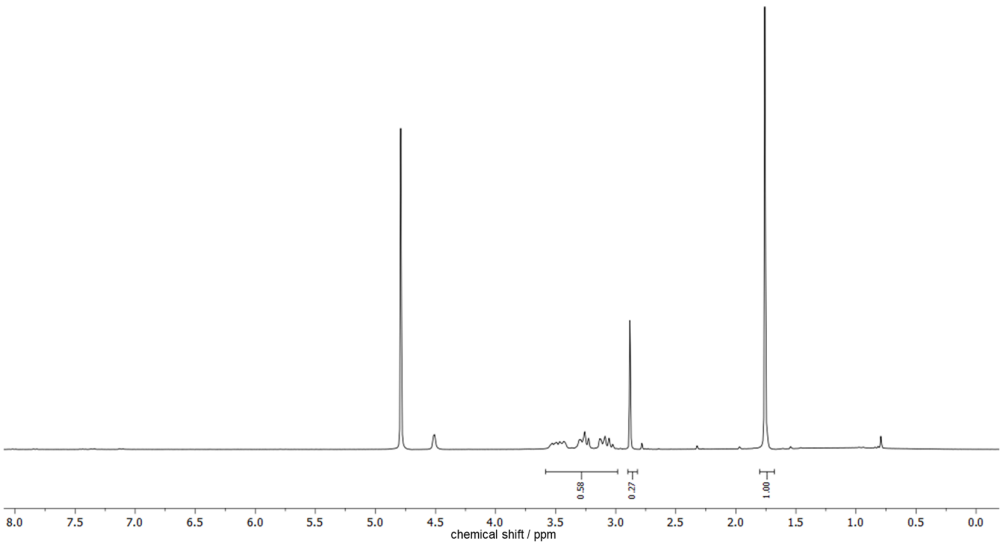

Figure 61. ^{1}H-NMR (D_2O/DCl, 300 MHz) of AcDex-S-S-Py (5 kDa).

6.5.2 Selected Standard Curves

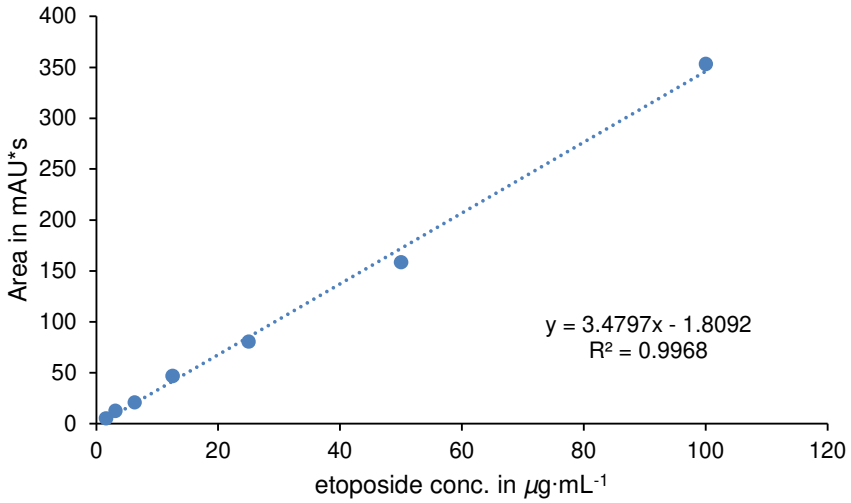

Figure 62. Standard curve of etoposide for determination of encapsulated etoposide in SpAcDex particles by absorbance measurement.

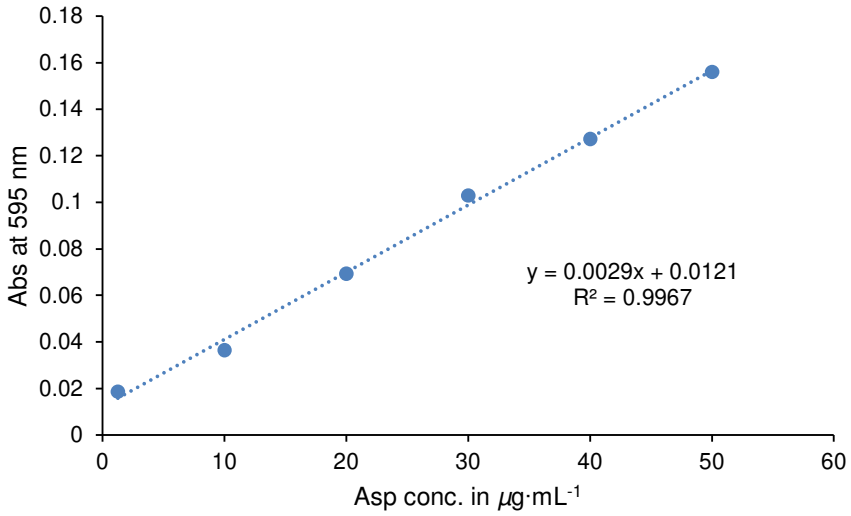

Figure 63. Standard curve of Asp for Bradford assay to determine encapsulated Asp in SpAcDex particles.

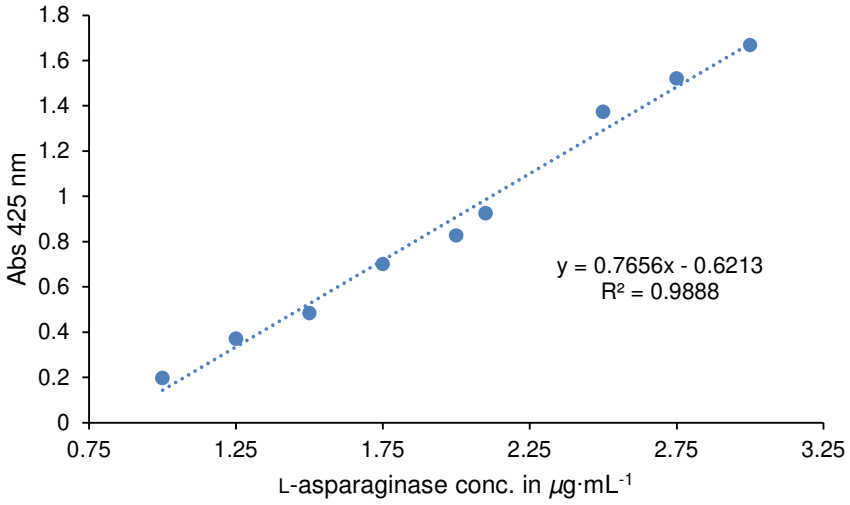

Figure 64. Standard curve of Asp activity for Nessler's reagent Asp activity assay to determine encapsulated active Asp in SpAcDex particles.

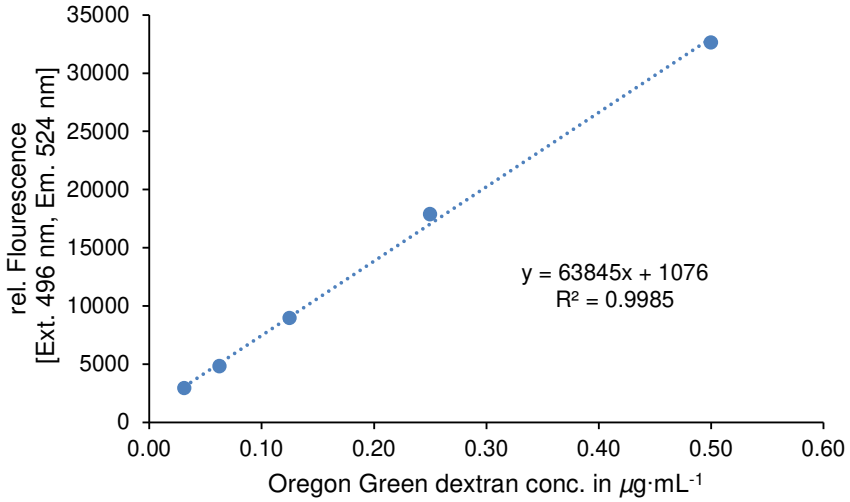

Figure 65. Standard curve of Oregon Green dextran for the determination of encapsulated Oregon Green dextran in SpAcDex particles by fluorescence measurement.

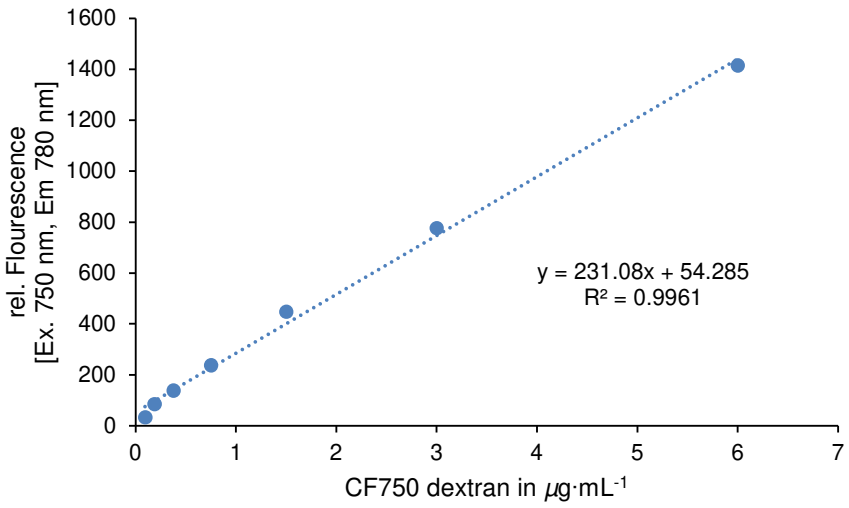

Figure 66. Standard curve of CF750 dextran for the determination of encapsulated CF750 dextran in SpAcDex particles by fluorescence measurement.

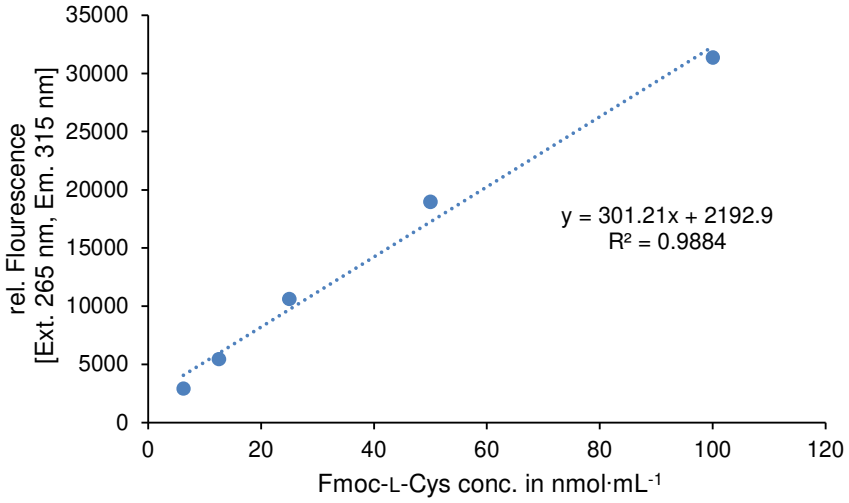

Figure 67. Standard curve of Fmoc-L-Cys for the determination of PEGylation on SpAcDex particles by fluorescence measurement.

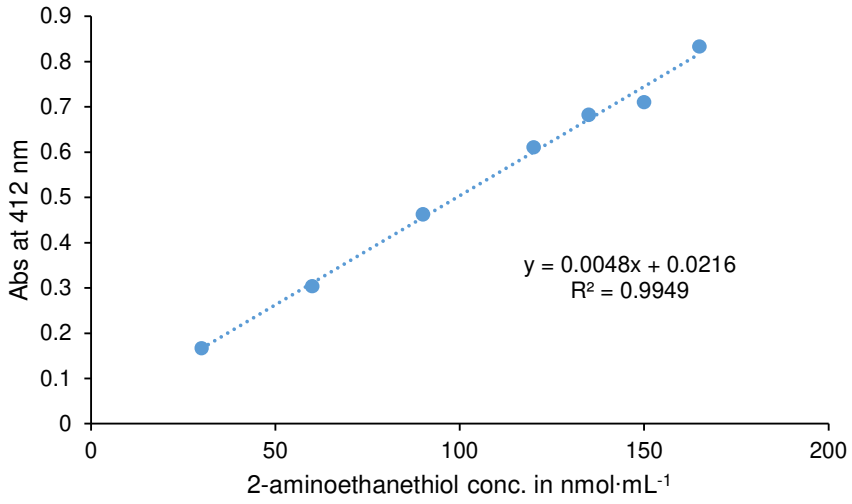

Figure 68. Standard curve of 2-aminoethanethiol conc. for the determination of PEGylation on SpAcDex particles by absorbance measurement.

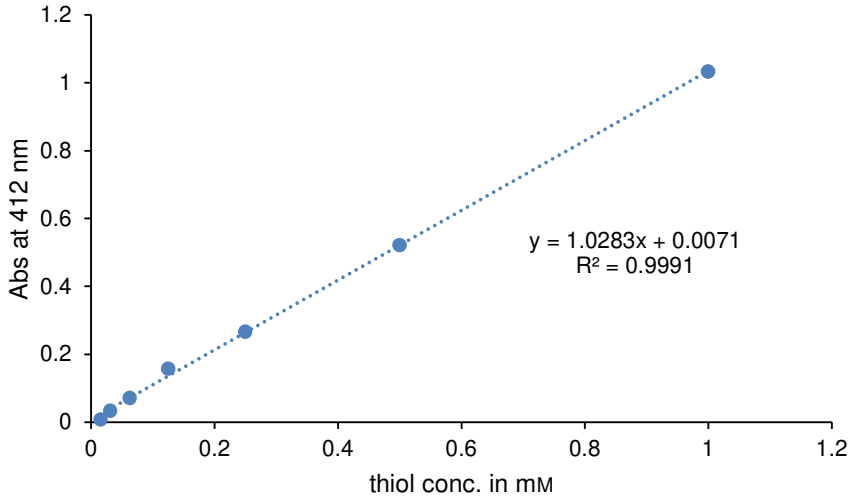

Figure 69. Standard curve of *N*-acetyl-L-cysteine for Ellman's assay to determine the SATA-modification on anti-DEC205.

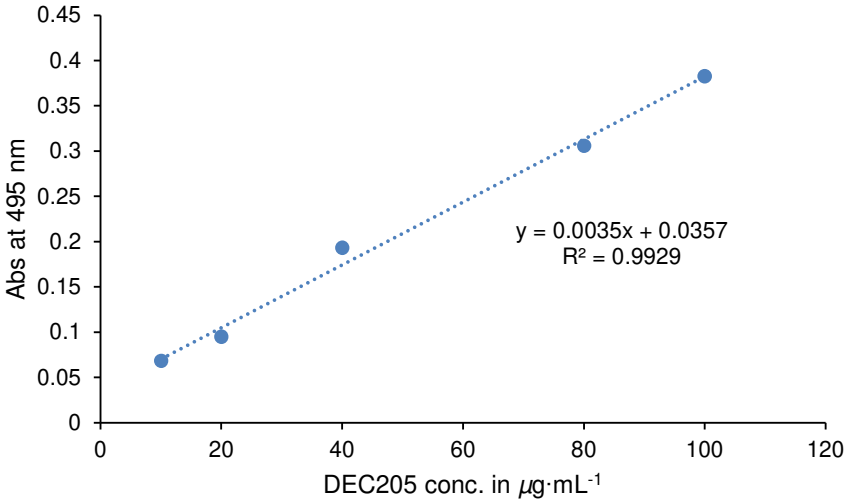

Figure 70. Standard curve of anti-DEC205 for Bradford assay to determine anti-DEC205 on the SpAcDex particles surface.

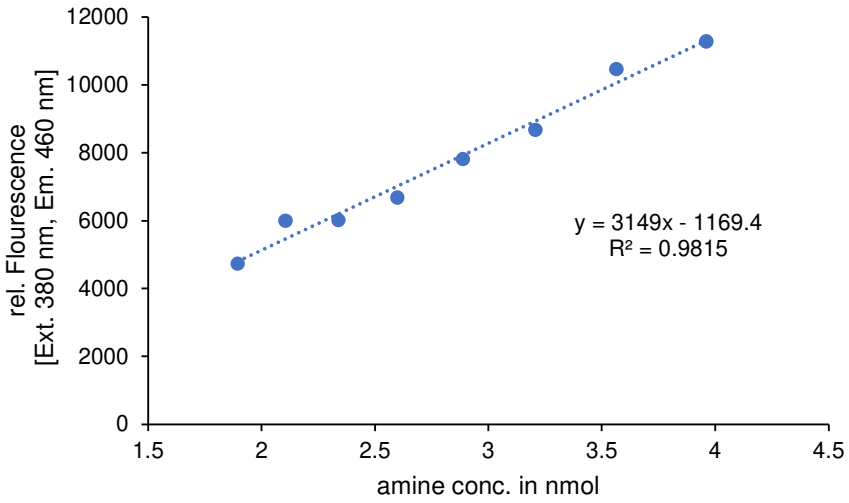

Figure 71. Standard curve of hexylamine for fluorescamine assay to determine SATP-modification on HRP.

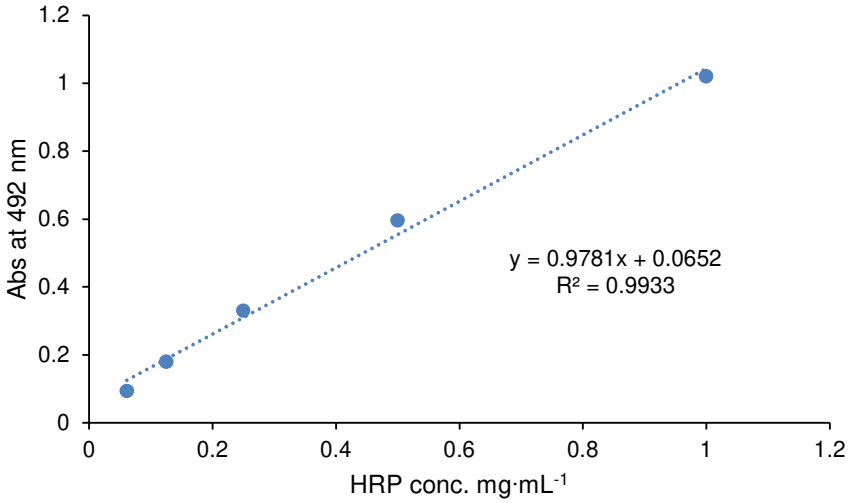

Figure 72. Standard curve of HRP for BCA assay to determine the HRP-content within HRP-AcDex particles.

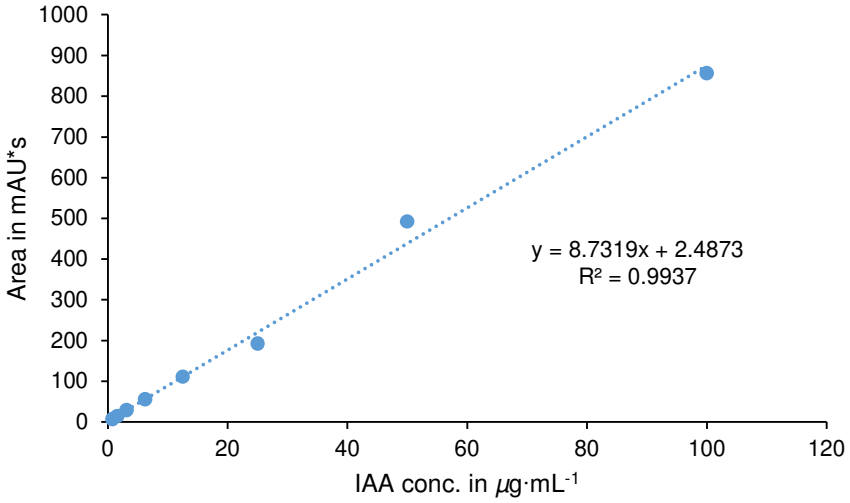

Figure 73. Standard curve of IAA for the determination of encapsulated IAA in HRP-AcDex particles by absorbance measurement.

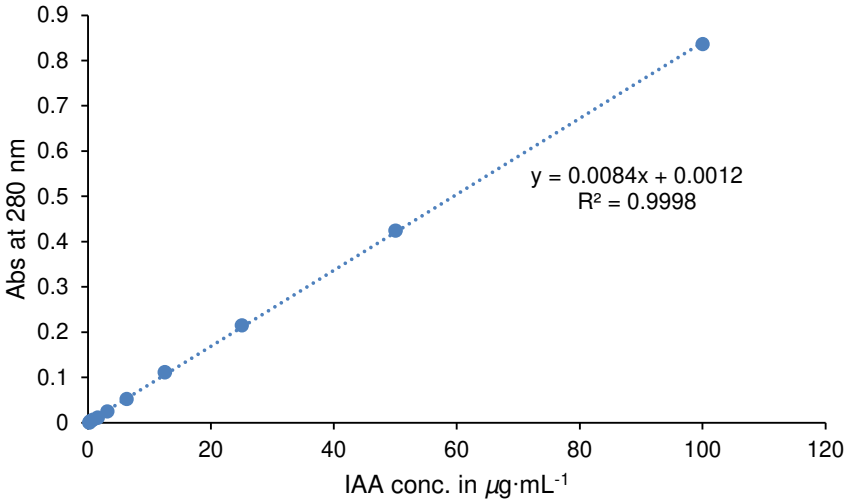

Figure 74. Standard curve of IAA for the determination of released IAA in HRP-AcDex particles by absorbance measurement.

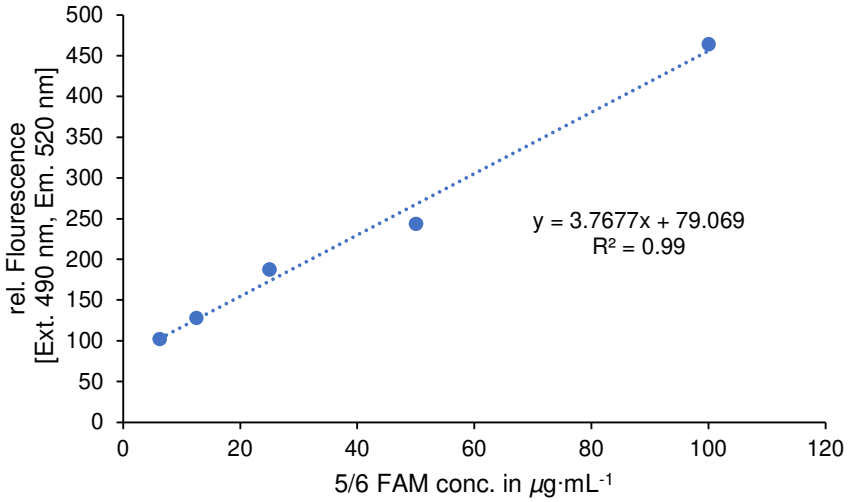

Figure 75. Standard curve of 5/6 FAM for the determination of encapsulated fluorescent dye in HRP-AcDex by fluorescence measurement.

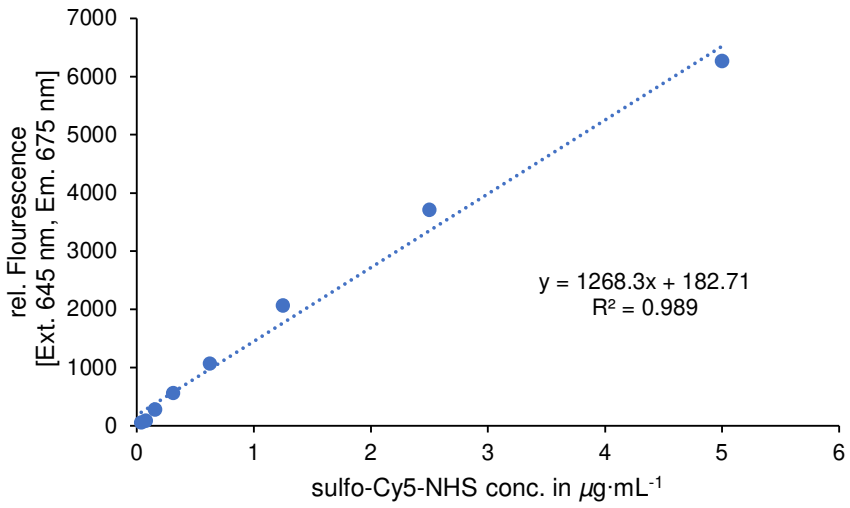

Figure 76. Standard curve of sulfo-Cy5-NHS for the determination of conjugated fluorescent dye to HRP by fluorescence measurement.